



**ELECTROCHEMILUMINESCENCE AND ORGANIC ELECTRONICS
OF DERIVATISED POLY(ANILINE SULPHONIC ACID)
LIGHT-EMITTING DIODES**

By

KERILENG MILDRED MOLAPO

BSc (Rhodes University)

BSc Honours (University of the Western Cape)

A thesis submitted in fulfillment of the requirements for the degree of
MAGISTER SCIENTIAE

Department of Chemistry

University of the Western Cape

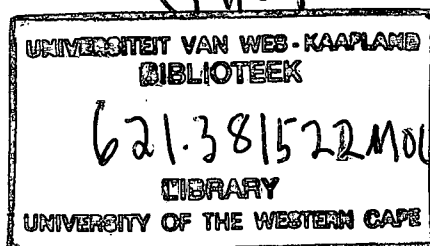
Supervisor: Prof. Emmanuel I. Iwuoha

DECEMBER 2011



UNIVERSITY *of the*
WESTERN CAPE

(THE)



DECLARATION

I declare that “Electrochemiluminescence and organic electronics of derivatised poly(aniline sulphonic acid) light-emitting diodes” is my own work, that it has not been submitted for any degree or examination in any other university and that all the resources I have used or quoted have been indicated and acknowledged by means of complete references.

Kerileng Mildred Molapo



Signed :

DEDICATION

This work is dedicated to my late Grandparents

Mme Leano Molapo

le

Rre Elisha Molapo



UNIVERSITY *of the*
WESTERN CAPE

ACKNOWLEDGEMENTS

Firstly I would like to thank the **Creator** of all things, true source of light and wisdom, origin of all being, the **God Almighty**, for blessing me with the grace to work with constancy, patience and method which carried me through out the course of my research work.

I would like to express my deep sense of gratitude to my supervisor Professor Emmanuel Iwuoha for the valuable encouragement, inspiration, continued fruitful discussions, advice and critical review of aspects of this study.

I thank the SensorLab management Prof. Iwuoha, Prof. Baker, Dr Jahed and Dr Ngece for creating a positive and conducive environment which gave me opportunity to step into an exciting research field, which I totally enjoyed working with in.

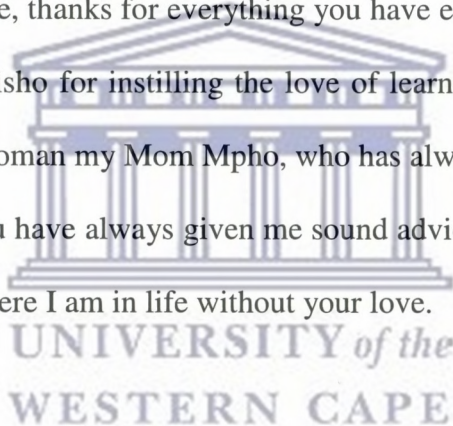
To Prof. Tia Keyes and Prof. Robert Forster, from the School of Chemical Sciences, Dublin City University of Ireland, thanks for hosting me during my two months visit, giving me a platform to learn enormously and introducing me to the field of Photophysics and Electrochemiluminescence. I would also like to extend my thanks to Anitha and Ciaran for their remarkable help throughout my visit.

My thanks are extended to all my research colleagues and friends in **SensorLab** in the University of Western Cape for the discussions we shared and for providing such a wonderful environment , being my family away from home and making Cape Town enjoyable .Thanks to Faiza “Sister Boss”, Peter “Second boss in charge”, Godfrey “Cousin”, Gcineka, Fanelwa, Stephen, Lundi, Lindsay, Euodia, Masikini and Nwabisa for making the Main Lab such a nice and friendly environment to work with in .

Special thanks go to my very good friend Kwena Modibane. Thank you Kwena e kgolo for being there for me and encouraging me and always believing in my potentials. To my two good friends Gcineka and Sekai, whom I met in the academic field, but have now become my sisters, thank you for the love, care, support and always making me happy.

Thanks to my friends, the one's we share childhood memories: Nthabiseng, Norma, Palesa, Kelebogile and Lindiwe, thanks for being very good friends, and for bearing with me even for the times I used to be very boring to you, due to having academic commitments.

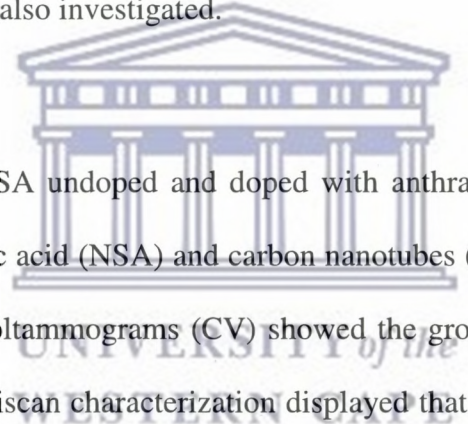
“Gratitude is the memory of heart”, I owe a giant thanks to the Molapo family the people who have brought me thus far in life, thanks for everything you have ever done for me. Thank you to my parents Mpho and Kagisho for instilling the love of learning within me, from a very young age. To a remarkable woman my Mom Mpho, who has always believed that I came for a great purpose in this life, you have always given me sound advice, love and encouragement and I certainly wouldn't be where I am in life without your love.



I want to lastly acknowledge the financial assistance for my MSc degree from South African Synthetic Oil Limited (SASOL) and National Research Foundation of South Africa (NRF).

ABSTRACT

Applications of electrochemiluminescent conjugated polymers offer promising solutions in addressing the problem of light emitting devices. However, the challenging problems that hamper their application in light emitting devices are loss of signal due to diffusion of the electrochemiluminescence (ECL) reagent out of the detection zone, limited ability to repeatedly cycle an individual luminophore and high reagent consumption. In this work, the main objective was to produce conducting polymers with enhanced electrochemiluminescence by tuning the properties of the polymer itself. The electrochemical and photophysical properties of films of polyaniline (PANI) and poly(8-anilino-1-naphthalene sulfonic acids) (PANSA) synthesized through electro- and chemical polymerization methods were also investigated.



The electrosynthesis of PANSA undoped and doped with anthracene sulfonic acid (ASA), 1,2-naphthaquinone-4-sulfonic acid (NSA) and carbon nanotubes (CNT) in acid medium was investigated and the cyclic voltammograms (CV) showed the growth of the polymer during polymerization. The CV multiscan characterization displayed that the growth of the polymer was dependent of the scan rate and the three redox couples were observed as indicative of the three redox states of typical polyaniline and its derivatives. The results also showed that the peak currents were diffusion controlled and the electron charge transport coefficient (D_e) of the electrosynthesized polymers was found to range between 10^{-8} and 10^{-9} $\text{cm}^2 \text{s}^{-1}$ for PANSA, PANSA-ASA, PANSA-NSA and PANSA-CNT. The D_e value indicates that the movement of electrons along the polymer chain was averagely fast. The transmission electron microscopy (TEM) was used to investigate the electronic morphology of the polymers and the TEM images showed an intertwinement of tubings which aggregate into a ring with a mixture of tubings and plastic sheets.

The chemical synthesis of PANI, PANSA and PANI-NSA was carried out by using monomers analine, 8-anilino-1-naphthalene sulfonic acid, and aniline with 1,2-naphthaquinone-4-sulfonic acid, respectively, using oxidants. All chemically synthesized polymers exhibited quinoid and benzoid bands typically see in polyaniline FTIR and Raman spectra confirmed the successfully formation of polymers. The CV characterization of these polymers showed distinctive redox peaks. This proved that the polymers were electroactive, conductive and exhibited reversible electrochemistry. The D_e of the electrosynthesized polymers was found to be $\sim 10^{-5} \text{ cm}^2 \text{ s}^{-1}$ for chemically synthesized polymers. The electric conductivity measurement showed to increase from 10^{-4} to 10^{-2} when aniline was polymerized with NSA dopant, this might be related to the process of electron transfer from dopant to polymer. Scanning electron microscopy for external morphology showed that the polymers were made of different nano-rods polymeric structures.

Photophysical properties of electro- and chemically synthesized PANSA and PANI were investigated through UV-vis absorption, fluorescence behaviour, and lifetime. The UV-vis absorption spectra of these polymers showed that they exhibited absorption bands corresponding to the polyemeraldine redox state of typical polyaniline. The effect of dopants resulted in the increase in solubility of the polymers with a small shift of absorption bands due to incorporation of dopants in to the backbone of the polymer. The fluorescence emission spectra of the electrochemically synthesized PANSA with and without dopants were observed to be similar and mirror image of the excitation spectra and corresponding to the electronic band of the benzoid ring in the polyemeraldine form confirming that the fluorescing molecule in these polymers were the benzoid rings. However, the emission spectra of the chemically synthesized PANSA and PANI were different to excitation spectra due to loss of symmetry upon excitation. The effects of chemically synthesized PANI,

PANSA and PANI-NSA addition on the photophysical properties of $[\text{Ru}(\text{bpy})_2(\text{picCOOH})]^{2+} \cdot (\text{ClO}_4^-)_2$ were investigated in order to understand the interaction of polymer and $[\text{Ru}(\text{bpy})_2(\text{picCOOH})]^{2+} \cdot (\text{ClO}_4^-)_2$. The analysis revealed that the presence of polyaniline and its derivatives enhanced the $[\text{Ru}(\text{bpy})_2(\text{picCOOH})]^{2+} \cdot (\text{ClO}_4^-)_2$ absorption band, photoluminescence and fluorescence lifetime. The enhancement observed from interaction of $[\text{Ru}(\text{bpy})_2(\text{picCOOH})]^{2+} \cdot (\text{ClO}_4^-)_2$ with polyaniline and its derivatives might be due to the excited state electron transfer from the PANI and PANSA excited state to the $[\text{Ru}(\text{bpy})_2(\text{picCOOH})]^{2+} \cdot (\text{ClO}_4^-)_2$.

It was further demonstrated in this work that it is possible to form polyaniline and PANSA doped with $[\text{Ru}(\text{bpy})_2(\text{picCOOH})]^{2+} \cdot (\text{ClO}_4^-)_2$ films on ITO electrode using potentiostatic growth method to favour ECL production. The results showed that all films generated ECL in the presence of Tripropylamine (TPA) as a co-reactant and their emission properties depend on time used to prepare the film. The enhancement of ECL signal was due to a positive electron transfer from the conducting polymer (PANI and PANSA) to $[\text{Ru}(\text{bpy})_2(\text{picCOOH})]^{2+} \cdot (\text{ClO}_4^-)_2$ complex. The results highlighted the potential of these polymeric luminophores usage in the manufacturing of the ECL devices.

TABLE OF CONTENTS

TITLE PAGE.....	i
DECLARATION.....	ii
DEDICATION.....	iii
ACKNOWLEDGEMENTS	iv
ABSTRACT.....	vi
TABLE OF CONTENTS	ix
LIST OF SYMBOLS	xvii
LIST OF ABBREVIATIONS	xix
LIST OF SCHEMES	xxiii
LIST OF TABLES	xxv
LIST OF FIGURES	xxvi
CHAPTER ONE:	1
<i>INTRODUCTION</i>	1
1.1. Background.....	1
1.2. Research Rationale and Motivation	2
1.3. Problem Identification	2
1.4. Research Feasibility and Impact.....	3
1.4.1. Feasibility.....	3
1.4.2. Impact	4
1.5. Research Aims and Objectives.....	5
1.5.1. Aims	5
1.5.2. Objectives	5
1.6. Thesis outline	6
1.6. References	7
CHAPTER TWO:.....	9
<i>LITERATURE REVIEW</i>	9
2.1. Luminescence.....	9

2.1.1. Electroluminescence (EL).....	9
2.1.2. Photoluminescence	10
2.1.3. Chemiluminescence	11
2.1.4. Electrochemiluminescence	12
2.2. Discovery and history of electrochemiluminescence.....	13
2.2.1. Background.....	13
2.2.2. Early experiments.....	14
2.3. Principles of electrochemiluminescence	14
2.3.1. Overview.....	14
2.4. ECL generation pathways	17
2.4.1. Annihilation ECL.....	17
2.4.2. Coreactant ECL.....	21
2.4.2.1. Types of Coreactants.....	23
2.4.2.1.1. Tripropylamine (TPA).....	23
2.4.2.1.2. Peroxide systems	25
2.5. ECL Luminophores	27
2.6. Electrochemiluminescence of ruthenium complexes	28
2.6. 1. Overview.....	28
2.6.2. Annihilation ECL of ruthenium complex.....	28
2.6.3. Coreactant ECL of ruthenium complex.....	30
2.7. Conducting Polymers (ICPs) for ECL electrode modification	31
2.7.1. Overview of polymers	31
2.7.2. History of polymers	31
2.7.3. Conducting Polymers	32
2.7.4. Electronics of electrically conducting polymers (ECPs).....	33
2.7.4.1. The band theory as a function of application of quantum theory.....	34
2.7.4.2. The band theory as a function of application of molecular orbital theory.....	35
2.7.4.3. The electronic properties of metals, semiconductors, and insulators	38
2.7.4.4. The electronic properties of semiconductors.....	38
2.7.4.4.1. The electronic properties of intrinsic semiconductors.....	39
2.7.4.4.2. The electronic properties of intrinsic semiconductors.....	40

2.7.5. Polyaniline.....	44
2.7.5.1. History.....	44
2.7.5.2. Structure of Polyaniline	44
2.7.5.3. Synthesis of polyaniline.....	45
2.7.5.4. Electrochemical polymerization	46
2.7.5.5. Chemical polymerization	46
2.7.5.6. Mechanism of polymerization	47
2.7.5.7. Properties of polyaniline.....	51
2.7.5.7.1. Switching and Optical properties of PANI.....	51
2.7.5.7.2. Conductivity properties of PANI.....	54
2.7.5.7.3. Solubility properties of PANI.....	56
2.8. Theoretical Background to the techniques used	57
2.8.1. Fundamentals of electrochemistry.....	57
2.8.1.1. Basic components of an electroanalytical system.....	57
2.8.1.2. Fundamentals of ECL	60
2.8.1.3. Electro analytical techniques.....	62
2.8.1.3.1. Cyclic voltammetry.....	62
2.8.1.3.2. Chronoamperometry	67
2.9. Spectroscopy and Photochemistry fundamentals	69
2.9.1. Luminescence.....	69
2.9.2. Nature of electronic states.....	70
2.9.2.1. Absorption.....	73
2.9.2.2. Fluorescence	74
2.9.2.3. Internal conversion	75
2.9.2.4. Intersystem crossing and Phosphorescence.....	75
2.9.2.5. Fluorescence Quenching	76
2.10. Spectroscopy techniques	77
2.10.1. Ultraviolet Visible (UV-vis) Spectroscopy	77

2.10.2. Fluorescence Spectroscopy	78
2.10.3. Time-Related Photon Counting (TCSPC)	79
2.10.4. Vibrational Spectroscopy	81
2.10.4.1. Fourier-Transform Infrared Spectroscopy	81
2.10.4.2. Raman Spectroscopy	81
2.11. Microscopy	82
2.11.1. Scanning electron microscopy (SEM)	82
2.11.2. Transmission electron microscopy (TEM)	83
2.12. Four point probe conductivity measurements	84
2.13. Conclusion	85
2.14. References	86
 CHAPTER THREE:	 98
ELECTROCHEMICAL SYNTHESIS and CHARACTERIZATION of POLY(8- ANILINO-1-NAPHTHALENE SULFONIC ACID)	 98
3.1. Introduction	98
3.2. Experimental method	99
3.2.1. Reagents and materials	99
3.2.2. Apparatus and measurement	99
3.2.3. Synthesis of Anthracene sulfonic acid (ASA)	100
3.2.4. Electrochemical synthesis of PANSA	101
3.3. Results and discussion	101
3.3.1. Polymerization of 8-anilino-1-naphthalene sulfonic acid (ANSA)	101
3.3.1.1. Polymerization of undoped ANSA	102
3.3.1.2. Effect of dopants during polymerization of ANSA	104
3.3.2. Cyclic voltammetric characterization of PANSA	109
3.3.2.1. Cyclic voltammetric characterization of undoped PANSA	109
3.3.2.2. Cyclic voltammetric characterization of doped PANSA	111
3.3.2.3. Estimation of kinetic parameters for undoped and doped PANSA	113
3.3.3. TEM characterization of PANSA	115

3.4. Proposed Mechanisms of electropolymerization of ANSA with and without dopants	119
3.4.1. Mechanism of electropolymerization of 8-anilino-1-naphthalene sulfonic acid..	119
3.4.2. Mechanism of electropolymerization of 8-anilino-1-naphthalene sulfonic acid (ANSA) in the presence of 1,2-Naphthaquinone-4- sulfonic acid (NSA).....	120
3.4.3 Mechanism of electropolymerization of 8-anilino-1-naphthalene sulfonic acid (ANSA) in the presence of Anthracene sulfonic acid (ASA)	121
3.4.4. Mechanism of electropolymerization of 8-anilino-1-naphthalene sulfonic acid (ANSA) in the presence of multiwalled carbon nanotubes (CNT).....	122
3.5. Conclusion.....	123
3.6. References	124
CHAPTER FOUR:	127
CHEMICAL SYNTHESIS and CHARACATERIZATION OF POLY (8-ANILINO-1-NAPHTHALENE SULFONIC ACID) AND POLYANILINE	127
4.1. Introduction	127
4.2. Experimental method.....	128
4.2.1. Reagents and materials	128
4.2.2. Apparatus and measurement	128
4.2.3. Chemical synthesis of Polyaniline (PANI) and Poly (8-anilino-1-naphthalene sulfonic acid) PANSA	130
4.2.3. Chemical synthesis of Polyaniline (PANI) with NSA dopant	130
4.3. Results and discussion.....	131
4.3.1. Chemical synthesis of PANI and PANSA	131
4.3.2. Cyclic voltammetric characterization of chemical synthesized polymers	132
4.3.2.1. Cyclic voltammetric characterization on gold electrode.....	132
4.3.3. Electrical conductivity measurement of polymer	137
4.3.4. FTIR Characterization of polymers.....	139
4.3.4.1. FTIR spectra of undoped PANI and PANSA.....	139
4.3.4.2. The effect of dopants on FTIR spectra of PANI.....	141
4.3.5. Raman Characterization of polymers.....	142
4.3.5.1. Rama spectra of PANI, PANSA and PANI-NSA.....	142
4.3.6. Scanning Electron Microscopy (SEM)	144
4.4. Conclusion.....	147

4.5. References	148
CHAPTER FIVE:	151
PHOTOPHYSICAL STUDIES OF ELECTRO and CHEMICALLY SYNTHESIZED POLY(8-ANILINO-1-NAPHTHALENE SULFONIC ACID) AND POLYANILINE .151	
5.1. Introduction	151
5.2. Experimental method.....	152
5.2.1. Reagents and materials	152
5.2.2. Apparatus and measurement	152
5.2.3. Synthesis of polymers.....	153
5.3. Results and Discussion	153
5.3.1. Photoluminescence Studies of electrosynthesized undoped and doped PANSA... 153	
5.3.1.1. UV-visible Spectroscopic Characterization.....	154
5.3.1.1.1. Electronic absorption of undoped PANSA.....	154
5.3.1.1.2. Effect of dopants on electronic absorption of PANSA	155
5.3.1.1.3. Band gap determination of undoped and doped PANSA	157
5.3.1.2. 2D Fluorescence Characterization of electrosynthesized PANSA	159
5.3.1.2.1. 2D Fluorescence spectra of undoped PANSA.....	160
5.3.1.2.2. Effect of dopants on 2D fluorescence spectra of PANSA.....	162
5.3.1.3. 3D Fluorescence Characterization of PANSA.....	165
5.3.1.3. 1. 3D fluorescence topographical spectra of undoped and doped PANSA	165
5.3.1.3.2. 3D fluorescence contour spectra.....	168
5.3.2. Photoluminescence Studies of chemically synthesized PANI and PANSA.....	170
5.3.2.1. UV-visible Spectroscopic Characterization of Chemically synthesized Undoped PANI and PANSA.....	170
5.3.4.2. Effect of NSA on electronic absorption of PANI.....	171
5.3.4.2. Effect of dopant on fluorescence spectra of PANI.....	175
5.3.4.3. Fluorescence quantum yield and lifetime of chemical synthesized PANI and PANSA.....	176
5.3.5. Photoluminescence Studies $([Ru(bpy)_2(picCOOH)]^{2+} \cdot (ClO_4^-)_2)$ with addition of polymers.....	180

5.3.5.1. UV-visible Spectroscopic Characterization of $[Ru(bpy)_2(picCOOH)]^{2+}.(ClO_4^-)_2$ with addition of chemically synthesized polymers	180
5.3.5.3. Fluorescence lifetime of Ru complex with addition of chemical synthesized polymers.....	185
5.4. Conclusion.....	187
5.5. References	189
CHAPTER SIX:	194
ELECTROCHEMILUMINESCENCE of POLY (8-ANILINO-1-NAPHTHALENE SULFONIC ACID) and POLYANILINE DERIVATIZED with RUTHENIUM (II) (bis-2,2-BIPYRIDYL)-2(4-CARBOXYLPHENYL) IMIDAZO[4,5-f][1,10]PHENANTHROLINE	194
6.1. Introduction	194
6.2. Experimental method.....	198
6.2.1. Reagents and materials	198
6.2.2. Apparatus and measurement	198
6.2.2.1. Electrochemistry	198
6.2.3. Electro chemical synthesis of the PANI and PANSA with Ru complex	199
6.2.3.1. Preparation of PANI- $[Ru(bpy)_2(picCOOH)]^{2+}.(ClO_4^-)_2$ and PANSA $[Ru(bpy)_2(picCOOH)]^{2+}.(ClO_4^-)_2$ film on Pt and Au disc electrode respectively.	199
6.2.3.2. Preparation of the films on ITO used to study ECL	200
6.3. Results and Discussion	201
6.3.1. Preliminary results	201
6.3.1.1. Film preparation and optimization.....	201
6.3.1.2. Electropolymerization of aniline (ANI) and $[Ru(bpy)_2(picCOOH)]^{2+}.(ClO_4^-)_2$	203
6.3.1.3. Electropolymerization of ANSA and $[Ru(bpy)_2(picCOOH)]^{2+}.(ClO_4^-)_2$	206
6.3.1.4. Optimized electropolymerization of ANSA and $[Ru(bpy)_2(picCOOH)]^{2+}.(ClO_4^-)_2$	208
6.3.2. Potentiostatic growth of PANI and PANSA in the presence $[Ru(bpy)_2(picCOOH)]^{2+}.(ClO_4^-)_2$ on ITO in HCL and H_2SO_4 respectively.....	211
6.3.3. CV characterization of PANI- $[Ru(bpy)_2(picCOOH)]^{2+}.(ClO_4^-)_2$ and PANSA- $[Ru(bpy)_2(picCOOH)]^{2+}.(ClO_4^-)_2$ films.....	214

6.3.4. Electrochemiluminescence study.....	217
6.3.4.1. ECL response of PANI-[Ru(bpy) ₂ (picCOOH)] ²⁺ .(ClO ₄) ₂ film	217
6.3.4.1. ECL response of PANSA-[Ru(bpy) ₂ (picCOOH)] ²⁺ .(ClO ₄) ₂ film	225
6.4. Conclusion.....	230
6.5 References	231
 CHAPTER SEVEN:	 235
CONCLUSIONS AND RECOMMENDATIONS.....	235
7.1.Conclusion.....	235
7.2. Recommendation for further study	237



LIST OF SYMBOLS

A	: Area of electrode
	: Cross-section area
C	: Coulomb
D_e	: Diffusion coefficient
E_g	: Band gap
E_{final}	: Final potential
$E_{initial}$: Initial potential
$E^{o'}$: Formal electrode potential
E^{o}_{donor}	: Formal potential reduction
$E^{o}_{acceptor}$: Formal potential oxidation
E_p	: peak potential
$E_{p,a}$: Anodic peak potential
$E_{p,c}$: Cathodic peak potential
ΔE_p	: Separation peak potential
F	: Faraday constant
I	: Current
I_o	: Scaling factor
$I_{p,c}$: Cathodic reaction
$I_{p,a}$: Current for the anodic reaction
I_p	: Peak current
$I(t)$: Impulse response function
k	: Overall relaxation rate
n	: Refractive index
	: Number of electrons transferred



n_{std}	: Refractive index of the standard
ρ	: Specific resistivity
Q	: Charge
R	: Sample resistance
S_0	: Ground singlet state
S_1	: Excited singlet state
T	: Triplet state
ν	: Scan rate
V	: Applied voltage
I^*	: Surface concentration
σ	: Specific conductivity
Φ_F	: Fluorescence quantum yield
Φ_F^{std}	: Fluorescence quantum yield of the standard
Φ_{PL}	: Photoluminescence quantum yield
τ	: Lifetime
λ	: Wavelength
Δ	: Crystal field strength
ΔG	: Gibbs energy

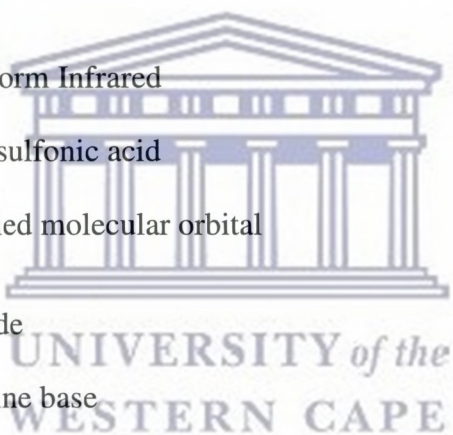


LIST OF ABBREVIATIONS

A	: Absorbance
AC	: Alternating current
AMI	: Advanced Metals Initiative
ANI	: Aniline
ANSA	: 8-anilino-1-naphthalene sulfonic acid
APS	: Ammonium persulphate
ASA	: Ananthracene sulfonic acid
A_{std}	: Absorbance of the standrad
BAS	: Bioanalytical Systems
BBQ	: Benzoidic-benzoidic-quinoidic
bpy	: 2,2'-bipyridyl
CB	: Conduction band
CCD	: Charge coupled device
CCl₃H	: Chloroform
CL	: Chemiluminescence
CNTs	: Carbon nanotubes
CV	: Cyclic voltammetry
DBSA	: Dodecyl-benzene sulfonic acid
DC	: Direct current
DMF	: Dimethyl formamide
DMSO	: Dimethyl sulfoxide
DPA	: 9,10-Diphenylanthracene
EB	: Emeraldine base
ECL	: Electrochemiluminescence



ECPs	: Electrically conducting polymers
EL	: Electroluminescence
EM	: Emeraldine
ES	: Emeraldine salt
F	: Fluorescence
F_g	: Fermi level
FPD	: Flat-panel display
FLIM	: Fluorescence lifetime imaging
F_{std}	: Area of the standard under an emission band
FTIR	: Fourier-Transform Infrared
HCSA	: 10-Champhor sulfonic acid
HOMO	: Highest occupied molecular orbital
ITO	: Indium tin oxide
LB	: Leucoemeraldine base
LC	: Ligand centred
LE	: Leucoemeraldine
LED	: Light emitting diodes
LEP	: Light emitting polymer
LUMO	: Lowest unoccupied molecular orbital
MCP	: Multi channel plate
MeCN	: Acetonitrile
MLCT	: Metal to ligand charge transfer



NIR	: Near infrared
NMP	: Methyl pyrrolidinone
NAMTS	: National Advanced Manufacturing Technology Strategy
NNS	: National Nanotechnology Strategy
NSA	: 1,2-Naphthaquinone-4-sulfonic acid
PADPA	: <i>p</i> -Aminodiphenylamine
PANI	: Polyaniline
PANSA	: Poly(8-anilino-1-naphthalene sulfonic acid)
PB	: Pernigraniline base
PE	: Pernigraniline
PL	: Photoluminescence
PLDs	: Polymer laser devices
PMAS	: Poly(2-methoxyaniline-5-sulfonic acid)
PMT	: Photo multiplier tube
PPy	: Polypyrroles
PPV	: Polyphenylene vinylenes
PT	: Polythiophenes
QDs	: Quantum dots
QBB	: Quinoidic-benzoidic- benzoidic
QBQ	: Quinoidic-benzoidic-quinoidic
SCE	: Saturated calomel electrode
SEM	: Scanning electron microscopy
Si-QDs	: Silicon-quantum dots
SPAD	: Single photon avalanche photodiode
TBABF₄	: Tetrabutylammonium tetrafluoroborate



TCSPC	: Time-correlated single photon counting system
TEM	: Transmission electron microscopy
THCOOH	: Thianthracenecarboxylic acid
THF	: Tetrahydrofuran
TPA	: Tripropylamine
UCD	: University College Dublin
UV	: Ultraviolet
UWC	: University of the Western Cape
VB	: Valence band
Vis	: Visible
2D	: Two dimension
3D	: Three dimension



LIST OF SCHEMES

Scheme 2.1: Photoluminescence showing transitions between the excited state and the ground state (Santhanam <i>et al.</i> , 1965).....	11
Scheme 2.2: Schematic diagram of a typical basic experimental apparatus used for the generation and measurement of ECL (Knight, 1999).....	15
Scheme 2.3: Structure of $[\text{Ru}(\text{bpy})_3]^{2+}$ and proposed mechanism for $[\text{Ru}(\text{bpy})_3]^{3+}/[\text{Ru}(\text{bpy})_3]^+$ ECL system (Richter, 2004).....	29
Scheme 2.4: Proposed mechanism for $\text{Ru}(\text{bpy})_3]^{2+}/\text{TPA}$ ECL system (Richter, 2004)...	30
Scheme 2.5: Oxidation of monomer during electrochemical polymerization of aniline (Morrin, 2002).....	48
Scheme 2.6: Radical coupling and Rearomatization during electrochemical polymerization of aniline (Morrin, 2002).....	48
Scheme 2.7: Chain propagation during electrochemical polymerization of aniline (Morrin, 2002).....	49
Scheme 2.8: Oxidation and doping of the polymer during electrochemical polymerization of aniline (Wallace <i>et al.</i> , 2009).....	50
Scheme 2.9: Chain propagation of the polymer during chemical synthesis polymerization of aniline (Wallace <i>et al.</i> , 2009).....	50
Scheme 2.10: Reduction of the pernigraniline salt to emeraldine salt during chemical synthesis polymerization of aniline (Wallace <i>et al.</i> , 2009).....	51
Scheme 2.11: The doping of EB with protons to form the conducting emeraldine salt (PANI/HA) form of polyaniline (a polaron lattice) (Stafström <i>et al.</i> , 1987).....	56

Scheme 2.12: Showing the possible physical effects resulting from the absorption of light, the highlighting is position of photoluminescence (Valeur, 2002).....	70
Scheme 3.1: Electropolymerization of 8-anilino-1-naphthalene sulfonic acid (ANSA) in 0.5 M H ₂ SO ₄ at -0.3 to 1.1 V and 0.05V s ⁻¹ scan rate.....	102
Scheme 3.2: Different oxidation states of poly (8-anilino-1-naphthalene sulfonic acid)	110
Scheme 4.1: Chemical synthesis of PANI, PANSA, and PANI-NSA.....	131
Scheme 6.1: Above shows the proposed tri- <i>n</i> -propylamine (TPA) and [Ru(bpy) ₂ (pic COOH)] ²⁺ . (ClO ₄) ₂ oxidation/ reaction sequence with abbreviations in parentheses.....	218



LIST OF TABLES

Table 2.1: Classification of types of luminescence.....	10
Table 3.1: Kinetic parameters of undoped and doped polymers.....	115
Table 4.1: Electrochemical parameters of PANI, PANSA and PANI-NSA	136
Table 4.2: Electrical conductivity parameters of chemically synthesized polymer.....	138
Table 4.3: Assignment of Raman vibrational bands & their relationship to structural changes and oxidation states (Lindfors <i>et al.</i> , 2002)	144
Table 5.1: UV-vis absorption wavelength and band gap related to the redox states of the undoped and doped PANSA	159
Table 5.2: Results summary of fluorescence properties of the polymers.....	162
Table 5.3: Fluorescence quantum yield of PANI, PANSA and PANI-NSA in DMSO.....	177
Table 5.4: Fluorescence lifetime of PANI, PANSA and PANI-NSA in DMSO.....	180
Table 5.5: Fluorescence lifetime of $[\text{Ru}(\text{bpy})_2(\text{picCOOH})]^{2+} \cdot (\text{ClO}_4^-)_2$ in MeCN with addition of chemically synthesized PANI, PANSA and PANI-NSA dissolved in DMSO	187
Table 6.1: Showing a summary of results obtained PANI and PANSA Films modulated with $[\text{Ru}(\text{bpy})_2(\text{picCOOH})]^{2+} \cdot (\text{ClO}_4^-)_2$, electropolymerized at different run timings at potential 0.7 and 0.5 V respectively and the final charge during the electropolymerization.....	214

LIST OF FIGURES

Figure 2.1: Preparation and electrochemiluminescence (ECL) of water-soluble carbon nanocrystals released into aqueous solution from a graphite rod by applying a scanning potential (Zheng <i>et al.</i> , 2009)	16
Figure 2.2: Molecular orbital diagram showing two alternative pathways for electron transfer between oxidised and reduced precursors A^- and A^+ . (A) Formation of an excited state and (B) direct population of ground state products (O'Reilly, 2008).....	20
Figure 2.3: Schematic representation of the energy terms in ECL processes (Kapturkiewicz, 2004)	21
Figure 2.4: (a) ECL and (b) cyclic voltammogram of 5.2 mM 2 THCOOH (Thianthracenecarboxylic acid) and 0.15 M TPA in pH 7.5 sodium phosphate buffer at 6 mm diameter Pt electrode at a scan rate of 100 mV/s (Miao and Choi, 2004). The behaviour of 1-THCOOH is similar except that the peak emission intensity is 6–7 times less intense that that of 2-THCOOH (Richards and Bard, 1995).....	24
Figure 2.5: Typical (shown uncharged) structures of conducting polymers (Walton and Lorimer, 2000).....	33
Figure 2.6: The formation of bands in a conducting solid in the 3rd period and overlap between the valence and conduction bands (Atkins, 2002).....	35
Figure 2.7: Molecular orbitals in a diatomic molecule (Atkins, 2002).....	36
Figure 2.8: Bonds in molecules and bands in solids (Jiles, 1994).....	37
Figure 2.9: Band structure diagram of an intrinsic semiconductor (Atkins, 2002; Jiles, 1994).....	40

Figure 2.10: Band structure diagram of an extrinsic n-type semiconductor (Jiles, 1994).....	42
Figure 2.11: Band structure diagram of an extrinsic p-type semiconductor (Jiles, 1994).....	43
Figure 2.12: Different oxidation states of polyaniline as base forms. $y = 1$ (leucoemeraldine), 0.5 (emeraldine) and 0 (pernigraniline) (Wallace <i>et al.</i> , 2002; Shimano and MacDiarmid, 2001; Masdarolomoor, 2006).....	45
Figure 2.13: Cyclic voltammogram of polyaniline film on a platinum electrode in 1 M HCL at a scan rate 0.1Vs^{-1} ; the potentials at which structure and colour changes occur and the change in the potential of the second redox reaction with pH are shown as well (Wallace, 2009).....	53
Figure 2.14: The different band gaps present in polyaniline redox states (Huang and MacDiarmid, 1993).....	54
Figure 2.15: Structure of 8-anilino-1-naphthalene sulfonic acid (ANSA).....	57
Figure 2.16: Potential-time excitation signal in cyclic voltammetric experiment (Wang, 2000).....	63
Figure 2.17: Solution phase cyclic voltammogram for the reduction reaction at a solid electrode (Bard and Faulkner, 2001).....	64
Figure 2.18: Plot of potential against time (Monk, 2001).....	68
Figure 2.19: Shows a trace of current against time in response to the potential step (Bockris <i>et al.</i> , 2000).....	68
Figure 2.20: Transition in electronic states showing the ground singlet, excited singlet and triplet states (Valeur, 2002).....	72
Figure 2.21: Jablonski diagram (Bard, 2004; Valeur, 2002).....	73

Figure 2.22: Possible electronic transitions of π , σ , and n (Valeur, 2002).....	77
Figure 2.23: Set-up for fluorescence spectroscopy (Lakowicz, 2006).....	79
Figure 2.24: Measurement of time interval between excitation and detection of photon and formation of the histogram (Lakowicz, 2006).....	80
Figure 2.25: Four point probes which have equal interspaces (s) (Aurelio, 2007).....	84
Figure 3.1: The typical cyclic voltammograms recorded during electrochemical synthesis of the (a) undoped PANSA, and doped with (b) Anthracene sulfonic acid (ASA), (c) 1,2-Naphthaquinone-4- sulfonic acid (NSA) and (d) Carbon nanotubes (CNT) respectively.....	105
Figure 3.2: The typical cyclic voltammograms recorded during polymerization of the dopants alone (a) Anthracene sulfonic acid, (b) 1,2-Naphthaquinone-4- sulfonic acid and (c) Carbon nanotubes.....	108
Figure 3.3: The typical cyclic voltammograms at 0.01, 0.02, 0.04, 0.06 and 0.08 V/s for (a) undoped PANSA, and doped with (b) Anthracene sulfonic acid (ASA), (c) 1,2-Naphthaquinone-4- sulfonic acid (NSA) and (d) Carbon nanotubes (CNT), respectively, in 0.5 M H ₂ SO ₄ at room temperature.....	112
Figure 3.4: TEM micrographs of doped PANSA-ASA (a-c) and PANSA-NSA (d-f)....	118
Figure 4.1: The typical cyclic voltammograms for (a) gold electrode, (b) undoped PANI, (c) PANSA and (d) doped PANI with 1,2-Naphthaquinone-4- sulfonic acid (NSA) at 0.01, 0.015, 0.02, 0.025, 0.03, 0.035, 0.04, 0.045 and 0.05 V s ⁻¹ using gold electrode in 1 M HCL.....	135
Figure 4.2: Peak current as a function of square root of scan rate for PANI, PANSA and PANI-NSA.....	136
Figure 4.3: FTIR spectra of PANI and PANSA.....	140
Figure 4.4: FTIR spectra of undoped PANI and PANI with dopant NSA.....	142
Figure 4.5: Raman spectra of PANI, PANSA and PANI-NSA.....	143

Figure 4.6: Scanning electron micrograph of PANI.....	146
Figure 4.7: Scanning electron micrograph of PANSA.....	146
Figure 4.8: Scanning electron micrograph of PANI-NSA.....	147
Figure 5.1: UV-visible spectra of undoped PANSA in DMSO.....	155
Figure 5.2: The forms of polyemeraldine salt (Huang and MacDiarmid, 1993).....	155
Figure 5.3: UV-visible spectra of doped PANSA with Anthracene sulfonic acid (ASA), 1,2-Naphthaquinone-4- sulfonic acid (NSA) and Carbon nanotubes (CNT) and undoped PANSA as a baseline in DMSO.....	156
Figure 5.4: Absorbance squared versus photon energy extrapolated to zero absorption undoped PANSA, the inset for band gaps for polyleucoemeraldine (LE) and polyemeraldine (EM).....	158
Figure 5.5: 2D Fluorescence spectra of undoped and doped PANSA with 1,2 Naphthaquinone-4- sulfonic acid (NSA), Carbon nanotubes (CNT) and Anthracene sulfonic acid (ASA).....	161
Figure 5.6: Fluorescence excitation and UV-vis absorption spectra of PANSA-CNT in DMSO, excited at 350 nm.....	164
Figure 5.7: 3D Fluorescence topographical spectra of (a) DMSO, (b) ANSA, (c) undoped and doped PANSA with (d) Anthracene sulfonic acid (ASA), (e) 1,2-Naphthaquinone-4- sulfonic acid (NSA) and (f) Carbon nanotubes (CNT), respectively, in DMSO.....	167
Figure 5.8: 3D Fluorescence contour spectra of (a) DMSO, (b) ANSA, (c) undoped and doped PANSA with (d) Anthracene sulfonic acid (ASA), (e) 1,2-Naphthaquinone-4- sulfonic acid (NSA) and (f) Carbon nanotubes (CNT), respectively, in DMSO.....	169
Figure 5.9: UV-visible spectra of undoped chemically synthesized PANI and PANSA in DMSO.....	171

Figure 5.10: UV-visible spectra of chemical synthesized PANI doped with NSA in DMSO.	
Figure 5.11: Fluorescence excitation, emission and UV-vis absorption spectra of PANI in DMSO, excited at 350 nm.....	174
Figure 5.12: Fluorescence excitation, emission and UV-vis absorption spectra of PANSA in DMSO, excited at 350 nm.....	174
Figure 5.13: Fluorescence excitation, emission and UV-vis absorption spectra of PANI-NSA in DMSO, excited at 350 nm.....	175
Figure 5.14: Typical fluorescence emission decay of PANSA in DMSO, when pulsed with a 450 nm laser source with a long pass-off filter of 530 nm, and the residual of a mono exponential tail fit.....	178
Figure 5.15: UV-vis absorption spectra of $[\text{Ru}(\text{bpy})_2(\text{picCOOH})]^{2+} \cdot (\text{ClO}_4^-)_2$ complex in MeCN (a) with addition of 10 μl of polymers and with addition of 10-150 μl of polymers dissolved in DMSO (b) PANI, (c) PANSA and (d) PANI-NSA.....	182
Figure 5.16: Fluorescence emission spectra of Ru complex in MeCN (a) with addition of 10 μl of polymers and with addition of 10-150 μl of polymers dissolved in DMSO (b) PANI, (c) PANSA and (d) PANI-NSA.....	184
Figure 5.17: A typical fluorescence emission decay of PANSA in DMSO, when pulsed with a 450 nm laser source with a long pass-off filter of 530 nm, and the residual of a mono exponential tail fit.....	185
Figure 6.1: Polymer mediated pathway, which takes place via polymer based charge carriers (Pickup, 1999).....	196
Figure 6.2: Super-exchange pathway (Pickup, 1999).....	196
Figure 6.3: Outer sphere electron transfer (Pickup, 1999).....	197

Figure 6.4: CV characterization of $[\text{Ru}(\text{bpy})_2(\text{picCOOH})]^{2+} \cdot (\text{ClO}_4^-)_2$ complex on ITO electrode in 0.1 M H_2SO_4 and HCl.....	202
Figure 6.5: Electrosynthesis of PANI and $[\text{Ru}(\text{bpy})_2(\text{picCOOH})]^{2+} \cdot (\text{ClO}_4^-)_2$ on a 0.072 cm^2 Pt electrode at a scan rate 0.1 V s^{-1} in HCL (1 M) ,the CV 1 st to the 20 th of the polymerization cycle.....	204
Figure 6.6: Cyclic voltamogram characterization at 0.01, 0.02, 0.04, 0.08 and 0.1 V s^{-1} for Pt-PANI- $[\text{Ru}(\text{bpy})_2(\text{picCOOH})]^{2+} \cdot (\text{ClO}_4^-)_2$ in 1M HCL film grown at 0.1 V s^{-1}	204
Figure 6.7: Cyclic voltamogram characterization of Pt –PANI- $[\text{Ru}(\text{bpy})_2(\text{picCOOH})]^{2+} \cdot (\text{ClO}_4^-)_2$ in an extended potential window of (0.02-0.16 V s^{-1}) at a scan rate of 0.1 V s^{-1} in HCL (0.1 M).....	205
Figure 6 .8: Electrosynthesis of PANSA and $[\text{Ru}(\text{bpy})_2(\text{picCOOH})]^{2+} \cdot (\text{ClO}_4^-)_2$ on a 0.0172 cm^2 Au electrode at a scan rate 0.05 V s^{-1} in H_2SO_4 (0.5 mM), the CV illustrates the 1 st to the 10 th polymerization cycle.....	207
Figure 6.9: Multi scan CV of Au-PANSA- $[\text{Ru}(\text{bpy})_2(\text{picCOOH})]^{2+} \cdot (\text{ClO}_4^-)_2$ at 0.01, 0.02, 0.04, 0.08 and 0.1 V s^{-1} in 0.5 M H_2SO_4 , film grown at 0.05 V s^{-1}	208
Figure 6.10: Electrosynthesis of PANSA and $[\text{Ru}(\text{bpy})_2(\text{picCOOH})]^{2+} \cdot (\text{ClO}_4^-)_2$ on a 0.0177 cm^2 Au electrode at a scan rate 0.1 V s^{-1} in H_2SO_4 (0.1mM), the CV illustrates the 1 st to the 10 th of the polymerization cycle is shown.....	209
Figure 6.11: Cyclic voltamogram characterization at 0.01, 0.02, 0.04, 0.08 and 0.1 V s^{-1} for Au-PANSA- $[\text{Ru}(\text{bpy})_2(\text{picCOOH})]^{2+} \cdot (\text{ClO}_4^-)_2$ in H_2SO_4 (0.1mM), film grown at 0.05 V s^{-1}	209
Figure 6.12: Cyclic voltamogram characterization, of Au–PANI- $[\text{Ru}(\text{bpy})_2(\text{picCOOH})]^{2+} \cdot (\text{ClO}_4^-)_2$ in an extended potential window of (0.02-0.16 V s^{-1}) at a scan rate of 0.1 V s^{-1} in H_2SO_4 (0.1 mM).....	210

Figure 6.13: Amperometric i-t response of PANI-[Ru(bpy)₂(picCOOH)]²⁺.(ClO₄⁻)₂ film modified ITO electrode upon applying a constant oxidative potential of 0.7 V for 810 seconds.....212

Figure 6.14: Amperometric i-t response of PANSA-[Ru(bpy)₂(picCOOH)]²⁺.(ClO₄⁻)₂ film modified ITO electrode upon applying a constant oxidatative potential of 0.5 V for 810 seconds.....213

Figure 6.15: Illustrating Blank ITO, in 1 mM [Ru(bpy)₂(picCOOH)]²⁺.(ClO₄⁻)₂ and 0.1 mM HCL (—) and (—) illustrates characterization of ITO-PANSA [Ru(bpy)₂(picCOOH)]²⁺.(ClO₄⁻)₂ at a scan rate of 0.1 V s⁻¹ in 0.1 mM HCL electropolymerized by potentiostatic growth for 810 s.....215

Figure 6.16: Illustrating Blank ITO, in 1 Mm [Ru(bpy)₂(picCOOH)]²⁺.(ClO₄⁻)₂ and 0.1 mM H₂SO₄ (—), and the characterization ITO-PANSA- [Ru(bpy)₂(picCOOH)]²⁺.(ClO₄⁻)₂ (—) at a scan rate of 0.1 V s⁻¹ in 0.1 mM H₂SO₄ electropolymerized by potentiostatic growth for 810 s.....216

Figure 6.17: Shows simultaneously recorded: Cyclic voltammogram (—) and electrochemiluminescence response (—) of ITO modified with PANI-[Ru(bpy)₂(picCOOH)]²⁺.(ClO₄⁻)₂ film electrodeposited for 1600 seconds from hydrochloric acid. TPA (50 mM) dissolved in PBS was the co-reactant used. The electropolymerization and the ECL were performed at a scan rate of 0.1 V s⁻¹ and Γ was 1.29 x 10⁻⁹ mol cm⁻².....219

Figure 6.18: Cyclic voltammogram (—) and electrochemiluminescence response (—) of ITO modified with PANI-[Ru(bpy)₂(picCOOH)]²⁺.(ClO₄⁻)₂ film electrodeposited for 810 seconds from hydrochloric acid. TPA (50 mM) dissolved in PBS was the co-reactant used.

The electropolymerization and the ECL were performed at a scan rate of 0.1 Vs^{-1} and Γ was $2.56 \times 10^{-10} \text{ mol.cm}^{-2}$ 221

Figure 6.19: The ECL responses of ITO modified with PANI-[Ru(bpy)₂(picCOOH)]²⁺.(ClO₄⁻)₂ film electrodeposited for 810 and 1600 seconds from hydrochloric acid. TPA (50 mM) dissolved in PBS was the co-reactant used. The electropolymerization and the ECL was performed at a scan rate was 0.1 Vs^{-1} 222

Figure 6.20: Shows the potential waveform of PANI-Ru complex that involves stepping 10 times from 5 to 16 V with a pulse width of 5 seconds, the supporting electrolyte is PBS that contains 50 mM TPA.....224

Figure 6.21: Shows the corresponding light signals of PANI-Ru complex, which are triggered by the potential stepping.....224

Figure 6.22: Cyclic voltammogram (—) and electrochemiluminescence response (—) of ITO modified with PANSA - [Ru(bpy)₂(picCOOH)]²⁺.(ClO₄⁻)₂ film electrodeposited for 810 seconds from sulphuric acid. TPA (50 mM) dissolved in PBS was the co-reactant used during ECL detection. The electropolymerization and the ECL were performed at scan rates of 0.05 and 0.1 Vs^{-1} respectively. Γ was $5.16 \times 10^{-13} \text{ Molcm}^{-2}$ 225

Figure 6.23: Cyclic voltammogram (—) and electrochemiluminescence response (—) of ITO modified with PANSA - [Ru(bpy)₂(picCOOH)]²⁺.(ClO₄⁻)₂ film electrodeposited for 90 seconds from sulphuric acid. TPA (50 mM) dissolved in PBS was the co-reactant used. The electropolymerization and the ECL were performed rates of 0.05 and 0.1 Vs^{-1} , respectively. Γ was $7.99 \times 10^{-12} \text{ mol.cm}^{-2}$ 226

Figure 6.24: The ECL responses of ITO modified with PANSA - [Ru(bpy)₂(picCOOH)]²⁺ film electrodeposited for 90 and 810 seconds from hydrochloric acid. TPA (50 mM) dissolved in PBS was the co-reactant used. The electropolymerization and the ECL were performed at a scan rate of 0.05 and 0.1 V s^{-1} , respectively.....228

Figure 6.25: Shows the potential waveform that involves stepping 10 times from 5 to 16 V with a pulse width of 5 seconds, the supporting electrolyte is PBS that contains 50 mM TPA of ITO- PANSAs -[Ru(bpy) ₂ (picCOOH)] ²⁺ .(ClO ₄) ₂ prepared for 90 seconds.....	229
Figure 6.26: Shows the corresponding light signals, which are triggered by the potential stepping.....	230



CHAPTER ONE:

INTRODUCTION

1.1. Background

Electrochemiluminescence (ECL) is applied for industrial applications that have considerable potential, such as clinical diagnostic, analytical chemistry, and light-emitting devices, due to selectivity, sensitivity for detection and quantification of molecules through generation of fluorescence light when electric current is applied on the materials. In ECL the electrochemical reaction allows for precise control over the time and position of the light emitting reaction. The control over time allows one to synchronise the luminescence and the biochemical reaction under study and control over position not only improves sensitivity of the instrument by increasing the signal to noise ratio, but also allows multiple analytical reactions in the same sample to be analyzed using an electrode array. The ECL generation fluorescent materials are based on inorganic semiconductor materials for light-emitting devices. Further progress in this ECL field mainly depends on discovery of new advanced materials, interfacial films and nanoparticle coatings, advances in microfluidics leading to total increase in ECL properties. There has been extensive use of polymers for enhancement of ECL properties. Electrochemiluminescent conjugated polymers constitute a new class of fluorescent polymers that emit light when excited by the flow of an electric current. These new generation fluorescent materials may now challenge the domination by inorganic semiconductor materials for the commercial market of light-emitting devices such as light-emitting diodes and polymer laser devices (PLDs).

1.2. Research Rationale and Motivation

The suitable ECL materials for application as a flat-panel display (FPD) are characterized by high intensity of brightness, excellent current efficiency and colour purity. The ECL materials for a FPD to display high brightness and high efficiency it requires optimum charge transport and balance throughout the light emitting layer (Lee, 2006; Fletcher, 2000), which is determined by the chemical structure and composition of the light emitting polymer (LEP). In this regard, the bipolar characteristics of conjugated polymers containing electron and ruthenium complex are responsible for energy transport which lead to enhancement of ECL signal (O'Reilly, 2010), which can be used to enhance the brightness and efficiency of devices (Lee, 2006). The application of conjugated polymers and ruthenium complex ECL in polymer light emitting diodes has been hampered by the formation of a long wave length excimer emission band. Excimer emission from aggregates formed by polymer chain π - π stacking in conjugated polymer usually results in low efficiency and poor colour purity (Grimsdale *et al.*, 2002). In this study the the focus is on the production of conducting polymer for use in ECL system. The polymers were polyaniline and poly (8-anilino-1-naphthalene sulfonic acid), synthesized electro and chemical polymerization. Each of the processable polymers was coupled with ruthenium complex.

1.3. Problem Identification

ECL materials emit light in much the same way as an electroluminescence (EL) and photoluminescence (PL) but ECL mainly involves the production of reactive intermediates from stable precursors at the surface of the electrode and these intermediates then undergo electron transfer reactions under a variety of conditions to form excited states that emit light. ECL is expected to emit light with across the wavelengths of the electromagnetic radiation

corresponding to the visible, ultraviolet and infra red and could be applied as energy efficient light sources. Many exciting ECL materials have been introduced already by several researchers (Bard, 2004). The challenging problem associated with ECL systems are factors such as loss of signal due to diffusion of the ECL reagent out of the detection zone, limited ability to repeatedly cycle an individual luminophore and high reagent consumption (Forster and Hogan, 2000). Highly branched organic molecules containing heteroatomic systems such as pyrans, naphthalides and triazine-branched conjugated polymers have been used to improve the luminescent properties (Wang *et al.*, 2010). However, these molecules are expensive and have several synthetic steps. Ruthenium complexes and conjugated polymers continue to play an important role in ECL based systems. Their dominance is mainly due to their nearly ideal reversible voltammetry and their attractive photophysical properties (O'Reilly, 2010). This study was based on production polymer materials doped with ruthenium (II) complex instead of branched. The polyanilino materials Ru complex-modified electrode was studied and evaluated as new generation ECL. South Africa's energy policies encourage technologies that can offer maximum energy savings. The ECL technology can be used in many applications and it falls into this category.

1.4. Research Feasibility and Impact

1.4.1. Feasibility

Previous studies have shown that tris(2,2'-bipyridyl)-ruthenium(II) is one of the most studied ECL compounds due to its ability to undergo ECL reactions in aqueous solutions and its good chemical, electrochemical, and photochemical stability, regenerability, and excellent luminescence properties (Miller *et al.*, 1972). But recently, Hun and Zhang (2011) found that as a typical ECL reagent, tris(2,2'-bipyridyl)-ruthenium(II) could still retain their ECL

property even after being used to dope the silica nanoparticles because the exterior nanosilica prevented the electroactive reagent from leaching out into the aqueous solution due to the electrostatic interaction. In the present study $\text{Ru}(\text{bpy})_2(\text{picCOOH})]^{2+} \cdot (\text{ClO}_4^-)_2$ was used and it electrostatically bound to polyaniline and poly(8-anilino-1-naphthalene sulfonic acid).

1.4.2. Impact

This study was in line with the objectives of the National Nanotechnology Strategy (NNS) which includes encouraging research on the design, synthesis, characterization, modelling and fabrication of novel nanomaterials and nanodevices; development of human resources; and stimulating new developments in technology missions such as advanced materials for advanced manufacturing. Polyaniline doped with nanomaterials demonstrates the development of novel nanomaterials which have applications in new ECL systems that will compete effectively with current light display systems. This project was also in alignment with the National Advanced Manufacturing Technology Strategy (NAMTS), and the Advanced Metals Initiative (AMI). NAMTS's mandate which includes research on light weight materials and advance production technologies which the electroluminescent polyanilino-light emitting devices project exemplifies. The combination with ruthenium containing compound stresses the beneficiation of the AMI objectives.

1.5. Research Aims and Objectives

1.5.1. Aims

The main aim of this work was to synthesize and study the photophysical and electrochemiluminescence properties of PANI and PANSA blended with $[\text{Ru}(\text{bpy})_2(\text{picCOOH})]^{2+} \cdot (\text{ClO}_4^-)_2$.

1.5.2. Objectives

- ✓ Electrosynthesis and characterization of undoped PANSA and doped with ananthracene sulfonic acid (ASA), 1,2-naphthaquinone-4-sulfonic acid (NSA) and carbon nanotubes (CNT) by cyclic voltammetric (CV) and transmission electron microscopy (TEM).
- ✓ Chemical synthesis and characterization of undoped PANI, PANSA and PANI doped with 1,2 naphthaquinone-4-sulfonic (NSA) by cyclic voltammetric (CV), electric conductivity, FTIR, Raman spectroscopy and Scanning electron microscopy (SEM).
- ✓ Studying photophysical properties of electro- and chemically synthesized polyaniline and its derivatives using UV-Vis, fluorescence spectroscopy and time correlated single photon counting (TCSPC).
- ✓ Studying photophysical properties of $[\text{Ru}(\text{bpy})_2(\text{picCOOH})]^{2+} \cdot (\text{ClO}_4^-)_2$ using UV-Vis, fluorescence spectroscopy and time correlated single photon counting (TCSPC).
- ✓ Investigation of the interaction of the polymer and $[\text{Ru}(\text{bpy})_2(\text{picCOOH})]^{2+} \cdot (\text{ClO}_4^-)_2$ and its impact in the photophysical properties of $[\text{Ru}(\text{bpy})_2(\text{picCOOH})]^{2+} \cdot (\text{ClO}_4^-)_2$
- ✓ Electrosynthesis of PANI- and PANSA- $[\text{Ru}(\text{bpy})_2(\text{picCOOH})]^{2+} \cdot (\text{ClO}_4^-)_2$ films on ITO electrode using potentiostatic growth method and characterization of the films using CV.

- ✓ Studying of the electrochemiluminescence properties of PANI- and PANSA-
([Ru(bpy)₂(picCOOH)]²⁺.(ClO₄⁻)₂) films using CV.

1.6. Thesis outline

This thesis attempts to tune the electrochemical and photophysical properties of polymeric systems to produce enhanced ECL. The Outline of the remaining chapters in this thesis

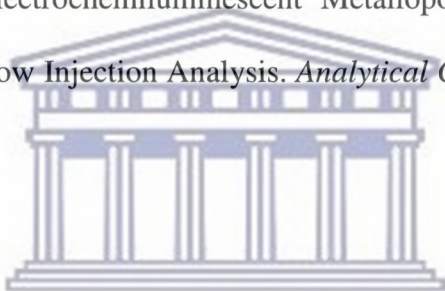
- ✓ **Chapter two** of the thesis focuses on the literature review, introducing the theoretical considerations and characterization methods and tools including: electrochemiluminescence, polymers, and conducting polymers.
- ✓ **Chapter three** of this thesis concentrates on the electropolymerization and characterization of 8-anilino-1-naphthalene sulfonic acid monomer. The PANSA polymers are doped with ASA, NSA and CNT.
- ✓ **Chapter four** deals with chemical synthesis of PANI, PANSA and PANI-NSA and characterization of the synthesized polymers.
- ✓ **Chapter five** focuses on photophysical properties of electro- and chemically synthesized polymers and Ru complex, focusing on the electronic absorption fluorescence behaviour and lifetime of the polymers.
- ✓ **Chapter six** examines the electro synthesis of polymers modulated with ruthenium complex and mainly focuses on their ECL properties.
- ✓ **Chapter seven** summarizes the main conclusions and recommendations of the thesis.

1.7. References

Bard, A. J. Introduction. In *Electrogenerated Chemiluminescence*, Bard, A.J.; Marcel Dekker. Inc: New York, (2004).

Fletcher, R. B., Lidzey, D. G., Bradley, D.D.C., Walker, S., Inbasekaran, M., Woo, E.P. High brightness conjugated polymer LEDs, *Synthetic Metals*, (2000) 111,151- 153.

Forster, R.J., Hogan, C.F. Electrochemiluminescent MetallopolymerCoatings: Combined Light and Current Detection Flow Injection Analysis. *Analytical Chemistry*, (2000) 72, 5576-5582.



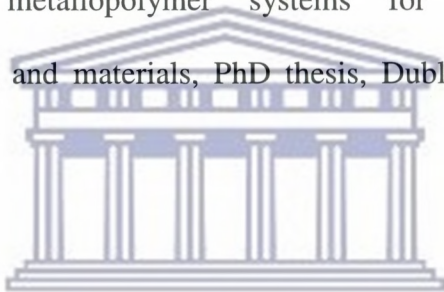
Grimsdale, A.C., Leclere, P., Lazzaroni, R., Mackenzie, J.D., Murphy, C., Setayesh, S. Correlation between molecular structure, microscopic morphology, and optical properties of poly(tetraalkylindenofluorene)s. *Advanced Functional Materials* (2002) 12, 729–33.

Hun, X., Zhang, Z. A novel electrogenerated chemiluminescence (ECL) sensor based on tris(2,2'-bipyridyl-ruthenium(II)-doped titania nanoparticles dispersed in Nafion on glassy carbon electrode. *Talanta* (2011), In Press.

Lee, R. H., Hsu, H. F, Chan, L. H, Chen, C.T. Synthesis and electroluminescence properties of novel tetraphenylsilane-oxadiazole-diphenyl(para-tolyl)amine polymer. *Polymer*, (2006) 47, 7001–7012.

Miller, L.L, Nordblom, G.D., Mayeda, E.A. A simple, comprehensive correlation of organic oxidation and ionization potentials, *Journal of Organic Chemistry* (1972) 37, 916–918.

O'Reilly, E., Conjugated metallopolymer systems for electrochemiluminescence enhancement; new approaches and materials, PhD thesis, Dublin City University, Ireland (2008).



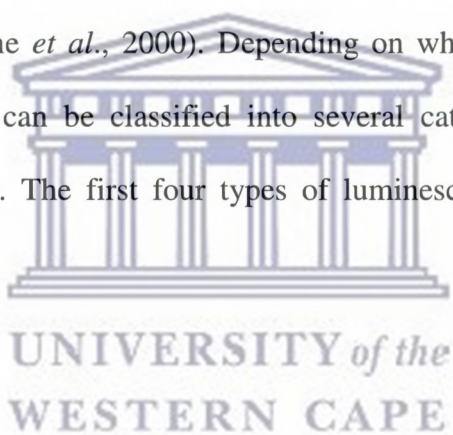
Wang, Y., Zhang, X., Han, B., Peng, J., Hou, S., Huang, Y., Sun, H., Xie, M., Lu, Z. The synthesis and photoluminescence characteristics of novel blue light-emitting naphthalimide derivatives, *Dyes and Pigments*, (2010) 86, 190-196.

CHAPTER TWO:

LITERATURE REVIEW

2.1. Luminescence

Luminescence is a general term which is used to describe light emission process that does not derive energy from the temperature of the emitting body (Valeur and Berberan-Santos, 2011). This means, the light is emitted from a substance that is not heated and is in the form of cold body radiation (Harvey, 1957). Luminescence can be caused by chemical, biochemical, or crystallographic changes, the motions of subatomic particles, or radiation-induced excitation of an atomic system (Dodeigne *et al.*, 2000). Depending on what phenomenon caused the light emission, luminescence can be classified into several categories, which are briefly explained in Table 2.1 below. The first four types of luminescence will be subsequently discussed.



2.1.1. Electroluminescence (EL)

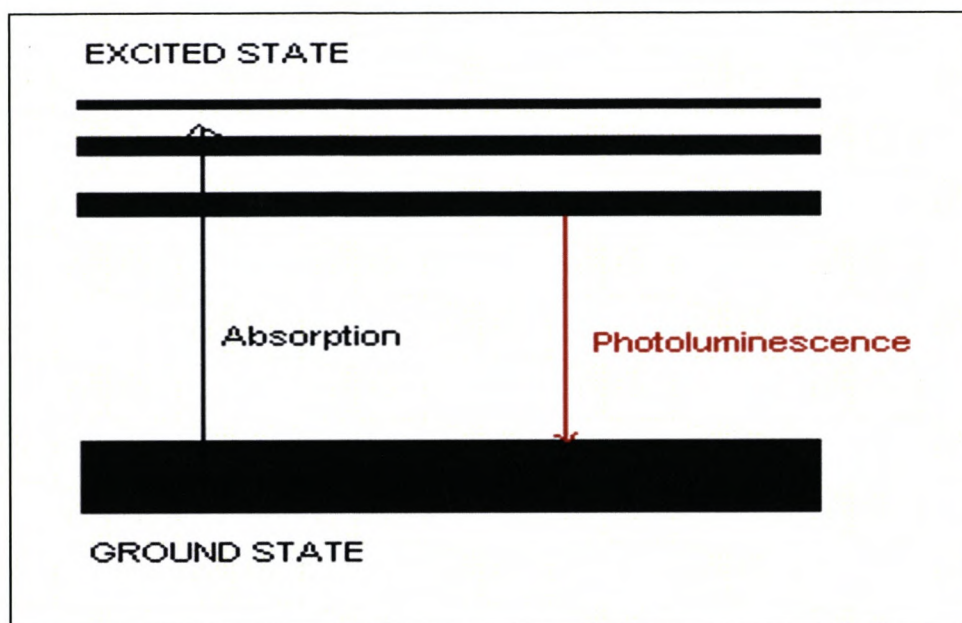
Electroluminescence (also called injection chemiluminescence and abbreviated EL), is an optical and electrical phenomenon in which a material emits light in response to the passage of an electric current (Ivey, 1963). EL process is closer to electrochemiluminescence (ECL) but it results from radiative recombination of electron-hole in the solid (Ivey, 1963), following injection of charge carriers (electrons and holes). The electrons and holes are normally separated by doping the material in order to form a p-n junction, in a light emitting device (LED) prior to the recombination (Ivey, 1963).

Table 2.1: Classification of types of luminescence

Excitation mode	Luminescence type
Injection of charge	Electroluminescence
Absorption of radiation	Photoluminescence
Electrochemical reaction	Electrochemiluminescence
Chemical reaction	Chemiluminescence Bioluminescence
Thermally activated ion recombination	Thermoluminescence
Sono waves	<u>Sonoluminescence</u>
Exited state (assuming ground singlet state)	Luminescence type
First exited singlet state	Fluorescence
Lowest triplet state	Phosphorescence

2.1.2. Photoluminescence

Photoluminescence (PL) is a light emission process that results from transitions between excited states and the ground state (Gfroerer, 2000). The behaviour of photoluminescence can be well understood by looking at the transitions between the lower energy state (ground state) and higher energy level (excited state) as shown in Scheme 2.1 (Santhanam *et al.*, 1965). In this process, a substance absorbs photons of light, which causes the excitation of substance from the lower energy state to a higher energy level and then returns back to a lower energy state. When it returns to the lower energy level, a photon of light is emitted.



Scheme 2.1: Photoluminescence showing transitions between the excited state and the ground state (Santhanam *et al.*, 1965).

2.1.3. Chemiluminescence

Chemiluminescence (CL) can be defined as the light emitted by the electronically excited product of a chemical reaction when it relaxes to the ground state (Jiang *et al.*, 2006; Weeks, 1992). The behaviour of a chemiluminescent reaction is given by the quantum yield, which determines the fraction of reacting molecules that actually produce light emission (Jiang *et al.*, 2006). Furthermore, the luminescence in CL is initiated and controlled by the mixing of reagents or careful manipulation of fluid flow (Campbell; 1988). In analytical chemistry, the main attraction of CL is the opportunity to carry out sensitive assays over a wide range of concentrations using relatively inexpensive equipment and usually combined with a complementary technique that confers specificity on the CL reaction (Knight, 1999). The most widely used complementary technique in biological studies is CL immunoassay where antibody labels such as acridinium esters have been used to detect analytes at picomolar concentrations (Eskola *et al.*, 2006; Jiang *et al.*, 2006; Weeks, 1992, Campbell; 1988). In

addition, CL compounds can be developed and used as substrates for enzyme labels; it is possible to increase the speed of ultrasensitive CL immune assays without impairing the sensitivity (Weeks, 1992; Jansen *et al.*, 1991).

2.1.4. Electrochemiluminescence

Electrochemiluminescence (also called electrogenerated chemiluminescence and abbreviated ECL), can be described as chemiluminescence produced as a result of electrochemical reactions (Jiang *et al.*, 2006; Richter, 2004; Knight, 1999). It involves the production of reactive intermediates from stable precursors at the surface of an electrode (Richter, 2004). These intermediates then react under a variety of conditions to form excited states that emit light. Generally, excitation pathways of ECL are closely related to their corresponding photoluminescent excitation pathways in Scheme 2.1 (Santhanam *et al.*, 1965). In addition, ECL has important advantages over CL and PL (Roda *et al.*, 2000), because (i) the luminescence in ECL is initiated and controlled by switching on or sweeping electrode potential to allow unstable reagents to react as soon as they are formed; (ii) the reactants produced *in situ* in the vicinity of an electrode surface to which appropriate potential is applied; and (iii) no external light source is required for excitation thereby significantly reducing background interference (Bard, 2004). Hence, this work mainly focuses in ECL, and it will be subsequently discussed thoroughly in the following sections.

2.2. Discovery and history of electrochemiluminescence

2.2.1. Background

Understanding the status of scientific knowledge that existed, especially in electrochemistry of organic molecule, before, ECL experiments arose in the middle 1960's is essential in order to understand what lead to the discovery of ECL (Hercules, 1964). During the 1950's, most organic electrochemistry studies were carried out in aqueous and partially aqueous solutions (Kolthoff and Lingane, 1952). The disadvantage associated with carrying out experiments in water is that, it has acidic and basic characteristic properties; hence proton transfer reactions are often coupled to electron transfers (Bard, 2004). Owing to this, electrode reactions normally results in the formation of waves. Furthermore, water can be oxidized to oxygen or reduced to hydrogen; hence making it to have a small potential window (Bard, 2004).

Currently, the accepted idea is that electrode reactions generally precede in elementary steps which involve single electron transfer (Bard, 2004). While during 1950's, the prevailing concepts of organic chemistry were largely based on "pushing" electron pairs, hence radical ions were not thought of as usual intermediates (Kolthoff and Lingane, 1952). The turning point, which altered things around was the introduction of the use of aprotic solvents, with large potential window such as acetonitrile (MeCN) (Bard, 2004). This solvent allowed difficult oxidations and reductions to be examined. However, the problem associated with using MeCN was that, it was often contaminated with small amounts of water and sometimes oxygen, and hence even with this solvent, electrogeneration of radical ions was not observed (Bard, 2004).

2.2.2. Early experiments

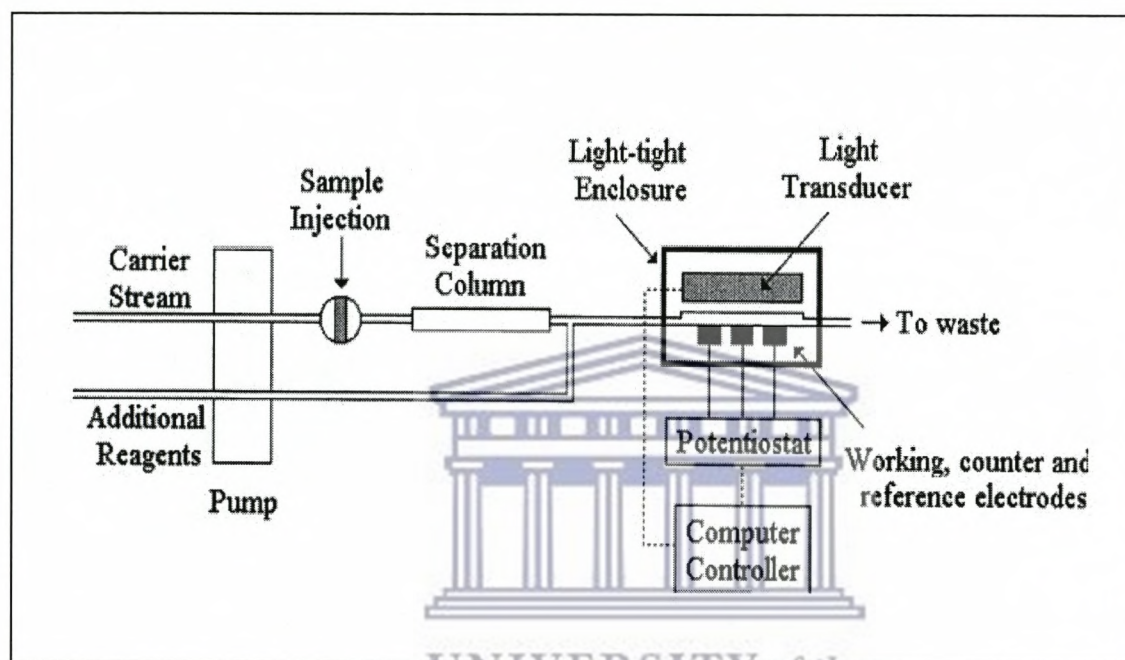
In 1927, electroluminescence was first observed by Dufford *et al.* (1927), during electrolysis experiment for solutions of Grignard compounds in anhydrous ether which lead to emission of light. Subsequently, light emission was also observed by Harvey in 1928 for luminol in alkaline solution (Harvey, 1957). However, no attention was given to the discovery at that time. Later, in the 1960s, there was much interest in the phenomena as a tool to study new compounds, complexes and clusters which exhibited novel photochemical and electrochemical properties (Hercules, 1964). Subsequently, chemiluminescence experiments were carried out in the 1960's involving radical ions used radical anions prepared chemically and reacted with different oxidants (Chandross and Sonntag, 1964). The experiments involved light emission, when a radical anion of 9,10-diphenylanthracene (DPA), produced by reduction with potassium in THF, reacted with the 9,10-dichloride of DPA (DPACl₂), Cl₂, benzoyl peroxide and related compounds (Bard, 2004). Following this, around the 1970s, ECL was observed by reacting electrogenerated tris-2,2'-bipyridylruthenium(III) [Ru(bpy)₃]³⁺ with tripropylamine (TPA) to create an electronically excited state that emits at approximately 610 nm (Tokel and Bard, 1972).

2.3. Principles of electrochemiluminescence

2.3.1. Overview

To conduct an ECL experiment, an electrochemical instrument that consists of an electrochemical cell and a light detector to measure light from the working electrode is required (Lu, 2010; Venkatanarayanan, 2010). In addition to that, a photomultiplier tube (PMT) is used as a light detector, a photodiode, and a charge coupled device (CCD) (Lu, 2010; Venkatanarayanan, 2010). This CCD is positioned to collect light from the working

electrode, and hence detect ECL. The part of the electrochemical cell is transparent so that the light generated at the electrode can reach the detector in the electrochemical instrument of flow-based systems (Venkatanarayanan, 2010). Moreover, the electrodes and the detector are contained within a light tight housing, which is normally a black box, to reduce background light (Bard, 2004).



Scheme 2.2: Schematic diagram of a typical basic experimental apparatus used for the generation and measurement of ECL (Knight, 1999).

Scheme 2.2 above illustrates the basic design concepts of ECL low cells (Scheme 2.2 has slightly changed in recent years) (Knight, 1999). However, a new novel ECL probe has been developed by Preston and Nieman (1996) and is used to take measurements in a similar fashion to a pH probe. They showed that the new approach does not require a conventional dark box to exclude ambient light.

A typical example of ECL behaviour is illustrated in Figure 2.1 for water-soluble carbon nanocrystals released into aqueous solution from a graphite rod conducted by Zheng *et al.*, (2009). The figure shows an electrochemical cell comprising of a graphite electrode and a platinum counter-electrode in a phosphate buffer solution. When applying a voltage to the set up, carbon nanocrystals are captured by the porous graphite and the nanocrystals, are then oxidized by the buffer solution and transform into a water-soluble phase. As a result, two types of carbon nanocrystal are produced and give a strong ECL response to a cycling potential, with strong emission of green visible light (Zheng *et al.*, 2009).

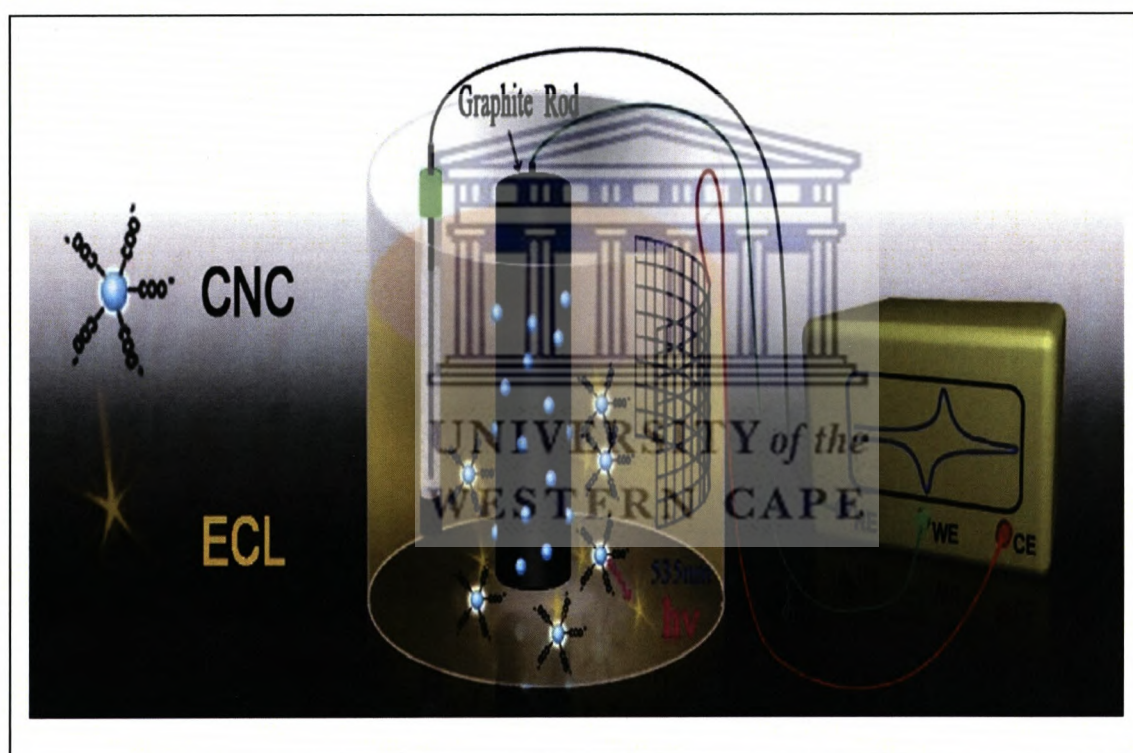


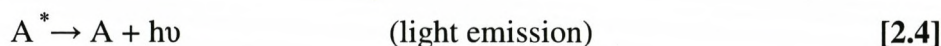
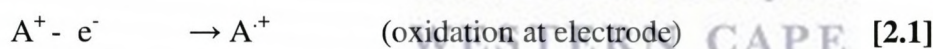
Figure 2.1: Preparation and electrochemiluminescence (ECL) of water-soluble carbon nanocrystals released into aqueous solution from a graphite rod by applying a scanning potential (Zheng *et al.*, 2009).

2.4. ECL generation pathways

ECL can be produced by two dominant pathways, namely the annihilation and coreactant pathways (Forster *et al.*, 2009; Richter, 2004). In each case two species are generated electrochemically, which further undergo an electron-transfer reaction to produce an emissive species (Forster *et al.*, 2009).

2.4.1. Annihilation ECL

Annihilation involves electron transfer reactions between an oxidized and a reduced species, through alternate pulsing of the electrode potential; both the oxidized and reduced forms of the luminophore are generated at the electrode (Forster *et al.*, 2009; Richter, 2004). These species then interact, resulting in formation of both ground state and electronically excited state, which then relaxes by emission (Forster *et al.*, 2009). The general mechanism is illustrated by Equation 2.1-2.4, and is coined to elaborate annihilation ECL pathway (Richter, 2004).



The corresponding free energy for the annihilation reaction, ΔG , can be determined using Equation 2.5 (Forster *et al.*, 2009).

$$\Delta G = nF(E^\circ_{\text{Donor}} - E^\circ_{\text{Acceptor}}), \quad [2.5]$$

The formal potentials for the ground-state reduction and oxidation processes are termed E°_{Donor} and $E^\circ_{\text{Acceptor}}$, respectively, and the difference between the two give the change in Gibbs energy (ΔG). In addition to that, the efficiency of the chemical reaction during ECL is determined by ECL quantum efficiency which is defined as the ratio of the number of photons emitted to the number of annihilations between the oxidized and reduced species (Richter, 2004).

It is well documented that in order to obtain an efficient **annihilation** ECL signal from a substrate The following characteristics are the basic prerequisites; Stable radical ions of the precursor molecules in the electrolyte have to be formed, good photoluminescence efficiency of a product of the electron transfer reaction and sufficient energy in the electron transfer reaction to produce the excited state (O'Reilly, 2008). Furthermore, the precursors participating in the homogeneous electron transfer leading to the light emitting excited state are generated at electrodes through heterogeneous electron transfer reactions (Forster *et al.*, 2009; Richter, 2004).

This phenomenon of homogeneous electron transfer can also be explained using Equation 2.1-2.4 above (Maloy, 2004). The oxidative properties are enhanced by the oxidized precursor radical A^+ (Equation 2.1). This precursor is located in the highest occupied molecular orbital (HOMO) and it represents a hole in the HOMO. While the reduced radical precursor $A^{\cdot-}$ (Equation 2.1), represents an electron in the lowest unoccupied molecular orbital (LUMO) and it enhances the reduction capacity. The homogenous electron transfer reaction can take place in two possible pathways (Figure 2.2) between the oxidized and reduced radicals

(Maloy, 2004). In the first instance which is called the energy dissipated mechanical mode, the electron can be transferred from the presently occupied LUMO of $A^{\bullet-}$ (the reduced radical), to the HOMO of oxidized radical precursor $A^{\bullet+}$ (Maloy, 2004). Although this is a thermodynamically favoured pathway, if the reaction transfer is too rapid, a large amount of energy will be irreversibly used, over short time frame in the vibrational modes, and this is very difficult to be achieved in a reacting system. On the contrary, in the second pathway the electron is transferred from $A^{\bullet-}$ LUMO to slightly less energetically demanding LUMO of $A^{\bullet+}$ as shown in Figure 2.2 The second pathway is known as the luminescent pathway(Maloy, 2004)).



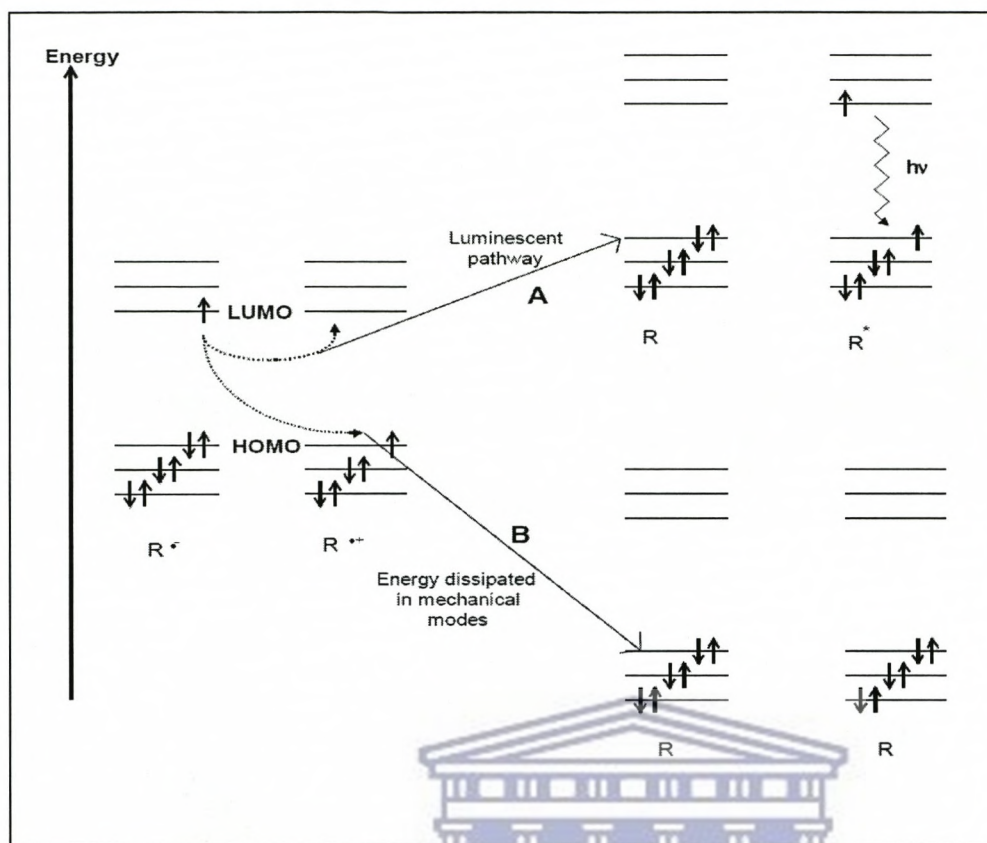


Figure 2.2: Molecular orbital diagram showing two alternative pathways for electron transfer between oxidised and reduced precursors A^{•+} and A^{•-}. (A) Formation of an excited state and (B) direct population of ground state products (O'Reilly, 2008).

In addition, these two pathways can be classified into two different ECL mechanisms. Whereby in the case of the luminescent pathway, the energy is less demanding and the reactions between A^{•+} + A^{•-}, lead to a formation of an excited state A* which is usually singlet state, and is accompanied by light emission, this mechanism is known as the S route (Forster *et al.*, 2009; Kapturkiewicz, 2004), as shown in Figure 2.3. In the second ECL mechanism, when the radical annihilation can not meet the energy requirements due to energy dissipation, the excited singlet state cannot be directly produced; hence a triplet- triplet annihilation takes place in order to indirectly generate a singlet excited state (Forster *et al.*, 2009; Bard, 2004).

This is illustrated in Equation 2.6- 2.7 below. It takes place by firstly forming an excited triplet state (Figure 2.3), which may generate a singlet state and this mechanism is classified as the T route (Forster *et al.*, 2009; O'Reilly, 2008; Kapturkiewicz, 2004). By doing this indirectly, the energy from the two electron transfer reactions is added together to generate sufficient energy to form the singlet excited state.

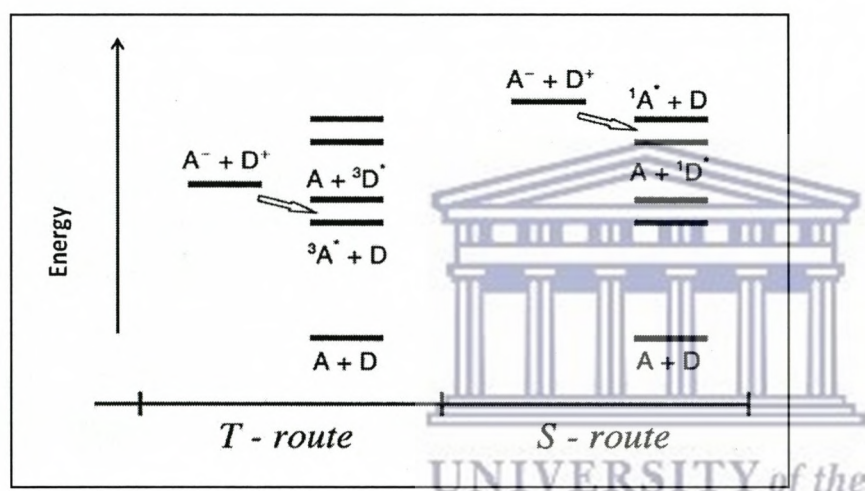


Figure 2.3: Schematic representation of the energy terms in ECL processes (Kapturkiewicz, 2004).

2.4.2. Coreactant ECL

In this pathway, both the luminophore and coreactant are present in the reaction solution (Forster *et al.*, 2009). The coreactant is a species that, upon oxidation or reduction, produces an intermediate that can react with an ECL luminophore to produce excited states (Forster *et al.*, 2009; Richter, 2004; Miao and Choi, 2004). This mechanism pathway occurs upon bond cleavage of the coreactant to form strong oxidants or reductants (Richter, 2004). It is also important to note that by applying either a single or double potential step, a signal ECL can

be generated. There are several types of good coreactants which can be used for ECL, and for a coreactant to be deemed good, it should adhere to the following prerequisites (Bard, 2004);

- In the potential window of interest during ECL, the coreactant should not give any signal or give any ECL background
- On or in close proximity of the electrode, it should be easy to oxidize or reduce the coreactant with the luminophore, and subsequently undergo a rapid chemical reaction which would give rise to an intermediate.
- This intermediate should possess adequate reducing or oxidizing energy to react with the oxidized or reduced luminophore to form the excited state.
- The reaction rate between the intermediate and the oxidized or reduced luminophore must take place rapidly.
- The coreactant should be soluble in the reaction mixture, and also the intermediates species generated electrochemically and chemically should be adequately stable in order for it to be able to react with the ECL precursor.
- The coreactant and its redox products should have no quenching effect on the luminescence of the ECL compound.

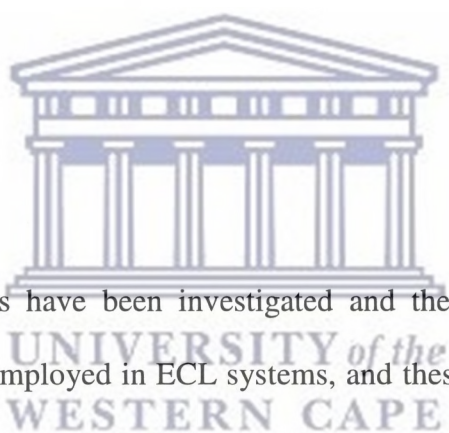
The first ECL coreactant was discovered by Bard's research group in 1977, using oxalate ion ($\text{C}_2\text{O}_4^{2-}$) which it was believed to produce the strong reductant $\text{CO}_2^{\bullet-}$ upon oxidation in aqueous solution (Miao and Choi, 2004):



The ECL luminophore can also be oxidized by the oxidizing potential as shown in Equation 2.9, the resultant intermediate $\text{D}^{\bullet+}$ interacts with the strong reductant $\text{CO}_2^{\bullet-}$ (Equation 2.10) to produce an excited state capable of emitting light (Equation 2.11).



Oxalate is often referred to as an “oxidative” or “oxidative-reductive” coreactant because of its ability to form a strong reducing agent upon electrochemical oxidation (Miao and Choi, 2004). In addition, the electrode typically only oxidizes *or* reduces the reagents in a single potential step in coreactant ECL, whereas in annihilation schemes a double-potential step (e.g., oxidation followed by reduction) is required to generate the highly energetic precursors (Richter, 2004).



2.4.2.1. Types of Coreactants

A number of ECL coreactants have been investigated and there are several coreactants, besides oxalate which can be employed in ECL systems, and these coreactants are discussed subsequently with their mechanisms in the following sections.

2.4.2.1.1. Tripropylamine (TPA)

TPA is also categorized under oxidative-reductive type of coreactant for ECL systems. Leland and Powell (Richter, 2004) were the pioneers of reporting ECL of $[Ru(bpy)_3]^{2+}$, employing tri-*n*-propylamine [TPA= $(CH_3CH_2-CH_2)_3N$] as a coreactant. In general when TPA is employed as the coreactant, upon application of potential to the reaction, direct oxidation of TPA at the electrode takes place giving rise to a first wave (Richter, 2004). A second wave also appears in the reaction, and its mechanism of formation starts with the

oxidation of TPA, which results in formation of a stable radical cation $\text{TPA}^{\cdot+}$ (Richter, 2004), which has a very short life time of approximately 0.2 ms (Bard, 2004). During its oxidation, a proton is lost from its α carbon, resulting in formation of a strongly reducing intermediate free radical TPA^{\cdot} (Richter, 2004; Miao and Choi, 2004). The TPA^{\cdot} proceeds on to reduce luminophore dication to give rise to a cation. The luminophore cation is further oxidized to form the excited state luminophore (Miao and Choi, 2004). Finally, the reaction between electrogenerated oxidized luminophore and TPA produces ECL emission. This is evident as the two waves formed are ascribed to the emission of light from the excited state luminophore, and they are shown below in Figure 2.4 for a typical example.

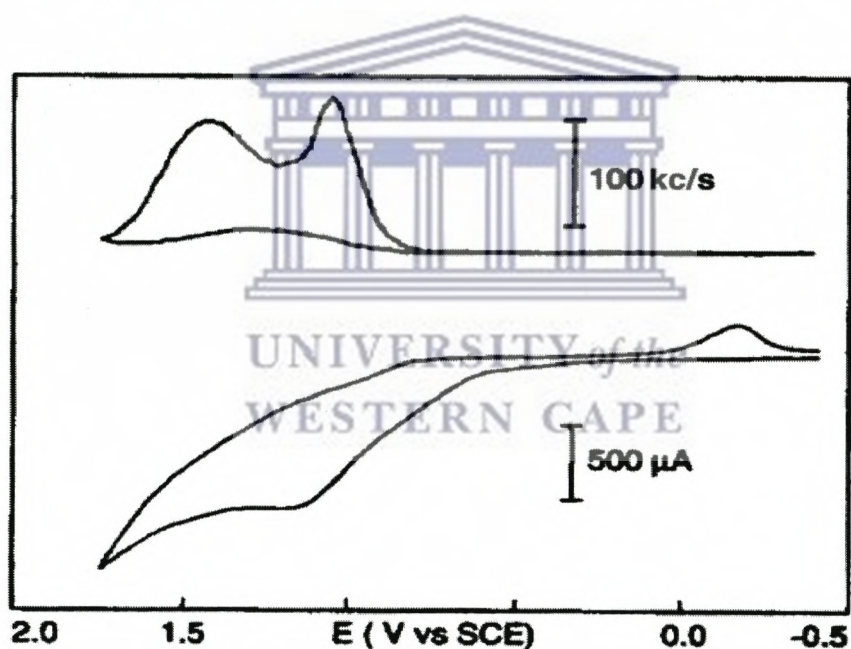
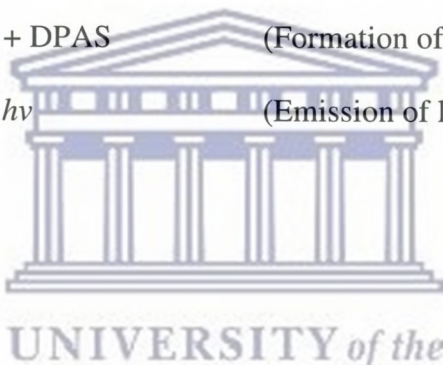
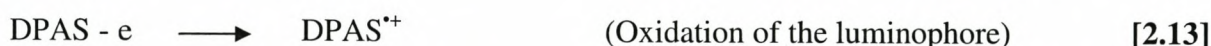
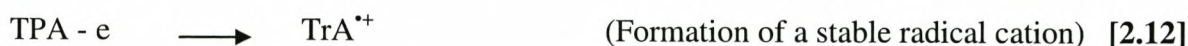


Figure 2.4: (a) ECL and (b) cyclic voltammogram of 5.2mM 2-THCOOH (Thianthracenecarboxylic acid) and 0.15 M TPA in pH 7.5 sodium phosphate buffer at 6 mm diameter Pt electrode at a scan rate of 100 mV/s (Miao and Choi, 2004). The behaviour of 1-THCOOH is similar except that the peak emission intensity is 6–7 times less intense than that of 2-THCOOH (Richards and Bard, 1995).

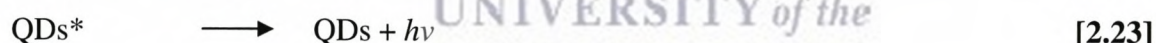
To elaborate this clearly, a specific example of a possible ECL mechanism which can take place, by employing 9, 10-diphenylanthracene-2-sulfonate (DPAS) as the luminophore and TPrA as the correactant is illustrated below in Equation 2.12-2.19 (Miao and Choi, 2004 ; Richards and Bard, 1995).



2.4.2.1.2. Peroxide systems

These coreactant systems are different from those of oxalate and TPA systems. This is because when a peroxide compound is reduced, it produces reactive oxidizing agent (Miao and Choi, 2004). Owing to this reason these systems are possible applicable coreactants in an ECL system. The electron density of the oxygen to oxygen bond (O-O) in a peroxide molecule is strongly affected by the functional group attached to the O-O bond and this strongly influences the reactivity of the oxidizing agent (Miao and Choi, 2004). If electron withdrawing functional groups are attached to the O-O bond, they increase reactivity of the oxidizing agent while on the contrary electron donating groups decrease reactivity of the peroxide system (Miao and Choi, 2004). Two peroxide systems will be further explained, and these are peroxydisulfate ($\text{S}_2\text{O}_8^{2-}$) and hydrogen peroxide (H_2O_2).

In **Peroxydisulfate** ($S_2O_8^{2-}$), the reduction of $S_2O_8^{2-}$ produces the strong oxidant, $SO_4^{\cdot-}$, this strong oxidant proceeds to undergo an electron-transfer reaction with an ECL luminophore to generate light (Richter, 2004). An example is given below where peroxydisulfate can be used as coreactant for the ECL emission of silicon-quantum dots (Si-QDs). In this system $SO_4^{\cdot-}$ is generated by electrochemically reducing peroxydisulfate, and the reduction takes place in the same potential window in which quantum dots (QDs) reduction occurs (Lei and Ju, 2011). The strong oxidant $SO_4^{\cdot-}$ then reacts with the negatively-charged QDs by injecting a hole into the highest occupied molecular orbital to produce an excited state of the QDs as illustrated in Equation 2.20-2.23 (Lei and Ju, 2011).



In **Hydrogen peroxide** (H_2O_2), in this system dissolved oxygen can be electrochemically reduced to H_2O_2 (Lei and Ju, 2011; Zou and Ju, 2004), which serves as a correactant in ECL (Equation 2.24-2.27). Zou and Ju (2004) were the pioneers of demonstrating that the electron-transfer reaction between electrochemically-reduced nanocrystal species and H_2O_2 can produce ECL emission from CdSe- QDs, this example is illustrated below.



2.5. ECL Luminophores

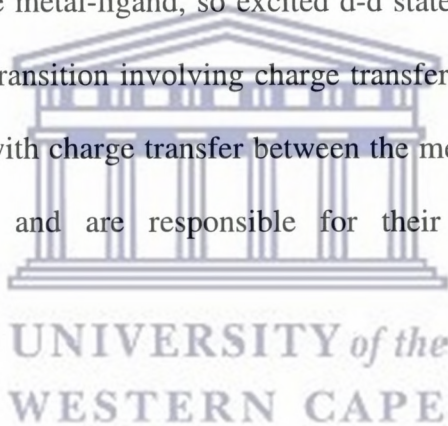
It is known that in order to generate ECL, alternating current (AC) and direct current (DC) electrolysis are normally used and the precursors may be generated sequentially at the electrode by cyclic voltammogram (CV) or potential step techniques or simultaneously at a rotating ring disk or double band electrode (Venkatanarayanan, 2010). The precursors are generated through annihilation reactions between reduced and oxidised forms of either an organic or inorganic luminophore or by using a coreactant that forms an energetic oxidant or reductant on bond cleavage (Richter, 2004).

Organic compounds known to produce ECL include luminal include , anthracene, 9,10-diphenylanthracene (DPA) coronene , phenothiazine, rubrene isobenzofurans, heterocyclic molecules like carbazoles have been reported (Richter, 2004). Furthermore, many metal inorganic complexes, and clusters display the electrochemical and spectroscopic qualities required of ECL luminophore such as tris(bipyridine) ruthenium(II) $[\text{Ru}(\text{bpy})_3]^{2+}$, $[\text{Ir}(\text{ppy})_3]$, $[\text{Os}(\text{bpy})_3]^{2+}$, $[\text{Re}(\text{CO})_3\text{Cl}(\text{phen})]^+$ (Richter, 2004). There are other complexes and/or clusters containing metals such as Ag, Al, Au, Cd, Cr, Cu, Eu, Hg, Ir, Mo, W, Pd, Pt, Re, Ru, Si, and Tb, that have also been reported (Richter, 2004). However, $[\text{Ru}(\text{bpy})_3]^{2+}$ was the first inorganic complex to display ECL and to date it has been the most useful inorganic complex ,in the investigation and development of ECL as an analytical tool, as most researches have used it in their work. Hence, electrochemiluminescence of ruthenium complexes will be further elaborated in the subsequent sections.

2.6. Electrochemiluminescence of ruthenium complexes

2.6. 1. Overview

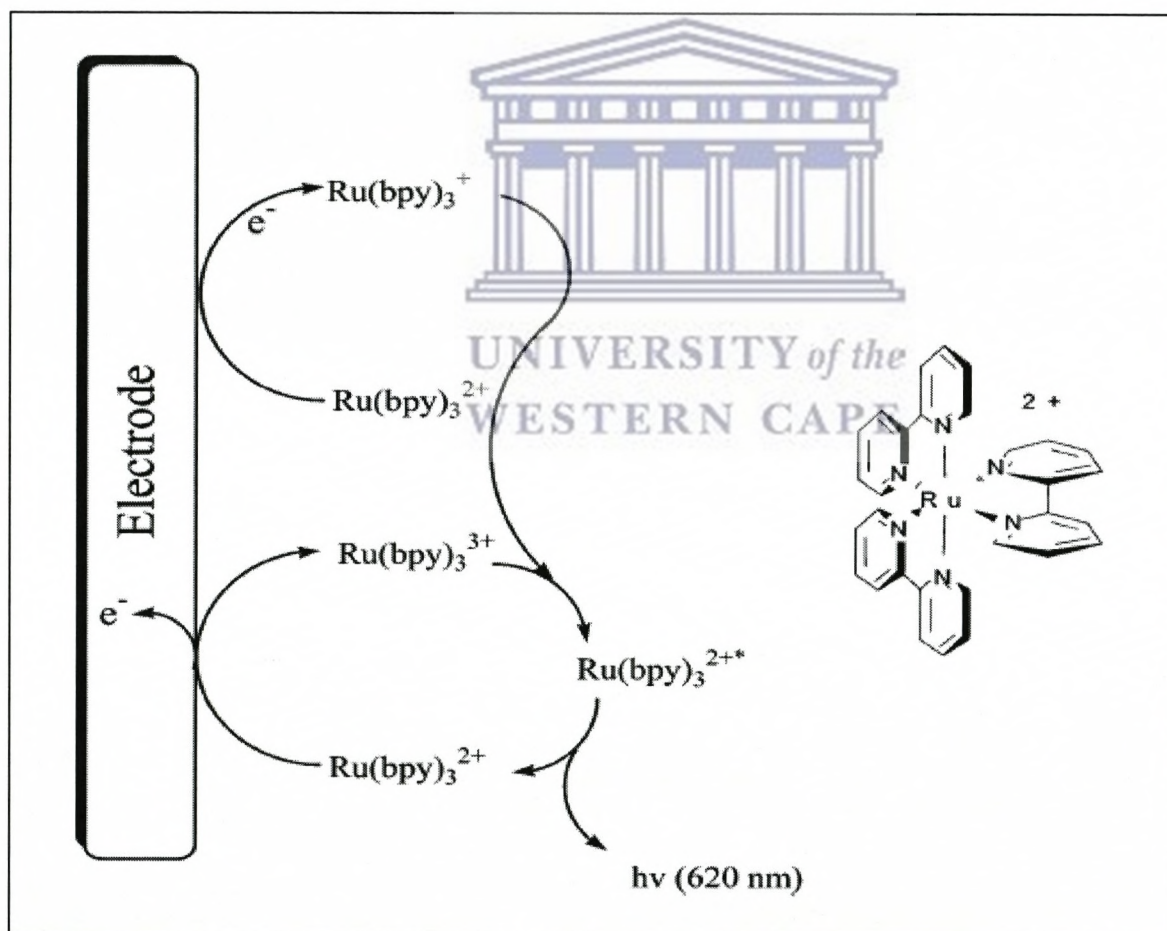
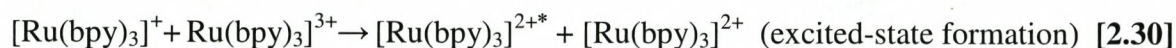
Ru complexes are transition-metal complexes, have six *d* electrons and the ability to undergo reversible one electron- transfer reactions at easily attainable potentials. The presence of ligands in the Ru complexes splits the *d*-orbital energy level into three lower (*t*) and two higher (*e*) orbitals and the extent of splitting is determined by the crystal-field strength Δ (Lakowicz, 1999). The six *d* electrons fill the three lower-energy *d* orbitals and then transitions between the orbitals $t \rightarrow e$ are formally forbidden. If *d-d* absorption occurs, the radiative rate is low and emission is not observed. In addition, electrons in the *e* orbitals are antibonding with respect to the metal-ligand, so excited *d-d* states are usually unstable. The metal-ligand results in a new transition involving charge transfer between the metal and the ligand. The metal complexes with charge transfer between the metal and the ligand have the lowest-energy excited states and are responsible for their electrochemiluminescence processes (Lakowicz, 1999).



2.6.2. Annihilation ECL of ruthenium complex

The ECL of ruthenium complexes has shown to be valuable in commercial applications and has been very common in the investigation ECL as an analytical technique, because it has been and is still widely employed by many researches as a luminophore (Richter, 2004). This can be ascribed to a few characteristics of this complex such as; is soluble in a variety of aqueous and non aqueous solvents and moreover it displays strong luminescence in the solvents which can dissolve it (Venkatanarayanan, 2010). For example, Scheme 2.3 shows ECL from $[\text{Ru}(\text{bpy})_3]^{2+}$ which was first reported in acetonitrile (MeCN) using

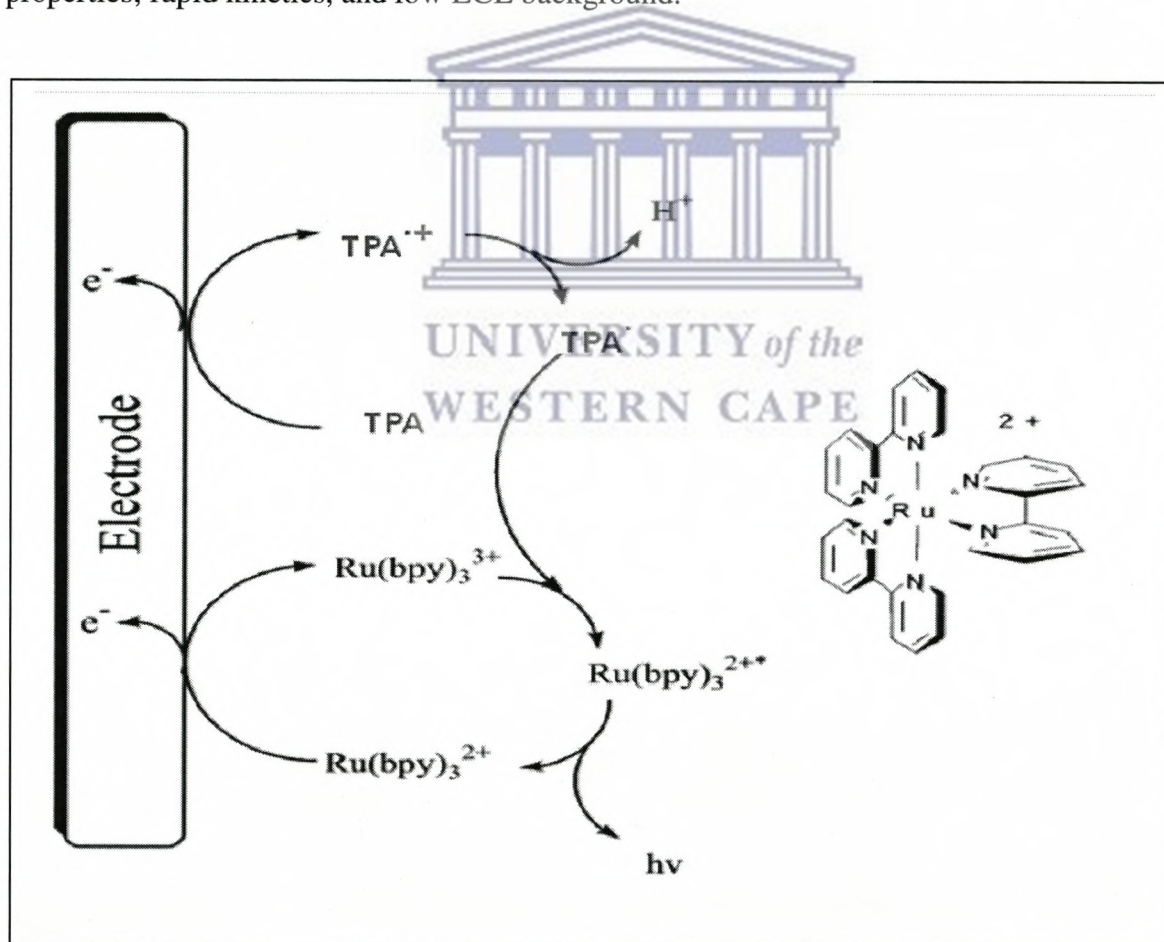
tetrabutylammonium tetrafluoroborate (TBABF₄) as the electrolyte (Richter, 2004). The ECL was generated by alternate pulsing of an electrode potential to form oxidized [Ru(bpy)₃]³⁺ and reduced [Ru(bpy)₃]⁺ as shown in Equation 2.28-2.31:



Scheme 2.3: Structure of [Ru(bpy)₃]²⁺ and proposed mechanism for [Ru(bpy)₃]³⁺/[Ru(bpy)₃]⁺ ECL system (Richter, 2004).

2.6.3. Coreactant ECL of ruthenium complex

In the case of ruthenium-bpy-based ECL, the amines especially tertiary amines such as TPA are the dominant coreactants as shown in Scheme 2.4 (Richter, 2004). TPA is either oxidized or reduced in the same potential step as the Ru complex as ECL. The potential scanning is normally one directional and through electron transfers or chemical reactions that follow electron transfer, the coreactant generates a product that reacts with the ECL luminophore to generate an excited state (Venkatanarayanan, 2010). Usually, this occurs upon bond cleavage of the coreactant to form strong oxidants or reductants for a coreactant to be termed “good”, it should have the following characteristics; good solubility, stability, electrochemical properties, rapid kinetics, and low ECL background.



Scheme 2.4: Proposed mechanism for Ru(bpy)₃²⁺/TPA ECL system (Richter, 2004).

It is well documented that the solution phase ECL system using Ru complex as luminophore has several disadvantages like loss of signal due to diffusion of the ECL reagent out of the detection zone, limited ability to repeatedly cycle an individual luminophore and high reagent consumption (Forster and Hogan, 2000). To overcome this problem immobilization of Ru complex ECL luminophore has been incorporated into ion exchange polymer composite films like nafion (Moretto *et al.*, 2010) on the electrode surface. Hence, in this work the focus is on conducting polymer for modification of electrode to incorporate Ru complex for electrochemiluminescence.

2.7. Conducting Polymers (ICPs) for ECL electrode modification

2.7.1. Overview of polymers

They are defined as large molecules, made from small repeating units that are held together by covalent bonds (Daintith and Martin, 2005). Monomers (mono=one) are the building blocks, which are the same repeating units which make up a polymer (poly = many in Greek). Polymers can exist as two units (dimer), three units (trimers) or several units (oligomers). The amount of repeating units is referred to as the degree of polymerization and is given the symbol X_n . They can be natural or synthetic; examples of polymers that exist in nature are DNA, natural rubber and cellulose and. etc.

2.7.2. History of polymers

Traditionally, polymers were coined as good electrical insulators and most of their applications have relied on their insulating properties (Epstein *et al.*, 1987). However, until three decades ago, researchers showed that certain class of polymers exhibit semiconducting

properties (Heeger, 2001). The first instance of polymer conduction was observed in 1963 by Bolto *et al.*, (1963). The research showed that some polypyrroles showed signs of conductivity Bolto *et al.*, (1963). This discovery was followed by work executed by Shirakawa and co-workers in 1977, who reported the first synthesis of doped polyacetylene by accidental, when one of the co-workers mistakenly added excessive amount of catalyst to an experiment which was done to polymerize acetylene (Wallace *et al.*, 2009). This resulted in formation of a silver film instead of the black powder. The new product had different optical properties compared to the normal black powder. They tried to oxidize the polyacetylene by using iodine vapour but that resulted in the increase of conductivity of the polymer. The discovery along with the extensive research in this area, contributed to authors receiving a Nobel Prize in Chemistry in 2000 to MacDiarmid, Heeger, and Shirakawa (Chiang *et al.*, 1978). Since this discovery reported by Shirakawa and co-workers, conducting polymers have received great attention in the field of science.



2.7.3. Conducting Polymers

A conducting polymer is an organic based polymer that can act as a semiconductor or a conductor. The most widely studies organic polymers are; polyaniline (PANI), polypyrroles (PPy), polythiophenes (PT) and polyphenylene vinylenes (PPV) as given in Figure 2.5 (Walton and Lorimer, 2000; Bolto *et al.*, 1963). They are conjugated, that is they have π electron delocalisation along their polymer backbone, hence giving them interesting optical and electrical properties (Wallace, 2009; Chiang *et al.*, 1978). Due to the collection of unique properties these polymers possess, they are suitable for applications in areas such as; energy storage (light weight batteries, capacitors), energy conversion (photovoltaic cells), optical signal processing (light emitting diodes) (Chiang *et al.*, 1978).

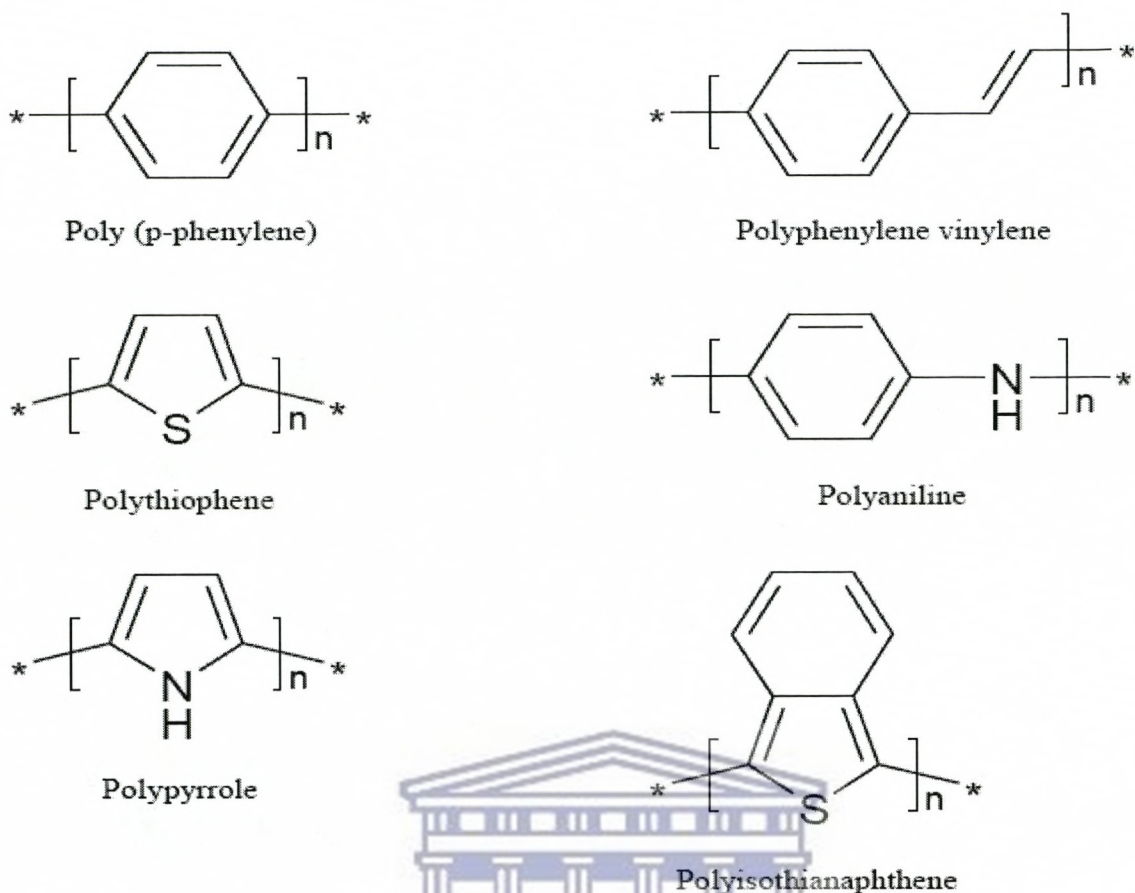


Figure 2.5: Typical (shown uncharged) structures of conducting polymers (Walton and Lorimer, 2000).

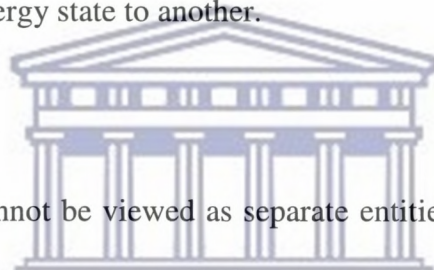
UNIVERSITY of the
WESTERN CAPE

2.7.4. Electronics of electrically conducting polymers (ECPs)

Conducting polymers are coined as extensively conjugated molecules, meaning they have alternating single and double bonds. In these molecules, electrons are able to move from one end of the polymer to the other through the extended p-orbital system. In electronic of ECPs, the Band theory is employed to explain the mechanisms of conduction in polymer. The theory originates from the formation of energy bands in polymer materials from discrete orbital energy levels found in single atom systems. In this regard, it is very vital to look at the review of band theory.

2.7.4.1. The band theory as a function of application of quantum theory

The physical chemistry approach to explanation of band theory is to relate it to an important application of the recently developed (and highly exciting) quantum theory of atomic structure (Atkins, 2002). The first major success of quantum theory was its explanation of atomic spectra, particularly that of the simplest atom, hydrogen. An important concept introduced by quantum mechanics was the notion that electrons in atoms could occupy only certain well-defined energy states (in contrast to classical mechanics which allows all possible energy values) and, in single (*i.e.* isolated) atoms these energy states were extremely sharp (Atkins, 2002). The resulting spectral emission lines which corresponded to electrons jumping from one 'allowed' energy state to another.



In a crystalline solid, atoms cannot be viewed as separate entities, because they are in close proximity with one another, and are chemically bonded to their nearest neighbour (Atkins, 2002). This leads to the concept that an electron on an atom 'sees' the electric field due to electrons on other atoms and the nature of the chemical bond implies that electrons on close-neighbour atoms are able to exchange with one another, causing the broadening of sharp atomic energy states into energy 'bands' in the solid (Atkins, 2002). This can be illustrated using an example below in Figure 2.6, that depicts 3p and 3s electron shells for a single metallic atom in the third period of the periodic table that overlap to become bands that overlap in energy (Atkins, 2002). The association of these bands is no longer solely with single atoms but rather with crystal as a whole. In other words, electrons may appear with equal probability on atoms anywhere else in the crystal.

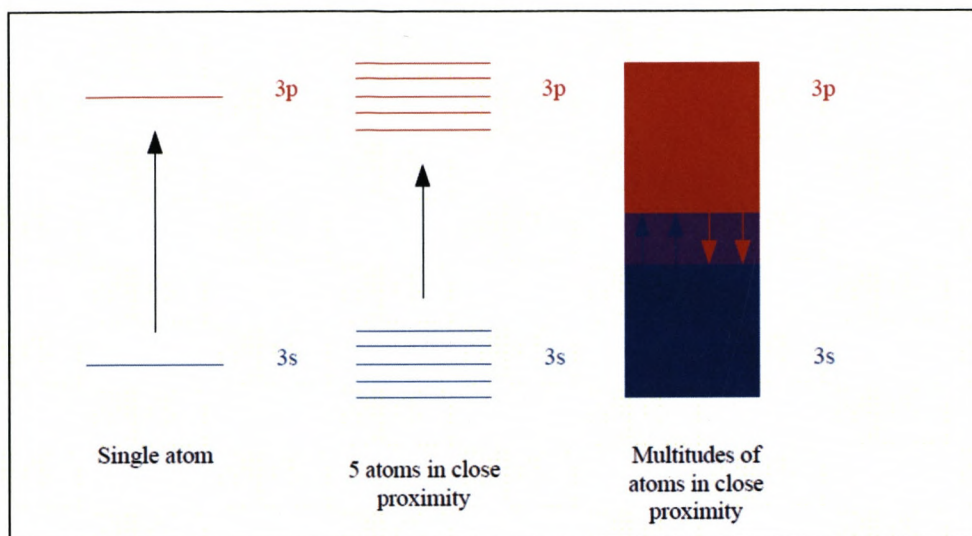
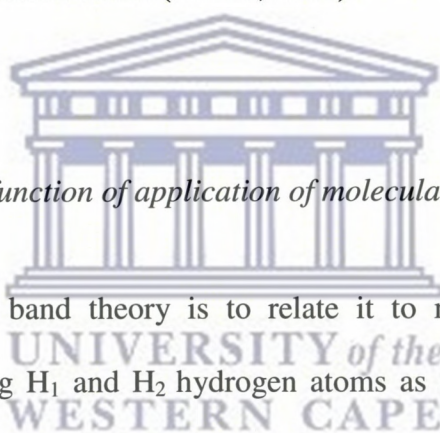


Figure 2.6: The formation of bands in a conducting solid in the 3rd period and overlap between the valence and conduction bands (Atkins, 2002).



2.7.4.2. The band theory as a function of application of molecular orbital theory

The “chemical approach” to band theory is to relate it to molecular orbital theory. In molecular orbital theory, using H_1 and H_2 hydrogen atoms as an example (Figure 2.7), an atomic molecular orbital from H_1 atom can overlap with an atomic molecular orbital of H_2 atom, resulting in the formation of two molecular orbitals known as the bonding and antibonding molecular orbitals (Atkins, 2002). These are delocalized over both atoms, and the bonding molecular orbital possess lower energy than the H_1 and H_2 atomic orbital, while the antibonding molecular orbital has higher energy.

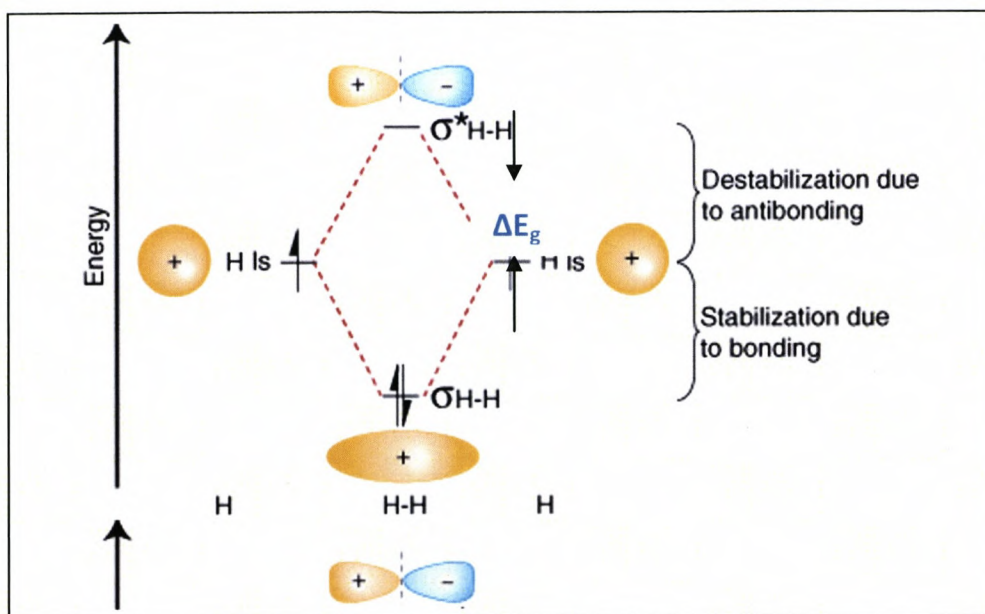


Figure 2.7: Molecular orbitals in a diatomic molecule (Atkins, 2002).

The energy band that results from the bonding orbitals of a molecule is known as the **valence band**, while the **conduction band** is as a result of the antibonding orbitals of the molecule (Atkins, 2002). The width of individual bands across the range of energy levels is called band width. The **valence band** represents the highest occupied molecular orbital (**HOMO**) and the **conduction band** represents the lowest unoccupied molecular orbital (**LUMO**). The gap between the highest filled energy level and lowest unfilled energy level is called band gap (E_g). This band gap represents a range of energies which is not available to electrons, and this gap is known variously as 'the fundamental energy gap', the 'band gap', the 'energy gap', or the 'forbidden gap' (Atkins, 2002). The level of electrons in a system which is reached at absolute zero is called the Fermi level (**Fg**) (Daintith and Martin, 2005). Combining the concepts explained in both atomic and molecular orbital theory, the electronic properties of metals, semiconductors, and insulators can be differentiated with reference to the band gap as shown in Figure 2.8 below.

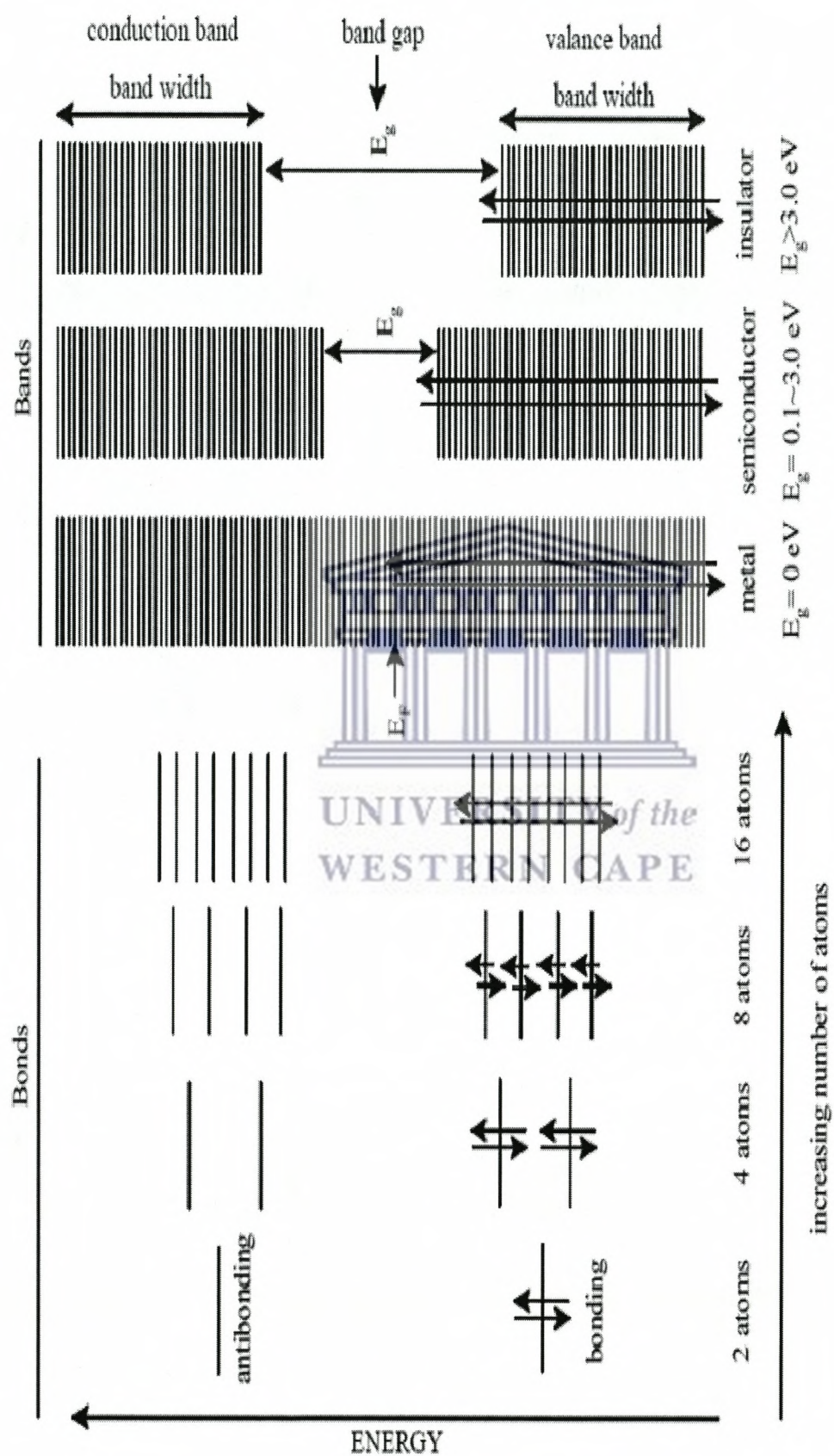


Figure 2.8: Bonds in molecules and bands in solids (Jiles, 1994).

2.7.4.3. The electronic properties of metals, semiconductors, and insulators

In metals there is no range of energies, which is deemed unavailable to electrons, that simply means forbidden gap or band gap in metals $E_g = 0$ eV (Figure 2.8). Hence metals always have a partially filled free-electron band, because the conduction and valence bands overlap, hence the electron can readily occupy the conduction band (Atkins, 2002).

Insulators have a band gap which is larger than 3 eV (Figure 2.8), the energy gap between the valence band (VB) and the conduction band (CB) is too large, hence the electron is not able to make that jump to detach from its atom, in order to be promoted to the valence band, consequently they are poor electrical conductors at ambient temperatures. Insulators can be defined as materials in which the valence bands are filled and the forbidden energy gap between valence band and conduction band is too great for the valence electrons to jump at normal temperatures from VB to the CB (Atkins, 2002).

2.7.4.4. The electronic properties of semiconductors

In semiconductors (Figure 2.8), there is a possibility of two scenarios which can allow a material to become a conductor. The first instance is that when the valence band is not completely filled, hence an electron can raise its energy to a higher level within the valence band, so that it can detach from its atom (Bott, 1998). This is coined as conduction within same band, and it requires a small amount of energy, hence many electrons are capable of accomplishing it. Second instance is when the Band gap is

very small, *i.e.* $E_g = 0.1 - 3 \text{ eV}$, hence electrons can raise their energy and detach from their atoms by jumping to a higher energy level in the conduction band (Bott, 1998).

There are several methods which can be used to excite electrons into the conduction band such as thermal or photochemical excitation. Once these electrons have reached the conduction band, they contribute to the electrical conductivity (Atkins, 2002). Furthermore, the holes which are created in the valence band, by the electrons jumping to the conduction band, also contribute to electrical conductivity. The number of electrons conduction band and the number of holes in valence band determine the electrical properties of intrinsic semiconductors (Bott, 1998).

However, another method known as **doping** is often also used to generate the charge carriers (electrons and holes). This method involves adding a different element into the material, and whether a semiconductor is pure (no different element added to it) or it is doped allows semiconductors to be categorised into either **intrinsic** or **extrinsic** semiconductors (Bott, 1998; Jiles, 1994).

2.7.4.4.1. The electronic properties of intrinsic semiconductors

The undoped semiconductors such as pure silicon are an example of an intrinsic semiconductor. These materials possess a relatively small forbidden energy gap (E_g). Hence because E_g is small, at 300K *i.e.* room temperature, the electrons can be thermally excited, causing them to be raised to higher energy in the conduction band, yielding about 10^{15} - 10^{20} conduction electrons (Jiles, 1994). Figure 2.9 demonstrates the concept of intrinsic semiconductors. As the temperature is increased, more

electrons are thermally excited to the conduction bands and leaving more holes in the valence band.

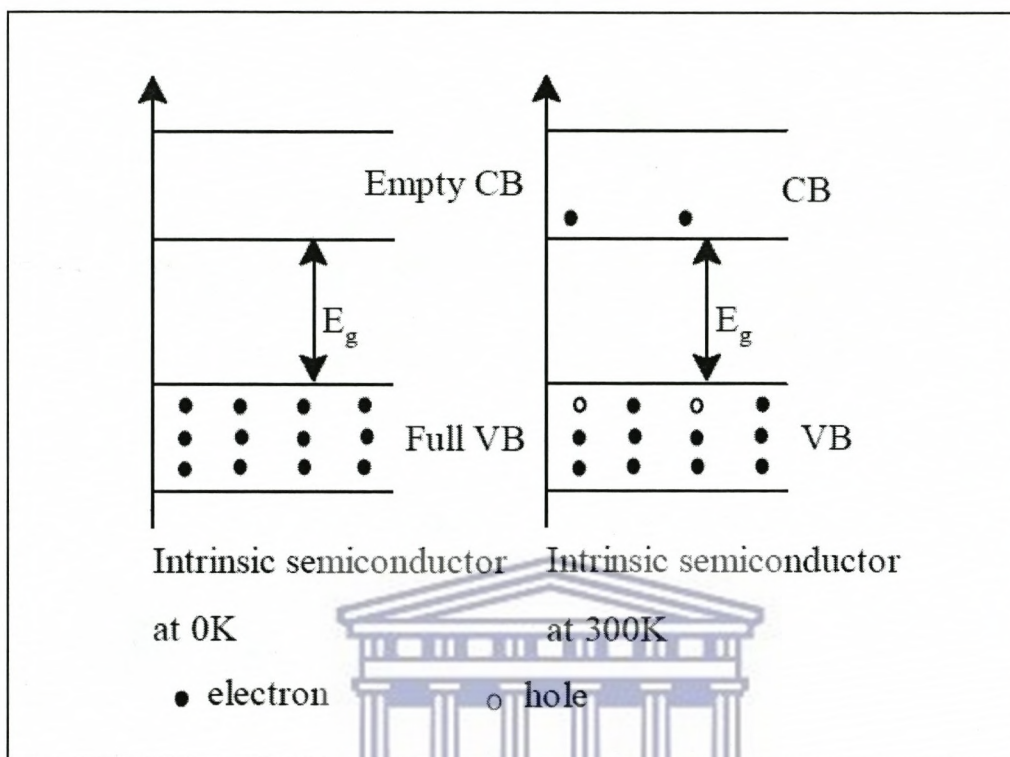
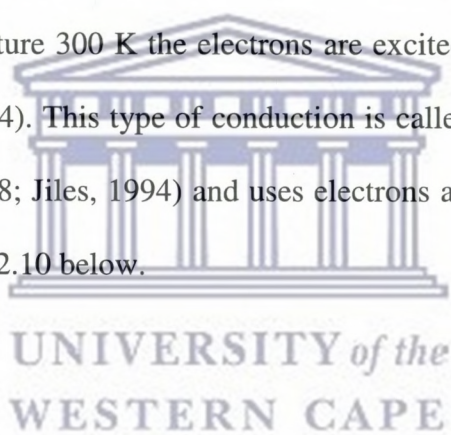


Figure 2.9: Band structure diagram of an intrinsic semiconductor (Atkins, 2002; Jiles, 1994.)

2.7.4.4.2. The electronic properties of intrinsic semiconductors

These are type of semiconductor materials which have another element or an impurity introduced into them. The impurity is known as the dopant, and the process of adding it is referred to as doping. Dopants are categorised into two groups *i.e* they can either be **donors** or **acceptors** (Atkins, 2002; Jiles, 1994). Examples of elements which are donors are phosphorus, arsenic and antimony and typical acceptor elements in extrinsic semiconductors are trivalent elements such as boron, aluminium, gallium and indium (Jiles, 1994).

Furthermore, in an extrinsic semiconductor there are two types of mechanisms for conduction that can occur. The first mechanism is when an acceptor element, is doped with a donor element that has a higher valence number (a measure of how many bonds an element can form) than it (Atkins, 2002). For example, Germanium (**Ge**) atom has 32 electrons distributed in four orbits. The outermost orbital is called the valence orbital, and it contains four electrons, hence it is tetravalent. If Ge is doped with Phosphorous (**P**), which has a valence orbital which contains five electrons (pentavalent), this creates an extra electron per atom (Jiles, 1994). This extra pair of electrons from donor **P** partially fills the conduction band because it occupies discrete levels near the bottom of the conduction band, around -0.1 eV of the band gap (Jiles, 1994). At room temperature 300 K the electrons are excited into the conduction band (Atkins, 2002; Jiles, 1994). This type of conduction is called **n-type** semiconductor (Atkins, 2002; Bott, 1998; Jiles, 1994) and uses electrons as the main charge carriers; it is illustrated in Figure 2.10 below.



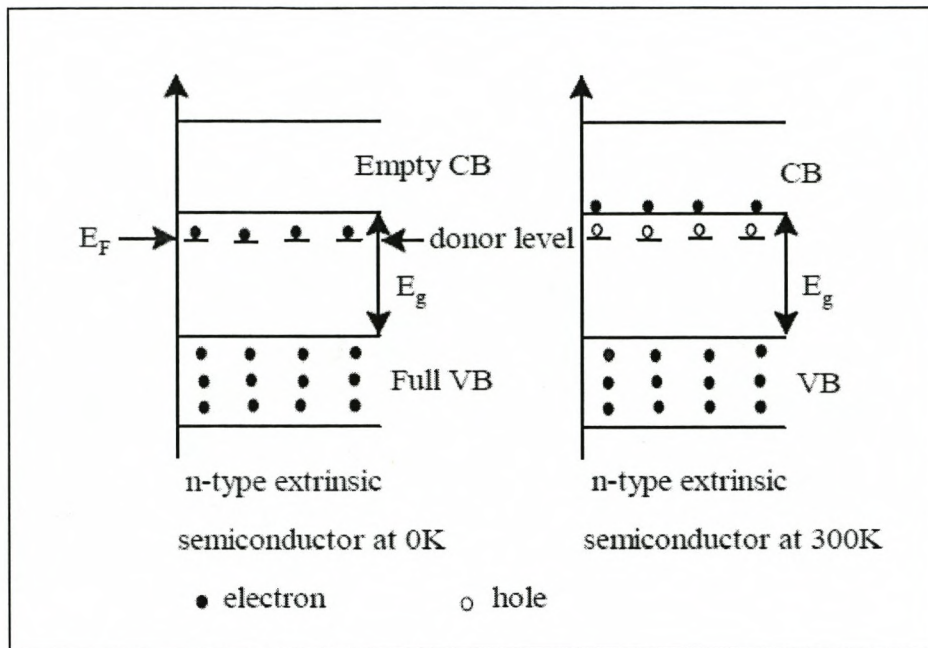


Figure 2.10: Band structure diagram of an extrinsic n-type semiconductor (Jiles, 1994).

In the second mechanism, a dopant with a lower valency than the material that is being doped is used, for example a trivalent dopant, such as Indium (**In**), can be used to dope Germanium (Jiles, 1994). In this scenario, only three covalent bonds are formed from the four possible bonds which could form. Here, the valence band is now depleted of some electrons because the fourth possible bond is vacant; hence this vacancy creates a hole for each electron missing from a bonding pair (Atkins, 2002). The main charge carrier here are the holes that are formed when the electrons move out of the valence shell. A trivalent dopant is characterized as an acceptor because it injects many holes which are the majority carriers of the charge, hence being responsible are the holes responsible for the conductivity of the crystal (Bott, 1998; Jiles, 1994). For this reason materials are called *p*-type semiconductors (Atkins, 2002; Bott, 1998; Jiles, 1994) as shown in Figure 2.11.

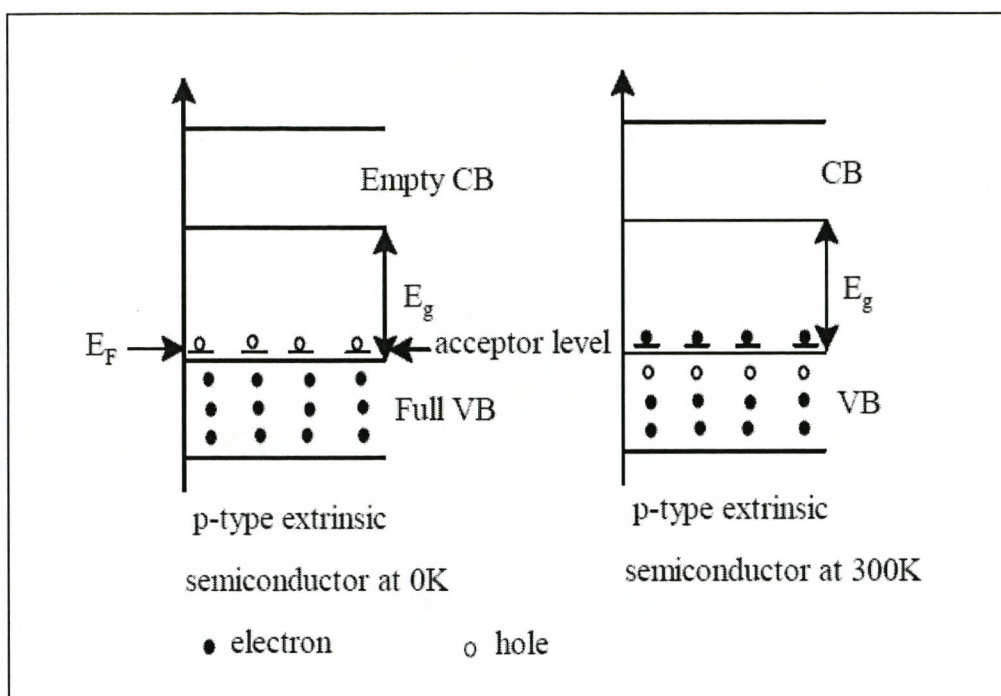


Figure 2.11: Band structure diagram of an extrinsic p-type semiconductor (Jiles, 1994).

In conclusion to the electronic properties of ECPs and the general band theory described in this section, provide a better understanding in design and synthesizing the type of conducting polymers, which have semiconducting properties and can be used as for electrode modification for ECL studies. As previously stated that there are many types of conducting polymers, hence in this work, the focus is on polyaniline due to its ease of synthesis and processing, environmental stability, and unique electrical properties, to date it is one of the most investigated conducting polymers, with industrial importance.

2.7.5. Polyaniline

2.7.5.1. History

Polyaniline (PANI) was initially discovered in 1834 by Runge, and it was referred to as aniline black (Letheby, 1862). Following this, Letheby carried out research to analyse this material in 1862 (Letheby, 1862). PANI is a mixed oxidation state polymer composed of reduced benzoid units and oxidized quinoids. Green and Woodhead (1912) discovered this interesting characteristic of polyaniline. Furthermore, Epstein *et al.*, (1987) discovered that PANI had characteristics of becoming a conductor from an insulator under certain conditions. Since then, the material has become a subject of great interest in research (Li *et al.*, 2009).



2.7.5.2. Structure of Polyaniline

PANI is a mixed oxidation state polymer composed of reduced benzoid units and oxidized quinoids (Lu *et al.*, 1986). It has an average oxidation state denoted as $1-y$ and can be found in three distinct oxidation states (Shimano and MacDiarmid, 2001; Green and Woodhead, 1912) as shown in Scheme 2.5 below. These are known to range from the fully reduced leucoemeraldine (LE) where $1-y=0$, to the half oxidized state known as emeraldine base (EB) which an oxidation state of $y = 0.5$ and finally the fully oxidized Pernigraniline ($1-y = 1$) with imine links (Wallace *et al.*, 2002; Masdarolomoor, 2006; Lu *et al.*, 1986). The EB is regarded as the most useful form of polyaniline due to its high stability at room temperature, it is composed of two benzoid units and one quinoid unit, respectively, that alternate and it is known to be a semiconductor (Masdarolomoor, 2006). Furthermore, EB can be doped in a non redox

reaction using an acid, resulting in an emeraldine salt (ES) and then in comparison with the other two forms, LE is easily oxidized while the pernigraniline (PE) is easily degraded (Masdarolomoor, 2006).

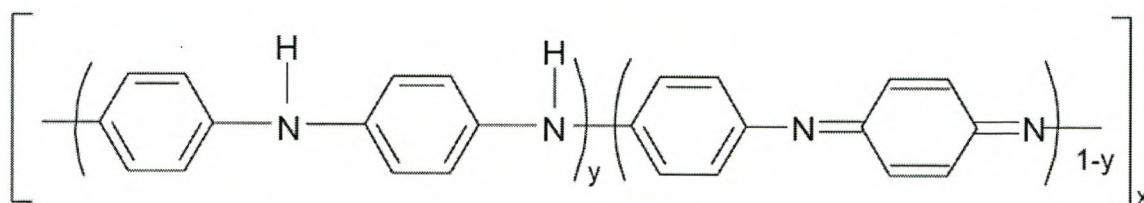


Figure 2.12: Different oxidation states of polyaniline as base forms. $y = 1$ (leucoemeraldine), 0.5 (emeraldine) and 0 (pernigraniline) (Wallace *et al.*, 2002; Shimano and MacDiarmid, 2001; Masdarolomoor, 2006).



2.7.5.3. Synthesis of polyaniline

There are two general synthesis methods which can be employed to synthesize conducting polymers; that is via electrochemical oxidation of the monomers or chemical synthesis (Terje *et al.*, 1998). Essentially during polymerization, monomers are used as starting materials to form low molecular weight oligomers (Wallace *et al.*, 2002). At potentials that are lower than where the monomers are oxidized, the low molecular weight oligomers are further oxidized to form a polymer (Wallace *et al.*, 2002). In the case of electrochemical polymerization, the monomers have to be oxidized by cycling between a potential window which will allow for the oxidation to take place and the formed polymer will then be electrodeposited onto the surface of the electrode (Wallace, 2002; Terje *et al.*, 1998). In the case of chemical synthesis, chemical oxidants such as ferric chloride (FeCl_3) and ammonium persulfate

$[(\text{NH}_4)_2\text{S}_2\text{O}_8]$ are employed and the polymer precipitates out of the chemical reaction solution (Terje *et al.*, 1998). There are several polymerization methods that are employed in order to synthesize PANI, such as the commonly used chemical or electrochemical oxidative polymerisation, or the rare methods such enzyme-catalyzed or photochemical initiated polymerization (Wallace *et al.*, 2002). The current work focuses on electrochemical and chemical polymerization and these will be further discussed.

2.7.5.4. Electrochemical polymerization

Electrochemical polymerization can be carried out by employing one of the three techniques. These are either; applying a constant voltage (potentiostatic), or a variable current and voltage (potentiodynamic) and the last method is applying a constant current (galvanostatic) to the aqueous solution of aniline. An electrolyte such as an acid (HA) is also needed for polymerization (Zotti *et al.*, 1988). It has several functions such as, to provide a sufficiently low pH so as to help solubilize the aniline monomer in water and to avoid excessive branching of undesired products but to instead to generate doped emeraldine salt (ES) form (Zotti *et al.*, 1988).

2.7.5.5. Chemical polymerization

In the preceding section, it was mentioned that for chemical polymerization to take place the monomers have to be oxidized and that ammonium persulfate $(\text{NH}_4)_2\text{S}_2\text{O}_8$ which has oxidation potential of $E_0 = 1.94 \text{ V}$ and ferric chloride (FeCl_3) with $E_0 = 0.77$

V are the most commonly used oxidizing agent (Maser *et al.*, 2008; Dong *et al.*, 2007; Green and Woodhead, 1912). However, there are other less commonly used oxidants such as; Hydrogen peroxide [H_2O_2 ; $E_0 = 1.78 \text{ V}$], Cerium (IV) Sulfate [$\text{Ce}(\text{SO}_4)_2$; $E_0 = 1.72 \text{ V}$] and Potassium dichromate [$\text{K}_2\text{Cr}_2\text{O}_7$; $E_0 = 1.23 \text{ V}$] (Green and Woodhead, 1912). Ferric chloride has the lowest oxidizing potential compared to the other four mentioned oxidizing agents but it has proved to be a useful oxidizing agent yielding up to great 200 000 Molecular weight of PANI (Green and Woodhead, 1912). Furthermore, it is required that the polymerization reaction solution has pH conditions that are acidic (<3) in order to avoid excessive formation of undesired branched product (Dong *et al.*, 2007).

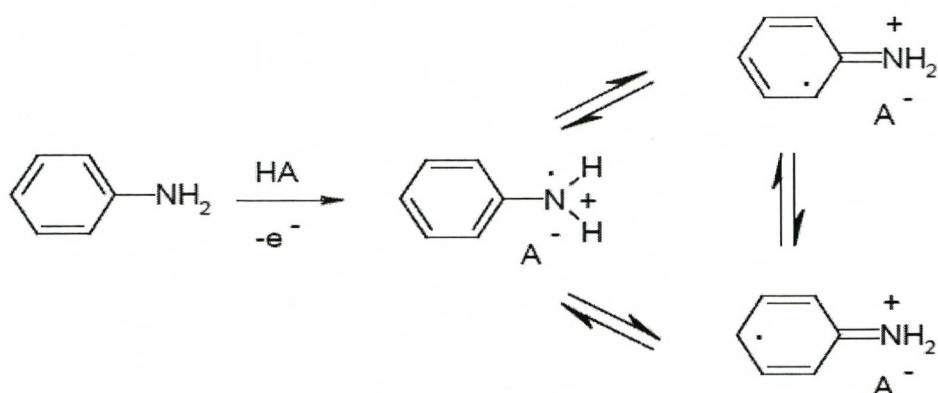


2.7.5.6. Mechanism of polymerization

Both the mechanism of chemical and electrochemical polymerization of aniline proceed via a radical propagation reaction, the initial steps (1 and 2) are common to both methods, but subtle differences appear in the initial product of the chain propagation step and product formation steps (3 and 4) (Morrin, 2002). The first two common initial steps are outlined below since they are common to both chemical and electrochemical polymerization, and the last steps (3 and 4) will be illustrated separately for chemical and electrochemical polymerization

Step 1: Oxidation of Monomer

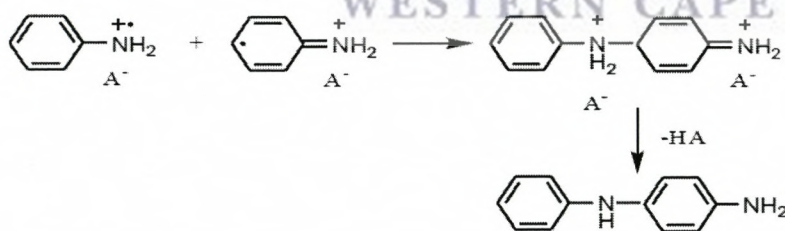
In the initial step as shown in Scheme 2.5 (Morrin, 2002), oxidation of aniline to a radical cation, which exists in three resonance forms, takes place. This step is the slowest step in the reaction, hence it's deemed as the rate determining step.



Scheme 2.5: Oxidation of monomer during electrochemical polymerization of aniline (Morrin, 2002).

Step 2: Radical coupling and Rearomatization

Head to tail coupling of the *N*- and *para*- radical cations (Scheme 2.6) takes place, yielding a dicationic dimer species (Morrin, 2002). This dimer then undergoes rearomatization to its neutral state, yielding its intermediate *p*-aminodiphenylamine known as PADPA. These processes are also accompanied by elimination of two protons.

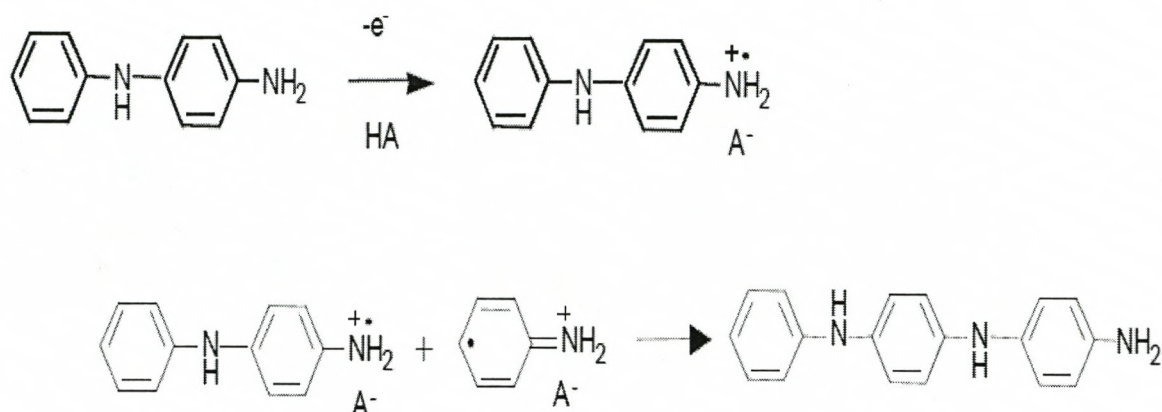


Scheme 2.6: Radical coupling and Rearomatization during electrochemical polymerization of aniline (Morrin, 2002).

Step 3 : Chain propagation for electrochemical synthesis

The dimer radical cation (centred on the para position; nitrogen atom) undergoes oxidation on the surface of the electrode. Chain propagation results from the radical

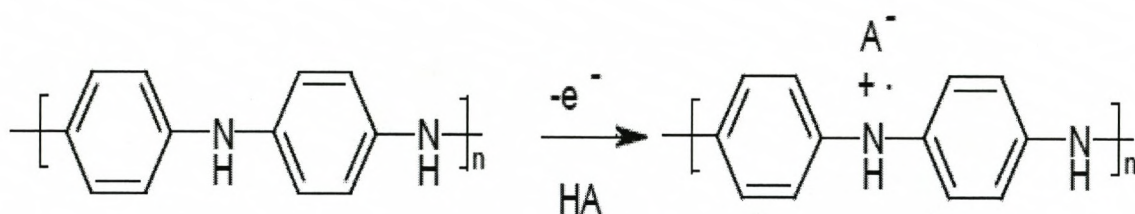
cation of the dimer coupling with an aniline cation as illustrated in Scheme 2.7 (Morrin, 2002).



Scheme 2.7: Chain propagation during electrochemical polymerization of aniline (Morrin, 2002).

Step 4 : Oxidation and doping of the polymer for electrochemical synthesis

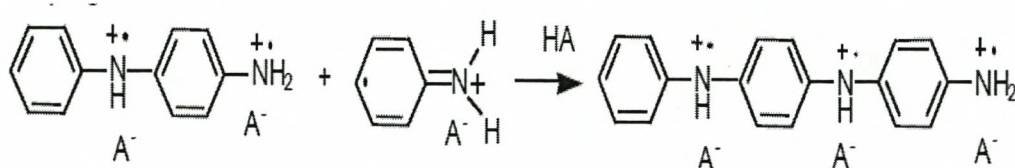
Scheme 2.8 shows the oxidation and doping of the polymer during electrochemical polymerization reaction in the presence of acid in the solution which dopes the formed polymer to yield PANI/HA.



Scheme 2.8: Oxidation and doping of the polymer during electrochemical polymerization of aniline (Wallace *et al.*, 2009).

Step 3 : Chain propagation for Chemical synthesis

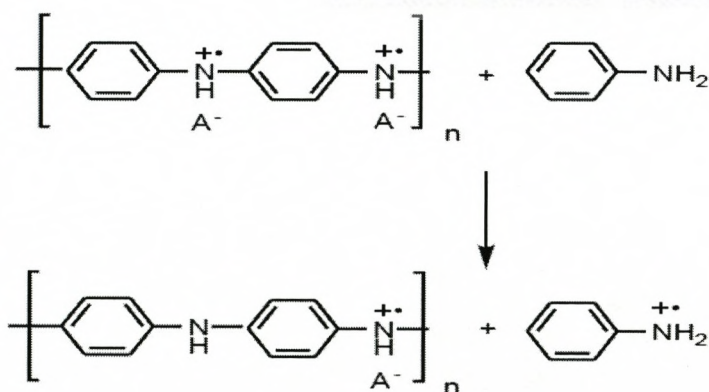
The chain propagation during the chemical synthesis of the polyaniline, the initial product in this step is the fully oxidized pernigraniline salt as shown in Scheme 2.9 below.



Scheme 2.9: Chain propagation of the polymer during chemical synthesis polymerization of aniline (Wallace *et al.*, 2009).

Step 4: Reduction of the Pernigraniline salt to Emeraldine salt(ES)

After consumption of all the oxidant in step 3, the pernigraniline salt is reduced by unreacted aniline to the green emeraldine (Scheme 2.10)



Scheme 2.10: Reduction of the pernigraniline salt to emeraldine salt during chemical synthesis polymerization of aniline (Wallace *et al.*, 2009).

2.7.5.7. Properties of polyaniline

It is well known that polyaniline has switching, optical, conductive and solubility properties that distinguish it from other conducting polymers (Wallace *et al.*, 2002).

2.7.5.7.1. Switching and Optical properties of PANI

These two properties fairly interlink and influence each other directly because as a result of PANI being able to switch between oxidation states, it directly influences the result of the UV spectrum (Wallace *et al.*, 2002), hence these two properties will be discussed concurrently. Once the conductive form of the PANI is formed i.e. emeraldine salt (ES), addition of acids and bases that protonate and deprotonate base sites in PANI, causes switching of PANI between oxidation states (de Albuquerque *et al.*, 2004; Wallace *et al.*, 2002). This leads to reaction solution pH dependence in the polymer oxidation states, hence, when the pH of the polymerization reaction is greater than four, PANI becomes non electroactive (de Albuquerque *et al.*, 2004). The loss of its electroactive characteristic is caused by failure of formation of the ES salt (de Albuquerque *et al.*, 2004). As previously mentioned, PANI is a mixed oxidation state polymer, ranging from the most reduced form leucoemeraldine which is yellow in colour, to the half oxidized form emeraldine which is green, and the violet fully oxidized pernigraniline (Nicolas-Debarnot, and Poncin-Epaillard, 20003) as shown in Figure 2.13. The electrochemical switching of polyaniline between oxidation states of PANI can be readily monitored by CV, illustrating how the structural switching corresponds to change of pH and redox potentials.

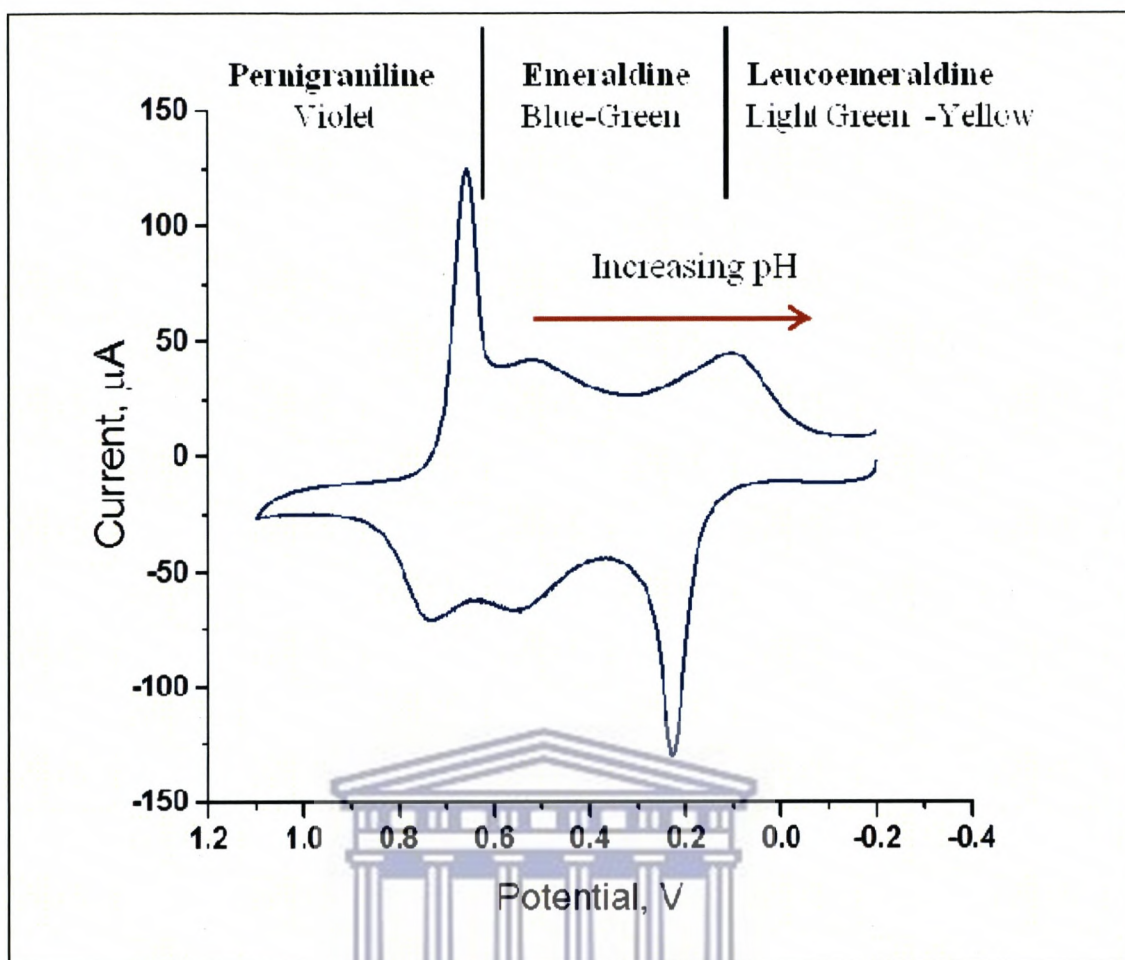


Figure 2.13: Cyclic voltammogram of polyaniline film on a platinum electrode in 1 M HCl at a scan rate of 0.1 Vs^{-1} ; the potentials at which structure and colour changes occur and the change in the potential of the second redox reaction with pH are shown as well (Wallace *et al.*, 2009).

In addition, the UV-visible spectrum of polyaniline is sensitive to oxidation state and transitions between oxidation states and is accompanied by visible optical colour change (de Albuquerque *et al.*, 2004). Hence, optical absorption can be used for quantification of electronic band gap structures, which link the signature transitions which take place during the switching between oxidation states of PANI. When quantifying the different oxidation states with UV, the electronic band structures are linked to the one of the oxidation states of PANI (Huang and MacDiarmid, 1993). The

PANI in the ES form exhibits three characteristic bands, one at 330 nm attributed to π - π^* band two bands at 430 and 800 nm in visible region band, which are due to π -polaron band and polaron- π^* band transitions (Huang and MacDiarmid, 1993) as illustrated in Figure 2.14.

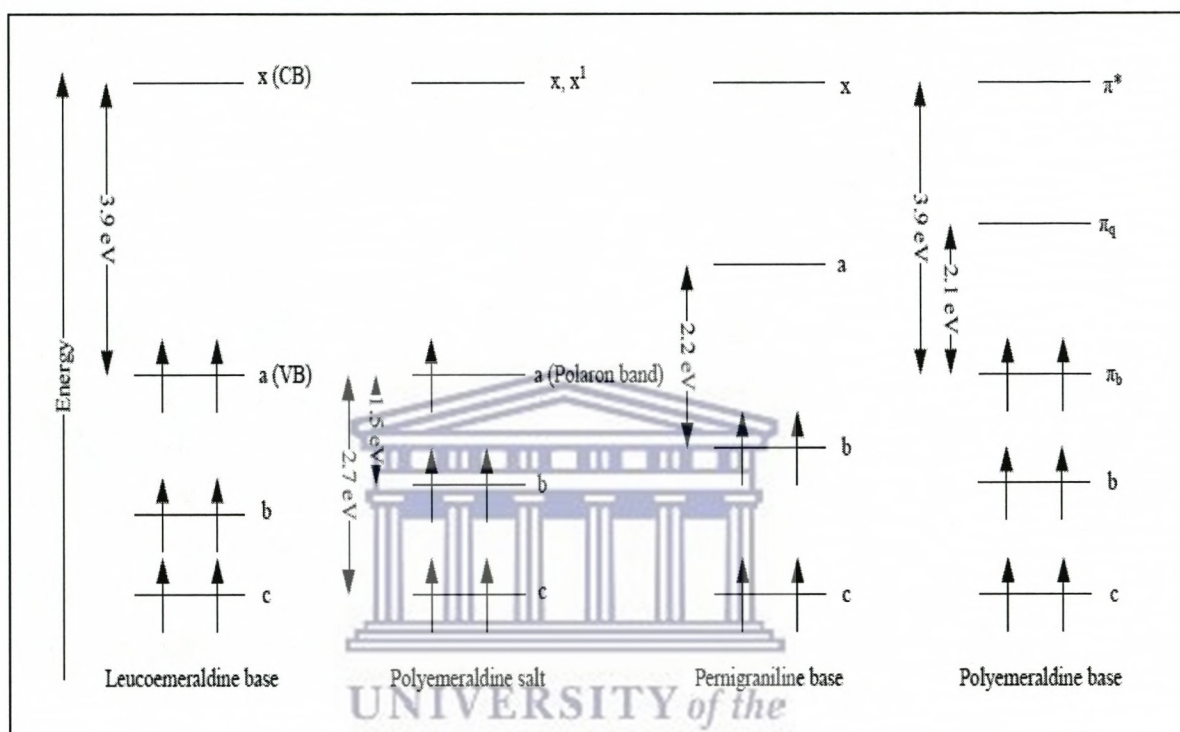
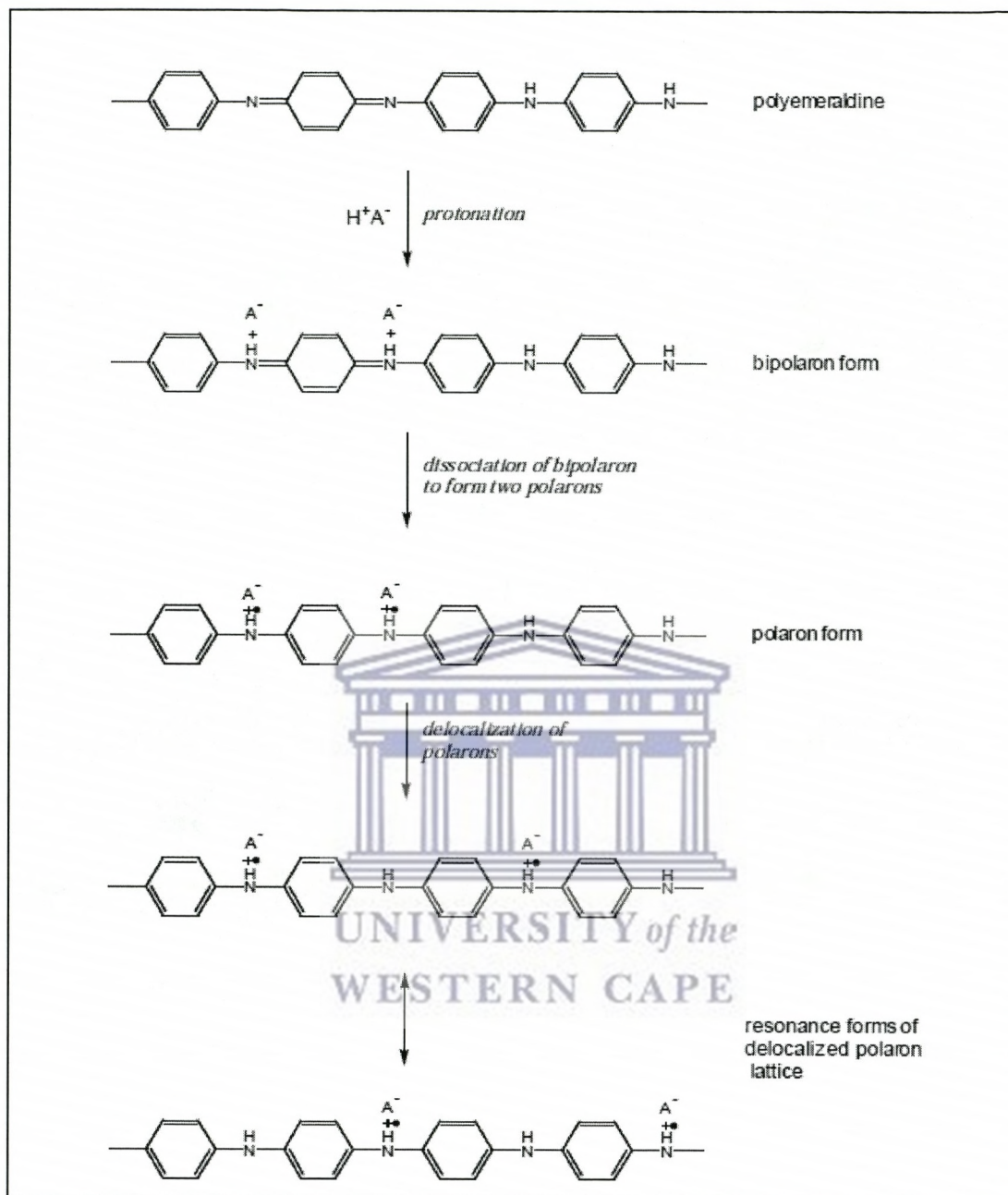


Figure 2.14: The different band gaps present in polyaniline redox states (Huang and MacDiarmid, 1993).

The emeraldine base form of PANI shows a low wavelength π - π^* band and a strong absorption band at ca. 600 nm, attributed to a local charge transfer between a quinoid ring and the adjacent imine-phenyl-amine units (intramolecular charge transfer exciton) (Wallace *et al.*, 2002). The reduced leucoemeraldine base (LB) form exhibits a band at ca. 320 nm attributed presumably to the π - π^* electronic transition (Huang and MacDiarmid, 1993). Pernigraniline base (PB) shows two bands at ca. 320 nm (π - π^* band) and at ca. 530 nm (Peierl gap transition) (Wallace *et al.*, 2002).

2.7.5.7.2. Conductivity properties of PANI

It was shown previously that the chain of polyaniline can be formed by various different combinations of the two repeating units known as the X and Y components of polyaniline. Owing to this reason, it has many unique properties and electronic conduction mechanism that seems to be unique among the rest of conducting polymers. What distinguishes PANI from other conducting polymers is the fact that its conductivity is varied by the degree of oxidation (variation in the number of electrons) and the degree of protonation (variation in the number of protons). Among the various oxidation states that PANI can exist in, the one that can be doped to a highly conductive state is the moderately oxidized emeraldine base (de Albuquerque *et al.*, 2004, Wallace *et al.*, 2002). This form of PANI has a structure which consists of equal proportions of amines ($-\text{NH}-$) and imine ($=\text{N}-$) sites. Through protonic acid doping, imine sites are protonated by acids HA to the bipolaron (dication salt) form (Stafström *et al.*, 1987). Which then undergo a further rearrangement to form the delocalized polaron lattice, which is a polysemiquinone radical-cation salt as shown in Scheme 2.11 below. The resulting emeraldine salt has conductivity on a semiconductor level of the order of 10^0 S cm^{-1} , many orders of magnitude higher than that of common polymers ($<10^{-9} \text{ S cm}^{-1}$) but lower than that of typical metals ($>10^4 \text{ S cm}^{-1}$) (Bhadra *et al.*, 2009). Kohlman *et al.*, (1997) explained that only 1% of the charge carriers which are available in the ES salt actually contribute to its observed conductivity and furthermore if all the available charge carriers were to contribute, the resulting conductivity at room temperature would be $\sim 10^5 \text{ S}^{-1} \text{ cm}$, which is comparable to that of copper.



Scheme 2.11: The doping of EB with protons to form the conducting emeraldine salt (PANI/HA) form of polyaniline (a polaron lattice) (Stafström *et al.*, 1987).

2.7.5.7.3. Solubility properties of PANI

The emeraldine base form of PANI is soluble in a number of organic solvents such as, dimethyl sulfoxide (DMSO), chloroform (CCl_3H), tetrahydrofuran (THF), dimethyl formamide (DMF), and methyl pyrrolidinone (NMP) (Spinks *et al.*, 2000). The dissolution in these various organic solvents is possible in this state that is the less ionic state of PANI. This is because in this state there are no cationic charges present in the polymer backbone. However the emeraldine salt is insoluble in aqueous solutions and most common organic solvents, because this state has got the cationic charges present in its backbone Spinks *et al.*, 2000). Cao *et al.* (1992) demonstrated that by introducing functionalised protonic acid dopants such as sulfonic acids ((10-champhor sulfonic acid (HCSA) and dodecyl-benzene sulfonic acid (DBSA) in the ES salt, solubility can be improved although it will be limited. The current work focuses on an aniline derivative which is N substituted with naphthalene sulphonic acid, and it is known as 8- anilino1-naphthalene sulfonic acid (ANSA), as given in Figure 2.15 below. It belongs to a family of substituted naphthalene's and viewed as an aniline substituted naphthalene sulfonic acid. The presence of naphthalene sulfonic acid enhances the properties of the polymer and for this reason makes ANSA to be important for electrode surface as polymer for interaction with Ru complex for electrochemiluminescence.

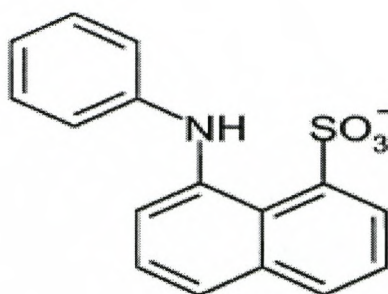


Figure 2.15: Structure of 8- anilino-1-naphthalene sulfonic acid (ANSA)

In this work, the aim was to synthesize conducting polymers for generation of ECL. This is because conducting polymers are extensively conjugated molecules, that means they have alternating single and double bonds and they also meet the above stated prerequisites. Specifically among the various conducting polymers which are known, PANI and its derivative, poly [8- anilino-1-naphthalene sulfonic acid] (PANSA), were the conducting polymers employed and so far, to the best of our knowledge, there is no work on enhancement of Ru complex ECL using these polymers. The ECL is related to photoluminescence. The photoluminescence was also employed as part of the analytical technique among other techniques in this work. Hence, the following section deals with the theoretical background to the techniques used in this study.

2.8. Theoretical Background to the techniques used

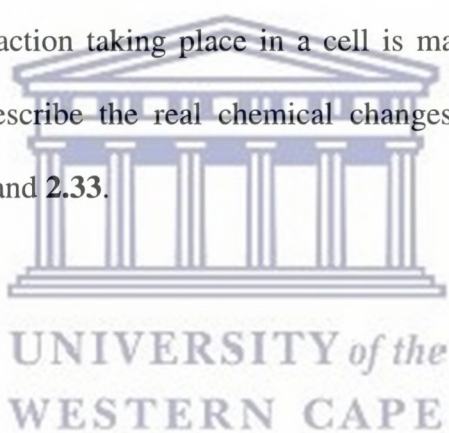
2.8.1. Fundamentals of electrochemistry

2.8.1.1. Basic components of an electroanalytical system

In an electrochemical system, chemical changes caused by the passage of an electric current and the production of electrical energy to a chemical reaction can be studied. In this kind of study the properties of collections of interfaces are called

electrochemical cells (Bard and Faulkner, 2001). These systems are defined generally as two electrodes (electronic conductors) separated by at least one electrolyte phase (ionic conductor). The key element is to study processes and factors that affect the transport of charge across the interface and chemical phases, between the *electrode* and *electrolyte*. In an electrolyte, charge is carried by the movement of electrons such as Na^+ , H^+ , Cl^- , in either water or non aqueous solvent and this charge, is carried through an electrode by movement of electrons and holes (Bard and Faulkner, 2001). It essential that the electrolyte is adequately conductive, that simply means it should have low resistance (Bard and Faulkner, 2001).

The overall chemical reaction taking place in a cell is made up of two independent *half-reactions*, which describe the real chemical changes at the two electrodes as shown in Equation 2.32 and 2.33.



The half reactions correspond to the chemical composition of the system near the electrodes responds to the interfacial potential difference at the corresponding electrode. The common interest is normally on the half reaction (Equation 2.32) that occurs at a particular electrode known as called the *working* (or *indicator*) *electrode* (Bard and Faulkner, 2001). There are several types of working electrodes, which are fabricated from different materials such as; those made from metals (e.g., Pt, Au), liquid metals (Hg, amalgams), carbon (graphite), and semiconductors (indium-tin oxide, Si) (Bard and Faulkner, 2001).

Since there are two independent half reactions, and the one that takes place at the working electrode, the second half reaction serves to standardize the reaction which is taking place at the working electrode (Equation 2.33). The standardization reaction occurs at an electrode called the *reference electrode* which is made up of phases having essentially constant composition (Bard and Faulkner, 2001). Since the reference electrode has a constant makeup, hence its potential is fixed. The *potential* of the working electrode is observed is with *respect to* the reference, and that is equivalent to observing or controlling the energy of the electrons within the working (Bard and Faulkner, 2001). Therefore any changes in the cell are attributed to the working electrode. Common reference electrodes are saturated calomel electrode abbreviated as SCE and it is denoted as $\text{Hg}/\text{Hg}_2\text{Cl}_2/\text{KCl}$ and silver/silver chloride (Ag/AgCl) (Bard and Faulkner, 2001).

The potential of the couple represents the energy needed at equilibrium to add an electron to A or to remove an electron from A^\cdot (Equation 2.32). When a negative potential is applied to an electrochemical cell, the electrons move from the electrode to the solution, hence, a reduction current occurs which causes the energy of the electrons is raised (Bard and Faulkner, 2001). The increase in energy is what causes the transfer of the electrons into vacant electronic states on species in the electrolyte. As the potential becomes more negative, it becomes more difficult to add electrons to A (reduce), while it becomes easier to remove (oxidize) electron from A^\cdot . On the contrary by applying a more positive potential to the electrochemical cell, causes the electrons on solutes in the electrolyte to transfer to the electrode as the energy is more favourable (Bard and Faulkner, 2001). The flow of electrons from solution to electrode is an oxidation current. The critical potentials at which these processes occur are

related to the standard potentials, E° , for the specific chemical substances in the system (Bard and Faulkner, 2001).

In an electrochemical cell, there is also an auxiliary electrode present, it is known as the *counter electrode*. It serves as a sink for electrons so that current can be passed from the external circuit through the cell. It is essential that this electrode conducts current well. In most cases the counter electrode consists of a metallic foil or thin platinum wire, although gold and sometimes graphite may be used (Bard and Faulkner, 2001).

2.8.1.2. Fundamentals of ECL

Bard (2004), explained that understanding the relationship between current $i(t)$ and radiant intensity $I(t)$, is important because these are the analytical variables in a quantitative study of electrogenerated chemiluminescence. In ECL, the observed chemiluminescence arises from the reaction of species generated electrochemically at a solution/electrode interface. Hence, it is important to understand concepts such as; mass transfer and mass transport of solution species to an electrochemical interface to generate the precursors for ECL.

When analysing the electroanalyte movement through solution, if the electron conduction through the electrode and electron transfer across the interface are both fast, then the rate that limits the overall rate of charge flow will be that at which the electroactive material moves from the solution towards the surface of the electrode where the process of electron transfer takes place. This type of movement is known as

mass transport, and proceeds via three separate mechanisms, namely migration, convection and diffusion (Monk, 2001).

Once the concepts of mass transfer and mass transport have been understood, it becomes easier to follow the concepts of ECL as the precursors undergo subsequent mass transfer and transport from the electrochemical interface to react in a spatial reaction zone within the diffusion layer produce excited state species. The rate at which the precursors react within in this diffusion layer directly influences the observed CL intensity (Bard, 2004).

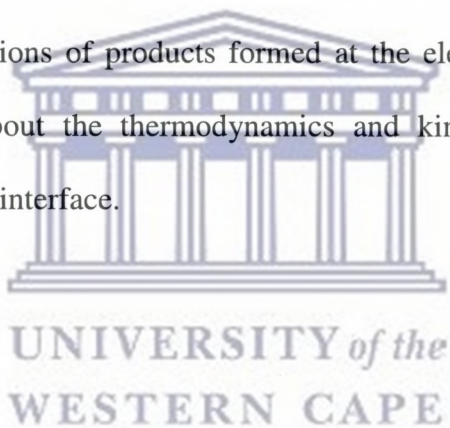
According to Forster *et al.* (2003), there are several assumptions that are made for an ideally responding redox polymer immobilized on an electrode surface, where, A_{Ox} and B_{Red} represent a reducible and oxidizable species in solution; these assumptions are: the redox couple O/R, is adsorbed on the electrode surface hence its concentration is too low to contribute to the Faradaic current. It is also assumed that the maximum surface coverage and free energy of adsorption are independent of the applied potential and are also proportional to the surface activity. Furthermore, all adsorption sites on the surface are harmonious and the oxidized and reduced forms occupy equal areas on the surface. In addition to that for it to be possible to observe an ideal response the entire potential drop occurs at the electrode polymer interface and the adsorbates do not interact laterally. Lastly the Faradaic and capacitive currents can be separated (Forster *et al.* 2003).

Voltammetry is examples of an electrochemical technique that can help one understand the thermodynamics and kinetics of electron transfer across the electrode polymer interface and within the polymer film.

2.8.1.3. *Electro analytical techniques*

2.8.1.3.1. *Cyclic voltammetry*

Cyclic voltammetry (CV) is the most widely used electrochemical technique, which gives qualitative information about the electrochemical reactions (Skoog *et al.*, 2004). It can be employed as a preliminary study, to obtain a fast overview before one starts to investigate ECL studies (Bard, 2004; Skoog *et al.*, 2004) also explained that although CV is frequently used for qualitative analysis, it offers a rapid means of determining the redox potentials of the electro active species. It allows one to study oxidation and reduction reactions of products, to detect reaction intermediates and to evaluate follow up reactions of products formed at the electrodes. Furthermore, CV provides information about the thermodynamics and kinetics of electron transfer across the electrode/film interface.



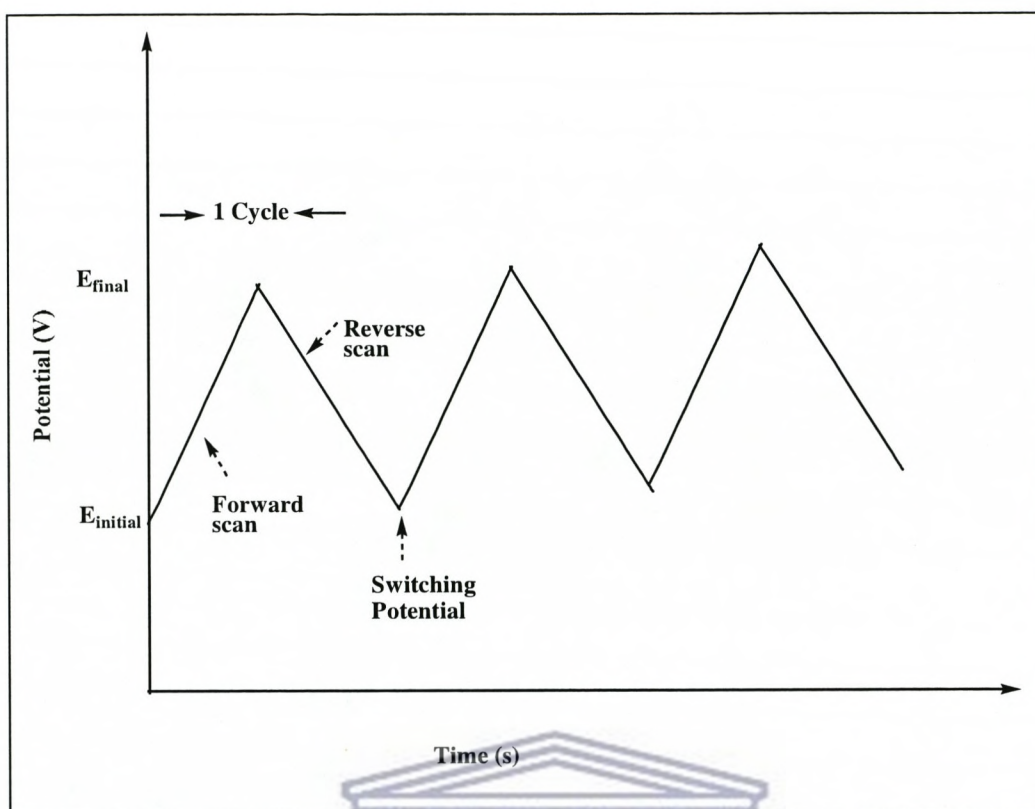


Figure 2.16: Potential-time excitation signal in cyclic voltammetric experiment (Wang, 2000).

During a CV experiment, the applied potential is firstly swept in one direction from the E_{initial} towards the E_{final} , from then the sweep direction is reversed back and the potential returns to E_{initial} , while the current is measured (Monk, 2001). This constitutes one complete cycle in cyclic voltammetry and a CV may use one full cycle, a partial cycle or several cycles, illustrated in Figure 2.16 above. A scan in the direction of more negative potentials is known as the forward scan, while one in the opposite direction is called reverse scan. The forward and reverse scans give rise to the triangular waveform illustrated in the figure above and the potential at which the scan is reversed is known as the switching potential (Monk., 2001).

In a typical CV experiment, the potential of the electrode is swept with time at a certain scan rate in a solution of compound(s) of interest in a solvent and supporting electrolyte. Typically the result obtained from this experiment is a plot of current versus applied voltage (I vs V), demonstrated in Figure 2.17 below.

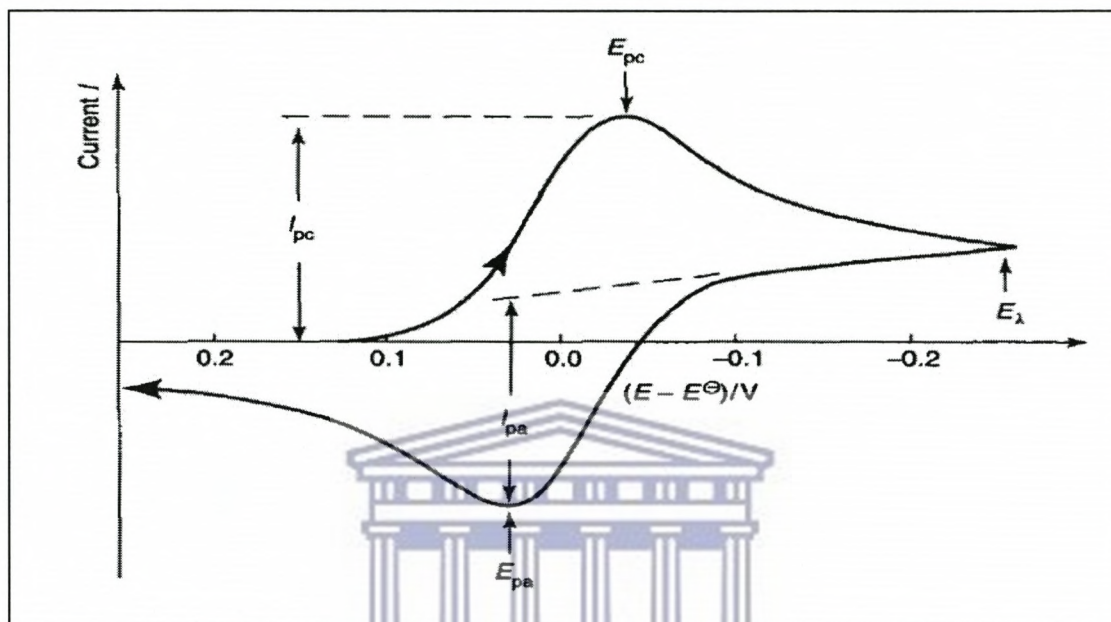


Figure 2.17: Solution phase cyclic voltammogram for the reduction reaction at a solid electrode (Bard and Faulkner, 2001).

The resulting voltammogram shows characteristic well-behaved system, i.e., one where fully reversible species in solution. The upper (cathodic) peak represents the reaction in Equation 2.34 while the lower (anodic) peak represents the electrode reaction (Equation 2.35).



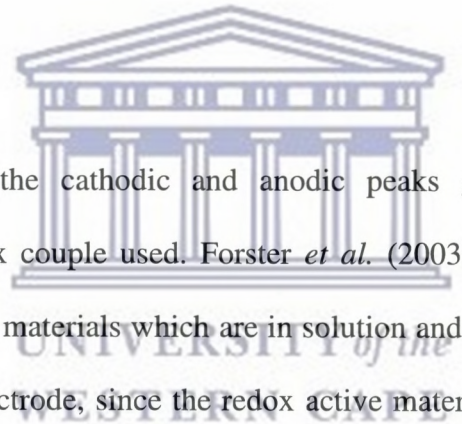
The voltammogram above shows important parameters such as i_{pa} and i_{pc} (anodic and cathodic peak current), E_{pa} and E_{pc} (anodic and cathodic peak potentials). For a

reversible electrode reaction at 25°C, the difference in the peak potentials ΔE_p is calculated according Equation 2.36 (Skoog *et al.*, 2004).

$$\Delta E_p = |E_{pa} - E_{pc}| = 0.059/n \quad [2.36]$$

Where n is the number of electrons transferred in the electrode reaction for a reversible couple. The electron transfer reactions at the electrode are rapid (nernstian systems) and the products of the reactions, e.g., the ion radicals, are stable, an analysis of the waves yields the formal electrode potential E° , which is centred between E_{pa} and E_{pc} which is calculated as in Equation 2.37 (Monk., 2001).

$$E^\circ = E_{pa} + E_{pc} / 2 \quad [2.37]$$



The position of both the cathodic and anodic peaks gives us thermodynamic information of the redox couple used. Forster *et al.* (2003) explained that there are differences in the CV of materials which are in solution and those which are adsorbed on the surface of the electrode, since the redox active materials adsorbed do not have to diffuse to or from the electrode surface. Owing to this reason, the resulting CV shapes of the surface adsorbed species are sharp and symmetrical compared to the solution phase species. This can be ascribed to the existence of fixed amounts of species on the electrode surface, which is not influenced by mass transport (Forster *et al.*, 2003).

In the case when the sample of interest is adsorbed on the surface of the electrode, the surface concentration (Γ) of the absorbed species could be estimated from a plot of

current (I_p) versus scan rate (v) in accordance with the Brown Anson model using the Equation 2.38 (Wang, 2000).

$$I_{pa} / v = \frac{n^2 F^2 \Gamma A}{4 RT} \quad [2.38]$$

The peak current (I_p) varies linearly with the scan rate (v) and, n is the number of electrons transferred, F is the Faraday constant, v is the scan rate, R is the gas constant, T is the absolute temperature, A is the real or microscopic area of electrode and Γ is the surface coverage or concentration of redox active adsorbate (mol. cm^{-2}). Wang (2000) also explained that, by using the charge (Q) consumed during the reduction or adsorption of the adsorbed layer, the surface coverage or surface concentration (Γ) can be calculated using Equation 2.39(a) and (b). Q is the charge passed during exhaustive electrolysis of the film after correction for double layer charging.

$$Q = nFA\Gamma \quad [2.39(a)]$$

$$\Gamma = Q/nFA \quad [2.39(b)]$$

where Q is the charge in Coulomb (C) and Γ is a surface coverage in mol.cm^{-2}

However, in many films electron self-exchange reactions between neighbouring oxidised and reduced sites causes electrochemical charge transport. As this electron hopping process takes place, it is also accompanied by charge compensating ions which are mobile. The Randles-Sevcik equation (as given in Equation 2.40 below) can be used to estimate the effective diffusion coefficient, D_e , corresponding to the diffusion of either electron or charge compensating counter ions (Bard and Faulkner, 2001).

$$I_p = 2.69 \times 10^{-5} n^{3/2} A D_e^{1/2} C v^{1/2} \quad [2.40]$$

where I_p is the peak current in A, A is the electrode area in cm^2 , D_e is diffusion coefficient in $\text{cm}^2 \text{s}^{-1}$, c is the concentration in mol/cm^3 and v is the scan rate in Vs^{-1} .

A plot of i_p vs $v^{1/2}$, should be linear and from its slope D_e can be evaluated (Wang, 2000).

2.8.1.3.2. Chronoamperometry

In a chronoamperometric experiment, current 'amp' is measured as a function of time 'chrono'. It is usual to commence with the solution around the electrode containing only one redox form of the analyte. During the chronoamperometry experiment, the potential is stepped from an initial potential E_1 to a second potential E_2 . At the potential (E_1) there is no electron modification that occurs and at E_2 the electrode reaction is complete, i.e. the current is limiting, this is illustrated by Figure 2.18 below (Monk, 2001).

UNIVERSITY of the
WESTERN CAPE

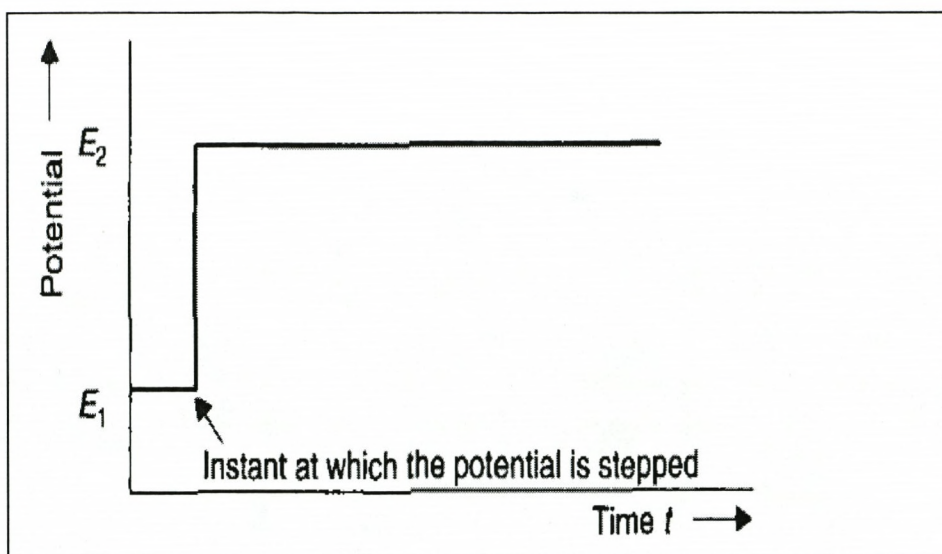


Figure 2.18: Plot of potential against time (Monk, 2001).

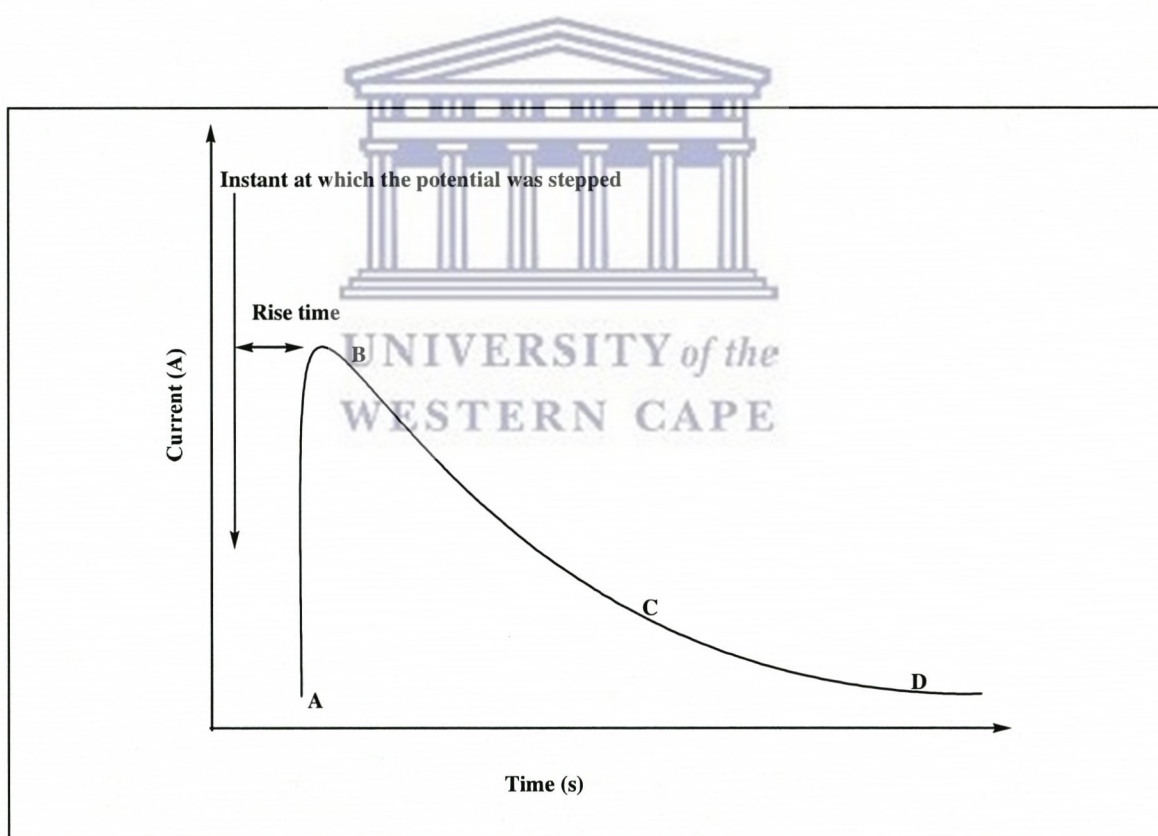


Figure 2.19: Shows a trace of current against time in response to the potential step (Bockris *et al.*, 2000).

In the Figure 2.19 above, the potential is firstly set on the pontetioostat at the desired value, and thus applied to the electrode. The current is initially used in the charging double layer up to the potential chosen (A to B). In addition to charging the double layer, the charge is also used to drive electrons across the interface, which is more demanding as the resistance is higher and this causes the current to decrease from B to C. From C-D, the double layer is almost charged and the current is starting to become constant. The effect of diffusion will be visible as time is increased (Bockris *et al*, 2000).

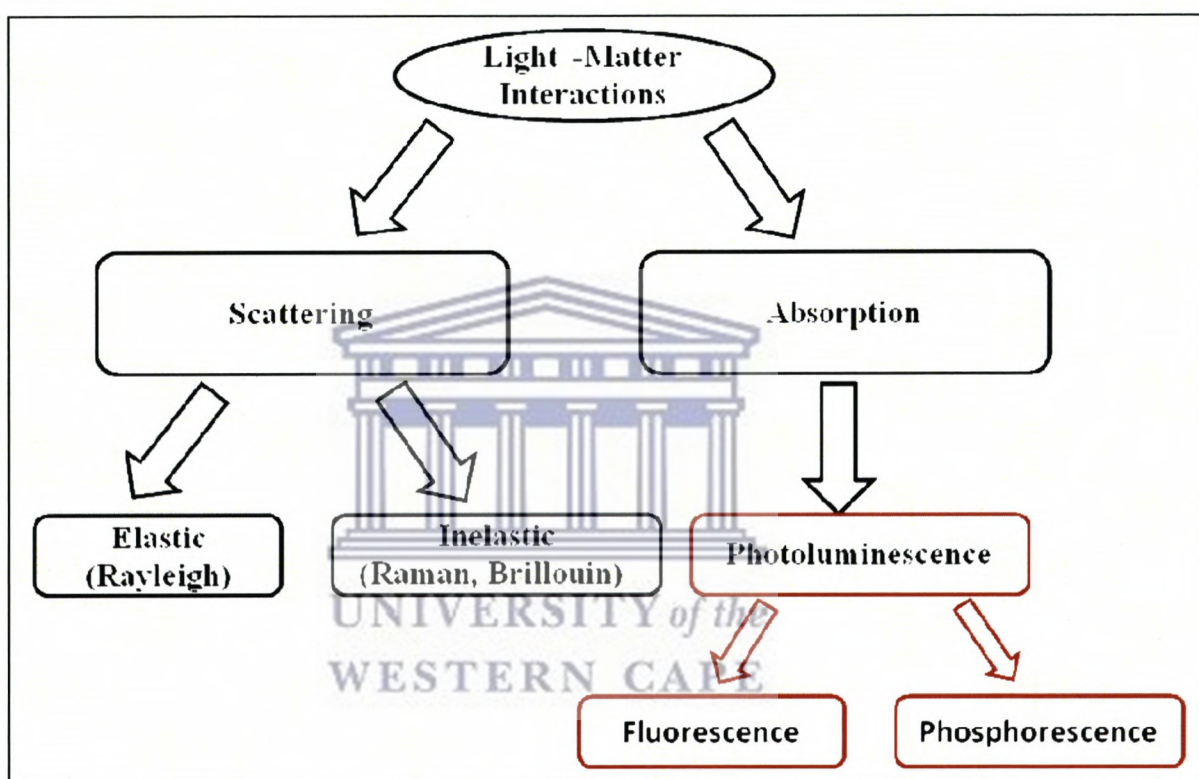
2.9. Spectroscopy and Photochemistry fundamentals

2.9.1. Luminescence

Luminescence was earlier explained in this work as a general term which is used to describe light emission process that does not derive energy from the temperature of the emitting body. To be more specific it is the emission of ultraviolet, visible or infrared photon from an electronically excited state species. This phenomenon was discovered in 1888 by a physicist and science historian called Eilhardht Wiedemann, to describe all those phenomena of light which are not solely conditioned by the rise of temperature (Valeur, 2002).

Furthermore, it was also mentioned that the various types of luminescence are classified according to the mode of excitation. The current section will focus on the type of luminescence in which the excitation mode is the absorption of a photon by a species, causing the excitation of the absorbing species from the lower energy state to a higher energy level and then returns back to a lower energy state. When it returns to

a lower energy level, a photon of light is emitted. The emission of photons accompanying the de excitation process is known as **photoluminescence** (fluorescence, phosphorescence or delayed phosphorescence) as shown Scheme 2.12 below. Prior to explaining the concept of photoluminescence and processes which can arise from it, it is useful to firstly explain the nature of electronic states, so that it can be easier to understand the concept of photoluminescence.



Scheme 2.12: Showing the possible physical effects resulting from the absorption of light, the highlighting is position of photoluminescence (Valeur, 2002).

2.9.2. Nature of electronic states

When explaining nature of electronic states, it essential to understand how electrons relate to orbitals, to give rise to electronic states. An *orbital* is a mathematical

expression, called a wave function that describes properties and characteristics of one electron in the vicinity of an atomic nucleus or of a system of nuclei as in a molecule (Valeur, 2002). An orbital is often represented as a three-dimensional region within which there is a high probability (95%) of finding the electron in. *Electronic states*, on the other hand, are concerned with the properties of all the electrons in all the orbitals. By combining all the wave functions of each electron housed in all the orbitals of a molecule; a wave function of an electronic state is formed, (Valeur, 2002). There are three kinds of states which an electron can exist in and these are; the ground, transition and excited state (Valeur, 2002). The state with lowest energy is called ground state, while transition state corresponds to a vibrationally excited ground state (*i.e.* ground state in a strained configuration), where as the excited electronic states is the one with much higher in energy than the ground state although it does not have excess vibrational energy. Electronic states of organic molecules can be categorized into two groups; *i.e.* singlet states which are denoted as *S* and triplet states *T*, and each electron state has got several vibrational levels (Lakowicz, 2006; 1999).

A pair of spin equal to $\frac{1}{2}$ and $-\frac{1}{2}$ electrons can be combined to form one of three possible electronic states of total spin equal to zero called the singlet state (S_0 , S_1 and S_2). In the singlet state, all the electrons the molecule have their spins paired, hence their spin equals zero. On the other hand the *triplet states* are those in which one set of electron spin have become unpaired and the spins are equal $\frac{1}{2}$ for each electron, hence, giving a total spin = 1 for the triplet state (illustrated by the Figure 2.20 below). At each of these electronic energy levels the fluorophores can exists in a number of vibrational energy levels denoted by ν_0 , ν_1 , ν_3 , etc. The vibrational levels arise because a molecule in a given electronic state may absorb small increments of energy

corresponding to changes in vibrational modes, although retaining the same electronic configuration (Valeur, 2002). The possible physical processes which follow absorption of a photon by a molecule are normally represented by a Jablonski diagram, which is illustrated in Figure 2.21 below, showing the absorption, fluorescence, intersystem crossing and phosphorescence.

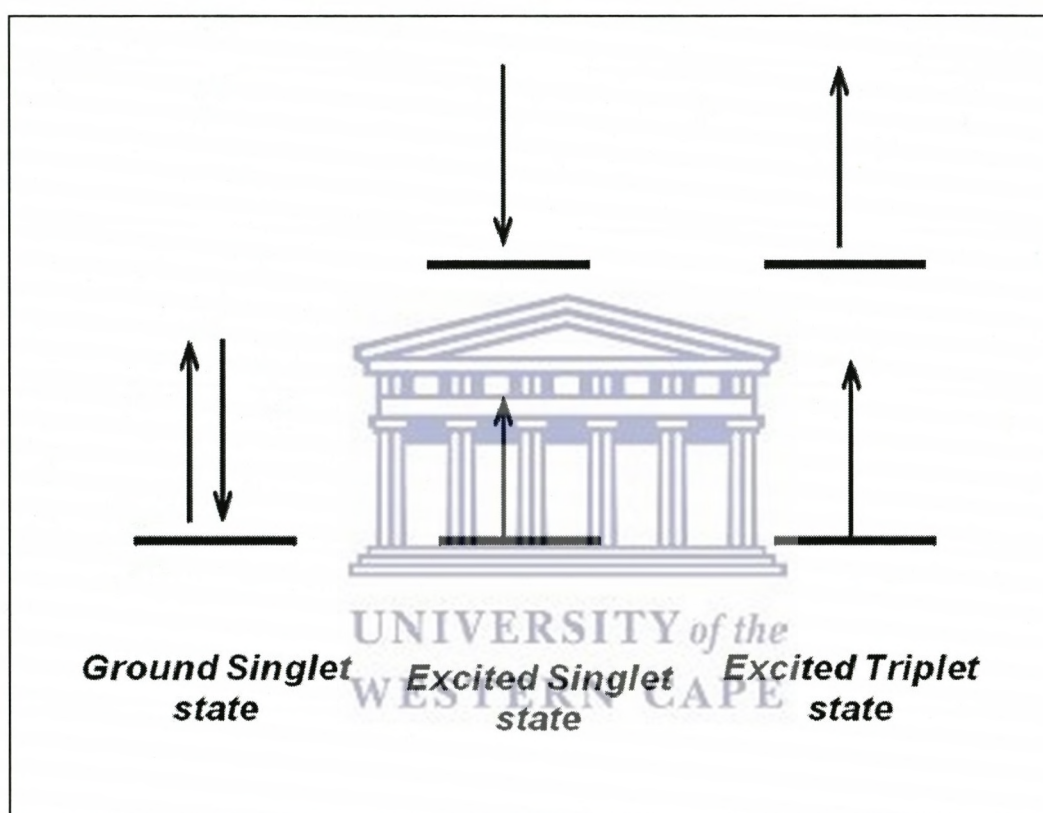


Figure 2.20: Transition in electronic states showing the ground singlet, excited singlet and triplet states (Valeur, 2002).

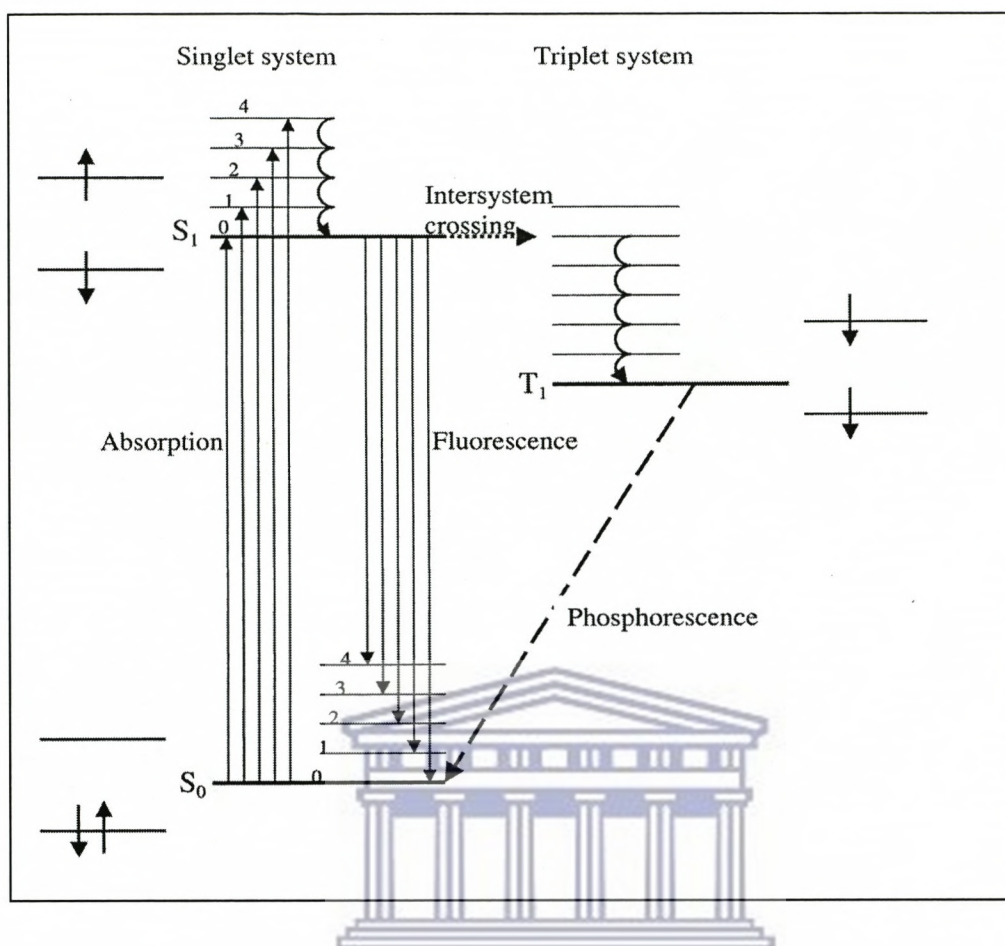


Figure 2.21: Jablonski diagram (Bard, 2004; Valeur, 2002).

2.9.2.1. Absorption

Prior to absorption at room temperature, all molecules are in the lowest vibrational level of the ground state. Upon applying UV radiation on a particular molecule, it absorbs the photons of light, and gets excited from the lower vibrational energy level v_0 of the ground state S_0 , to one of vibrational levels in the electronic excited state S_1 (Valeur, 2002). Following light absorption, several processes usually occur such as and these are fluorescence, phosphorescence, internal conversion and intersystem crossing (illustrated by Figure 2.21 above)

2.9.2.2. Fluorescence

Upon absorption, once a molecule arrives at the lowest vibrational level of an excited singlet state (Figure 2.20), it can do a number of things, one of which is to return to the ground state. When it returns to a lower energy level, a photon of light is emitted this process is known as *fluorescence*. Therefore it can specifically be defined as the emission of light from singlet-excited states, in which the electron in the excited orbital is paired (of opposite sign) to the second electron in the ground-state orbital (Valeur and Berberan-Santos, 2011). Return to the ground state is spin-allowed and occurs rapidly by emission of a photon. It was shown that emission rates of fluorescence are typically 10^8 s^{-1} , so that a typical fluorescence lifetime is near 10 ns (Valeur, 2002). Fluorescence spectral data are generally presented as emission spectra and if a molecule that absorbed UV radiation does not fluoresce it means it lost its energy through another process. The efficiency of fluorescence yield is measured by the number of molecules taking part in an event for every photon absorbed by the molecule, and known as fluorescence quantum yield (Φ_F) and is calculated according to Equation 2.41.

$$\Phi_F = \Phi_F^{std} \frac{F \cdot A_{std} \cdot n^2}{F_{std} \cdot A \cdot n_{std}^2} \quad [2.41]$$

where F and F_{std} are the areas under the fluorescence curves of the molecule and the standard, respectively. A and A_{std} are the respective absorbances of the sample and standard at the excitation wavelengths and n and n_{std} are the refractive indices of the solvents used for the sample and standard, respectively.

2.9.2.3. Internal conversion

There other alternative routes besides fluorescence which molecules can take in order to return to the ground state, these are known as radiationless processes (Valeur, 2002). They are deemed radiationless processes because the molecules in an excited singlet state may return to the ground state without the emission of a photon, converting all the excitation energy into heat and this process is called *internal conversion* (Valeur and Berberan-Santos, 2011).

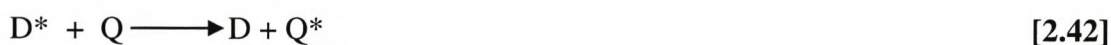
2.9.2.4. Intersystem crossing and Phosphorescence

Molecules in the excited singlet state S_1 state can also undergo a spin conversion, that is the spin can be reversed. For example, if the molecule's spin is equal to $1/2$, when it becomes reversed and the spin becomes equal to $-1/2$, it moves to the excited triplet state, T_1 and this process is called *intersystem crossing*. The probability of this happening is increased if the vibrational levels of these two states overlap (Lakowicz, 2006). A process of vibrational relaxation occurs causing the molecule in T_1 to finally return to the lowest vibrational level of the electronic ground state S_0 . Transition from the T_1 to S_0 is forbidden hence the molecule returns via vibrational relaxation, and as a result, the rate constants for triplet emission are several orders of magnitude smaller than those for fluorescence. Emission from T_1 is termed *phosphorescence* and is generally shifted to longer wavelengths (lower energy) relative to fluorescence (Valeur and Berberan-Santos, 2011; Valeur, 2002).

2.9.2.5. Fluorescence Quenching

Fluorescence quenching refers to any process that decreases the fluorescence intensity of a sample (Lakowicz, 2006). There are a wide variety of quenching processes that include excited state reactions, molecular rearrangements, ground state complex formation, and energy transfer (Valeur, 2002). Quenching experiments can be used to determine the accessibility of quencher to a fluorophore, monitor conformational changes, monitor association reactions of the fluorescence of one of the reactants changes upon binding (Lakowicz, 2006). There are two basic types of quenching: static and dynamic (collisional) (Valeur and Berberan-Santos, 2011). Both types require an interaction between the fluorophore and quencher. In the case of dynamic quenching the quencher must diffuse to the fluorophore during the lifetime of the excited state. Upon contact the fluorophore returns to the ground state without emission of a photon. In the case of state quenching a complex forms between the fluorophore and the quencher, and this complex is non-fluorescent. The formation of this complex does not rely upon population of the excited state.

An excited state (D^*) can be quenched by another molecule (a quencher, Q) to produce the ground state (Valeur, 2002), i.e.



where Q^* can often decay to the ground state without emission. Quenching can occur by either energy transfer or electron transfer. Energy transfer, sometimes called Förster transfer, is favored by the electronic energy of D^* being greater than that of Q^* and a large overlap of the emission band of D^* with the absorption band of Q (Lakowicz, 2006). The energy transfer occurs by a direct electrodynamic interaction between D^* and Q and occurs at short distances between the reactants (Valeur, 2002).

2.10. Spectroscopy techniques

2.10.1. Ultraviolet Visible (UV-vis) Spectroscopy

Ultraviolet-visible spectroscopy is an analytical technique used to measure electronic absorption of the molecule in the ultraviolet-visible region of the spectrum which is commonly applied in analytical chemistry for the quantitative determination of different analytes, such as highly conjugated organic compounds, transition metal ions and biological macromolecules with analyses usually carried out in solutions (Skoog *et al.*, 2004). The light in the visible and adjacent (near-UV and near-infrared) ranges is used resulting in absorption or reflectance of any chemical involved and molecules undergo electronic transitions in this region of the spectrum. The absorption spectrum shows a number of absorption bands corresponding to structural groups and electronic transitions within the molecule (Valeur, 2002). For example, the different electronic transitions are shown in Figure 2.22.

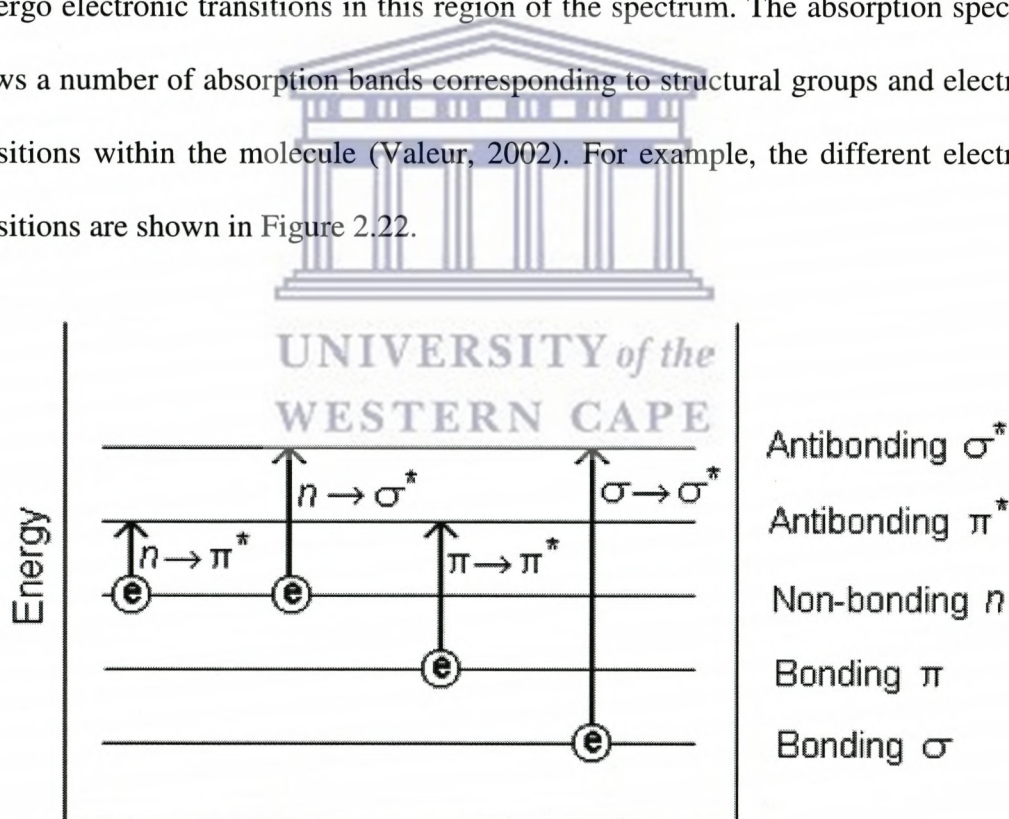
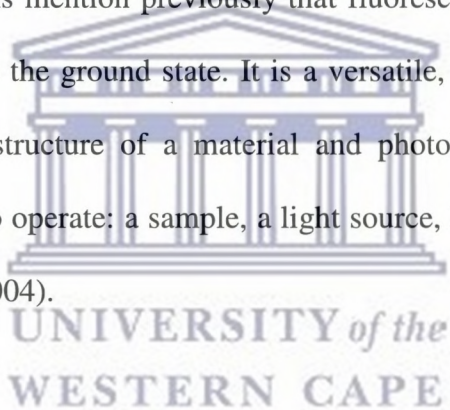


Figure 2.22: Possible electronic transitions of π , σ , and n (Valeur, 2002).

It can be seen that when an electron σ bonding is excited to the anti-bonding ($\sigma - \sigma^*$ transitions) a large energy is required and observed at around 200 nm. The $n - \sigma^*$ transitions is due to the non-bonding electrons and has less energy in the range 150 - 250 nm. Most electronic absorption of organic compounds is based on transitions of n or π electrons to the π^* excited state which is observed between 200 - 700 nm.

2.10.2. Fluorescence Spectroscopy

The fluorescence technique (Figure 2.23) is the analytical technique used to study the photoluminescence behaviour of the material and is a complementary technique to UV-Vis spectroscopy. As mention previously that fluorescence deals with transitions from the excited state to the ground state. It is a versatile, non-destructive method of probing the electronic structure of a material and photoluminescence requires the following components to operate: a sample, a light source, light filtering system and a detector (Skoog *et al.*, 2004).



In addition, the light from the light source hits the sample causing production of excitons as well as electron interactions and some of these interactions cause an emission of light, which is then filtered to its different energies and then recorded by the detector (Valeur, 2002). The fluorescence can be used to get the number of defects that are in a type of electronic molecule. The fluorescent lifetime of a molecule is the parameter describing the time evolution of the decay of the fluorescent radiant intensity (Lakowicz, 2006). The measurement of fluorescence lifetimes can be obtained using fluorescence technique and this is a field which has grown significantly in recent years, in particular with relation to fluorescence lifetime imaging (FLIM) of live cells and in the study of proteins (Cosgrave *et al.*, 2010).

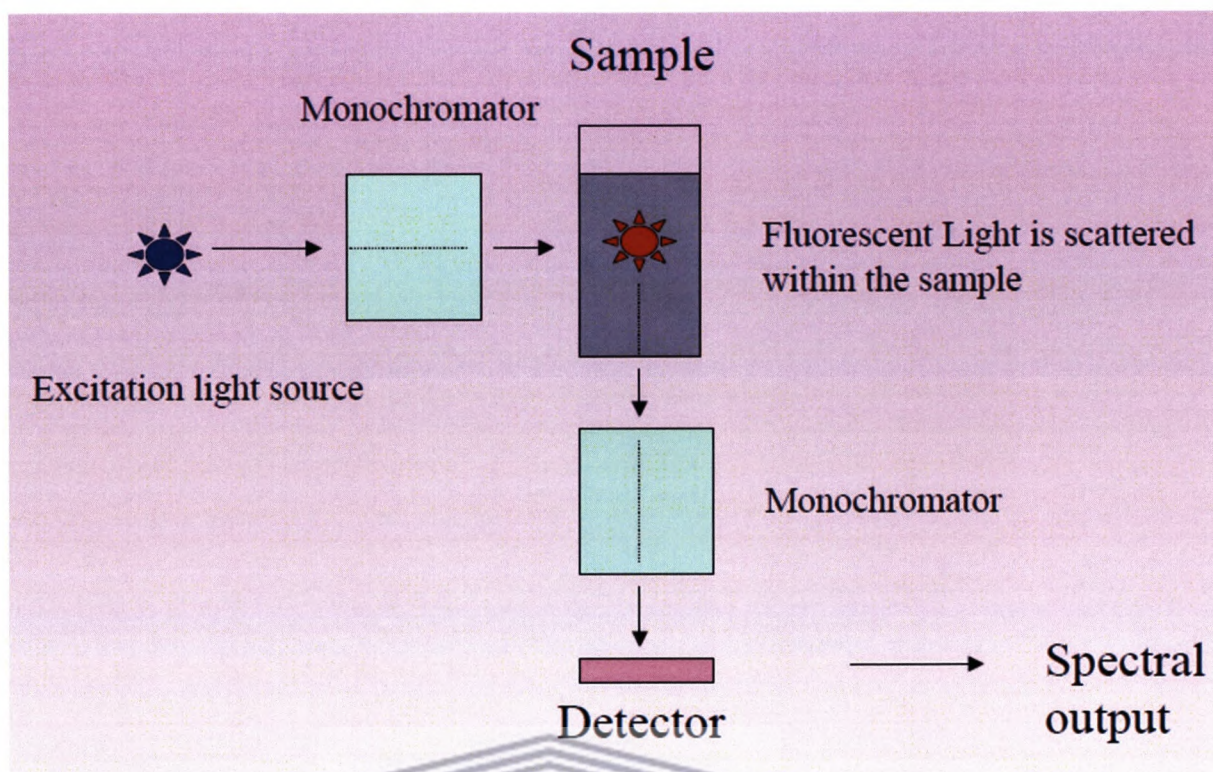


Figure 2.23: Set-up for fluorescence spectroscopy (Lakowicz, 2006).

2.10.3. Time-Correlated Photon Counting (TCSPC)

This technique is based on the fact that from a fluorescence signal, registration of single photons can be timed and this can be done repeatedly with precision. The reference for the timing is the corresponding excitation pulse. Excitation is carried out with pulsed laser (MHz repetition rate). Hence, its principle is based on the measurement of time interval between excitation and detection of photon. In principle this is done by initially measuring time difference between the photon event and the corresponding excitation. For this purpose both signals are converted to electric signals. For the fluorescence photon this is done via the single photon detector. There are several detectors that can be used such as photomultiplier tube (PMT), multi channel plate (MCP) or a single photon avalanche photodiode (SPAD) can be used.

Any of the detectors can be used provided that its probability of registering more than one photon per cycle is low. This is to guarantee that the histogram of photon arrivals represents the time decay one would have obtained from a single shot time-resolved analog recording (Lakowicz, 2006).

For the excitation pulse it may be done via another detector if there is no electrical sync signal supplied by the laser. It is important to note that all conversion to electrical pulses must provide a digital timing result which must accurate as possible. The histogram is collected in a block of memory, where one memory cell holds the photon counts for one corresponding time bin (Lakowicz, 2006). These time bins are often referred to as time channels. Each possible timing value must be corresponded to one memory cell or histogram channel, and this is achieved by addressing the timing with the histogram memory. Following that the addressed histogram cell is incremented. After collection of sufficient counts the histogram memory can be read out. And its data can be used for display and e.g. fluorescence lifetime calculation. The results obtained are a plot counts versus time difference in a histogram. The diagrams below illustrate how the histogram is formed over multiple cycles (Lakowicz, 2006).

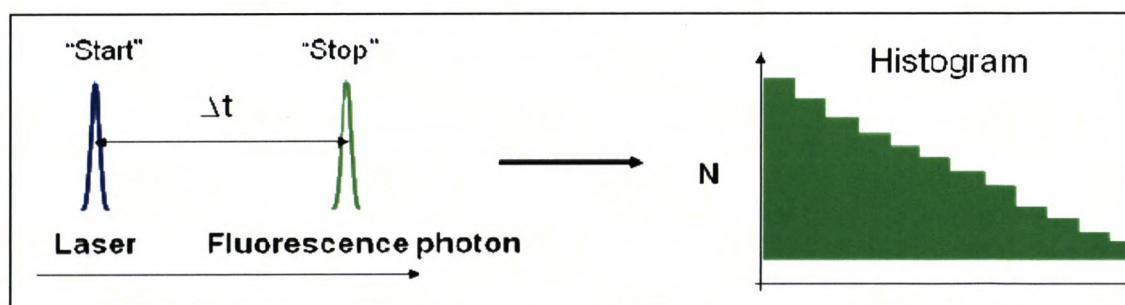
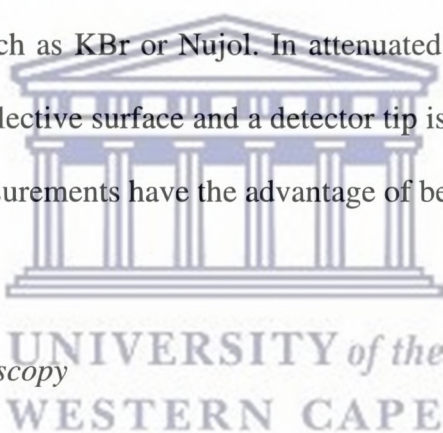


Figure 2.24: Measurement of time interval between excitation and detection of photon and formation of the histogram (Lakowicz, 2006).

2.10.4. Vibrational Spectroscopy

2.10.4.1. Fourier-Transform Infrared Spectroscopy

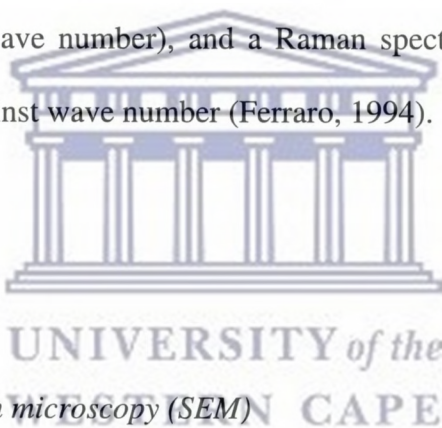
FTIR provides information about vibrational absorption of the molecule revealing the functional groups present in the molecule (Skoog *et al.*, 2004). FTIR spectroscopy uses IR beam from the spectrometer is directed onto the sample at an angle greater than the critical angle, so that the infrared light undergoes internal reflection. At each point of internal reflection an evanescent wave is produced, which is absorbed by the sample in direct contact with the reflective surface (Skoog *et al.*, 2004). In this work, attenuated total reflectance was used to acquire FTIR spectra of pure samples without the need for a matrix such as KBr or Nujol. In attenuated total reflectance FTIR, the sample is placed on a reflective surface and a detector tip is screwed down into contact with the sample. Its measurements have the advantage of being easy to perform.



2.10.4.2. Raman Spectroscopy

Raman spectroscopy is a very useful technique for material identification and is used for both quantitative and qualitative analysis (Ferraro, 1994). It is based on inelastic scattering of monochromatic light, usually from a laser source and it involves illuminating a sample with monochromatic light and using a spectrometer to examine light scattered by the sample. The inelastic scattering is when the frequency of photons in monochromatic light changes upon interaction with a sample. Photons of the laser light are absorbed by the material and then re-emitted. Frequency of the re-emitted photons is shifted up or down in comparison with original monochromatic frequency, which is called the Raman effect (Ferraro, 1994).

The Raman effect is normally an optical phenomenon observed when a small portion (approximately 1 in 10^7 photons) of light incident on a sample surface is scattered inelastically (Ferraro, 1994). This light is scattered at a wavelength different to the one incident on the molecule and this difference in wavelength is called the Raman Shift. The Raman scattering takes place when an incident light is absorbed by an electron, promoting it to a virtual state. This distorts the electronics of a molecule momentarily, causing the bond to form a temporary dipole and then the bond then vibrates back to its ground state, causing the dipole to vanish (Ferraro, 1994). The Raman shift results from a change in the wavelength of the emitted light relative to the wavelength of absorption (change in wave number), and a Raman spectrum plots versus emission (scattering) intensity against wave number (Ferraro, 1994).



2.11. Microscopy

2.11.1. Scanning electron microscopy (SEM)

SEM is a useful tool to provide images of external morphology of the polymer. SEM utilizes a focused beam of high-energy electrons generated from a cathode filament that systematically scans across the surface of a specimen (Atkins, 2002). This electron beam is generated within an electron gun, accelerated by a high voltage and formed into a fine probe by electromagnetic lenses filament are accelerated towards an anode which contains sample material and focused through one or two magnetic, condenser lenses to generate a highly focused electron beam with a very fine focal spot of 0.4 – 5 nm (Mavundla, 2010). SEM uses pairs of deflector plates or scanning coils that form part of the lenses of microscope and the first lens that influences the beam is the

condenser lens, which causes the beam to converge and pass through a focal point just above a condenser aperture. The final lens demagnification determines the diameter of the spot size of the electron beam at the specimen, which in turn determines the specimen resolution. The electron beam is deflected horizontally or vertically across the sample so that it scans a rectangular area of the sample surface in a raster-like manner. The interaction of the highly accelerated electron beam with atoms in the surface of the material results in the emission and scattering of electrons which are picked up by a detector leading to the morphological image. In this work, the SEM technique was employed for investigation of the morphology of the polymers.

2.11.2. Transmission electron microscopy (TEM)

TEM is a microscopic technique operational which is used to provide image electronic structure of the material when a beam of electrons is transmitted through an ultra thin specimen, interacting with the sample as it passes through. The electrons behave as a light source with much lower wavelengths making it possible to obtain resolutions a thousand times better than using light microscopes, owing to the small de Broglie wavelength of the electrons. Some of the electrons are scattered and disappear from the beam, whereas at the bottom of the microscope the unscattered electrons hit a fluorescent screen, which gives rise to a "shadow image" of the sample depending on the density of the material present (Kenkel *et al.*, 1994). The image is created by the interaction of the electrons with the sample which is magnified and focused onto an imaging device. The TEM is one of the important major analysis methods in physical and biological sciences to exam fine details, even as small as a single column of atoms, which is tens of thousands times smaller than the smallest resolvable object in a

light microscope (Kenkel *et al.*, 1994). Hence, in this study the TEM technique was used for morphological characterization of the synthesized polymers.

2.12. Four point probe conductivity measurements

A four point probe system can be used to measure the resistance of a material, in order to determine the resistivity of a thin film. It is made up of four point probes, which are thin collinear wires made from tungsten. These probes interact with the film, and during this interaction current (I) is passed between the two outer probes, while the voltage (V) is measured in between the two inner probes (Aurelio, 2007).

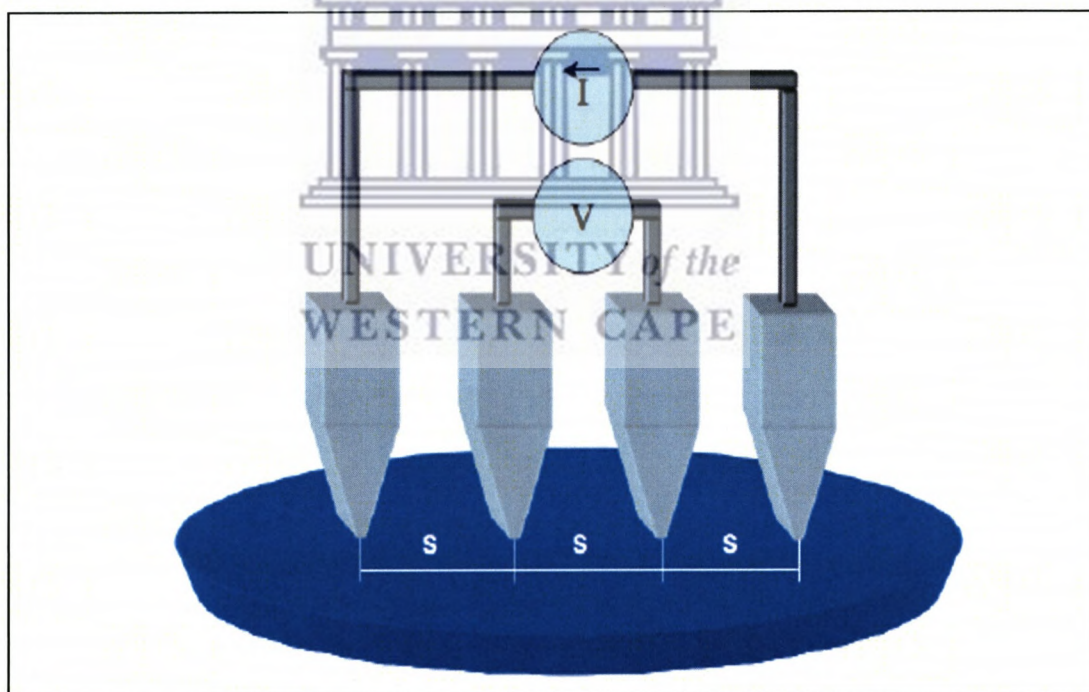


Figure 2.25: Four point probes which have equal interspaces (s) (Aurelio, 2007).

The specific resistivity (ρ) is a measure of how strongly a material opposes the flow of current hence when it is low the material readily allows the movement of electric

charge (Equation 2.43 and 2.44). Its reciprocal is specific conductivity (σ) which is a measure of the materials ability to conduct an electric current.

$$\rho = RA/t \quad [2.43]$$

$$\sigma = 1/\rho \quad [2.44]$$

where ρ is its resistivity, R is the sample resistance, A is the cross-sectional area, t is the thickness, and σ is the conductivity (Aurelio,2007)..

2.13. Conclusion

In conclusion, this chapter presented a review of relevant literature related to electrochemiluminescence. The chapter initially briefly introduces the basic concepts of luminescence and electrochemiluminescence followed by citing relevant literature related to Ru complex luminophore. Furthermore, few important key concepts regarding modification of conducting polymers which will be used to modify the electrode for ECL studies were also introduced. The review showed that ECL can be generated into pathways by annihilation and coreactant pathways and Ru complex showed to played vital role in ECL generation. It can be incorporated with conducting polymers for enhance of ECL properties. The conducting polymers of interest were polyaniline and its derivatives due to the electro-activity to interact with the ruthenium complex for enhancement of the photoluminescence and electrochemiluminescence properties.

2.14. References

de Albuquerque, J.E., Mattoso, L.H.C., Faria, R.M., Masters, J.G., MacDiarmid, A.G., Study of the interconversion of polyaniline oxidation states by optical absorption spectroscopy. *Synthetic Metals* (2004) 146, 1-10.

Aurelio, D. Development of low roughness, low resistance bottom electrodes for tunnel junction devices, Msc thesis, Technical University of Lisbon, (2007).

Atkins, P. W., Physical Chemistry, 7th ed, Oxford University Press: Oxford, (2002).

Bard, A. J. Introduction. In *Electrogenerated Chemiluminescence*, Bard, A.J. Ed; Marcel Dekker. Inc: New York, (2004).

Bard, A. J., Faulkner, L.R. Electrochemical methods. Fundamentals and applications, 2nd ed, John Wiley & Sons Inc: New York, (2001).

Bhadra, S., Khastgir, D., Singha, N. K., Lee, J. H., Progress in preparation, processing and applications of polyaniline, *Progress in Polymer Science* (2009) 34 , 783-810.

Bockris, J.O.M., Reddy, A.K.N, Gamboa-Aldeco, M. Modern Electrochemistry, Fundamentals of Electrode Processes 2nd ed , Kluwer Academic/Plenum: New York, (2000).

Bolto, B., McNeill, R., Weiss, D. Electronic Conduction in Polymers. III. Electronic Properties of Polypyrrole", *Australian Journal of Chemistry* (1963) 16, 1090-1103.

Bott, A.W. Electrochemistry of semiconductor, *Current separation*, (1998) 17, 87-91.

Campbell, A.K. Chemiluminescence: Principles and Applications in Biology and Medicine, VCH Verlagsgesellschaft, Ellis Horwood, Chichester: England, (1988).

Chandross, E.A., Sonntag, F.I. Normal chemiluminescent electron transfer reaction *Journal of the American Chemical Society* (1964) 15, 155-196

Chiang, C. K., Druy., M, A., Gau, S. C., Heeger, A. J., Louis, E. J., MacDiarmid, A. G., Park Y. W., Shirakawa, H. Synthesis of highly conducting films of derivatives of polyacetylene, (CH)_x, *Journal of the American Chemical Society*, (1978) 100, 1013-1015.

Cosgrave, L., Devocelle, M., Forster, R. J., Keyes, T. E. Multimodal cell imaging by ruthenium polypyridyl labelled cell penetrating peptides, *Chemical Communications*, (2010) 46, 103 -105.

Daintith, J., Martin, E., *Oxford Dictionary of Science*, 5th ed, Oxford University Press: New York , (2005).

Dodeigne, C., Thunus, L., Lejeune, R. Chemiluminescence as diagnostic tool, A review, *Talanta* (2000) 51, 415–439.

Dong, B., He, B. L., Xu, C.L., Li, H. L., Preparation and electrochemical characterization of polyaniline/multi-walled carbon nanotubes composites for supercapacitor. *Materials Science and Engineering* (2007) 143,7-13.

Dufford, R. T., Nightingale, D., Gaddum, L.W. Luminescence of Grignard compounds in the electromagnetic fields, *Journal of the American Chemical Society* (1927) 49, 1858-1864.

Epstein, A. J., Ginder, J. M., Zuo, F., Bigelow, R. W., Woo, H., Tanner, D. B., Richter, A. F., Huang, W. and MacDiarmid, A. G., "Insulator-to-metal transition in polyaniline", *Synthetic Metals* (1987) 18,303-309.

Eskola, J., Mäkinen, P., Oksa, L., Loikas, K., Nauma, M., Jiang Q., Håkansson, M., Suomi, J., Kulmala, S. Competitive Immunoassay by hot electron-induced electrochemiluminescence detection and using a semiautomatic electrochemiluminometer, *Journal of Luminescence* (2006) 118,238- 244.

Ferraro, J. R. Introduction to Raman Spectroscopy, Academic Press: New York, (1994).

Forster, R. J., Bertoncello, P., Keyes, T. E. Electrogenerated chemiluminescence, *Annual Review of Analytical Chemistry* (2009) 2 ,18.1–18.27

Forster, R.J., Hogan C.F., Electrochemiluminescent MetallopolymerCoatings: Combined Light and Current Detection Flow Injection Analysis. *Analytical Chemistry*, (2000)72 , 5576-5582.

Forster, R. J., Keyes, T. E., Vos, J. Interfacial supramolecular assemblies. John Wiley and Sons: England,(2003).

Gfroerer, T. H., Mayers, R.A. (ed), Encyclopedia of analytical chemistry: photoluminescence in analysis of surfaces and interfaces, *John Wiley & Sons Ltd, Chichester* (2000) 12, 9209–9231.

Green, A. G., Woodhead, A. E., "CXVII-Aniline-Black and Allied Compounds, *Journal of the Chemistry Society Transitions* (1912) 101, 1117.

Harvey, E. N., A History of Luminescence; American Philosophical Society: Philadelphia, (1957).

Heeger, A. "Semiconducting and metallic polymers: the fourth generation of polymeric materials", *Synthetic Metals* (2001) 125 , 23-42.

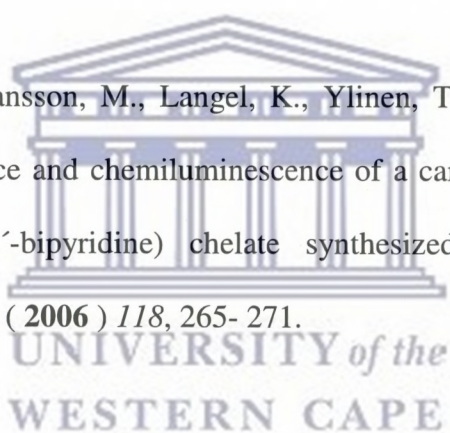
Hercules, D.M., Chemiluminescence resulting from electrochemically generated species , *Science* (1964) 145, 808.

Huang, W. S., MacDiarmid, A. G. Optical properties of polyaniline, *Polymer* (1993) 34, 1833-1845.

Ivey F., Electroluminescence and Related Effects; Academic Press: New York, (1963).

Jansen ,E.H.J.M., Zomer, G., Van, P.C. Chemiluminescence Immunoassays in Veterinary and Food Analysis, In: *Luminescence Techniques in Chemical and Biochemical Analysis, Practical Spectroscopy* ,SerieBaeyens, W.R.G., De-Keukeleire D., Korkidis, K. Eds; Marcel Dekker: New York, (1991).

Jiang, Q., Sun, S., Håkansson, M., Langel, K., Ylinen, T., Suomi, J., Kulmala, S., Electrochemiluminescence and chemiluminescence of a carboxylic acid derivative of Ruthenium(II) Tris-(2,2'-bipyridine) chelate synthesized for labeling purposes, *Journal of Luminescence* (2006) 118, 265- 271.



Jiles, D. Introduction to the Electronic Properties of Materials, Chapman & Hall: London, (1994).

Kapturkiewicz, A. Electron transfer and spin up-conversion processes In *Electrogenerated Chemiluminescence*, Bard, A.J. Ed.; Marcel Dekker. Inc: New York, (2004), 163–211.

Kenkel, J., Analytical Chemistry for Technicians, Lewis Publishers: Boca Raton, United States of America, (1994).

Knight, A. W. A review of recent trends in analytical applications of electrogenerated chemiluminescence, *Trends in analytical chemistry* (1999) 18, 47-62

Kohlman, R., Zibold, S. A., Tanner, D. B., Ihas, C. G., Ishiguro, T., Min, Y. G., MacDiarmid A. G. Epstein A. *Journal of Physical Review Letters* (1997) 78 , 3915-3918.

Kolthoff, I.M., Lingane, J.J. *Polarography*, 2nd ed., Interscience: New York, (1952).

Lakowicz, J. R., Principles of Fluorescence Spectroscopy, 3rd ed, Springer, (2006).

Lakowicz, J. R., Long-Lifetime Metal-Ligand Complexes; Principles of Fluorescence Spectroscopy; Plenum Publisher: New York, (1999).

Lei, J., Ju, H. Fundamentals and bioanalytical applications of functional quantum dots as electrogenerated emitters of chemiluminescence, *Trends in Analytical Chemistry* (2011), In press.

Letheby, H. On the production of a Blue Substance by the electrolysis of Sulphate of Aniline, *Journal of the Chemistry Society* (1862) 15, 161.

Li, D., Huang, J., Kaner, R. B. Polyaniline Nanofibers: A Unique Polymer Nanostructure for Versatile Application", *Accounts of Chemical Research* (2009) 42, 135-145.

Lu, F. L., Wudi, F., Nowak, M., Heeger, A.J. Phenyl-capped octaaniline (COA): An excellent model for polyaniline, *Journal of the American Chemistry Society* (1986) 108, 8311 - 8313.

Lu, Y. Preparation of novel polypyridyl ruthenium complex polymers with high sensitivity for electrogenerated chemiluminescence via copolymerization, *Photochemical Photobiological Science* (2010) 9, 392–397.

Malog, J.T. ECL Theory Mass transfer and homogenous kinetics In *Electrogenerated Chemiluminescence*, Bard, A.J Ed.; Marcel Dekker. Inc: New York, (2004) , 101–162.

Masdarolomoor, F., Novel nanostructured conducting polymer systems based on sulfonated polyaniline, PhD Thesis, Department of Chemistry, University of Wollongong (2006).

Maser, W. K., Sainz, R., Martínez, M. T., Benito, A. M. Electroactive polymer-carbon nanotube composites: smart organic materials for optoelectronic applications, *Contributions to Science*, (2008) 4, 187-192.

Miao, W., Choi, J. Coreactants In *Electrogenerated Chemiluminescence*, Bard, A.J. Ed.; Marcel Dekker. Inc: New York, (2004); 212-217.

Monk, P.M.S., *Fundamentals of Electroanalytical Chemistry*, John Wiley & Sons Ltd.: England, (2001).

Moretto, L. M., Kohls, T., Badocco, D., Pastore, P., Sojic, N., Ugo, P. J. *Electroanalytical Chemistry* (2010) 640, 35-41.

Morrin ,A. Characterisation and optimisation of an amperometric biosensor for use in electrochemical immunosensing. Report for Transfer to PhD Register. Dublin City University, Ireland (2002).

Nicolas, D.D. Poncin, E.F. Polyaniline as a new sensitive layer for gas sensors, *Analytica Chimica Acta* (2003) 475, 1-15.

O'Reilly, E. Conjugated metallopolymer systems for electrochemiluminescence enhancement; new approaches and materials, PhD thesis, Dublin City University, Ireland (2008).

Preston, J. P., Nieman, T. A. An electrogenerated chemiluminescence probe and its application utilizing tris(2,2'-bipyridyl)ruthenium(II) and luminol chemiluminescence without a flowing stream, *Analytical Chemistry* (1996) 68 ,966-970.

Richards, T.C., Bard, A.J. Electrogenated chemiluminescence. emission from sodium 9,10-diphenylanthracene-2-sulfonate, thianthrenecarboxylic acids, and chlorpromazine in aqueous media. *Analytical Chemistry* (1995) 67, 3140–3147.

Richter, M. M. Electrochemiluminescence (ECL), *Chemical Reviews* (2004) 104, 3003-3036.

Roda, A., Pasini P., Guardigli M., Baraldini, M., Musiani, M., Mirasoli, M., Fresenius J. *Analytical Chemistry* (2000) 366, 752.

Santhanam, K.S.V., Bard, A.J. Chemiluminescence of electrogenerated 9,10 diphenylanthracene anion radical *American Journal of Chemical Society* (1965) 87, 139-140.



Shimano, J.Y., MacDiarmid, A.G. Polyaniline, a dynamic block copolymer: key to attaining its intrinsic conductivity, *Synthetic Metals* (2001) 123, 251-262.

Shirakawa, Y.W.H. Synthesis of highly conducting films of derivatives of polyacetylene, (CH)_x. *Journal of American Chemical Society* (1978) 100, 1013-1015.

Skoog, D. A., West, D. M., Holler, F. J. Fundamentals of Analytical Chemistry, 8th ed, Saunders College Publishing, Fort Worth:Canada,(1992).

Spinks, G.M., Innis, P.C., Lewis, T.W., Kane, Maguire, L.A.P., Wallace, G.G. Current state and Future Directions of Research and Development in Conducting Polymers, *Materials Forum*, (2000) 24, 125-166.

Stafström, S., Brédas, J.L., Epstein, A.J., Woo, H.S., Tanner, D.B., Huang, W.S., MacDiarmid, A.G., Polaron lattice in highly conducting polyaniline: Theoretical and optical studies. *Physical Review Letters* (1987) 59, 1464 - 1467.

Terje ,A. Skotheim, R.L.E., John R. R. *Handbook of conducting polymers*. 2nd ed. Marcel Dekker : New York ,(1998).

Tokel, N.E., Bard, A. J. Electrogenenerated chemiluminescence. IX. Electrochemistry and emission from systems containing tris(2,2'-bipyridine)ruthenium(II) dichloride, *Journal of the American Chemical Society* (1972) 94, 2862-2863.

Valeur, B., Berberan-Santos, M. N. A brief history of fluorescence and phosphorescence before the emergence of quantum theory, *Journal of Chemical Education* (2011) 88, 731-738.

Valeur, B., *Molecular fluorescence: principles and applications*, WILEY-VCH: Germany,(2002).

Venkatanarayanan, A. Nanomaterials for Electrochemiluminescent Biosensor, PhD Thesis. Dublin City University, Ireland (2010).

Wallace, G. G., Spinks, G. M., Teasdale, P. R. Conductive electroactive polymers : intelligent materials systems.: CRC Press, Boca Raton,(2002).

0

Wallace, G. G., Spinks, G.M., Kane-Maguire, L.A.P , Teasdale, P.R. *Conductive Electroactive Polymers: Intelligent Polymer Systems*, 2nd ed., CRC Press: Boca Raton, (2009) .

Walton, D., Lorimer, P. *Polymers*, 1st ed, Oxford University Press: Oxford, (2000).

Wang, J. Analytical Electrochemistry. 2nd Ed., JohnWiley & Sons Inc: New York, (2000).



Weeks, I., Svenhla, G. Chemiluminescence Immunoassay, Wilson's Comprehensive , *Analytical Chemistry* (1992) 29, Elsevier, Amsterdam.

Zheng, L., Chi, Y., Dong, Y. Lin, J., Wang, B. Electrochemiluminescence of water-soluble carbon nanocrystals released electrochemically from graphite, *Journal of the American Society* (2009) 131, 4564–4565.

Zou, G. Z., Ju, H. X. Electrogenated Chemiluminescence from a CdSe Nanocrystal Film and Its Sensing Application in Aqueous Solution, *Analytical Chemistry* (2004) 76, 6871-6876.

Zotti, G., Cattarin, S., Comisso, N. Electrodeposition of polythiophene, polypyrrole and polyaniline by the cyclic potential sweep method, *Journal Electroanalytical Chemistry* (1988) 235, 259-273.



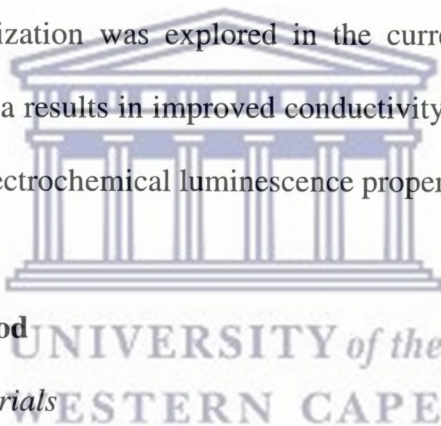
CHAPTER THREE:

ELECTROCHEMICAL SYNTHESIS AND CHARACTERIZATION OF POLY(8-ANILINO-1-NAPHTHALENE SULFONIC ACID)

3.1. Introduction

The previous chapter reviewed the relevant literature concerning ECL and conducting polymers while the current chapter deals with the electrochemical synthesis of undoped PANSA and PANSA modulated with anthracene sulfonic acid (ASA), 1,2-naphthaquinone-4- sulfonic acid (NSA) and carbon nanotubes (CNT). Polyaniline and its derivatives are conducting polymers of the semi-flexible rod polymer family that can be electrically synthesized in the presence of an acidic medium by anionic oxidation of the aniline polymer onto an electrode surface. They are of potential industrial importance because of their electrical conductivity and electroactivity. It is well documented that the method of electrochemical polymerization permits polymers with desired properties to be obtained by simply controlling polymerization conditions (the potential and current values, time of polymerization, material of electrode, etc.) (Shirakawa *et al.*, 1977). The other advantage of this electrochemical polymerization method is the possibility to avoid by-products which can form in the chemical synthesis process. However, one of the major challenging problems is that these polymers are difficult to process because they are insoluble in most common solvents. A common approach used to improve polyaniline's solubility is the introduction of sulfonic acid groups onto the polymer backbone. This can be achieved by treating the polymer with fuming sulfuric acid after polymerization or by polymerizing/copolymerizing substituted aniline derivatives (Bhandari *et al.*, 2011;

Bansal et al., 2009). Recently, Ngece *et al.* (2011) reported on electropolymerization of 8-anilino-1-naphthalene sulfonic acid (ANSA) in the presence of sulfuric acid to produce PANSA, and incorporating the enzyme cytochrome P450-2E1 (CYP2E1) for the detection of TB treatment drugs. ANSA is an aniline monomer which is substituted with naphthalene sulfonic acid, and it can be successfully electropolymerized to PANSA. The PANSA polymers in this study were electrosynthesized via oxidative polymerization of monomer ANSA in the presence of dopants, such as ASA, NSA or CNT. Dopants normally increase the surface area of the conducting polymer which significantly differs from the macroscopic properties. The opportunity of further increasing the solubility and surface area of the conducting polymers by adding bulky dopants during polymerization was explored in the current chapter. The increased solubility and surface area results in improved conductivity of the polymer which is known to enhance photo-electrochemical luminescence properties of polymers.



3.2. Experimental method

3.2.1. Reagents and materials

Electropolymerization was achieved by the use of 8-anilino-1-naphthalene sulfonic acid, ammonium hydrate salt 97% (ANSA) (Sigma-Aldrich) in the polymerization medium, sulphuric acid 95-98% (Fluka). The chemical reagent anthracene was purchased from Sigma-Aldrich. CNT (Cheap tubes INC.USA), and NSA (Fluka)

3.2.2. Apparatus and measurement

All electrochemical experiments were carried out with a BAS 100W integrated automated electrochemical workstation BioAnalytical Systems (BAS, West Lafayette, IN, USA) controlled by a computer and a conventional three-electrode system with a

0.0172cm² gold (Au) disk as the working electrode, a platinum (Pt) wire auxiliary electrode and Ag/AgCl reference electrode with a 3 M NaCl salt bridge solution, all purchased from BAS. All the results obtained using cyclic (CVs) were recorded with a computer interfaced to the electrochemical workstation. The working electrode was cleaned by polishing it in aqueous slurries of 1, 0.3, and 0.05 μ m, alumina powder respectively (Bueheler, IL, USA) and before proceeding to the next alumina powder; the electrode was rinsed with deionized water and sonicated for 10 minutes. The polished electrodes were then scanned in H₂SO₄ (0.1M) in a potential window of 0.025 to 0.12 V with reference to an Ag/AgCl electrode, to ascertain that they were clean bare electrodes.

3.2.3. *Synthesis of Anthracene sulfonic acid (ASA)*

A 10 mL of fuming H₂SO₄ was diluted with 10 mL H₂SO₄ (6 M) the resulting solution was diluted to 100 mL in a volumetric flask. Following that, 50 mL of the above solution was added to a round bottom flask that contained 2 g of anthracene. The contents were heated to boiling in an oil bath at 120 – 140 °C fitted with a condenser and thermometer. The mixture was refluxed for 3 hours with constant shaking to immerse reactants into solution. The mixture was then poured into crushed ice for 20 minutes and the unreacted anthracene was filtered off. Then 10 mL of a 50% NaOH was added to the mixture and put in a refrigerator to crystallize, to form a white anthracene sulfonic salt. The salt was then hydrolysed to form the anthracene sulfonic acid (Klink, 2007).

3.2.4. Electrochemical synthesis of PANSA

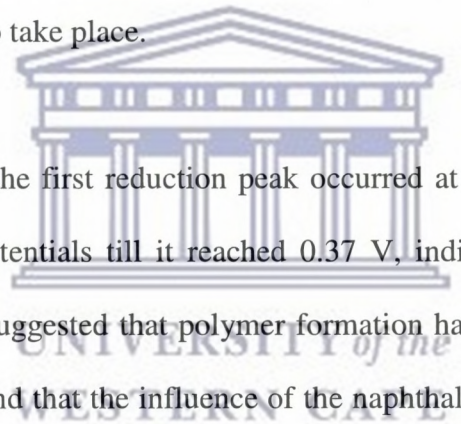
The electropolymerization of ANSA was performed in a cell solution containing 0.01 M of the ANSA monomer in 20 mL 0.5 M H₂SO₄ solution degassed with argon for five minutes. The potential was cycled from -0.3 V to +1.1 V, at a potential scan rate of 0.05 Vs⁻¹. An argon blanket was maintained on top of the cell solution during the polymerization process which was stopped after 10 voltammetric cycle.

3.3. Results and discussion

3.3.1. Polymerization of 8-anilino-1-naphthalene sulfonic acid (ANSA)

Electropolymerization of the monomer 8-anilino-1-naphthalene sulfonic acid (ANSA) was achieved by sweeping the potentials in the range -0.3 to 1.1 V for several cycles at a scan rate of 0.05V.s⁻¹ in an acidic medium, using a gold working electrode and the cyclic voltammograms (CVs) were recorded simultaneously during the synthesis process. It is well documented that an acidic medium (pH < 3) is required for polymerization of aniline to form conducting polymer (Bansal *et al.*, 2009; Masdarolomoor *et al.*, 2008; Cao *et al.*, 1989), so in this study, 0.5 M H₂SO₄ was used as an acidic medium for polymerization of ANSA monomer. The polymerization was carried out with and without dopants as given in Scheme 3.1.

This redox couple was attributed to the electrochemistry of *p*-benzoquinone formed in the polymerization process. Mazeikiene *et al.* (2006) observed similar behaviour of one redox couple in electropolymerization of ANSA in the presence of 0.1 M sulfuric acid and as well as PANI polymerized in the presence and absence of sodium dodecyl sulphate. During the anodic sweep, there was an anodic shift in the polymerization peak potential that is the initial anodic peak appeared at 0.50 V in the first cycle, and shifted to the higher potentials in subsequent cycles, until it reached 0.52 V. From this it can be deduced that oxidation of ANSA on the polymer involved charge transportation across the polymer film, possibly via electron hopping. Hence, making it difficult or being more energetically demanding for oxidation of ANSA on an already deposited film to take place.



In the cathodic sweep, the first reduction peak occurred at 0.40 V for the first cycle and shifted to lower potentials till it reached 0.37 V, indicating that reduction was easier. This behaviour suggested that polymer formation had taken place. From these observations, it was found that the influence of the naphthalene sulphonic acid moiety makes the 8-anilino-1-naphthalene sulfonic acid to be self-limiting upon polymerization; that is, a different behaviour from the electropolymerization of aniline, which is well known to be of a self-accelerating character (Mazeikiene *et al.*, 2006). In addition, naphthalene sulfonic acid moiety of 8-anilino-1-naphthalene sulfonic acid monomer is also known to act as self-dopant which changes the behaviour of the polymer (Bhandari *et al.*, 2011).

3.3.1.2. Effect of dopants during polymerization of ANSA

The effect of dopants on polymerization of ANSA was investigated and presented in Figure 3.1 (b) to (d). Figure 3.1(b) represents the CV of the anthracene sulfonic acid modulated PANSA (PANSA-ASA) which displays one redox couple with well defined oxidation-reduction peaks indicating that the PANSA-ASA film is electroactive (Mirmohseni and Wallace, 2003). The PANSA-ASA voltammogram showed similar behaviour of one redox couple as that of polymerization of undoped PANSA with increase in cathodic-anodic peaks. The anodic peak potentials shifted from 0.43 V for the first polymerization cycle towards higher potentials such as 0.50 V for the last cycle and the cathodic sweep, showed the first reduction peak occurred at 0.43 V for the first cycle and shifted to lower potentials until it reached 0.39 V on the last cycle. This also indicated easier reduction than oxidation redox response. A noticeable increase in the peak currents was observed with the increase in the number of cycles.



UNIVERSITY of the
WESTERN CAPE

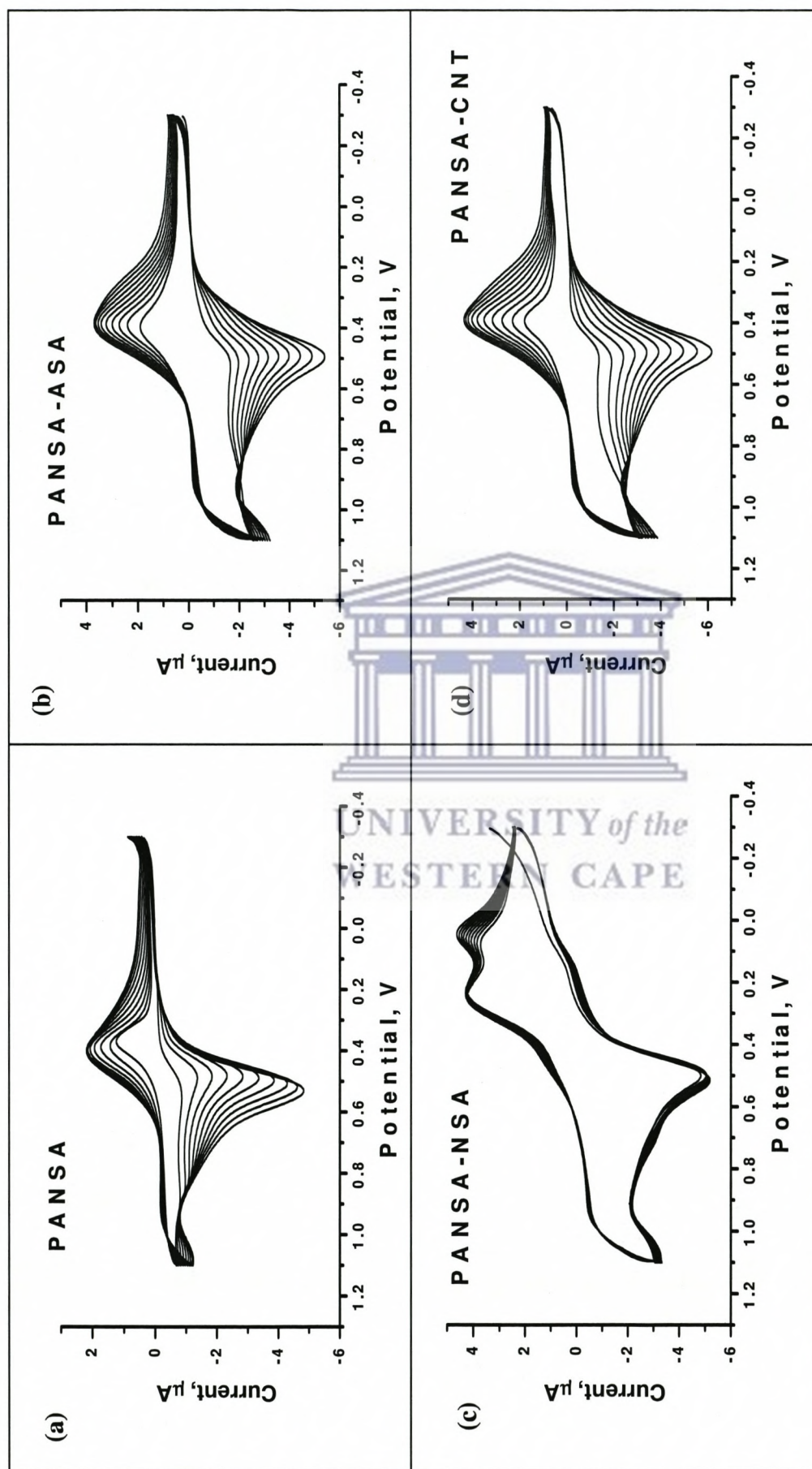


Figure 3.1: The typical cyclic voltammograms recorded during electrochemical synthesis of the (a) undoped PANSA, and doped with (b) Anthracene sulfonic acid (ASA), (c) 1,2-Naphthaquinone-4- sulfonic acid (NSA) and (d) Carbon nanotubes (CNT) respectively

Figure 3.1(c) represents the CV of PANSA doped with 1.2 Naphthaquinone-4- sulfonic acid (PANSA-NSA), the voltammogram showed different behaviour from that of polymerization of undoped PANSA. A very small and insignificant shift of peak potentials was observed as compared to those of undoped PANSA. In addition, change in peak currents was also very small. This can be attributed to difficulty in charge and electron delocalization along polymer chains at the scan rate of 0.05 V.s^{-1} , leading to failure of formation of radical cations (polarons) and dications (bipolarons) which normally initiate polymerization, hence no polymer growth was observed. Hence, further investigation of the whether the dopants could be polymerized was carried out. This was done in order to ascertain that what was formed, was a film of the polymer, not a film resulting from the polymerization of the dopants. The results of these investigations are presented in Figure 3.2 below. When comparing the CV obtained from the polymerization of NSA in $0.5 \text{ M H}_2\text{SO}_4$ at 0.05 Vs^{-1} in (Figure 3.2 (b)) and the voltammogram resulting from electropolymerization of PANSA doped with NSA under the same conditions (Figure 3.1 (c)) the voltammograms are almost identical, confirming the failure of formation of radical cations, during polymerization and resulting in CV which is just a result of cycling the dopant alone. Owing to these observations, it was deduced that in order to polymerize PANSA in the presence of NSA as dopant, electropolymerization must be carried out at a slower scan rate (0.02 V.s^{-1}). This was carried out under normal conditions as stated before, with a slower scan rate of 0.02 V.s^{-1} and successful polymerization took place. The film was characterized and the results are presented in Figure 3.3.

The CV of PANSA doped with carbon nanotubes is given in Figure 3.1(d), it was seen that the oxidation peak observed on the anodic sweep of PANSA-CNT was attributed to the production of the ANSA monomer radical cation in the polymerization process. The shifts of

the voltammetric peak potentials of PANSA–CNT film were very small as compared to those of undoped PANSA although there is a considerable increase in peak current. Such a remarkable enhancement in peak current properties of the PANSA–CNT composite was due the dopant effect or charge-transfer from the quinoid unit of PANSA to the CNT, but the extent of the increase depends on the nature of the substituent and dopant present in the aniline ring (Gajendran and Saraswathi, 2008; Lin and Wu, 2009). Furthermore cyclic voltammograms recorded during polymerization of the carbon nanotubes alone is given in Figure 3.2(c), it was seen that polymerization of CNT alone showed no growth as compared to PANSA-CNT., confirming that it is not possible to polymerize carbon nanotubes alone and polymerization observed in Figure 3.1(d) relies on the presence of the monomer .



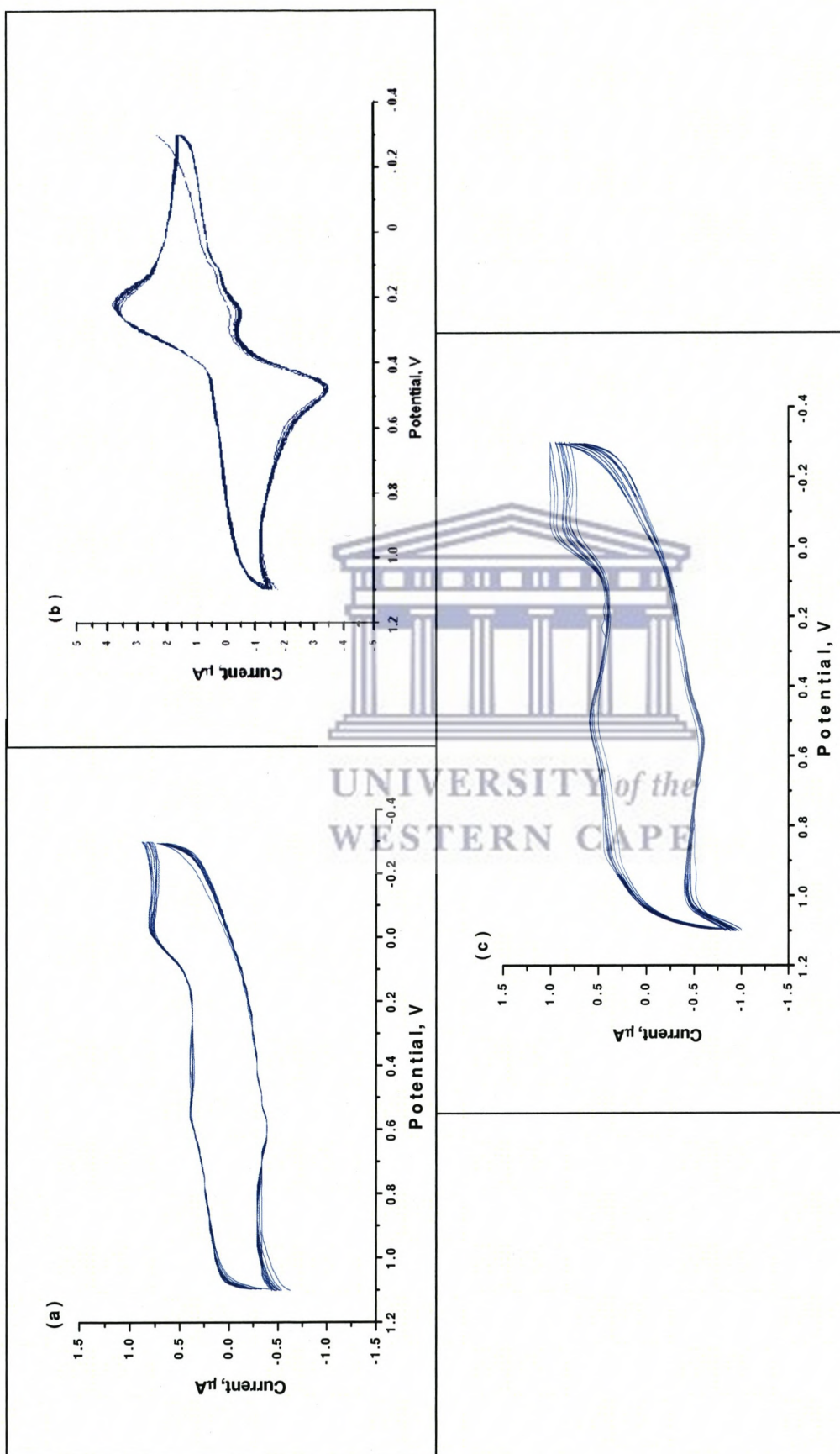
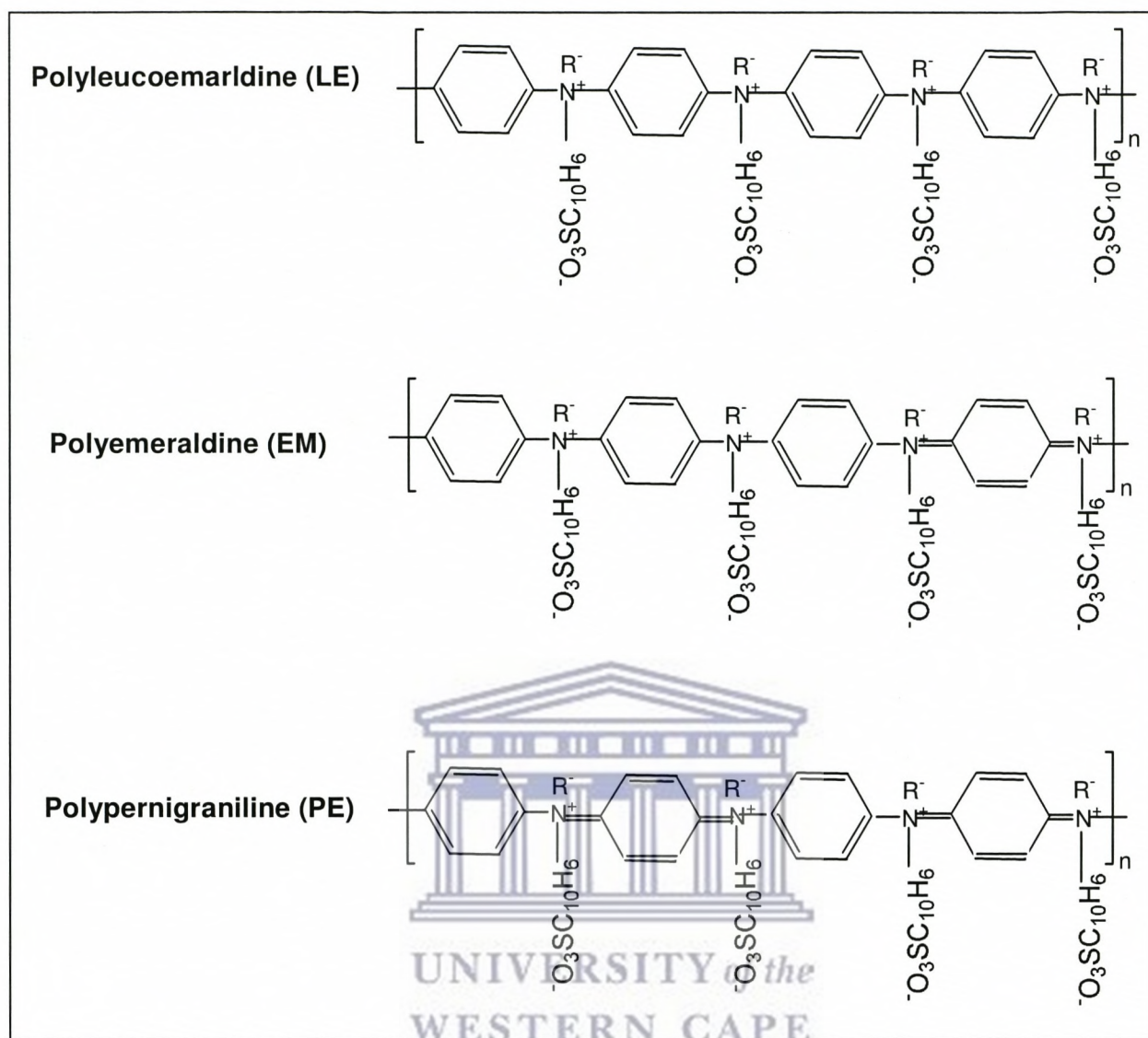


Figure 3.2: The typical cyclic voltammograms recorded during polymerization of the dopants alone (a) Anthracene sulfonic acid, (b) 1,2-Naphthaquinone-4-sulfonic acid and (c) Carbon nanotubes.

3.3.2. Cyclic voltammetric characterization of PANSA

3.3.2.1. Cyclic voltammetric characterization of undoped PANSA

Characterization of the polymer film-coated on the electrode was achieved by placing it in a monomer-free background electrolyte (0.5 M H_2SO_4) and CV's of the film-coated electrode at different scan rates (0.01, 0.02, 0.04, 0.06, and 0.08 Vs^{-1}) were recorded and presented in Figure 3.3. It was seen that three redox couples were observed in all polymers particularly being more conspicuous at the lower scan rates. This evidence of three redox couples was not observed during polymerization due to the high scan rate of 0.05 Vs^{-1} used during the electrochemical synthesis of these polymers. Three redox couples were indicative of three oxidation states in this PANSA as shown in Scheme 3.2. The voltammograms of this polymer showed a similar electrochemistry to that of polyaniline (Wallace *et al.*, 2002). As seen in Scheme 3.2, the most reduced form, commonly known as polyleucoemeraldine, consists of phenylene rings joined together by amine type nitrogens. In fully oxidized PANSA, termed pernigraniline, phenylene rings with benzenoid type sequence of bonds and rings of quinoid type of bonds are present in the ratio 1:1 and are separated by imine nitrogens. In half oxidized PANSA (polyemeraldine) imine and amine nitrogens are in equal numbers but the ratio of benzenoid type rings to the quinoid type ones is 3:1. However in the case of PANSA, at high scan rates these redox couples merged into one redox couple confirming the self-limiting character of PANSA as observed during polymerization (Figure 3.1). Ngece *et al.* (2011) observed two redox peaks in CV characterization of Au/PANSA electrode using 0.1 M, pH 7.4 phosphate buffer as the supporting electrolyte. Bhandari *et al.* (2011) also observed two redox couples using copolymers in different molar ratios of aniline and ANSA in ethanol media corresponding to the formation of polaronic and bipolaronic forms.



Scheme 3.2: Different oxidation states of poly(8-anilino-1-naphthalene sulfonic acid)

In undoped PANSA ((Figure 3.3(a)) showed three oxidation states. The first anodic peak A, was an oxidation peak due to the polyleucoemeraldine radical cation and the redox process A/A' which occurred at approximately (E_{p_a} ; ~ 0.1 V and E_{p_c} ; ~ -0.05 V), corresponded to the transformation of PANSA from the reduced leucoemeraldine (LE) state to the partly oxidized emeraldine state (EM). As PANSA was further oxidized, a transition from (LE) state to pernigraniline (PE) redox state of PANSA occurred, giving rise to the redox couple C/C'

which was observed at approximately 0.60 and 0.05 Vs⁻¹). It is well documented that redox reaction of p-benzoquinone (Iwuoha *et al.*, 1999), gives rise to the redox process B/B', observed at approximately 0.35 and 0.30 V.

3.3.2.2. Cyclic voltammetric characterization of doped PANSA

The effect of ASA dopant (Figure 3.3(b)) on the polymer showed to decrease the peak current of the three redox couples, particularly A'/A redox couple which was obtained to be lower than the one observed in undoped PANSA. This was related to electronic and steric effect caused by the dopant which implies that the presence of ASA dopant in the polymer chain induces some non - planar configurations that decreases the conjugation along the polymer backbone (Bansal *et al.*, 2009). The NSA dopant (Figure 3.3(c)) showed a decrease or flat in peak current of C'/C redox couple due to steric effect of the dopant, however during polymerization at 0.05 Vs⁻¹ scan rate the growth of polymer was not observed as shown in Figure 3.1(c). Figure 3.3(d) shows the effect of doping PANSA with CNT in CV characterization also showed increase in peak current as observed during polymerization, since the addition of CNTs to a polymer improves the electrical and mechanical properties of the neat polymer matrix (Lin and Wu, 2009).

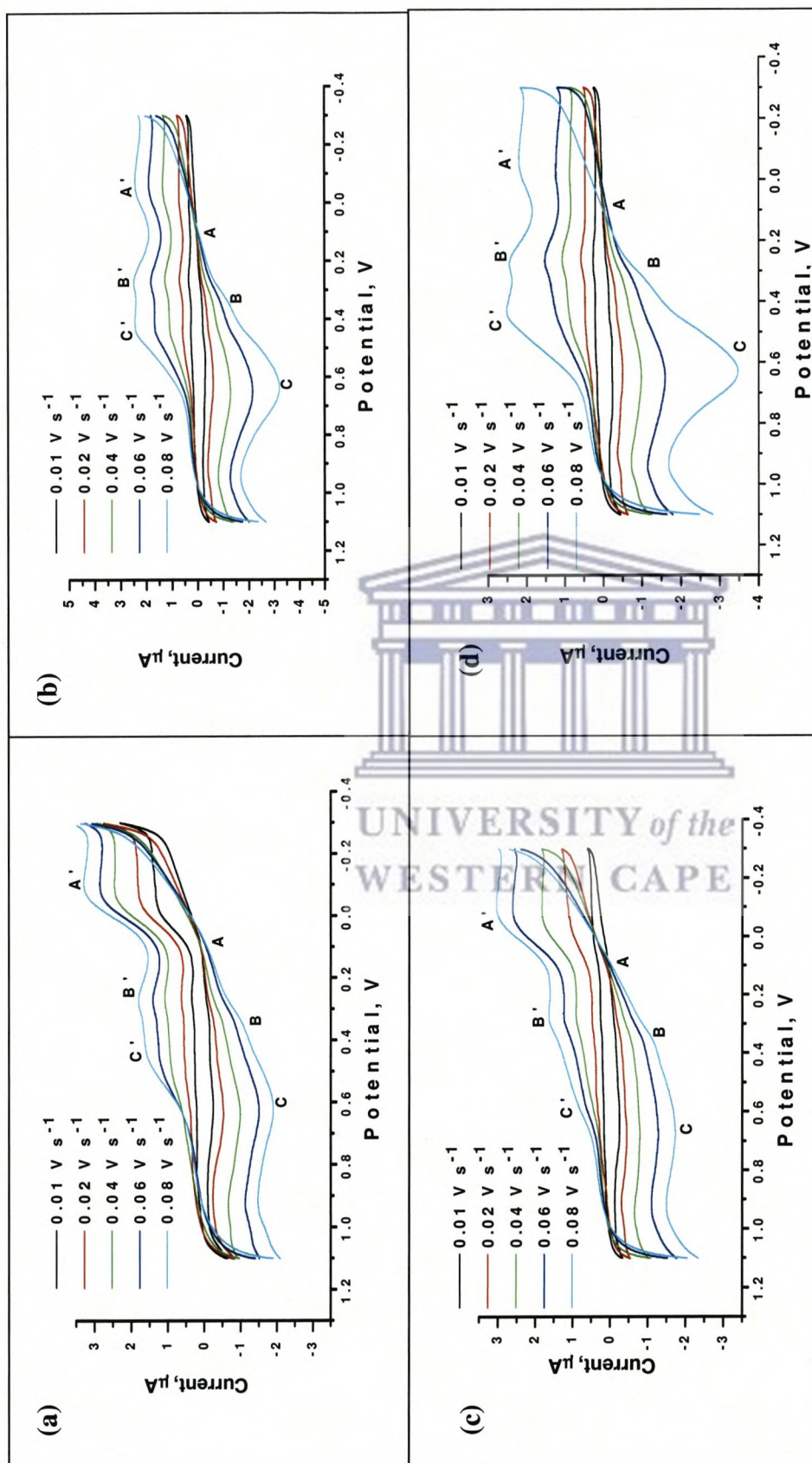


Figure 3.3: The typical cyclic voltammograms at 0.01, 0.02, 0.04, 0.06 and 0.08 V s^{-1} for (a) undoped PANSA, and doped with (b) Anthracene sulfonic acid (ASA), (c) 1,2-Naphthaquinone-4-sulfonic acid (NSA) and (d) Carbon nanotubes (CNT), respectively, in 0.5 M H_2SO_4 at room temperature.

3.3.2.3. Estimation of kinetic parameters for undoped and doped PANSA

The multiscan voltammograms of the undoped and doped forms of the PANSA film in Figure 3.3 above illustrated that, upon increasing the scan rates during the study an increase in the magnitude of the peak currents was observed, which was accompanied by shift of peak potentials towards more negative values. From this, it can be deduced that the peak currents are diffusion controlled and the process of charge transportation is taking place along the polymer chain possibly via an electron hopping process probably through the benzene rings (Brahim *et al.*, 2003). Furthermore, because the peak currents are diffusion controlled, hence the Randel- Sev'cik equation (Bard and Faulkner, 2001), was used to evaluate the diffusion coefficient (D_e) and given in Equation 2.40 (as given in chapter two).

$$I_p = 2.69 \times 10^{-5} n^{3/2} A D_e^{1/2} C v^{1/2} \quad [2.40]$$

Where n represents the number of electrons involved the reaction, $C = \Gamma$ is the surface concentration of the PANSA film (Mol cm^{-2}), v is the scan rate (V s^{-1}), A is the electrode area of the electrode (0.0211 cm^2).

The surface concentration Γ (Mol cm^{-2}) corresponding to this green film was investigated using the Brown Anson model (Brown and Anson, 19770), whereby a plot of I_p against v using Equation 2.38 (as given in chapter two).

$$I_{pa} / v = \frac{n^2 F^2 \Gamma A}{4 RT} \quad [2.38]$$

Where F is the Faraday constant ($96,584 \text{ C/mol}$), R is the universal gas constant ($8.314 \text{ J mol}^{-1} \text{ K}^{-1}$) and T is the temperature of the system (298 K).

As polymerization proceeds, the deposition of polymer on the electrode occurs as scanning cycles proceeds resulting in the formation of a thin film on the surface. Hence the film thickness can be estimated from the voltametric charge that is passed during polymerization (Cooper and Hall, 1993), using Equation 3.1 (Iwuoha *et al.*, 1997; Focke and Wnek, 1988).

$$\frac{I_{pc}}{\nu^{1/2}} = \frac{0.4463 (nF)^{3/2} D_e \Gamma A}{L(RT)^{1/2}} \quad [3.1]$$

Where L represents the polymer thickness.

The diffusion coefficient (D_e) was found 1.68×10^{-8} , 3.42×10^{-8} , 5.47×10^{-9} and 2.19×10^{-8} cm^2s^{-1} for undoped PANSA, PANSA-ASA, PANSA-NSA and PANSA-CNT, respectively (Table 3.1). The value indicates that the movement of electrons along the polymer chain was averagely fast and agrees well with other diffusion coefficient values reported for doped polyaniline (Michira *et al.*, 2007; Iwuoha *et al.*, 1997). However, D_e PANSA-NSA was found to be small as compared to undoped PANSA. Surface concentration (Γ) was found to be 1.06×10^{-9} , 2.11×10^{-9} and 1.69×10^{-9} mol cm^{-2} for undoped PANSA, PANSA-ASA and PANSA-CNT, respectively (Table 3.1). The surface concentration of PANSA-NSA was found to be the same as undoped PANSA. Form these observations, it was seen that the surface concentration in the range of 10^{-9} mol cm^{-2} was consistent with the value 6.27×10^{-9} mol cm^{-2} that was reported by Michira *et al.*, (2007), of in studies polyaniline.

The thickness of the undoped PANSA was calculated to be 14 nm, which was very close to the value reported by Iwuoha *et al.* (1997), where the thickness of polyaniline was estimated to be 16 nm. The study also showed that introduction of the dopants ASA and CNT increased the film thickness by 39 and 23.5 nm, respectively. However, there was no increase in film thickness of PANSA doped with NSA.

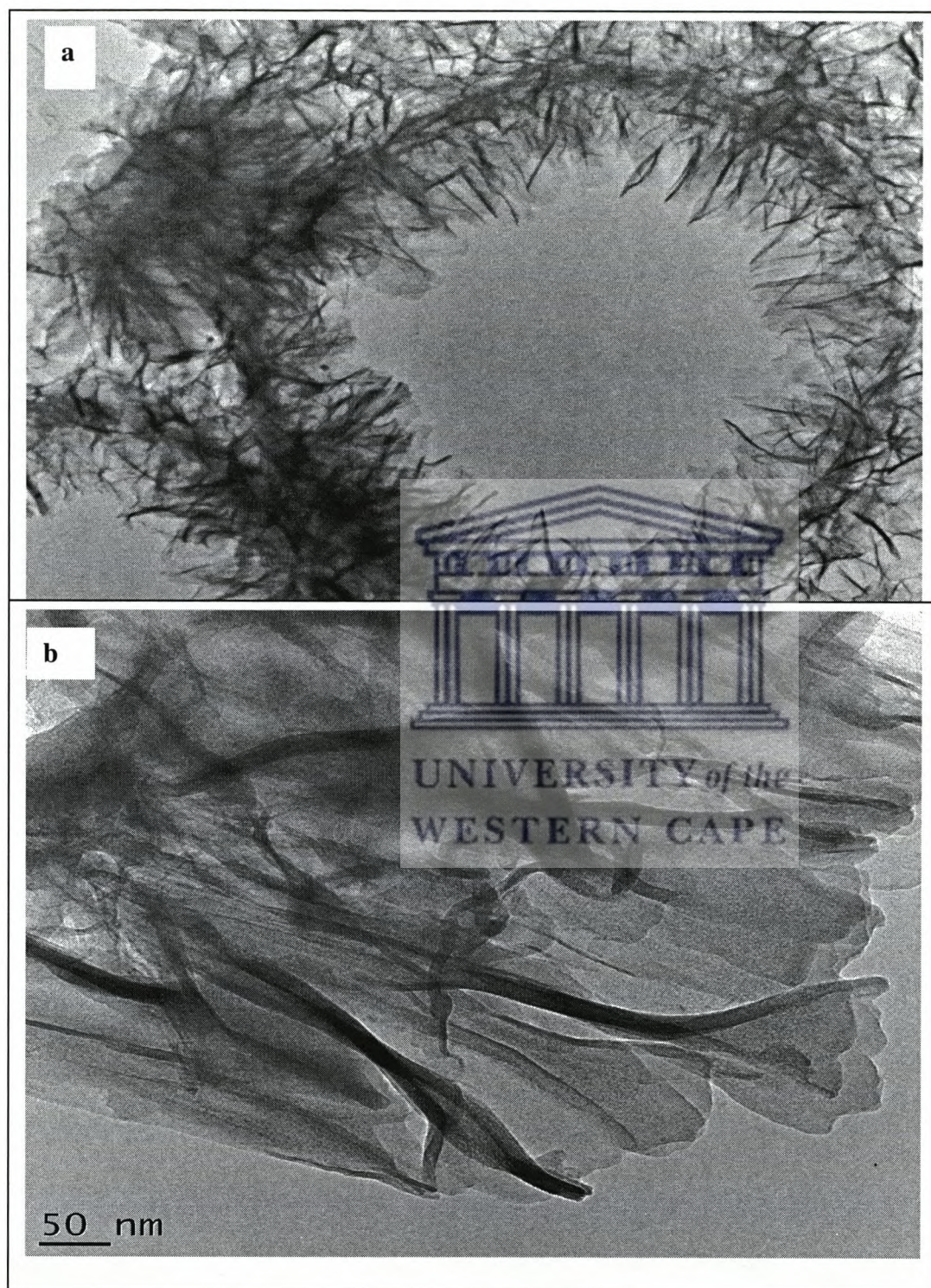
Table 3.1: Kinetic parameters of undoped and doped polymers

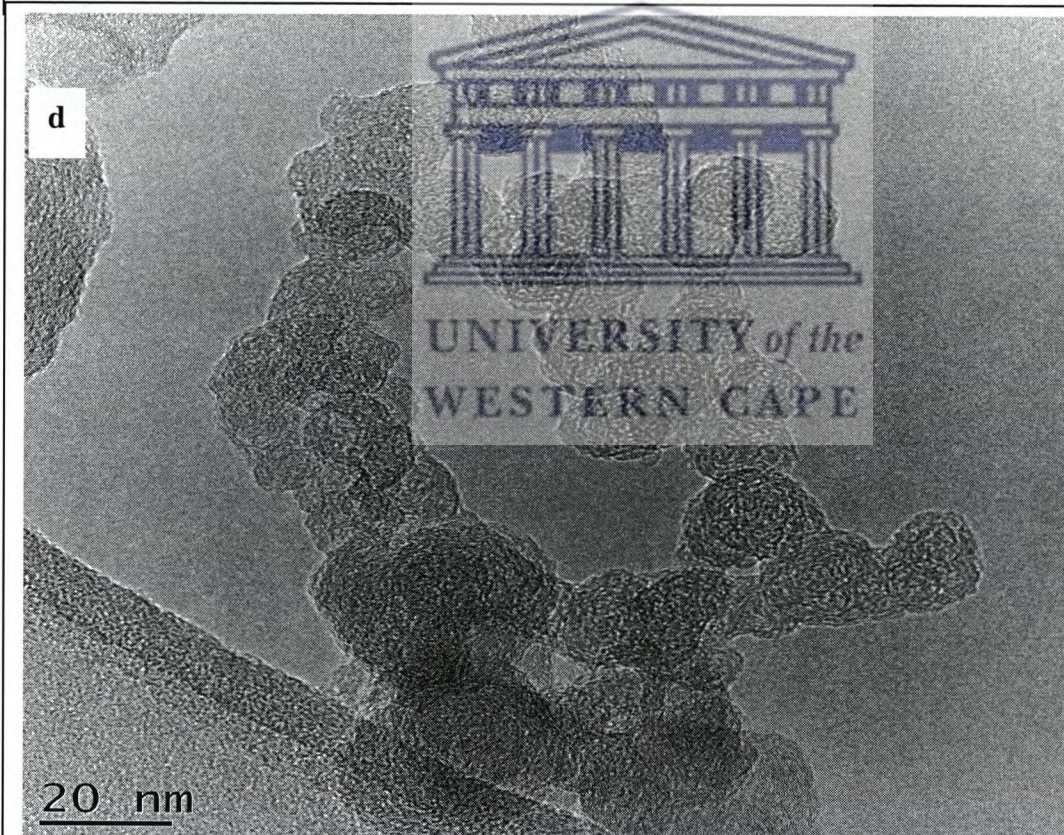
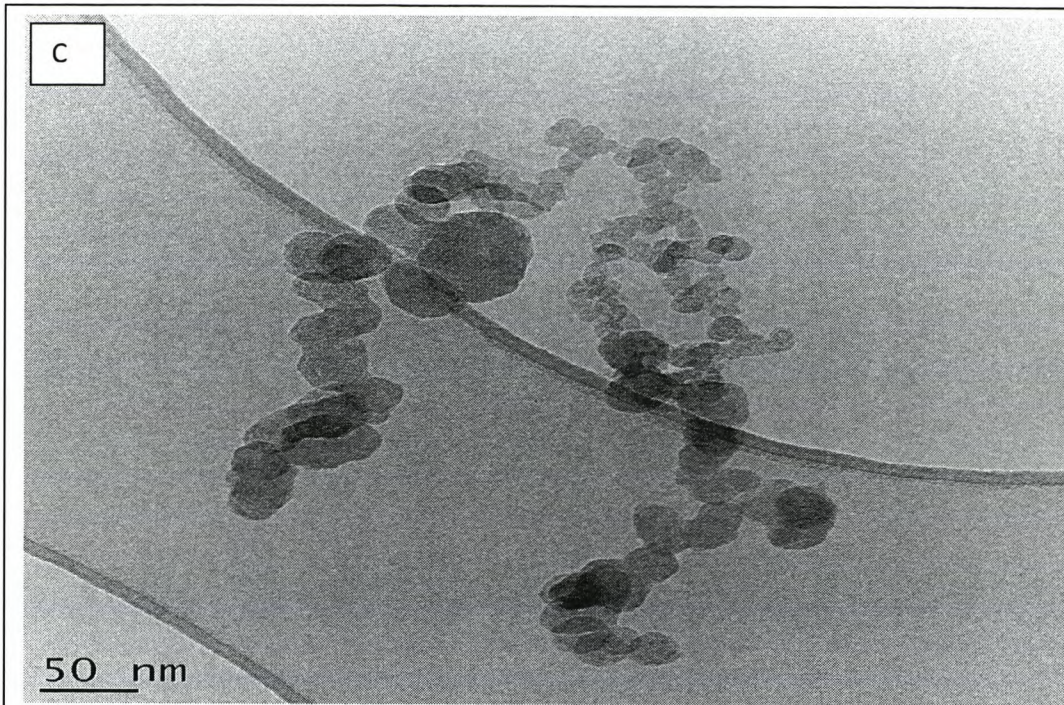
Polymer	I^* (mol cm ⁻²)	D_e (cm ² s ⁻¹)	L (nm)
PANSA	1.06 x 10 ⁻⁹	1.68 x 10 ⁻⁸	14
PANSA-ASA	2.11 x 10 ⁻⁹	3.42 x 10 ⁻⁸	39
PANSA-NSA	1.06 x 10 ⁻⁹	5.47 x 10 ⁻⁹	8.0
PANSA-CNT	1.69 x 10 ⁻⁹	2.19 x 10 ⁻⁸	23.5
POLYANILINE (Michira <i>et al.</i> , 2007)	6.27 x 10 ⁻⁹	6.41 x 10 ⁻⁷	-
POLYANILINE (Iwuoha <i>et al.</i> , 1997)	1.89 x 10 ⁻⁷	6.42 x 10 ⁻⁸	16

3.3.3. TEM characterization of PANSA

The electronic morphology and structure of PANSA-ASA and PANSA-NSA were investigated using TEM. It is generally agreed upon that morphology of the resultant polymers can be as diverse as there are many different polymer chains, dopant structures synthetic routes and conditions (Wan *et al.*, 2003). Figure 3.4 (a) and (b) present the TEM micrograph of PANSA-ASA and shows an intertwinement of tubings which aggregate into a ring with a mixture of tubings and plastic sheets (Figure 3.4a). These plastic sheets were observed in between the tubings, and they result from the presence of the dopant ASA in the polymer (Figure 3.4b). The results of PANSA-NSA are represented in Figure 3.4(c)-(d) and they show that the PANSA-NSA is made of spherical polymers which agglomerate into bigger spheres, causing circular aggregations which are observed in Figure 3.4(c) and (e). Higher magnification shows that these circular aggregations are real polymeric long coiled tubes. The polymer coils may be attributed to the multi scans which are carried out during

electropolymerization, which result in repetition of deposition of the polymer film, causing coils.





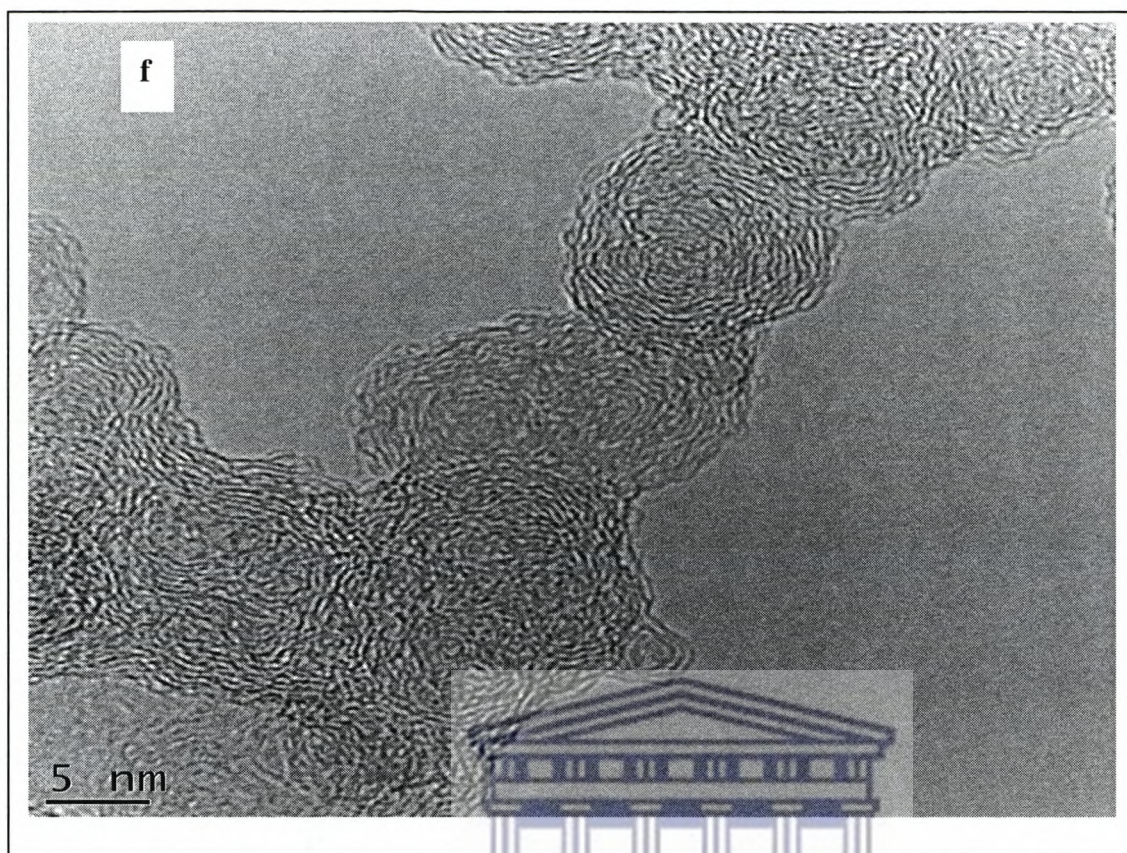
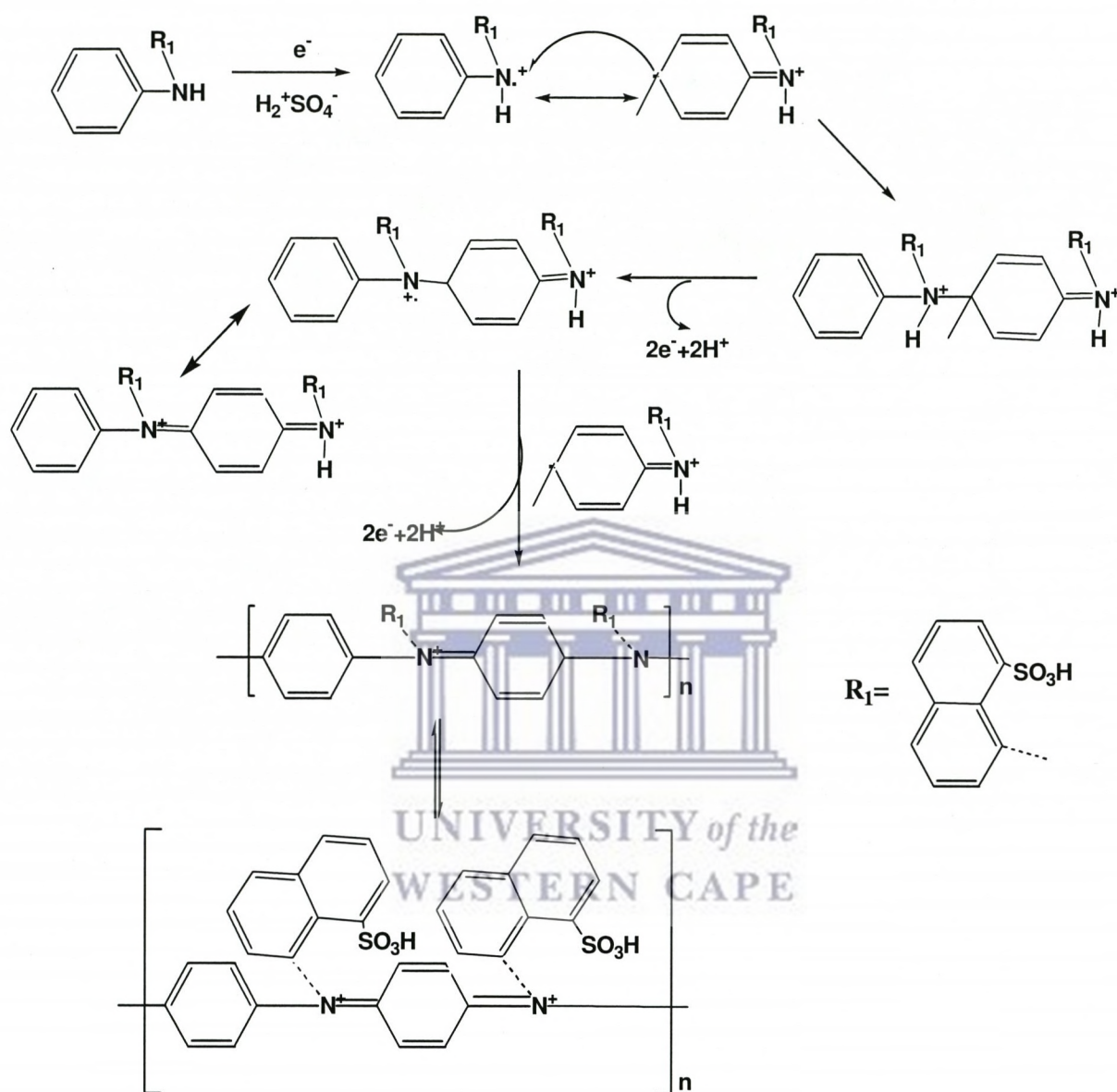


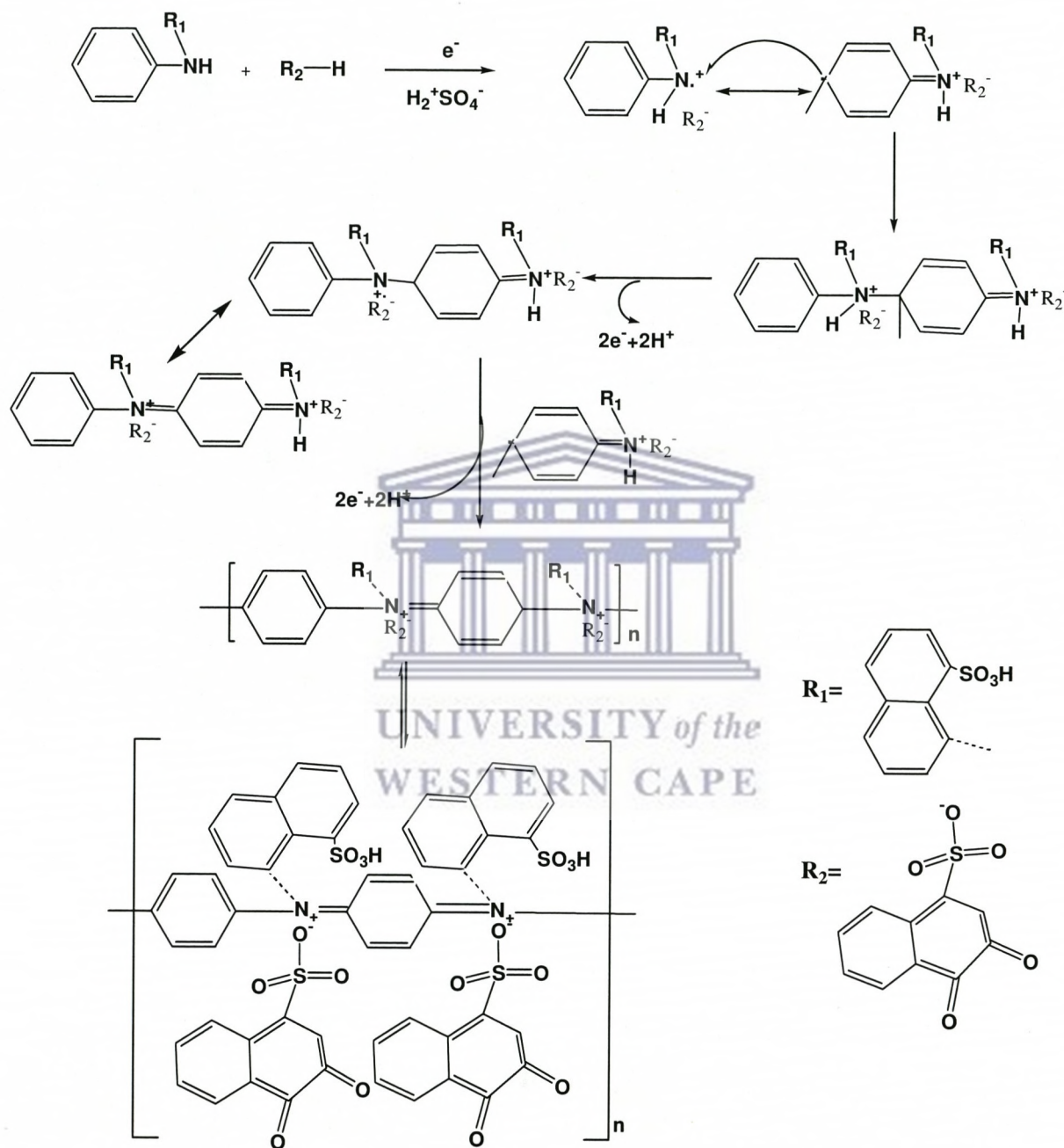
Figure 3.4: TEM micrographs of doped PANSA-ASA (a-c) and PANSA-NSA (d-f).

3.4. Proposed Mechanisms of electropolymerization of ANSA with and without dopants

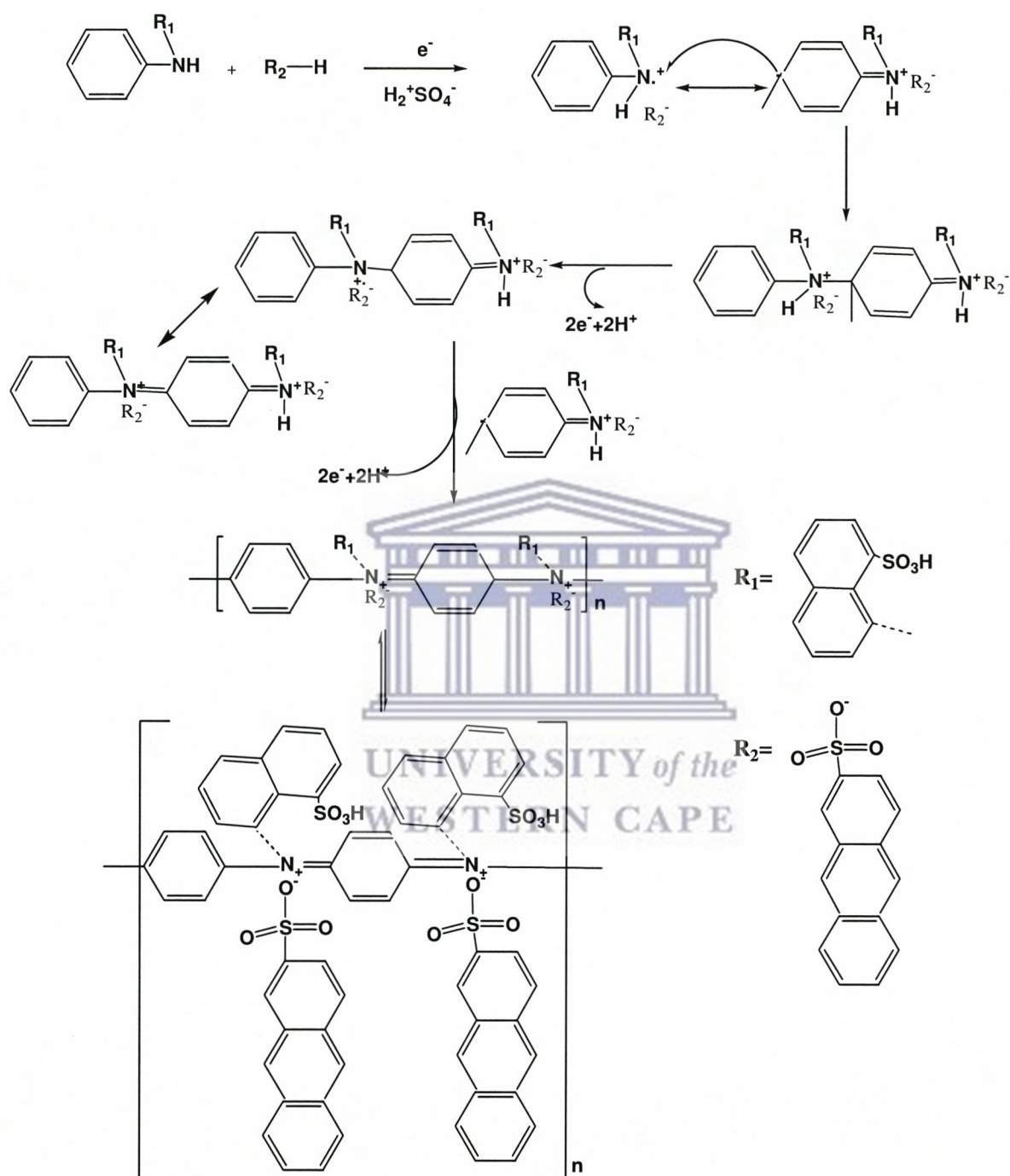
3.4.1. Mechanism of electropolymerization of 8-anilino-1-naphthalene sulfonic acid



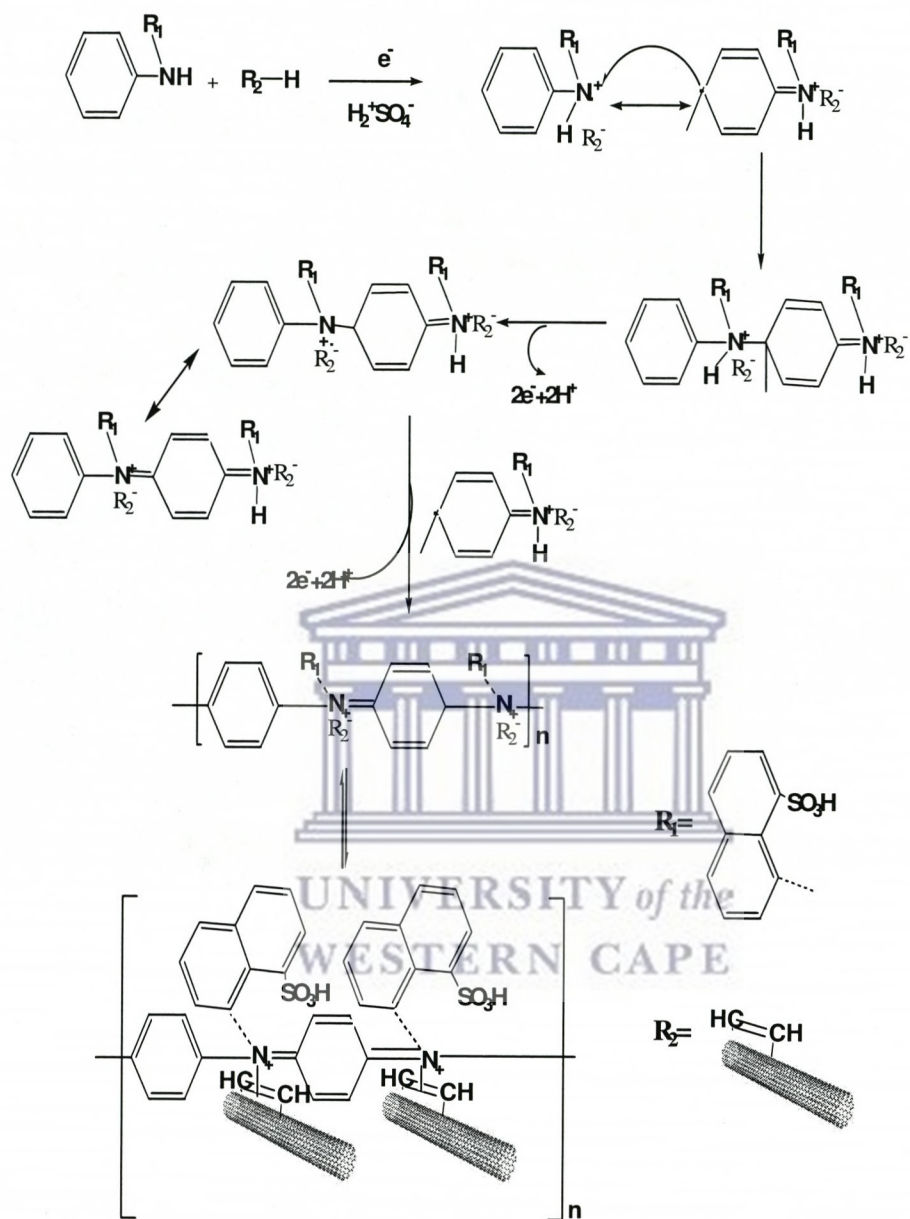
3.4.2. Mechanism of electropolymerization of 8-anilino-1-naphthalene sulfonic acid (ANSA) in the presence of 1,2-naphthaquinone-4- sulfonic acid (NSA)



3.4.3 Mechanism of electropolymerization of 8-anilino-1-naphthalene sulfonic acid (ANSA) in the presence of anthracene sulfonic acid (ASA)

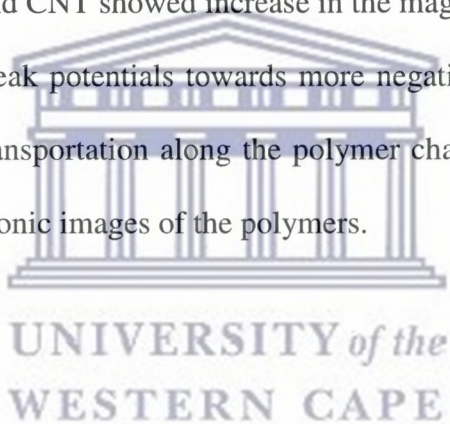


3.4.4. Mechanism of electropolymerization of 8-anilino-1-naphthalene sulfonic acid (ANSA) in the presence of multiwalled carbon nanotubes (CNT)



3.5. Conclusion

In conclusion, polymerization of monomer 8-anilino-1-naphthalene sulfonic acid (ANSA) was carried out by electrosynthesis with and without dopants on the Au electrode in the presence of sulfuric acid as electrolyte solution. The monomer ANSA has N-substituted aniline ring with naphthalene sulfonic acid. The existence of naphthalene sulfonic group in the polymer chain improved the solubility. The dopants were used as electro donor to the polymer for fine tuning and processability as well as increasing solubility of the polymer. The growth of the polymers was monitored by CV during electropolymerization and displayed redox couples typical for polyaniline. The multiscan voltammograms of the undoped PANSA and doped with ASA, ANSA and CNT showed increase in the magnitude of the peak currents and accompanied by shift of peak potentials towards more negative values upon increasing the scan rates due to charge transportation along the polymer chain. TEM revealed that the plastic sheets and tubings electronic images of the polymers.



3.6. References

Bard, A. J., Faulkner, L. R. Electrochemical methods. Fundamentals and applications, 2nd ed, John Wiley & Sons Inc: New York, (2001).

Bansal, V., Bhandari, H., Bansal, M. C., Dhawan, S. K. Electrical and optical properties of poly(aniline-co-8-anilino-1-naphthalene sulphonic acid) -A material for ESD applications, *Indian Journal of Pure and Applied Physics* (2009) 47, 667-675.

Bhandari, H., Choudhary, V., Dhawan, S. K. Influence of self-doped poly(aniline-co-4-amino-3-hydroxy-naphthalene-sulfonic acid) on corrosion inhibition behaviour of iron in acidic medium, *Synthetic Metals* (2011) 161, 753-762.

Brown, A.P., Anson, F.C. Cyclic and differential pulse voltammetric behaviour of reactants confined to the electrode surface, *Analytical Chemistry* (1977) 49, 1589–1595.

Cao, Y., Andreatta, A., Heeger, A.J., Smith, Synthesis of Acid Doped Conducting Polyaniline, *Polymer* (1989) 30, 2305.

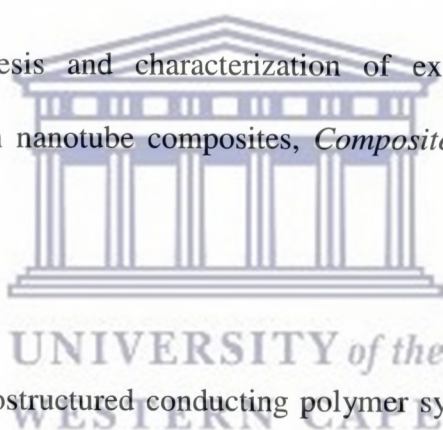
Focke, W.W., Wnek, G.E. Conduction mechanisms in polyaniline (emeraldine salt), *Journal of Electroanalytical Chemistry* (1988) 256, 343–352.

Gajendran, P., Saraswathi, R. Polyaniline–carbon nanotube composites, *Pure Applied Chemistry* (2008) 80, 2377–2395,

Iwuoha, E.I., De-Villaverde, D.S., Smyth, M.R., Reactivities of organic phase biosensors. The amperometric behaviour of horseradish peroxidase immobilised on a platinum electrode modified with an electrosynthetic polyaniline film, *Biosensors and Bioelectronics* (1997) 12, 753-754.

Klink, M. J. Development of polyaniline nanotube electrocatalysts and sensor devices for phenolic-pollutants, PhD Thesis, Department of Chemistry, University of the Western Cape, South Africa, (2007).

Lin, Y.W., Wu, T.M. Synthesis and characterization of externally doped sulfonated polyaniline/multi-walled carbon nanotube composites, *Composites science and Technology* (2009) 69, 559-2565.



Masdarolomoor, F., Novel nanostructured conducting polymer systems based on sulfonated polyaniline, PhD Thesis, Department of Chemistry, University of Wollongong, Australia, (2006)

Mazeikiene ,R., Niaura, G., Malinauskas, A. Raman spectroelectrochemical study of self-doped copolymers of aniline and selected aminonaphthalenesulfonates, *Electrochimica Acta* (2006) 51, 1919-1920.

Michira, I., Akinyeye, R., Somerset, V., Klink, M.J., Sekota, M., Al-Ahmed A., Baker P.G.L., Iwuoha, E.I., Synthesis, characterization of novel polyaniline nanomaterials and application in amperometric biosensors, *Macromolecular Symposia* (2007) 255, 57-69.

Mirmohseni, A., Wallace, G. G. Preparation and characterization of processable electroactive polyaniline-polyvinyl alcohol, *Polymer* (2003) 44, 3523-3528.

Ngece, R. F., West, N., Ndagili, P.M., Olowu, R., Williams, A., Hendricks, N., Mailu, S., Baker, P., Iwuoha, E. A silver nanoparticle/poly (8-anilino-1-naphthalene sulphonic acid) bioelectrochemical biosensor system for the analytical determination of ethambutol, *International Journal of Electrochemical Science* (2011) 6, 1820 –1834.

Shirakawa, H., Lowis, E.J., MacDiarmid, A.G. Synthesis of electrically conducting organic polymers: halogen derivatives of polyacetylene, $(CH)_x$, *Journal of Chemical Society of Chemical Communications* (1977), 578 – 580.

Wan, M., Wei, Z., Zhang, Z., Zhang, L., Huang, K., Yang, Y. Studies on nanostructures of conducting polymers via self-assembly method, *Synthetic Metals* (2003) 135, 175–182

CHAPTER FOUR:

CHEMICAL SYNTHESIS AND CHARACTERIZATION OF POLY (8-ANILINO-1-NAPHTHALENE SULFONIC ACID) AND POLYANILINE

4.1. Introduction

The previous chapter dealt with electrochemical polymerization of undoped and doped ANSA with ASA, NSA and CNT and also looked at characterization of the electro polymerized PANSA. This chapter deals with the chemical synthesis, and characterization, of undoped, PANSA, PANI, and PANI doped with NSA. The aniline polymerization by chemical synthesis is based on the aniline oxidation using suitable oxidants such as ammonium persulphate (APS), sodium chlorate, potassium dichromate, fenton reagent, hydrogen peroxide, etc, in a solution containing mineral or organic acids (Wallace *et al.*, 2009). Bai *et al.* (2007) reported polyaniline which was chemically, synthesized as cluster nanorods by binary oxidant system employing potassium dichromate and ammonium persulphate (APS). The resultant polyaniline product is normally dark green product “emeraldine” form and treatment of the product by alkaline or ammonium solution converts it into dark blue emeraldine base (Wallace *et al.*, 2002).

Several studies have been done on chemical synthesis of polyaniline and its derivatives which include alkoxy (Yin *et al.*, 2008). It is reported that the substituents in polymer chains decrease the stiffness of the polymers making it easier to dissolve (Yin *et al.*, 2008). The disubstituted polyaniline like poly (2,5-dimethoxyaniline) has been reported to have conductivity similar to that of polyaniline and are soluble in most organic solvents (Palys *et*

al., 2000). Other types of synthesized polyaniline are, the ones which sulfonic acids substituted (Masdarolomoor *et al.*, 2008), the sulfones are known to improve its processability and solubility. The other method involves chemical synthesis of polyaniline in the presence of dopant using the oxidant (Maser *et al.*, 2008). It is believed that the incorporation of the dopants into conducting polymers is to form soluble conducting polymeric nanostructures. Hence, this work presents chemical synthesis of polyaniline and poly(8-anilino-1-naphthalene sulfonic acid) via oxidative polymerization of their respective monomers using ferric chloride as an oxidant and the bulky dopant, NSA was also used to modulate during PANI.

4.2. Experimental method

4.2.1. Reagents and materials

Aniline (99%), 8-anilino-1-naphthalene sulfonic acid, ammonium hydrate salt 97% (Sigma-Aldrich), ammonium per sulphate (APS), $(\text{NH}_4)_2\text{S}_2\text{O}_8$, 98%, dimethyl formamide (DMF, 99%) and ferric chloride (FeCl_3) were purchased all purchased from from Sigma Aldrich.

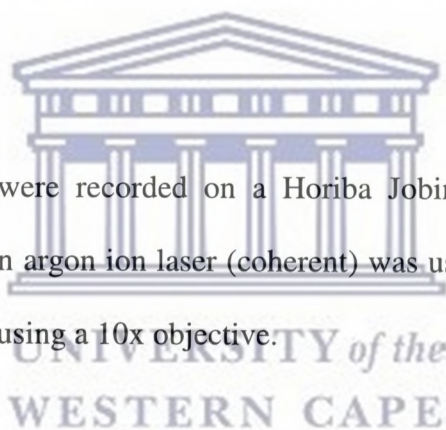
4.2.2. Apparatus and measurement

All electrochemical experiments were carried out using a BAS 100W integrated automated electrochemical workstation BioAnalytical Systems (BAS, West Lafayette, IN, USA) controlled by a computer. A conventional three-electrode system with a 0.0201 cm^2 gold (Au) disk was used as the working electrode, a platinum (Pt) wire auxillary electrode and Ag/AgCl reference electrode with a 3 M NaCl salt bridge solution, all purchased from BAS. All the results obtained using cyclic (CVs) were recorded with a computer interfaced to the electrochemical workstation. The working electrode was polished using alumina micro-polish and polishing pads (Buehler, IL, USA)

A conventional collinear four point probe instrument (Veeco Instruments FPP-100) was used to record resistance for conductivity measurements. The four probes which are made from tungsten were placed on the pellet and a current was passed through the pellet while the voltage was measured. The samples were prepared by making a paste of the polymers, and pressing it into pellets which were 1mm thick.

Infrared spectrums were recorded using the FTIR spectrometer (Perkin Elmer Spectrum 100) to identify the chemical structure of PANI and PANSA respectively. A small amount of material was placed on the diamond coated detector and pressed onto the electrode for FTIR measurements.

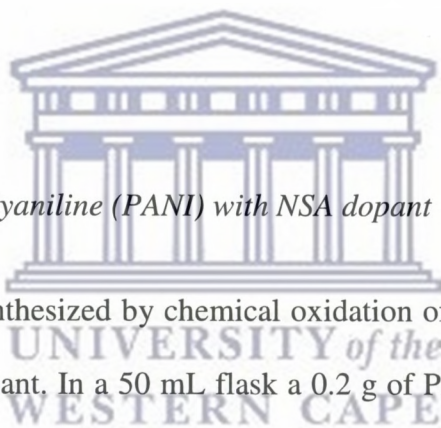
Resonance Raman spectrums were recorded on a Horiba Jobin-Yvon Labram HR 2000 confocal Raman microscope. An argon ion laser (coherent) was used to excite at 488nm. The laser was focused onto the film using a 10x objective.



The morphology of the synthesized materials was investigated using the Hatachi S- 3000 N scanning electron microscope. The samples were prepared by placing some of the synthesized material onto an aluminum stub. A carbon sticky tape was placed on the aluminium stub for adhesion of the material. The samples used for RAMAN and SEM were prepared by dissolving the polymers in DMSO, drop coating the solution on an ITO electrode (7 x 50 x 0.9 mm unpolished float glass with $R_s = 8-12 \Omega$), and allowing them to dry overnight

4.2.3. Chemical synthesis of Polyaniline (PANI) and Poly (8-anilino-1-naphthalene sulfonic acid) PANSA

PANI and PANSA were synthesized by chemical oxidation of their respective monomers. In a 50 mL flask a 0.2 g of the monomer (aniline (ANI) or ANSA) was dissolved in a solution of 2 mL HCl in 20 mL distilled water. The solution was stirred for 30 min at 50 °C where after 0.48 g of APS and 0.375 g of FeCl₃ was added respectively in the solution. The resultant mixture was stirred for another 3 h at 50 °C. The contents of the reaction were placed in the oven at 70 °C overnight to evaporate the solvents. The remaining contents were washed with ethanol and dried at 70 °C.



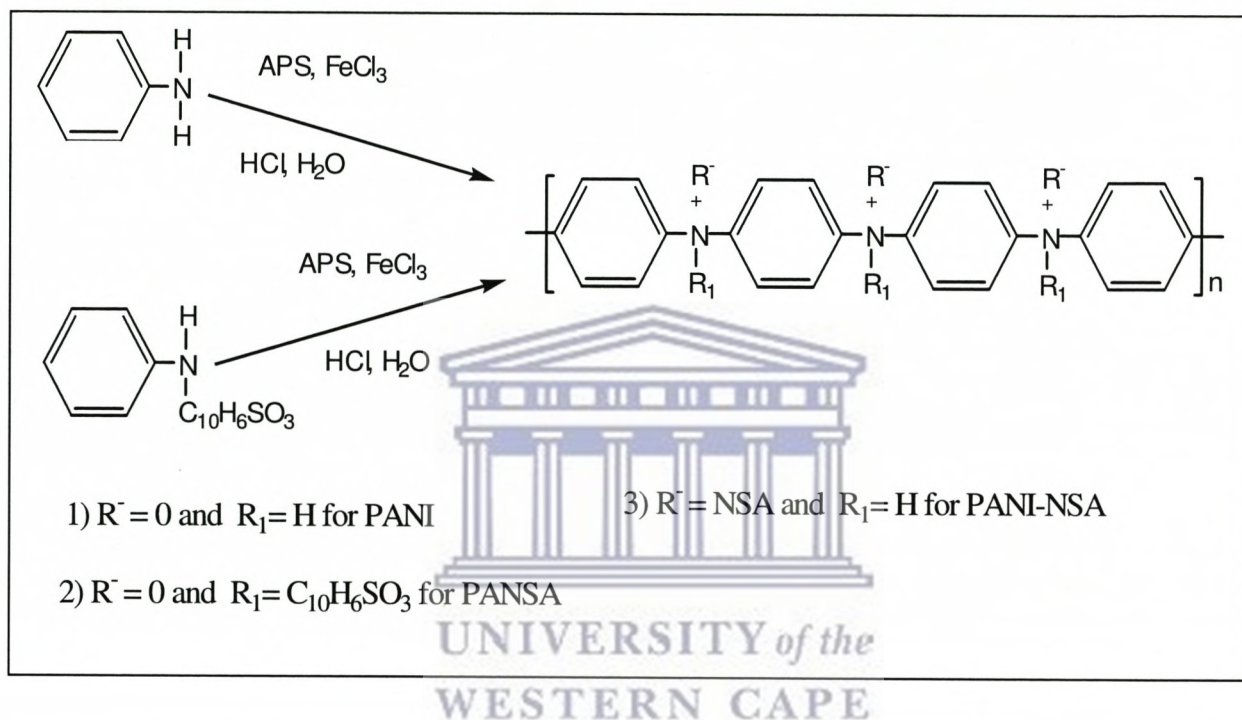
4.2.3. Chemical synthesis of Polyaniline (PANI) with NSA dopant

PANI doped with NSA was synthesized by chemical oxidation of aniline monomer with the presence of their respective dopant. In a 50 mL flask a 0.2 g of PANI and 0.001 g of dopant were dissolved in a solution of 2 mL HCl in 20 mL distilled water. The solution was stirred for 30 min at 50 °C where after 0.48 g of APS and 0.375 g of FeCl₃ was added respectively in the solution. The resultant mixture was stirred for another 3 h at 50 °C. The contents of the reaction were put in the oven at 70 °C overnight to evaporate the solvents. The remaining contents were washed with ethanol and dried at 70 °C.

4.3. Results and discussion

4.3.1. Chemical synthesis of PANI and PANSA

The chemical synthesis of the PANI and PANSA were achieved by oxidation of monomer aniline and monomer 8-anilino-1-naphthalene sulfonic acid, respectively, using ammonium persulphate as a suitable oxidant (Scheme 4.1).



Scheme 4.1: Chemical synthesis of PANI, PANSA, and PANI-NSA

It is well documented that the chemical synthesis of polyaniline and its derivatives by $(\text{NH}_4)_2\text{S}_2\text{O}_8$ is believed to proceed, in its initial stages, by a mechanism similar to that of electrochemical polymerization (Bansal *et al.*, 2009; Masdarolomoor *et al.*, 2008; Cao *et al.*, 1989). Scheme 4.1 shows the mechanism of polymerization of PANI and PANSA. The mechanism involves formation of the aniline radical cation and coupling of N- and para-radical cations which occurs with subsequent rearomatization of the dication of p-aminodiphenylamine (Bansal *et al.*, 2009). It is then oxidized to the diradical dication.

Although “head-to-tail” (i.e., N-para) coupling is predominant, some coupling in the ortho-position also occurs, leading to defects in conjugation in the resultant polymer (Bansal *et al.*, 2009). In this work, the green product polymers were obtained; the green coloured product obtained is indicative of formation of polyaniline that is in its emeraldine redox state green in colour (Wallace *et al.*, 2002).

4.3.2. Cyclic voltammetric characterization of chemical synthesized polymers

4.3.2.1. Cyclic voltammetric characterization on gold electrode

CV characterization of PANI, PANSA and PANI-NSA was achieved by using gold electrode in a monomer-free background electrolyte (HCL) at different scan rates (0.010, 0.015, 0.020, 0.025, 0.030, 0.035, 0.040, 0.045 and 0.050 Vs⁻¹) and were recorded and presented in Figure 4.1. Figure 4.1(a) represents the CV characterization of gold electrode alone; it showed one peak at $E_{pc} \sim 0.5$ V which was typical of a gold bare electrode, its peak current is very small, hence its contribution will be insignificant to the peaks observed at the same region when the polymers are characterized. The multiscan voltammogram of PANI is presented in Figure 4.1(b) and results showed one redox couple as indicative of the merging of three known oxidation states of polyaniline (Ngece *et al.*, 2011). Furthermore, it demonstrates that as the number of voltammetric cycles increased peak currents also increased. This indicated that polyaniline structures were conductive and diffusion of electrons along the polymer chain was also taking place. The redox couple observed at $E_{pa} \sim 0.42$ V and $E_{pc} \sim 0.50$ V due the polyleucoemeraldine radical cation, transformation of PANI from the reduced leucoemeraldine (LE) state to the partly oxidized emeraldine state (EM), and further oxidized to pernigraniline (PE). The multiscan voltammograms of this PANI showed a similar electrochemistry to that of chemical synthesized polyaniline reported before (Mavundla, 2010).

The CV characterization of PANSA is presented in Figure 4.1(c) and it is similar to that of PANI, it demonstrated the presence of one typical redox response exhibiting one redox couple, with a E° of 0.47 V Ngece (2007) explained that this redox couple is ascribed to the electrochemistry of *p*-benzoquinone formed during polymerisation process. The peak current also increased; as the scan rate increased. The effect of NSA dopant (Figure 4.1(d)) on the PANI followed the same trend of results as PANI, but with its redox couple that had a E° of 0.52 V. However, its peak current was lower as compared to PANI with no dopant; this might be due to electronic and steric effect caused by the presence of NSA dopant in the PANI polymer chain, inducing some non planar configurations that decrease the conjugation along the polymer backbone (Bansal *et al.*, 2009). The voltammograms in all polymers further showed that an increase in peak currents with an increase in scan rate. This was indicative that the peak current was diffusion controlled and from this observation the Randel-Sevcik equation (Bard and Faulkner, 2001), was used to evaluate the diffusion coefficient (D_e) Equation 2.40 presented in chapter two, which is evaluated from the slope of I_{pc} vs square root of the scan rate (Figure 4.2).

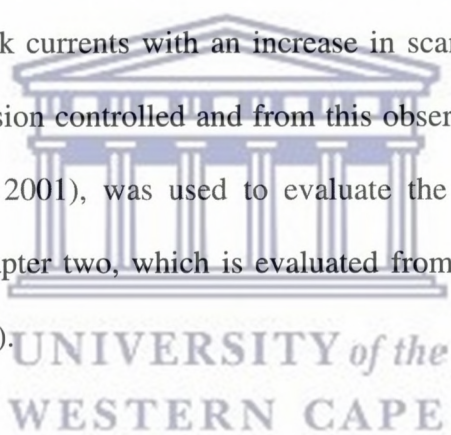


Table 4.1 compares the diffusion coefficient (D_e), average formal potential (E°), change potential (ΔE) and the ratio of current cathodic and anodic peaks (I_{pc}/I_{pa}). The E° was obtained to be ~0.5 V in all polymers. The ΔE values were ~0.12 V (PANI), 0.074 V (PANSA) and 0.051 V (PANI-NSA). The D_e values were found to be 1.37×10^{-5} , 0.34×10^{-5} and $0.28 \times 10^{-5} \text{ cm}^2 \text{ s}^{-1}$ for PANI, PANSA and PANI-NSA, respectively, and these values were in range with the one reported by Mavundla (2010) in studies undertaken for chemical synthesis PANI in which D_e was $0.93 \times 10^{-5} \text{ cm}^2 \text{ s}^{-1}$. This suggested that charge transportation along the polymer chain will be more efficient in PANI due to the high D_e value, so if that is

the case then, the conductance of PANI is expected to be higher than that of PANSA and the PANI-NSA composite.



UNIVERSITY *of the*
WESTERN CAPE

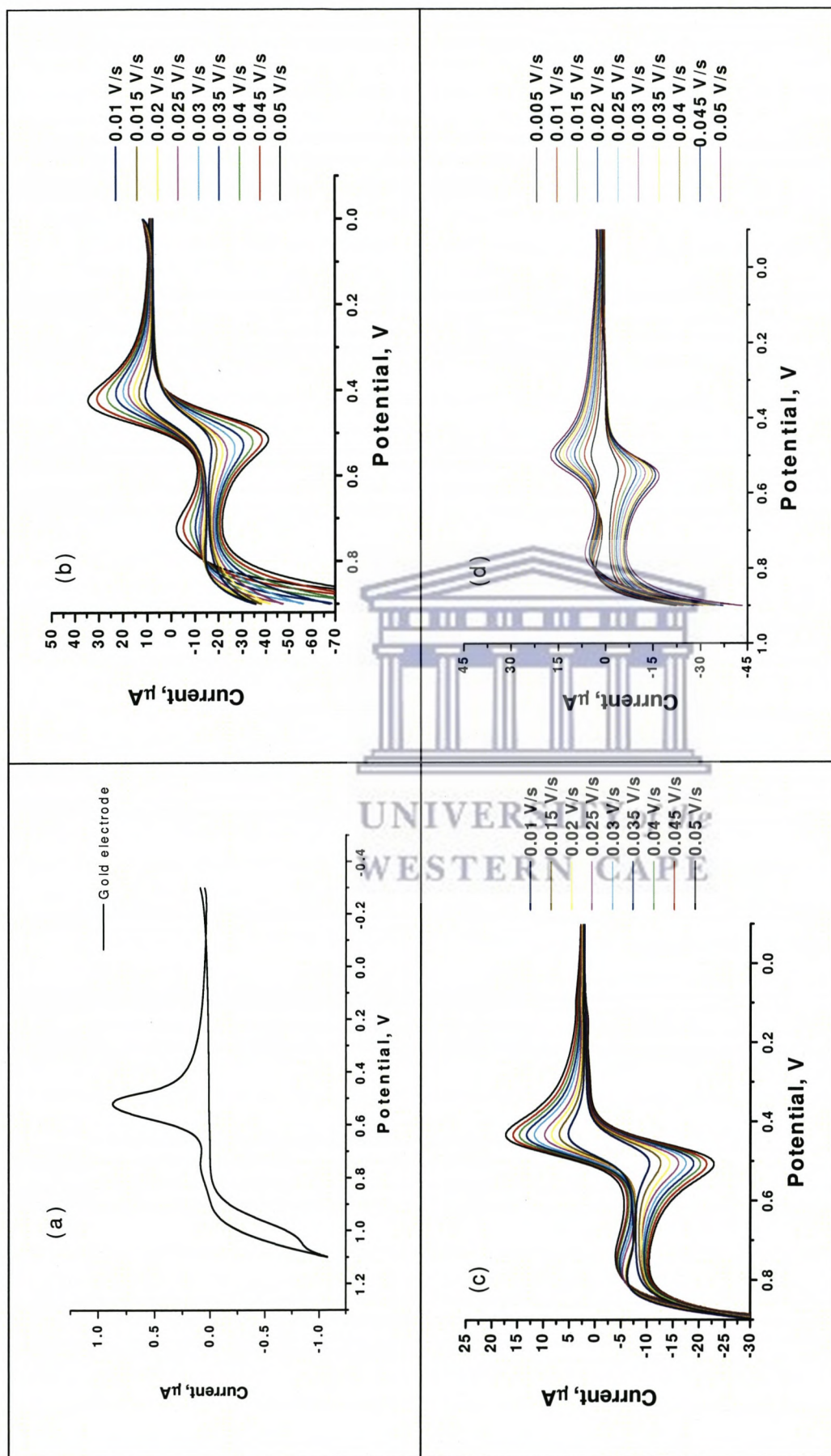


Figure 4.1: The typical cyclic voltammograms for (a) gold electrode, (b) undoped PANI, (c) PANSA and (d) doped PANI with 1,2-Naphthaquinone-4-sulfonic acid (NSA) at 0.01, 0.015, 0.02, 0.025, 0.03, 0.035, 0.04, 0.045 and 0.05 V s^{-1} using gold electrode in 1M HCl.

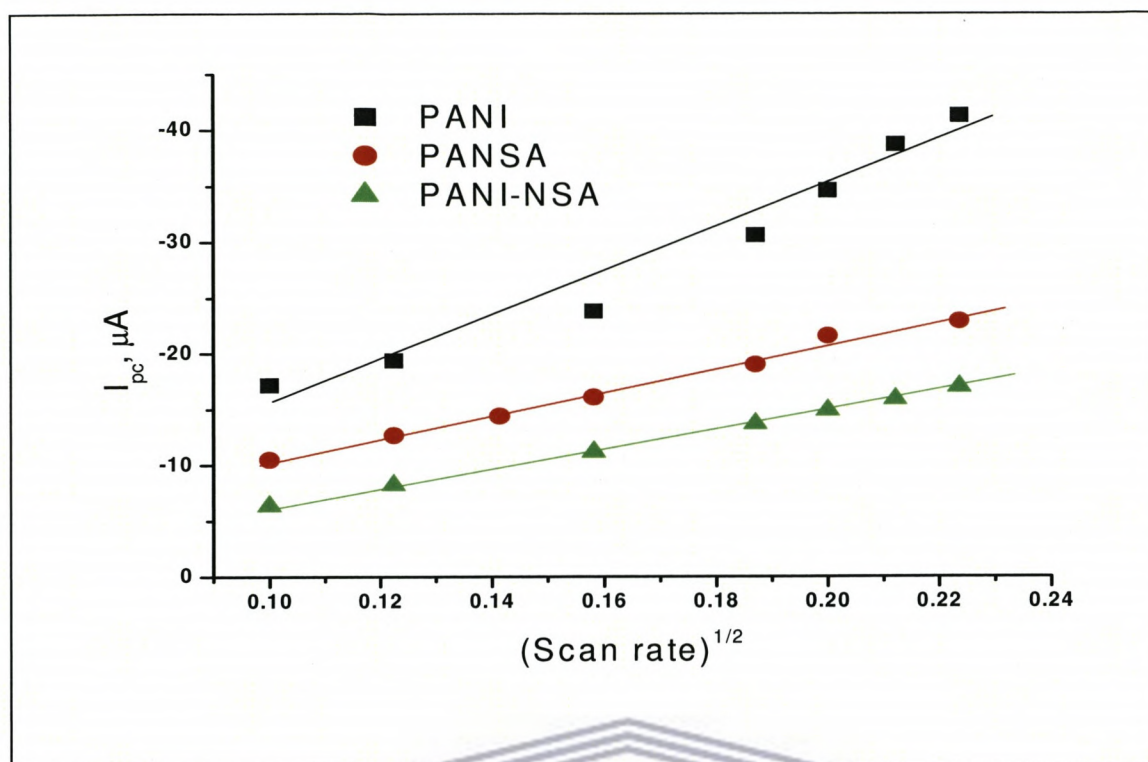


Figure 4.2: Peak current as a function of square root of scan rate for PANI, PANSA and PANI-NSA

Table 4.1: Electrochemical parameters of PANI, PANSA and PANI-NSA

Polymer	E^o (V)	ΔE (V)	I_{pc}/I_{pa}	D_e ($\times 10^{-5} \text{ cm}^2 \text{ s}^{-1}$)
PANI	0.47	0.118	1.32	1.37
PANSA	0.47	0.074	1.35	0.34
PANSA-NSA	0.52	0.051	1.00	0.28

The diffusion coefficient was seen to decrease in PANI > PANSA > PANI-NSA (Table 4.1) which was caused by the substituted naphthalene sulfonic acid in PANSA that increases the inter-chain distance between the polymer units and thus impede electron-hopping across the units. The effect of dopant NSA was seen to have low diffusion coefficient due to the steric hindrance emanating from the bend bulky NSA as compared to PANI.

4.3.3. Electrical conductivity measurement of polymer

The electrical conductivity measurements of chemically synthesized PANI, PANSA and PANI were performed using four-point probe technique. The specific resistivity (ρ) was calculated by using Equation 2.43 and 2.44 (given in chapter two). It is a measure of how strongly a material opposes the flow of current hence when it is low the material readily allows the movement of electric charge. Its reciprocal is specific conductance (σ) which is a measure of the materials ability to conduct an electric current.

$$\rho = RA/t \quad [2.43]$$

$$\sigma = 1/\rho \quad [2.44]$$

Where ρ is its resistivity, R is the sample resistance, A is the cross-sectional area, t is the thickness, and σ is the conductivity.




Table 4.2 shows the electrical resistivity followed this trend PANI-NSA < PANSA < PANI, with PANI, having the highest electrical resistivity and PANI-NSA being the lowest. It is well documented that the conductivity of the materials relies on microscopic and macroscopic conductivity (Chen *et al.*, 2003). The microscopic conductivity depends on the doping level, conjugation length, and chain length while the macroscopic conductivity is related to some external factors such as the compactness of the samples (Chen *et al.*, 2003). It was observed that the calculated conductivity increased from 10^{-4} to 10^{-2} Sm^{-1} (PANI-NSA > PANSA > PANI). When aniline was polymerized in the presence NSA as a dopant, it had the lowest resistivity and hence PANI-NSA had the highest specific conductivity (Table 4.2). PANSA conductivity was higher than the one of PANI. The raising of the conductivity in both PANSA and PANI-NSA might be related to electron transfer from the dopant to polymer in PANI-NSA composite whereas in PANSA might be from the naphthalene sulfonic acid group

to the polymer. The sulfonic groups in the polyaniline are known to act as self-doping agents and increase conductivity of the material (Bhandari *et al.*, 2011).

Table 4.2: Electrical conductivity parameters of chemically synthesized polymer

Sample	Voltage (mV)	Current (μA)	R Ω	P $\Omega \text{ m}$	σ S m^{-1}
PANI	34.0	3.5	959.24	4345.34	2.3×10^{-4}
	36.0	4.02			
	246	19.8			
Average	105	9.11	959.24	4345.34	2.3×10^{-4}
Standard deviation	122	9.26			
PANSA	310	0.905	62.48	283.03	3.53×10^{-3}
	147	0.112			
	70	0.05			
Average	175.7	0.36	62.48	283.03	3.53×10^{-3}
Standard deviation	98.82	0.477			
PANI-NSA	15	0.26	12.55	56.86	1.76×10^{-2}
	28	0.33			
	100	0.2			
Average	47.67	0.263			
Standard deviation	45.79	0.0651			

It should be noted that the above results have a certain margin of experimental error, which was evaluated with the standard deviation. The errors resulted from using a pellet instead of a uniform thin film, since the technique was designed for measurements of thin films. Furthermore, since a pellet was not flat as a uniform film, during the experiment the probe entered the pellet instead of scanning on top of it. The pellets were used due to solubility challenges, and difficulty in formation of uniform films on ITO with dissolved chemically synthesized polymers.

4.3.4. FTIR Characterization of polymers

4.3.4.1. FTIR spectra of undoped PANI and PANSA

The FTIR spectra of PANI and PANSA are shown in Figure 4.3. The spectra of PANI and PANSA exhibited the characteristic bands in the 400 - 4000 cm^{-1} range, and showed the bands at ~ 1298 and 800 cm^{-1} due to the out of plane C-H bending vibrations as indicative of the para coupling. That means the polymerization occurred at 1-4 position for both polymers. IR spectrum of the PANI showed principal absorptions at $\sim 1579, 1422, 1309, 1150, 1068, 980, 602$ and 596 cm^{-1} whereas for PANSA were shown at $\sim 1591, 1412, 1345, 1148, 1095, 1006, 872$ and 591 cm^{-1} .

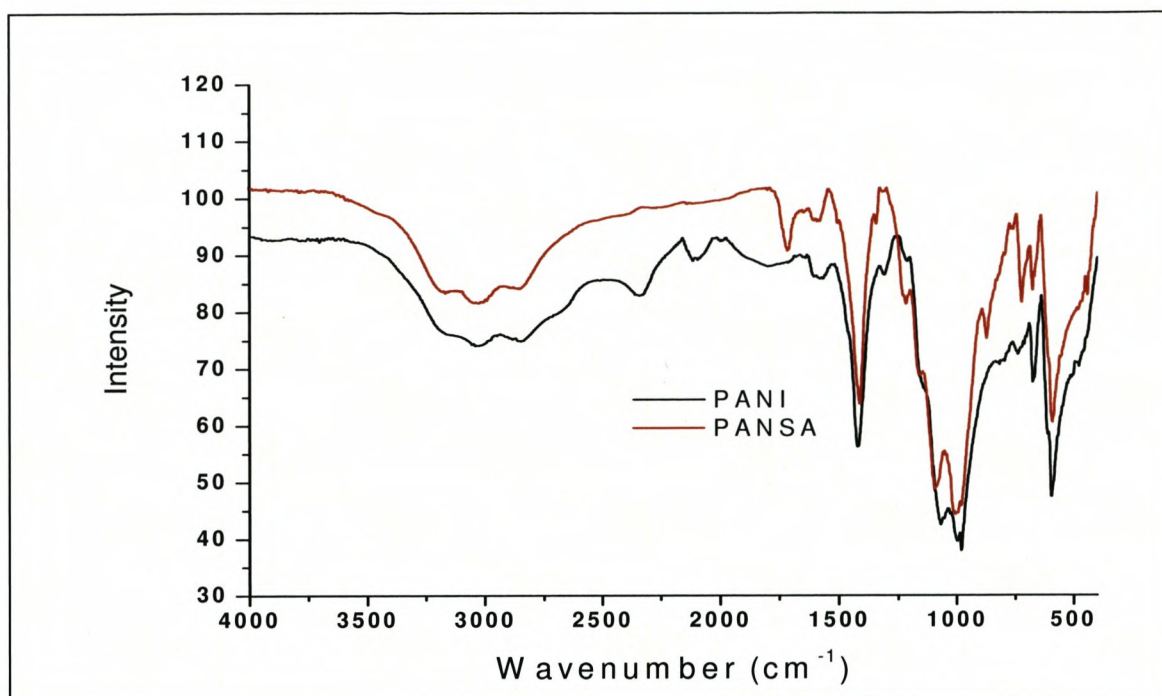
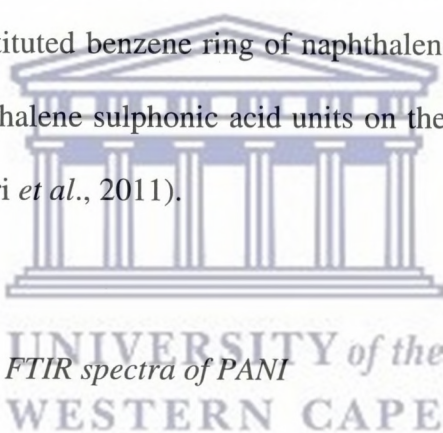


Figure 4.3: FTIR spectra of PANI and PANSA

The peaks at $\sim 1579 \text{ cm}^{-1}$ for PANI and 1591 cm^{-1} for PANSA were assigned to the C=N and C=C stretching modes for the quinoid in the polymer backbone (Zeng and Ko, 1998). The corresponding stretching vibration band for the C-N of quinoidic-benzoidic-quinoidic (QBQ), QBB, and BBQ occurred at $\sim 1422 \text{ cm}^{-1}$ for PANI and 1412 cm^{-1} for PANSA. The peak at 1309 cm^{-1} and the short peak at 1150 cm^{-1} in PANI were ascribed to N-H bending in PANI and the symmetric component of the C-C (or C-N) stretching modes. In PANSA, the bands at $\sim 1345 \text{ cm}^{-1}$ and 1148 cm^{-1} were due to the symmetric component of the C-C (or C-N) stretching modes. Furthermore, the bands at ~ 1068 and 980 cm^{-1} (PANI) and 1095 and 1006 cm^{-1} (PANSA) were due to the in-plane and out-of-plane C-H bending modes, respectively (Bansal *et al.*, 2009). The band at $\sim 1150 \text{ cm}^{-1}$ is considered to be a measure of the degree of electron delocalization in polymer chains and thus it is a characteristic peak related to polyaniline conductivity (Lee *et al.*, 2003). The presence of the stretching vibration of both

quinoid and benzoid group in PANI and PANSA showed the existence of half oxidized polymers (polyemeraldine form).

These results are in good agreement with those reported with Draman *et al.* (2009), and characteristic of PANI in its emeraldine base form. The broad bands between 3200-2900 cm^{-1} were observed in both PANI and PANSA, these bands corresponded to the formation of intermolecular or intramolecule of hydrogen bond due to the presence of hydrogen atom present at N- atom of aniline unit (Bansal, 2009) or SO_3H group of the naphthalene sulphonic acid unit in PANSA. However, the spectrum of PANSA showed a characteristic band at around 733 cm^{-1} which was assigned to the aromatic C-H out-of-plane bending vibration for three adjacent H in the tri-substituted benzene ring of naphthalene sulphonic acid unit. This indicated the inclusion of naphthalene sulphonic acid units on the backbone of the polymer, acting as a self-doping (Bhandari *et al.*, 2011).



4.3.4.2. The effect of dopants on FTIR spectra of PANI

The effect of dopants on chemical synthesis of PANI was investigated and presented in Figure 4.4. The FTIR spectrum of PANI-NSA shows peak at $\sim 1610 \text{ cm}^{-1}$, which were due to the stretching vibrations of quinoidic (Q) groups in the back bone of polymer. The sharp peak at 1423 cm^{-1} was assigned to various C-N stretching vibrations of QBQ, QBB, and BBQ, suggesting the dominance of the benzoid and quinoid ring structure, as observed in both undoped chemically synthesized PANI and PANSA. The other peaks between 1060 and 980 cm^{-1} were due to the in-plane and out-of-plane C-H bending modes. A characteristic band at around 832 cm^{-1} was due the presence of aromatic C-H out-of-plane bending vibration of naphthalene sulphonic acid.

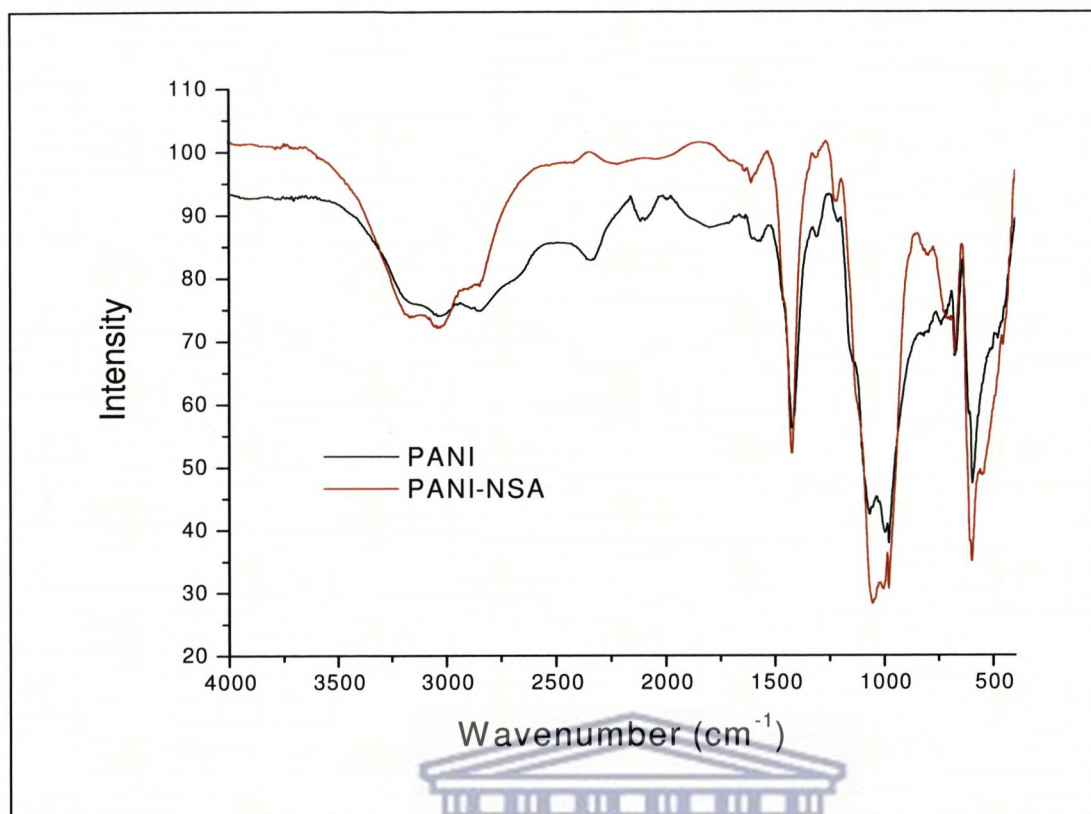


Figure 4.4: FTIR spectra of undoped PANI and PANI with dopant NSA.

4.3.5. Raman Characterization of polymers

4.3.5.1. Raman spectra of PANI, PANSA and PANI-NSA

Figure 4.5 presents the Raman spectra of the PANI, PANSA and PANI-NSA. The Raman bands PANI appeared at 1601, 1564, 1531, 1484, 1323, 1249, 1183, 1000, 804, and 605 cm^{-1} . The band assignments of the Raman absorption peaks are given in Table 4.3 (Lindfors *et al.*, 2002). The characteristic Raman bands at ~ 1601 , 1564 and 1183 cm^{-1} were due to C=C, C–C and C–H stretchings of benzoid and quinoid structure (Quillard *et al.*, 1995) in the polymer ring. The Raman bands at 1484, 1323 and 1249 cm^{-1} , characteristic of the C=N stretching in quinoid, semiquinone radical and C–H bending in quinonoid ring, respectively, confirming the existence of typical half oxidized polymer (polyemeraldine form). The other small bands

at ~ 1000 , 804 , and 605 cm^{-1} for PANI were assigned to in plane C-H bending of quinoid, benzoid symmetry ring stretching and ring deformation of semiquinoid, respectively.

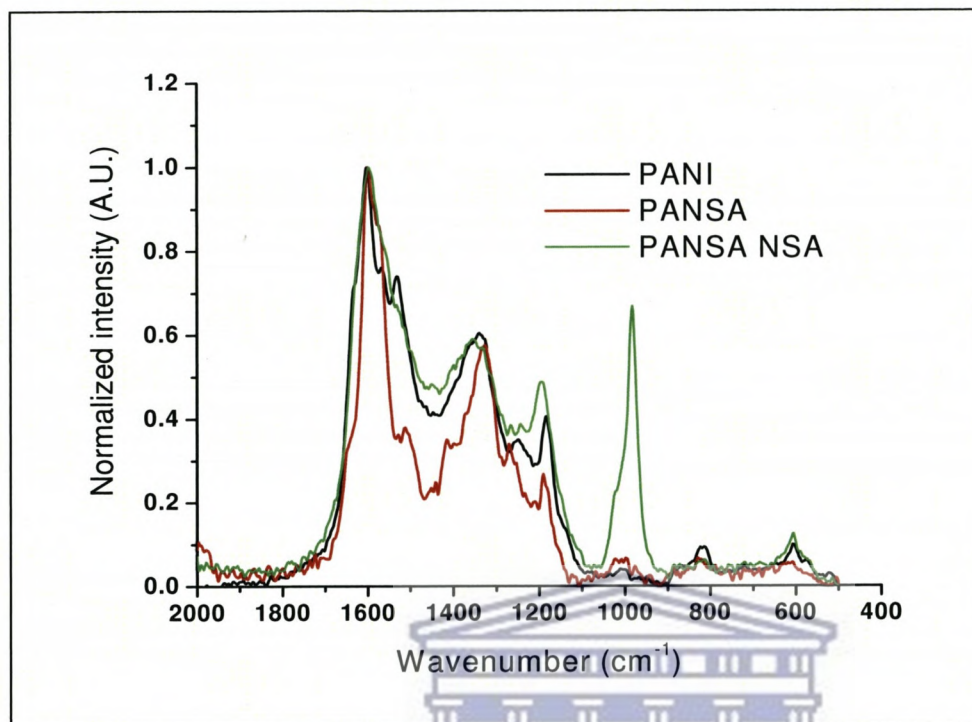


Figure 4.5: Raman spectra of PANI, PANSA and PANI-NSA.

The PANSA Raman showed absorption bands at 1597 , 1512 , 1414 , 1323 , 1270 , 1191 , 1000 , 821 and 607 cm^{-1} due to C=C, C=N, C-C and C-N stretchings of benzoid and quinoid structure in the polymer ring, confirming the existence of typical half oxidized polymer (polyemeraldine form). Furthermore, the band at 1270 cm^{-1} was due to the presence of SO_3H group in the PANSA and bands at 1000 , 821 and 607 cm^{-1} were assigned to in plane C-H bending of quinoid, benzoid symmetry ring stretching and ring deformation of semiquinoid, respectively. The incorporation of NSA group in PANI showed intense absorption band at 983 cm^{-1} .

Table 4.3: Assignment of Raman vibrational bands & their relationship to structural changes and oxidation states (Lindfors *et al.*, 2002)

Wavenumber/cm-1	Assignment	Radical Structure
1610	C-C	Benzoid
1577	C=C	Quinoid
1503	C=N	Quinoid
1410	C-C	Quinoid
1341	C-N ⁺	Semiquinoid*
1213	C-N	Benzoid
1000	In plane C-H bending	Quinoid
810	Symm ring stretching	Benzoid
600	Ring deformation	Semiquinoid*

4.3.6. Scanning Electron Microscopy (SEM)

The morphology and structure of PANI, PANSA and PANI-NSA were investigated. The effect of the naphthalene sulfonic acid group and NSA dopant on the monomer morphologies prepared under the same conditions was clearly observed in the SEM images. It is well known that SEM morphology of the resultant polymers can be as diverse as there are main polymer chains, dopant structure, synthetic routes and conditions (Wan *et al.*, 2003). SEM micrographs which display the morphology PANI, PANI-NSA and PANSA are shown in Figure 4.6-4.8. The micrograph of PANI in Figure 4.6 displays “rod-like hexagonal structures”, which are between 200-40 nm in size. The hexagonal structures in PANI were also

observed and reported before studies of synthesis and characterization of novel nanophase hexagonal Poly(2,5-dimethoxyaniline) (Mavundla *et al.*, 2010).

In Figure 4.7, the micrograph of PANSA showed the cylindrical broken nano rod clusters which arise from the salt like properties of naphthalene sulfonic group which is present in the ANSA monomer. When PANI was doped with NSA (Figure 4.8), nano-rod like structures was also observed. It was clearly that the surface of the nano-rods was covered with micelles, which were spherical. Mavundla (2010) explained that polymerization normally takes place at the micelle/water interface because the oxidants used are water soluble, and these micelles normally grow when salts are present in the polymerization reaction solution In PANI-NSA composite, NSA is the salt and as the polymerization proceeds, the micelles form as agglomerated spheres on the nano-rod like polymeric structures. This confirmed the incorporation of the NSA dopant along the backbone of polyaniline of the PANI-NSA, and presence of naphthalene sulfonic acid group in the polymer chain of the PANSA.

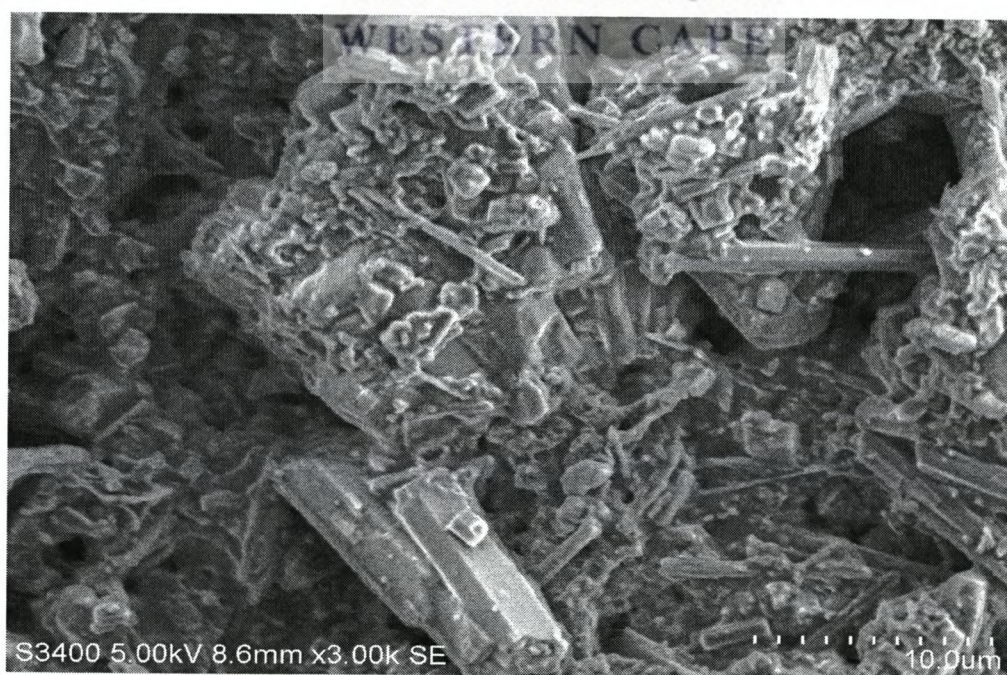


Figure 4.6: Scanning electron micrograph of PANI

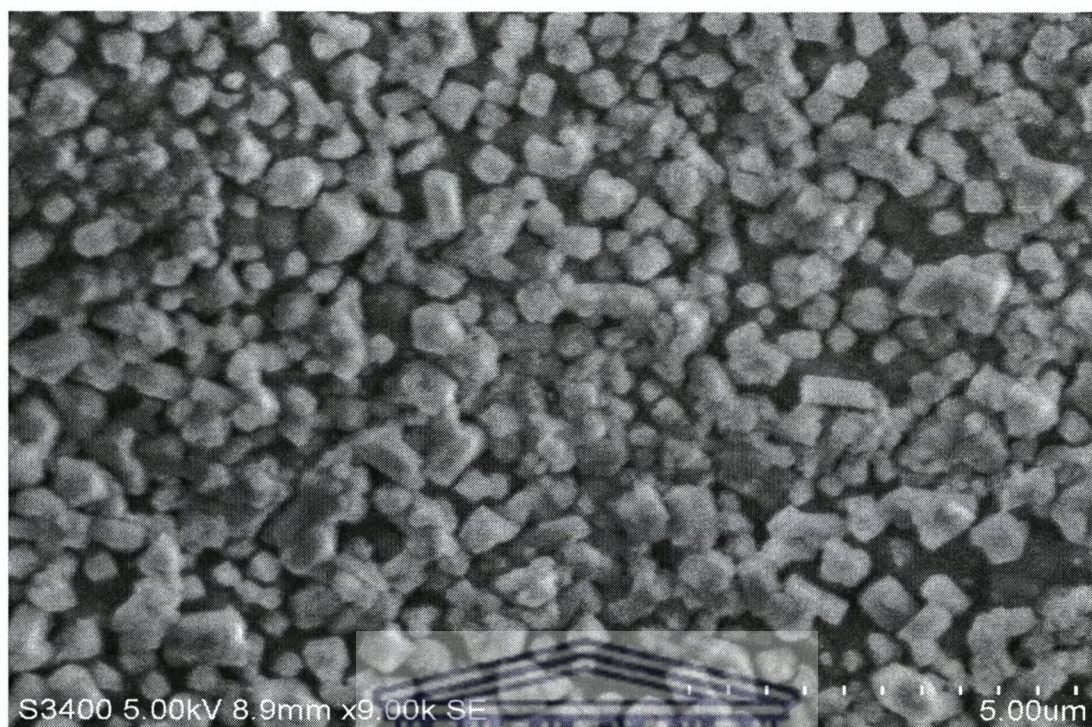


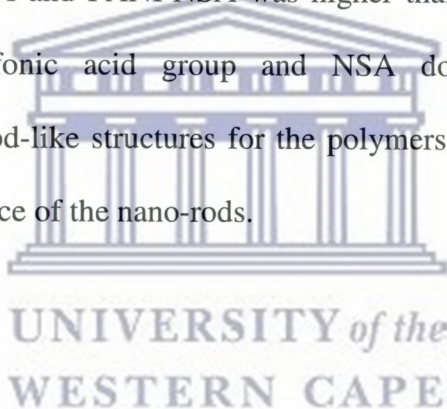
Figure 4.7: Scanning electron micrograph of PANSA



Figure 4.8: Scanning electron micrograph of PANI-NSA

4.4. Conclusion

The conducting PANI and PANSa and PANI-NSa were synthesized chemically through oxidation of the monomer using oxidant. All polymers studied exhibited quinoid and benzoid bands typically of polyaniline FTIR and Raman spectra which confirmed the polymers were formed. The presence of the sulfonate functionality in PANI-NSa suggested that the NSa groups were incorporated into the polymer backbones. Cyclic voltammetric characterization of the polymer pastes showed distinctive redox peaks, which prove that the polymer films on the Au electrode were electroactive and conductive and exhibited reversible electrochemistry. The conductivity of the nanostructured polymers was measured and results showed that specific conductivity of PANSa and PANI-NSa was higher than that of PANI due to the presence of naphthalene sulfonic acid group and NSa dopant, respectively. SEM micrographs displayed nano-rod-like structures for the polymers, and the presence of salts introduced micelles on the surface of the nano-rods.



4.5. References

Bai, X., Li, X., Li, N., Zuo, Y., Wang, L., Li, J., Qiu, S. Synthesis of cluster polyaniline nanorod via a binary oxidant system, *Materials Science and Engineering* (2007) 27, 695-699.

Bansal, V., Bhandari, H., Bansal, M. C., Dhawan, S. K. Electrical and optical properties of poly(aniline-co-8-anilino-1-naphthalene sulphonic acid) -A material for ESD applications, *Indian Journal of Pure and Applied Physics* (2009) 47, 667-675.

Bhandari, H., Choudhary, V., Dhawan, S. K. Influence of self-doped poly(aniline-co-4-amino-3-hydroxy-naphthalene-sulfonic acid) on corrosion inhibition behaviour of iron in acidic medium, *Synthetic Metals* (2011) 161, 753-762.

Bard, A. J., Faulkner, L. R. Electrochemical methods. Fundamentals and applications, 2nd ed, John Wiley & Sons Inc: New York, (2001).

Cao, Y., Andreatta, A., Heeger, A.J., Smith, M. Synthesis of Acid Doped Conducting Polyaniline, *Polymer* (1989) 30, 2305.

Chen, A., Wang, H., Zhao, B., Li, X. The preparation of polypyrrole-Fe₃O₄ nanocomposites by the use of common ion effect, *Synthetic Metals* (2003) 139, 411-415.

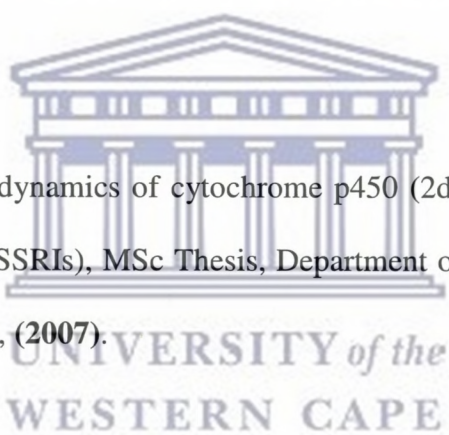
Lindfors, T., Ivaska, A. Potentiometric and UV-vis characterisation of N-substituted polyanilines, *Journal of Electroanalytical Chemistry* (2002) 53, 569-71.

Masdarolomoor, F., Innis, P.C., Wallace, G.G. Electrochemical synthesis and characterisation of polyaniline/ poly(2-methoxyaniline-5-sulfonic acid) composites, *Electrochimica Acta* (2008) 53, 4146–4155.

Maser, W. K., Sainz, R., Martínez, M. T., Benito, A. M., Electroactive polymer-carbon nanotube composites: smart organic materials for optoelectronic applications, *Contributions to Science*, (2008) 4, 187-192.

Mavundla, S. E. One-dimensional nanostructured polymeric materials for solar cells applications, PhD Thesis, Department of Chemistry, University of the Western Cape, South Africa, (2010).

Ngece, R. F., Electrochemical dynamics of cytochrome p450 (2d6) biosensors for selective serotonin re-uptake inhibitors (SSRIs), MSc Thesis, Department of Chemistry, University of the Western Cape, South Africa, (2007).



Ngece, R. F., West, N., Ndangili, P.M., Olowu, R., Williams, A., Hendricks, N., Mailu, S., Baker, P. , Iwuoha E., A silver nanoparticle/poly (8-anilino-1-naphthalene sulphonic acid) bioelectrochemical biosensor system for the analytical determination of ethambutol, *International Journal of Electrochemical Science* (2011) 6, 1820 –1834

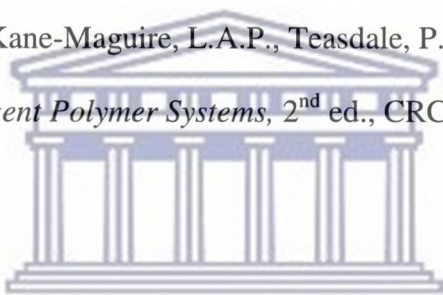
Lee, D., Char, K., Lee, W., Woo, S., Park, Y. Structural changes of polyaniline/montmorillonite nanocomposites and their effects on physical properties, *Journal of Materials Chemistry* (2003) 13, 2942-2947.

Palys, B., Kudelski, A., Stankiewicz, A., Jackowska, K., Influence of anions on formation and electroactivity of poly-2,5-dimethoxyaniline. *Synthetic Metals* (2000) 108, 111-119.

Quillard, S., Berrada, K., Louarn, G., Lefrant, S., Lapkowski, M., Pron, A. In situ Raman spectroscopic studies of the electrochemical behaviour of polyaniline, *New Journal of Chemistry* (1995) 19,365.

Wallace, G. G., Spinks, G. M., Teasdale, P. R., Conductive electroactive polymers : Intelligent materials systems., CRC Press: Boca Raton, (2002).

Wallace, G. G., Spinks, G.M., Kane-Maguire, L.A.P., Teasdale, P.R. *Conductive Electroactive Polymers: Intelligent Polymer Systems*, 2nd ed., CRC Press: Boca Raton, (2009).



Wan, M., Wei, Z., Zhang, Z., Zhang, L., Huang, K., Yang, Y. Studies on nanostructures of conducting polymers via self-assembly method, *Synthetic Metals* (2003) 135, 175–182.

Yin, P., Kilmartin, P. A., Formation of poly-2,5-dimethoxyaniline on steels, *Current Applied Physics* (2004) 4, 141-143.

CHAPTER FIVE:

PHOTOPHYSICAL STUDIES OF ELECTRO AND CHEMICALLY SYNTHESIZED POLY(8-ANILINO-1-NAPHTHALENE SULFONIC ACID) AND POLYANILINE

5.1. Introduction

The previous two chapters dealt with electro and chemical syntheses of polymers. Chapter three focused on electrochemical synthesis of undoped PANSA and PANSA doped with ASA, NSA and CNT and also looked at characterization of these polymers, while chapter four deal with chemical synthesis of PANI and PANSA, and PANI doped with NSA. The current chapter investigates photophysical properties of these electro and chemically synthesized polymers with and without dopants synthesized in chapter three and four, and relates them to their electronic signatures which can provide powerful insights about the structure of the polymer. In addition, this chapter also deals with the photoluminescence properties and lifetime studies of the chemically synthesized polymers. Furthermore, luminescence studies investigates the interaction of the polymers with $[\text{Ru}(\text{bpy})_2(\text{picCOOH})]^{2+} \cdot (\text{ClO}_4)_2$ and how the interaction impacts the photophysical behaviour of $[\text{Ru}(\text{bpy})_2(\text{picCOOH})]^{2+} \cdot (\text{ClO}_4)_2$ were also carried out.

The use of polymers as support matrix or confining transition metal complexes is also well known (Masdarolomoor, 2006) to enhance photoluminescence between metal centres either by covalently binding the metal to the polymers or via electrostatic interaction. The photoluminescence properties of polyaniline derivatives are of great interest for optoelectronic device applications (Heeger, 2001). Chen *et al.* (2007) suggested that the

fluorescence of conjugated polymer can be described in terms of semiconductor band theory. Therefore, upon photo excitation of these polymers, the electrons from the valence band are excited to the conduction band, causing migration along the polymer backbone. The excited electron and the oppositely charged “hole” attract one another. Photoluminescence occurs when the excited electron recombines with the hole; a photon is emitted (fluorescence). Poly(2-methoxyaniline-5-sulfonic acid) has been shown to display interesting photoluminescence (Draman *et al.*, 2009; Kane-Maguire *et al.*, 2004). The good photoluminescence features of such conducting polymers provide increased scope in the area of metal based ECL.

5.2. Experimental method

5.2.1. Reagents and materials

The $[\text{Ru}(\text{bpy})_2(\text{picCOOH})]^{2+} \cdot (\text{ClO}_4)_2$ was kindly synthesized and provided by Mr Ciaran Dolan, of the Tia Keyes research group from school of chemical sciences, Dublin city university Ireland, Aniline (99%), 8-anilino-1-naphthalene sulfonic acid (ANSA), ammonium hydrate salt 97% (Sigma-Aldrich), ammonium per sulphate (APS), dimethyl sulfoxide(DMSO, 99%) and ferric chloride (FeCl_3) were all purchased from Sigma (Sigma-Aldrich), sulphuric acid (95-98%) was purchased from Fluka.

5.2.2. Apparatus and measurement

The photophysical properties of the chemically polymerized films were investigated by measuring UV/Vis spectrums using Jasco V-670 UV/Vis/NIR spectrophotometer. Fluorescence emission and excitation spectrums of both the electropolymerized films were undertaken using a Cary Eclipse Fluorescence spectrometer (in Dublin city university, Ireland). These measurements were conducted in Hellma quartz cuvettes of either 1 cm or 0.2

cm optical path lengths. For the electrochemically synthesized polymers UV-Vis and fluorescence spectrums were recorded on the Nicolet Evolution 100 [Thermo Electron Cooperation, UK] and Horiba NanoLog 3-22- Triax [HORIBAJOBIN YVON, USA] respectively (in SensorLab UWC, South Africa). The Luminescence lifetimes were obtained using a Picoquant Fluotime 100 TCSPC system, exciting at 468 nm and detecting at 600 nm using a narrow band pass dielectric filter .The instrument response function was measured using scattering Ludox time response AM-30 colloidal silica solution (DCU, Ireland).

5.2.3. Synthesis of polymers

The electrosynthesis of PANSA undoped and doped with ASA, NSA and CNT were reported in chapter three, the chemical synthesis of undoped PANI, PANSA and PANI doped with NSA were presented in chapter four.



5.3. Results and Discussion

5.3.1. Photoluminescence Studies of electrosynthesized undoped and doped PANSA

Photoluminescence analysis was carried in this study to investigate the photophysical behaviour of undoped and doped PANSA molecules by using UV-vis spectroscopic, 2D and 3D fluorescence techniques.

5.3.1.1. UV-visible Spectroscopic Characterization

UV-visible spectroscopy is a useful tool for monitoring the possible changes in the absorption band which exists as intense peaks. Therefore, in this study this technique was employed to investigate the electronic absorption characteristic of PANSA and its interaction with the dopants. The UV-Vis spectra of undoped and doped PANSA were recorded in DMSO.

5.3.1.1.1. Electronic absorption of undoped PANSA

The spectrum of undoped PANSA (Figure 5.1) exhibited two characteristic bands at ~274 and 368 nm, these can be ascribed to π - π^* transitions and formation of polaronic (cations) and bipolaronic (dications) bands of polyemeraldine salt and is associated with the extent of conjugation between phenyl rings in the polymer ring (Figure 5.2). The observed band at 274 nm displayed a hypsochromic shift, which is a shift of spectral band position to lower wavelength as compared to the one of polyaniline (320 nm) reported before by Michira *et al.* (2007). This can be ascribed to the presence naphthalene sulfonic acid in the polymer backbone, which causes steric hindrance in the polymer chain. In addition, the presence of naphthalene sulfonic acid group also increases the torsional angle which reduces the conjugation length along the polymer (Bhandari *et al.*, 2011), and this causes shifting of π - π^* transition to lower wavelength. The similar UV-vis absorption bands were observed by Bhandari *et al.* (2011), using copolymers of aniline with ANSA in ethanol media, which was synthesized by chemical oxidative polymerization of aniline with ANSA and the absorption bands showed blue shift due to the presence of ANSA unit in the polymer matrix.

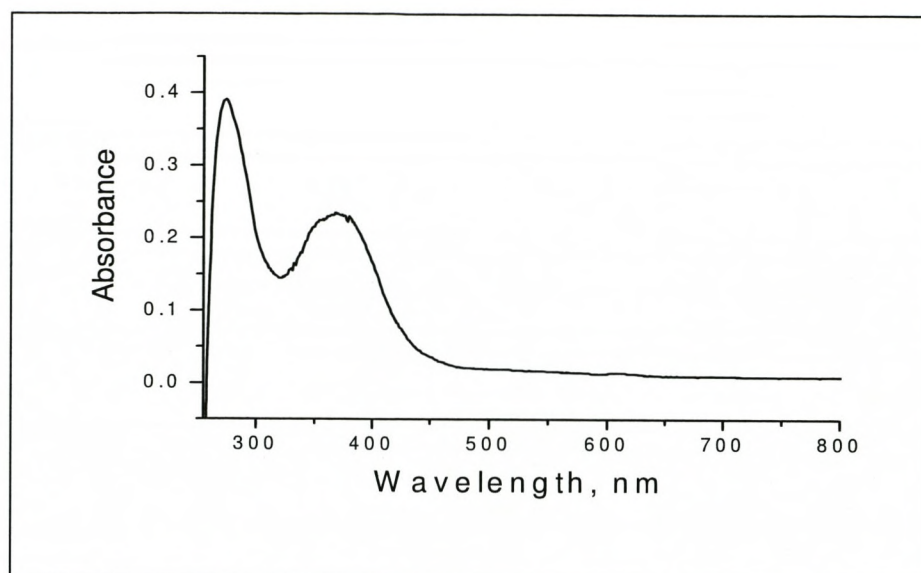


Figure 5.1: UV-visible spectra of undoped PANSA in DMSO.

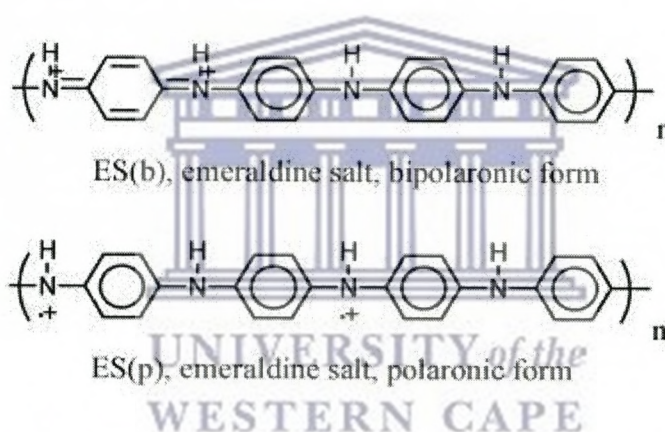


Figure 5.2: The forms of polyemeraldine salt (Huang and MacDiarmid, 1993).

5.3.1.1.2. Effect of dopants on electronic absorption of PANSA

The effects of how the dopants modulated the structure of PANSA were investigated using UV-Vis absorption spectra. The introduction of the dopants on the structure of PANSA showed lower absorption band with small change in absorption maximum wavelength as compared to undoped PANSA (Figure 5.3). Since, the fundamental process of doping is a charge-transfer reaction between an organic polymer and a dopant (Bhandari *et al.*, 2011).

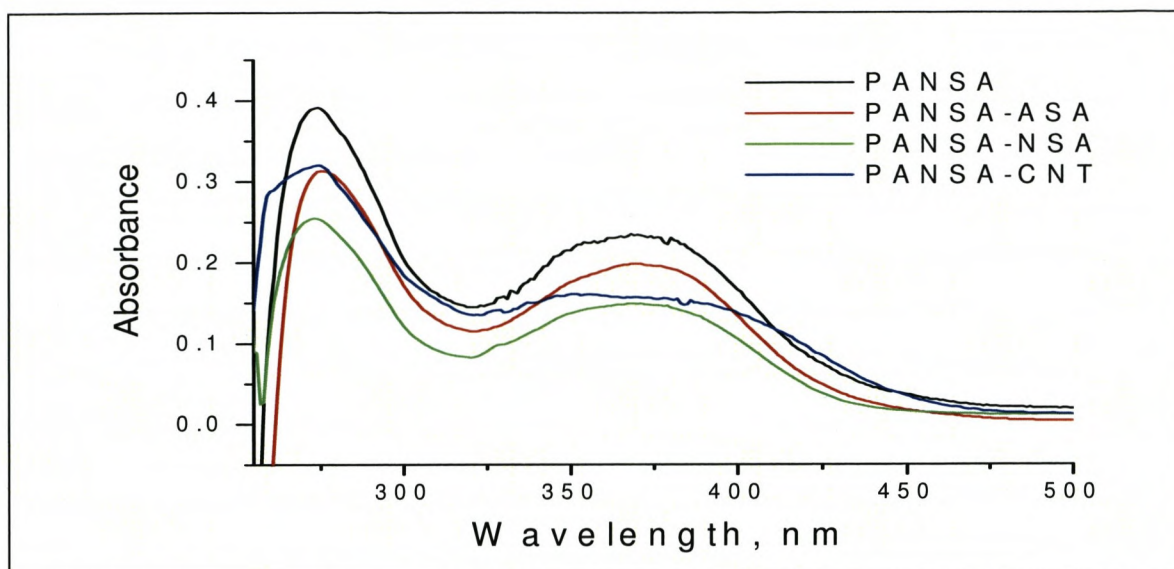


Figure 5.3: UV-visible spectra of doped PANSA with Anthracene sulfonic acid (ASA), 1,2-Naphthaquinone-4- sulfonic acid (NSA) and Carbon nanotubes (CNT) and undoped PANSA as a baseline in DMSO.

The success of these techniques is based on the fact that doping structurally modulates the structure of the resultant PANSA leading to change in band gap in its spectrum, because of doping, new electronic energy levels are introduced between the valence and conducting band of the polymer in the gap (Michira *et al.*, 2007). In the UV-vis spectra of doped PANSA (Figure 5.3), a small shift of < 2 nm was observed for bipolaronic bands in all dopants as compared to undoped, owing to the influence of dopants on the PANSA. However, a bathochromic shift was very small which was limited by the self-doping of the PANSA due to the presence of negatively charged sulfonate groups in PANSA structure. A similar observation of small bathochromic shift absorption bands observed in this work, was also observed by Bansal *et al.*, (2009) during synthesis of PANSA using para toluene sulphonic acid as a dopant in DMSO.

5.3.1.1.3. Band gap determination of undoped and doped PANSA

From the signature UV-vis absorption transition bands of undoped and doped PANSA (Figure 5.3), the band gaps of PANSA were estimated according to a method used by Misra *et al.*, (2005), by converting normal absorption spectra into a plot of absorbance squared versus the photon energy ($h\nu$). The extrapolation of the straight-line portion of absorbance squared-photon energy plot to zero absorption of the polymers (illustrated in Figure 5.4), this information obtained of band structure of polymer, can be related to the redox state of the polymer. The inserts in Figure 5.4 indicate a proposed band structure for the polyemeraldine salt, relating the band gaps based on theoretical calculations described above Results revealed the energy band gaps of the undoped PANSA to be 2.85 and 3.95 eV corresponding to polyemeraldine salt of PANSA (Figure 5.4). It was seen that the band of 2.85 eV for polyemeraldine salt was due to the localized benzoid highest occupied molecular orbital to quinoid lowest unoccupied molecular orbital excitation (Hopkins *et al.*, 1996), while the other band gap of 3.95 eV was attributed to phenyl rings which are connected by amine nitrogen. The effect of dopants on band gap of PANSA showed similar redox states with undoped PANSA with energy gaps corresponding to polyemeraldine salt with the first band gap of 2.90, 2.85 and 2.65 eV and the second of 3.95, 4.00 and 3.80 eV for PANSA-ASA, PANSA-NSA and PANSA-CNT, respectively, (Table 5.1).

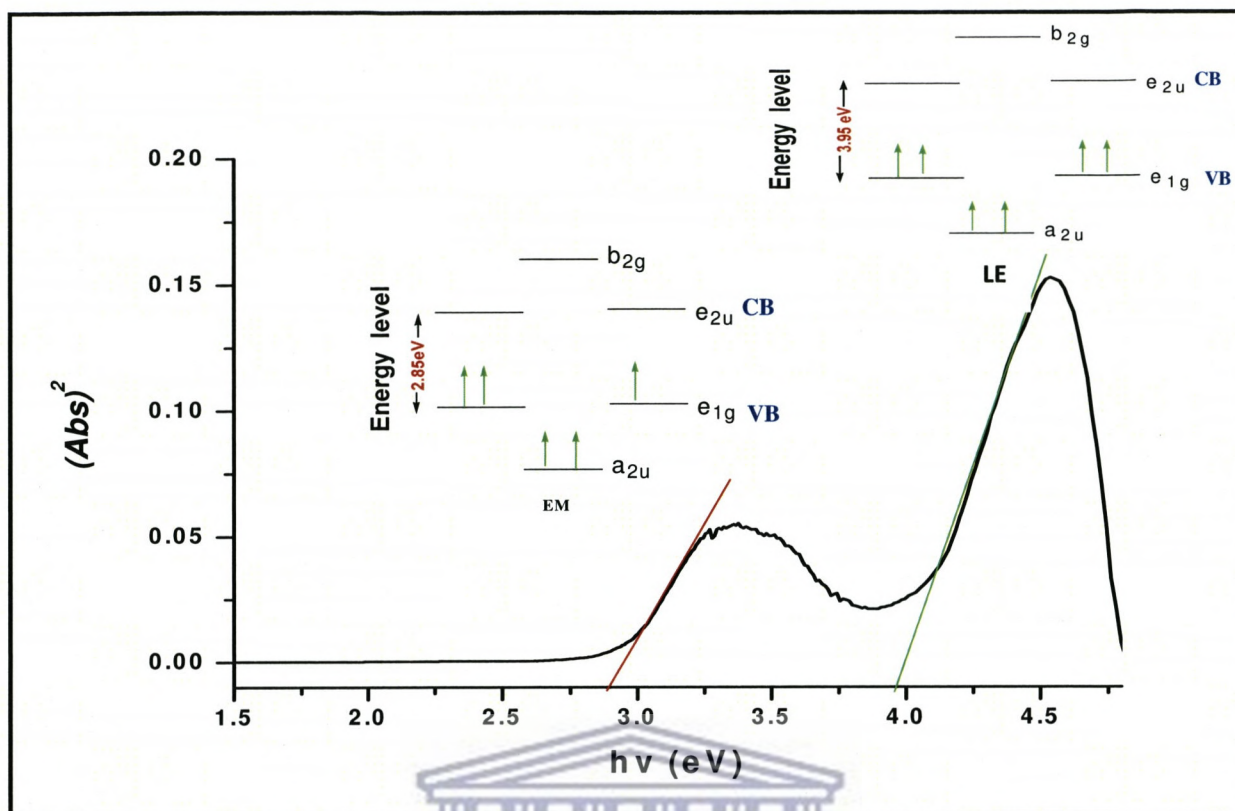


Figure 5.4: Absorbance squared versus photon energy extrapolated to zero absorption undoped PANSA, the inset for band gaps for polyleucoemeraldine (LE) and polyemeraldine (EM).

UNIVERSITY of the
WESTERN CAPE

Table 5.1: UV-vis absorption wavelength and band gap related to the redox states of the undoped and doped PANSA

Polymer	Absorption λ (nm)	Band gap (eV)	PANSA redox states
PANSA	274	3.95	Polyleucoemeraldine
	368	2.85	Polyemeraldine salt
PANSA-ASA	276	3.95	Polyleucoemeraldine
	370	2.90	Polyemeraldine salt
PANSA-NSA	273	4.00	Polyleucoemeraldine
	369	2.85	Polyemeraldine salt
PANSA-CNT	275	3.80	Polyleucoemeraldine
	369	2.65	Polyemeraldine salt



5.3.1.2. 2D Fluorescence Characterization of electrosynthesized PANSA

Fluorescence spectroscopic analysis was employed for further investigation of photoluminescence behaviour of undoped and doped PANSA because this important analytical technique is suitable for multicomponent analysis due to its inherent sensitivity, selectivity and versatility. Basically in fluorescence, a molecule absorbs light photons from the UV-visible light spectrum, which is known as excitation, causing transition to a high-energy electronic state and then rapidly emits light photons as it returns to its ground state, in less than 10^{-9} sec (Gfroerer, 2000). The 2D fluorescence spectra of undoped and doped PANSA were recorded in DMSO and the excitation wavelength for measuring polyaniline samples was set at 350 nm.

5.3.1.2.1. 2D Fluorescence spectra of undoped PANSA

The fluorescence spectra of undoped PANSA are presented in Figure 5.5, displays the showed excitation and emission spectra. Emission spectrum was red shifted with respect to excitation spectra, typical for polyaniline derivatives. It was observed at 481 nm whereas excitation spectrum was observed at around 383 nm when it was excited with 350 nm light. The excitation wavelength of 350 nm was chosen so that it fell within the range of the $\pi-\pi^*$ absorption envelope of the benzoid units centered at 360 - 380 nm (observed from absorption spectrum). In addition, the emission spectrum of this PANSA was noticed to be a mirror image of the excitation spectrum. This was probably due to the vibrational spacing in the ground state (S_0) that is often similar to the first excited single state (S_1) for large molecule (Mehamod, 2002).

The emission wavelength observed was different to previous studies which report a photoluminescence spectrum of polyaniline in NMP solution with λ_{\max} at 420 nm when it was excited with 340 nm light (Shimano and MacDiarmid, 2001). However, photoluminescence studies of poly(2-methoxyaniline-5-sulfonic acid) showed emission spectrum at around 600 nm when irradiated at wavelengths between 350 and 530 nm (Kane-Maguire, 2004). In addition, a large Stokes shift of 98 nm was obtained from the spectra in this work (Table 5.2), suggesting that the molecular geometry of the excited state was strongly different from that of the ground state.

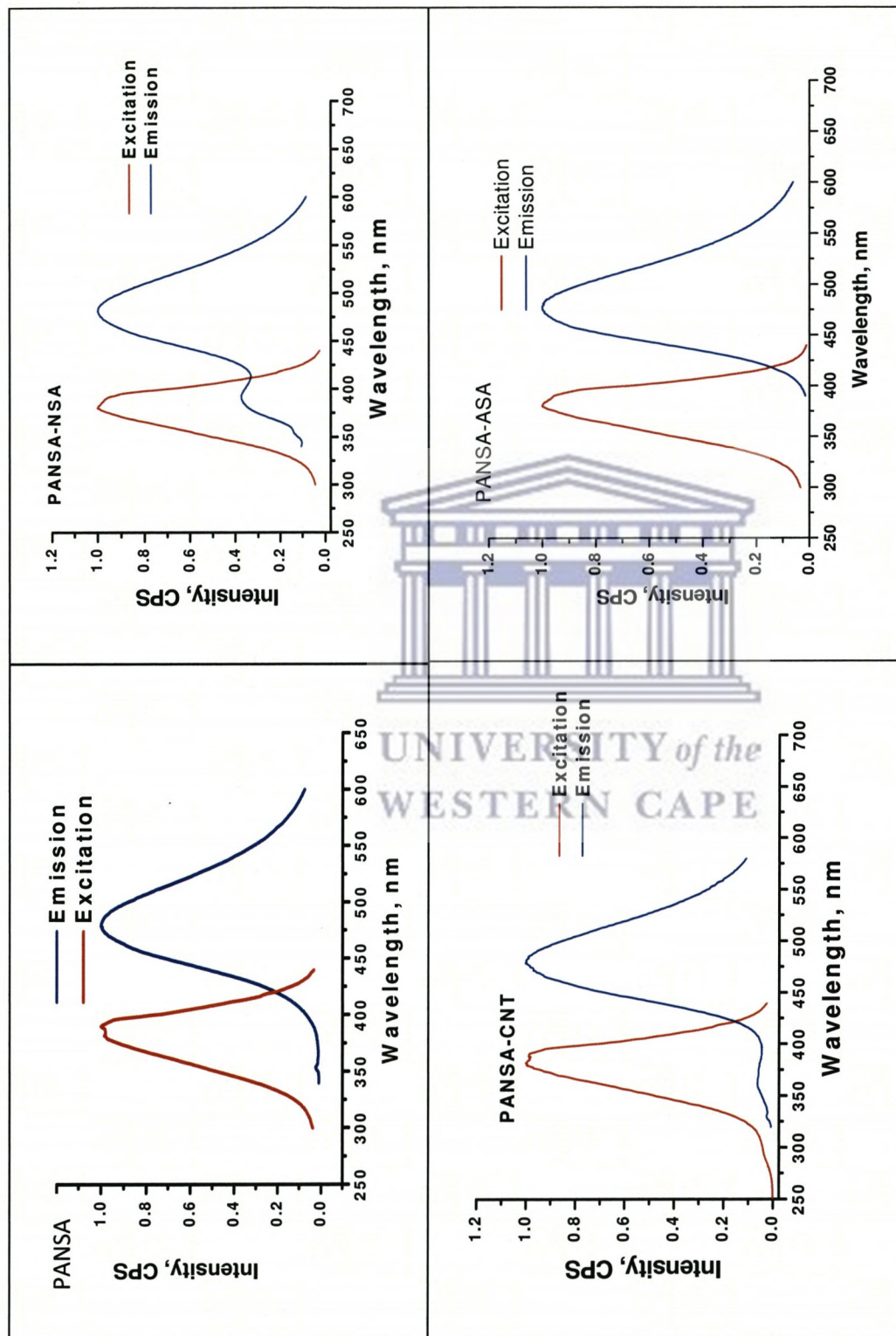


Figure 5.5: 2D Fluorescence spectra of undoped and doped PANSA with 1, 2 Naphthaquinone-4- sulfonic acid (NSA), Carbon nanotubes (CNT) and Anthracene sulfonic acid (ASA).

Table 5.2: Results summary of fluorescence properties of the polymers

Polymer	Fluorescence		Stoke's shift(nm)
	Ex. (nm)	Em. (nm)	
PANSA	383	481	98
PANSA-ASA	381	481	100
PANSA-NSA	380	481	101
PANSA-CNT	382	481	99



5.3.1.2.2. Effect of dopants on 2D fluorescence spectra of PANSA

The fluorescence emission spectra (Figure 5.5) of the doped PANSA were also red shifted with respect to their excitation spectra and they were observed at 481 nm whereas excitation spectra were observed at around 381, 380 and 382 nm and with a stoke's shift of 100, 101 and 99 nm for PANSA-ASA, PANSA-NSA and PANSA-CNT, respectively, as shown in the inset table. The behaviour was similar to the one of undoped PANSA. However, the emission spectrum of PANSA-NSA showed an additional shoulder at around 400 nm and did not form a mirror image of its excitation spectrum. This was probably due a loss of symmetry of the molecule upon excitation or because the vibrational spacing in the ground state (S_0) for large molecule is different to the first excited single state (S_1) (Mehamod, 2002).

It is well documented that in most polymers the chromophore responsible for fluorescence is the benzoid group and it was also found that quinoid groups are actually responsible for the quenching effect of photoluminescence (Son *et al.*, 1989; Shimano and MacDiarmid, 2001). Hence, the observed excitation spectra provided information about the absorption spectra of the excited fluorescent molecule in the excited state. The fluorescence excitation spectra are usually compared to the corresponding absorption spectra from UV/vis spectra and should ideally resemble the latter (Gfroerer, 2000). In addition, the excitation spectra also show if the emitted PANSA molecule has a similar molecular geometry to that of the ground state or whether any geometrical changes have occurred in the PANSA molecule upon excitation (Gfroerer, 2000). Therefore, the observed excitation peak at ~380 nm was attributed to the benzoid groups causing the emission in the polymers at ~481 nm. From these observations of fluorescence spectra, the undoped and doped PANSA forms exhibited one emission wavelength. Leading to the deduced conclusion that only one molecule is fluorescing and that molecule was common to all samples, which is the benzoid groups of PANSA itself. The dopants did not fluoresce, hence this observation of common emission of 481 nm for all polymers despite of modulation with different dopants. These observations demonstrated that the photoluminescence features of PANSA itself were maintained although the dopants were introduced. The excitation and emission observed for these polymers at ~380 and 481 nm equated to ~3.0 and 2.2 eV band gaps, respectively. These excitation wavelengths and energy gaps were close in energy to the $\pi - \pi^*$ absorption band of these polymers at ~370 nm and ~2.7-3.0 eV, respectively which was associated with its benzoid units. For example, this was shown in Figure 5.6 for fluorescence excitation and UV-vis absorption spectra of PANSA-CNT.

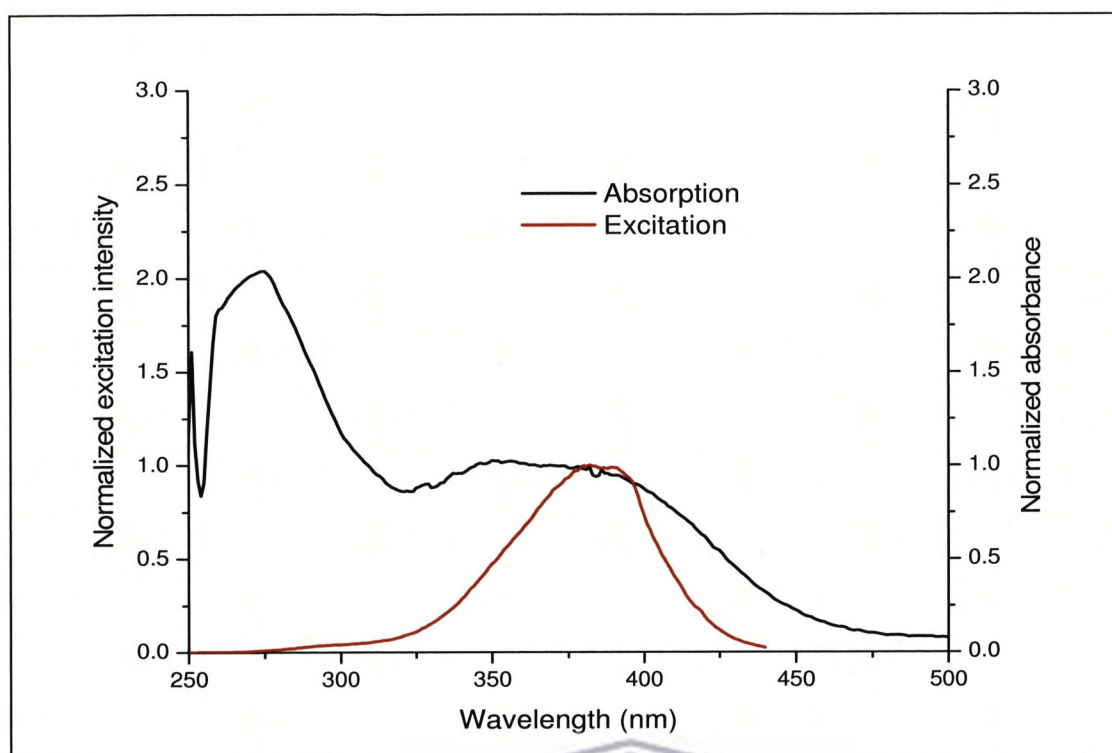


Figure 5.6: Fluorescence excitation and UV-vis absorption spectra of PANSA-CNT in DMSO, excited at 350 nm.

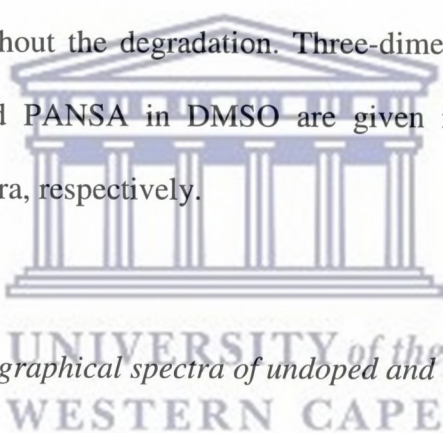
The excitation spectrum was shown to correspond with the absorption band at around 380 nm, as evidence that the fluorescing molecule was due to the benzoid ring of polyemeraldine (EM) salt of the PANSA-CNT.

However, it was shown that emission from the polyemeraldine excited state was believed to be self-quenched by adjacent quinoid groups in its structure (Son *et al.* 1989). However, several studies by Shimano and MacDiarmid (2001) and others (Cochet *et al.*, 2001; Chen *et al.*, 1996) showed that photoluminescence from polyemeraldine base (EB) films cast from solvents such as N-methylpyrrolidinone (NMP) and the emitting units in photoactivated *EB were considered to be the benzoid groups. However, Thorne *et al.* (1992) showed that the

fully reduced leucoemeraldine base (LB) form exhibits a strong emission centred at around 410 nm when irradiated at 300-350 nm due to benzoid groups.

5.3.1.3. 3D Fluorescence Characterization of PANSA

Three-dimensional fluorescence was also used for characterization of these materials. Since, single-wavelength measurements of fluorescence can be limited for the analysis of complicated multi-oxidation states of the polymer containing several overlapping emissions and/or excitation spectra. Bosco *et al.* (2006) used 3D fluorescence studies to resolve the species present in the reaction mixture, quantify the concentration of phenol and its principal degradation of products throughout the degradation. Three-dimensional photoluminescence spectra of undoped and doped PANSA in DMSO are given in Figure 5.7 and 5.8 for topographical and contour spectra, respectively.



5.3.1.3. 1. 3D fluorescence topographical spectra of undoped and doped PANSA

In 3D topographical fluorescence, one axis is the excitation wavelength scale, a second axis represents the emission wavelength and the other axis is that of intensity. The DMSO and monomer (ANSA) topographical spectra are also illustrated in Figure 5.7 (a) and (b), respectively. It was necessary to measure the solvent alone in order to ascertain that the DMSO does not actually give fluorescence background and the monomer as the baseline for better understanding of PL properties of the starting material so as to be able to evaluate the differences between monomer and polymer PL properties. There was no emission observed for DMSO solvent alone, however there is an insignificant effect of reyleigh scattering at 340 mn excitation and between 460 and 520 nm for emission. The emission of monomer

spectrum was observed, with photoluminescence intensity of 8×10^3 CPS both emission and excitation spectra due the phenyl rings in the monomer. When exciting the polymers at the 350 nm, topographical peaks of undoped PANSA (Figure 5.7(c)) were observed at the excitation and emission wavelengths of 380-400/500-540 nm. The topographical emission and excitation spectra showed to be broad and featureless with PL intensity of 1.4×10^5 CPS, which was much greater than the intensity of the monomer. The PL of this undoped PANSA might be to the fluorescing behaviour of benzoid group in polymer.

The effect of dopants on the polymer resulted in the increase in photoluminescence intensity of emission and excitation spectra of about 1.6×10^5 and 2×10^5 CPS for polymers modulated with ASA (Figure 5.7(d)) and NSA dopants (Figure 5.7(e)), respectively. The increase in photoluminescence intensity was attributed to the separation of benzoid groups in polyemeraldine salt (ES) due to their electrostatic repulsion. This observation of benzoid groups contributing to increased photoluminescence is consistent with the results from the UV absorption and 2D fluorescence spectrums discussed above, which indicated that the absorption resulted from absorption of the benzoid groups, which gave rise to fluorescence emission observed in 2D spectrums shown earlier. Furthermore, increased photoluminescence intensity enhancement might be due to transfer of energy from the dopant to PANSA (Ameen, 2009). However, CNT dopant (Figure 5.7(f)) showed a similar photoluminescence intensity of emission-excitation spectra with undoped PANSA.

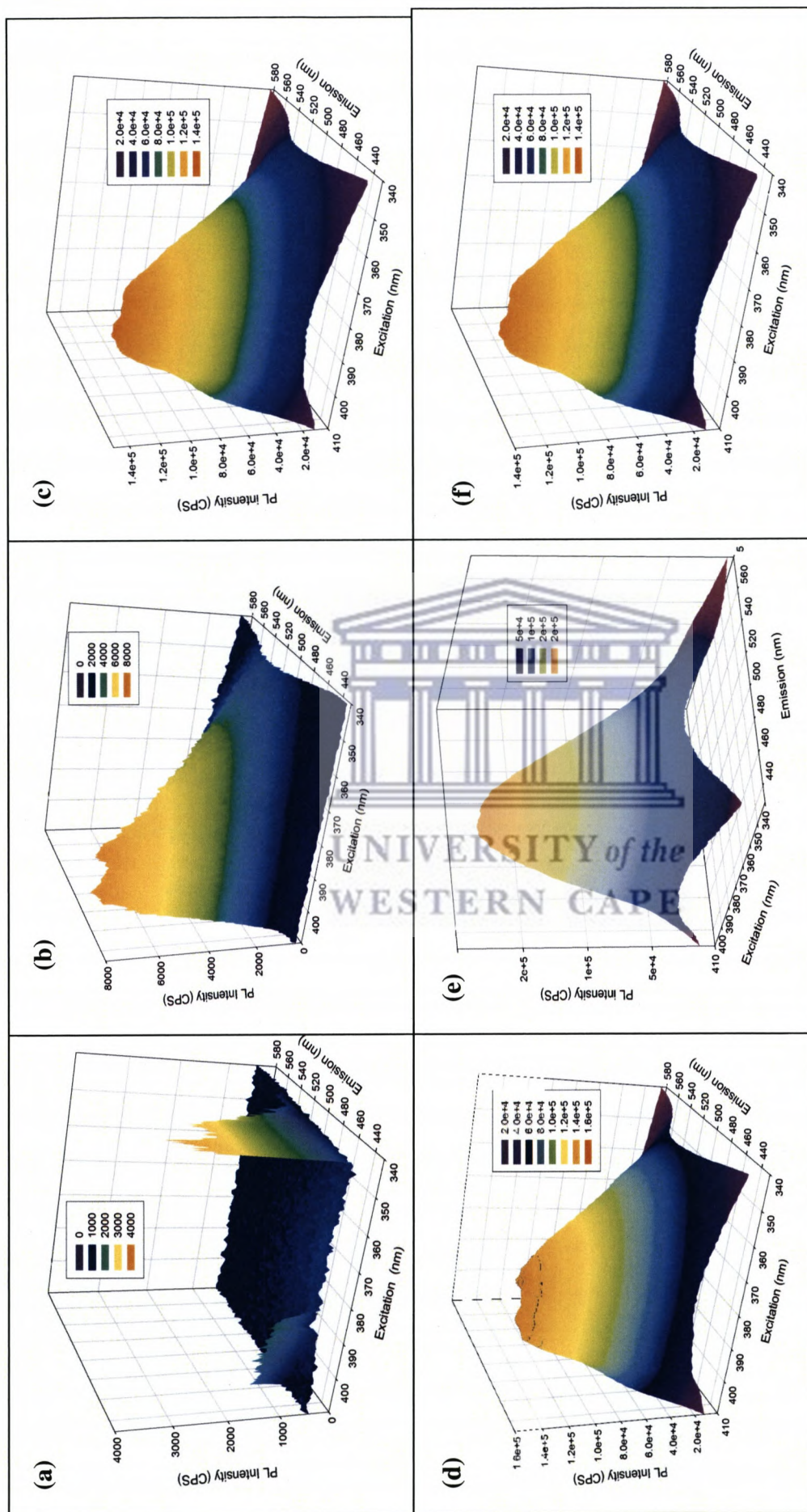


Figure 5.7: 3D Fluorescence topographical spectra of (a) DMSO, (b) ANSA, (c) undoped and doped PANSA with (d) Anthracene sulfonic acid (ASA), (e) 1,2-Naphthaquinone-4- sulfonic acid (NSA) and (f) Carbon nanotubes (CNT), respectively, in DMSO.

5.3.1.3.2. 3D fluorescence contour spectra

A 3D photoluminescence contour study was carried out to map the emission responses for these polymers. In 3D contour photoluminescence, one axis is the excitation wavelength scale and second axis represents the emission wavelength. It was seen in Figure 5.8(a), there was no excitation and emission wavelengths for DMSO spectrum; contour showed an agreement with the topographical spectrum observed for this solvent, confirming that DMSO does give any fluorescence background. The monomer contour spectra is given in Figure 5.8(b), the excitation wavelength centered at 410 nm resulted in photoluminescence (PL) emission centered at 490 nm with contour photoluminescence intensity of 7×10^3 CPS. The contour photoluminescence peaks of undoped PANSA (Figure 5.8(c)) were located at the excitation/emission wavelengths centered around 380/480 nm with contour intensity of 1.8×10^5 CPS. Similar excitation/emission wavelengths obtained under 2D fluorescence confirming that PANSA is in its emeraldine salt redox state. Zhou (2009), observed contour photoluminescence emission wavelength at 510nm for poly (2-methoxyaniline-5-sulfonic acid) (PMAS) when excited at 355 nm, the contour photoluminescence resulting from the emeraldine salt form of the PMAS. The introduction of dopants during electropolymerization of PANSA showed contour photoluminescence intensity of emission and excitation spectra of about 1.4×10^5 , 4×10^4 and 1.2×10^5 CPS for ASA (Figure 5.8(d)), NSA dopants (Figure 5.8(e)) and CNT (Figure 5.8(d)), respectively. The 3D contour fluorescence was in agreement to 2D fluorescence showing photoluminescence of polyemeraldine salt (EM) in the polymers.

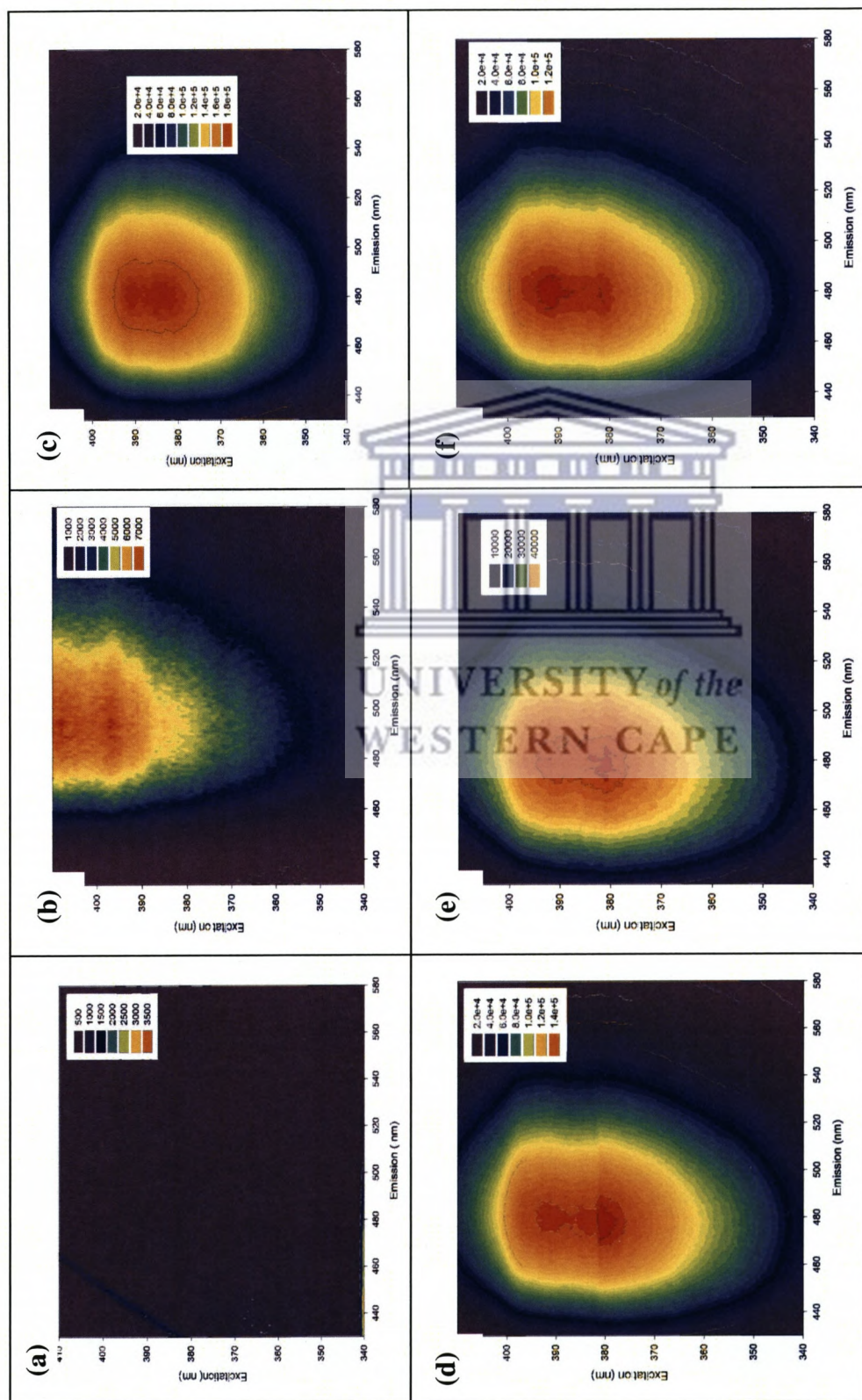


Figure 5.8: 3D Fluorescence contour spectra of (a) DMSO, (b) ANSA, (c) undoped and doped PANSA with (d) Anthracene sulfonic acid (ASA), (e) 1,2-Naphthaquinone-4- sulfonic acid (NSA) and (f) Carbon nanotubes (CNT), respectively, in DMSO.

5.3.2. Photoluminescence Studies of chemically synthesized PANI and PANSA

5.3.2.1. UV-visible Spectroscopic Characterization of Chemically synthesized Undoped PANI and PANSA

The UV-Vis spectra of chemically synthesized PANI and PANSA are shown in Figure 5.9. The UV-Vis spectra of PANI showed a peak between 300 and 350nm and a broad peak starting from 500 to 750 nm. The band at around 300-350 nm was due to π - π^* transition of benzoid rings while the peak at around 500-750 nm was due to charge transfer excitons of quinoid structure (Kohut-Svelko *et al.*, 2005; Kulkarni *et al.*, 2004). The observed bands were similar to the one obtained by Mavundla (2010), using chemical synthesized PANI for solar cell applications. These bands were characteristics of polyemeraldine base (EB) of PANI, because EB redox state of polyaniline is known to have low wavelength ascribed to π - π^* band and a strong band at around 600 nm that has been attributed to a local charge transfer between a quinoid ring and the adjacent imine-phenyl-amine units giving rise to an intramolecular charge transfer exciton (Mavundla, 2007; Kohut-Svelko *et al.*, 2005; Kulkarni *et al.*, 2004). However, Dong *et al.* (2007) observed pernigraniline form of polyaniline in the preparation of polyaniline/multi-walled carbon nanotubes composites for supercapacitor.

When comparing the UV-Vis spectra of chemical synthesized PANI and PANSA, it was seen that the shapes of the peaks were different. The peak observed between 250-300 nm due to the π - π^* transitions of the benzoid groups in PANSA, exhibited a hypsochromic shift with respect to PANI which was observed at 300-350 nm. Furthermore the peak observed between 380-400 nm in PANSA, which can be ascribed to charge transfer excitons of quinoid structure has also shifted to shorter wavelengths, when comparing it to PANI which was observed between 500-750 nm. These shifts were due to the attachment of naphthalene

sulphonic acid in the polymer backbone and might enhance the conductivity and reactivity of the PANSA.

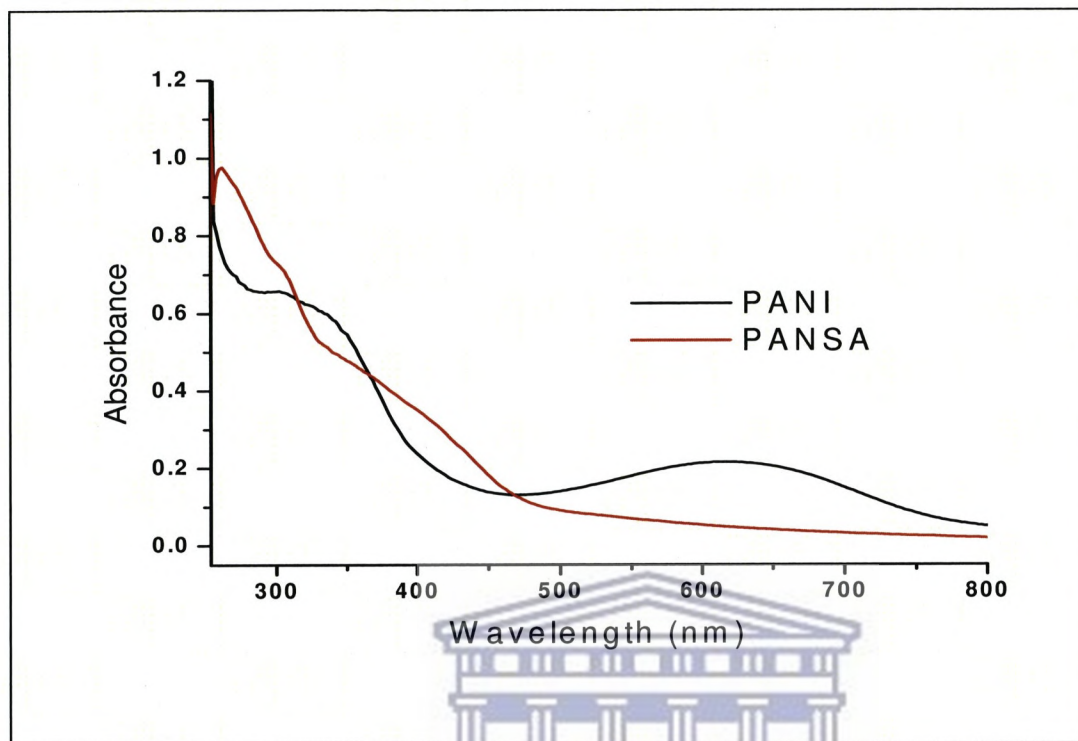


Figure 5.9: UV-visible spectra of undoped chemically synthesized PANI and PANSA in DMSO

UNIVERSITY of the
WESTERN CAPE

5.3.4.2. Effect of NSA on electronic absorption of PANI

The effect of NSA as a dopant on PANI was investigated by employing UV-vis spectral characterization of the composite PANI-NSA in DMSO, and comparing it to that of PANI with no dopant (Figure 5.10). The results show that there are two peaks observed in both polymers with maxima at ~ 320 and 620 nm corresponding to π - π^* transition centered on the benzoid unit and quinoid exciton band, respectively. The introduction of dopants showed no effect on the electronic absorption of PANI. The addition of dopants was expected to modulate the structure of PANI (Michira *et al.*, 2007). Lin *et al.* (2009) showed that the

introduction of CNT in the polymer resulted in the appearance of a new band around 290 nm. In addition to this, there was a considerable blue shift of about 30 nm of the π - π^* transition band as compared to polymer (Lin *et al.*, 2009).

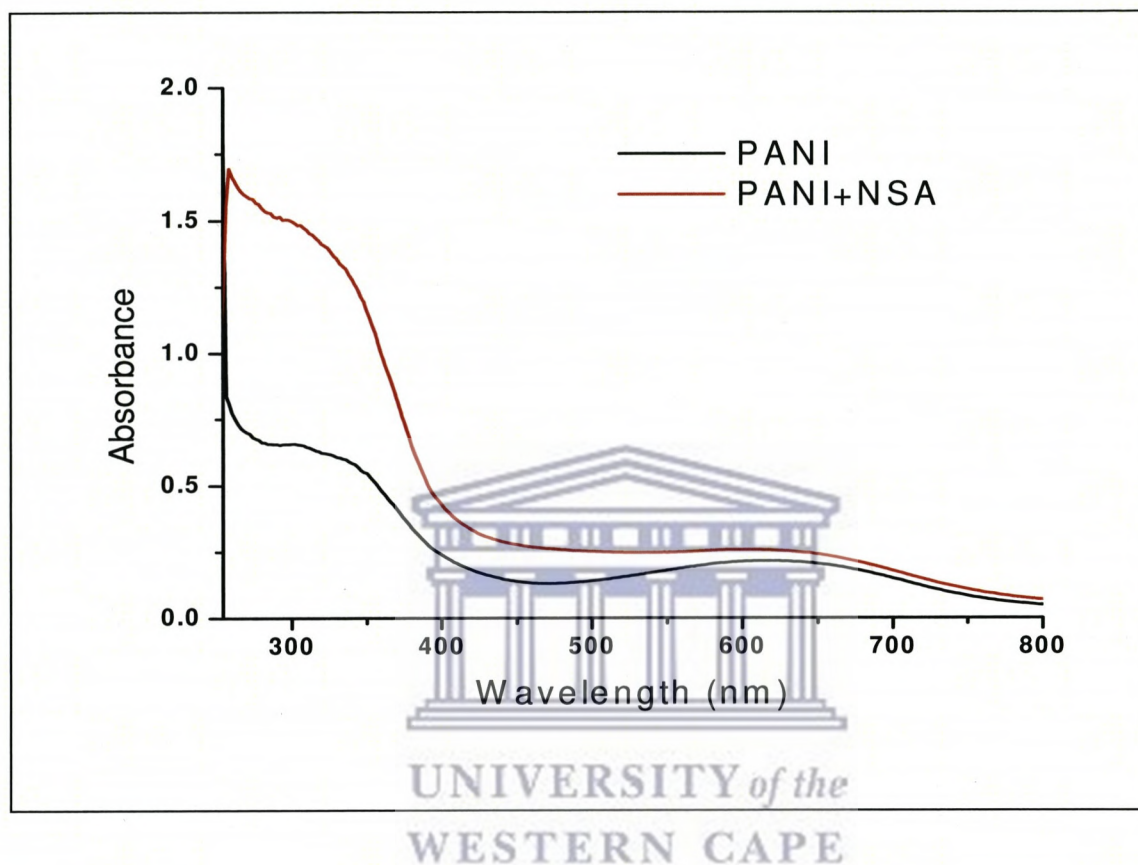
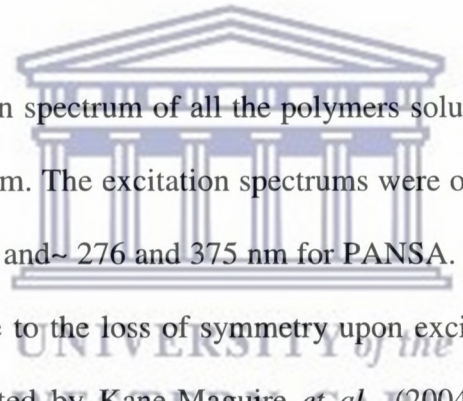


Figure 5.10: UV-visible spectra of chemical synthesized PANI doped with NSA in DMSO.

5.3.2.3. Fluorescence Spectroscopic Characterization of Chemical synthesized Undoped PANI and PANSA

The fluorescence spectra of PANI and PANSA in DMSO are presented in Figures 5.11 and 5.12, respectively, showing the absorption, fluorescence emission and excitation spectra. The maximum emission of PANI and PANSA was observed at 470 and 485 nm when the polymer solutions were excited at 308 and 313 nm, respectively. As explained previously the EB state of PANI is composed of a series of alternating two benzoid units and one quinoid unit Hence

the observed emissions were due benzoid groups of the EB redox state of the polymer. However, no emission from quinoid units absorption at around 600 nm (PANI) and 400 nm (PANSA) was observed. Infact the quinoid units are known to quench the adjacent benzoid groups (Son *et al.*, 1989; Shimano and MacDiarmid, 2001). The fluorescence spectrum of PANSA exhibited a bathochromic shift with respect to PANI, this is because the different of self doping agent and self doping level caused by the presence of the naphthalene sulfonic acid in the polymer backbone (Masdarolomoor *et al.*, 2008). The presence of the naphthalene sulfonic acid in the polymer backbone gave rise to maximum emission at higher wavelength. In addition, the emission spectrum of both polymers was observed to the red shifted as compared to absorption and excitation spectra.



It was noticed that the emission spectrum of all the polymers solutions did not give a mirror image of the excitation spectrum. The excitation spectrums were observed to have two peaks at ~ 276 and 375 nm for PANI and ~ 276 and 375 nm for PANSA. The difference in emission and excitation spectra was due to the loss of symmetry upon excitation. This observation is different from that demonstrated by Kane-Maguire *et al.*, (2004), which showed that the emission spectra of PANI as a mirror image of excitation spectra, because of the vibrational spacing in the ground state (S_0) of that is often similar to the first excited single state (S_1) for large molecule (Mehamod, 2002).

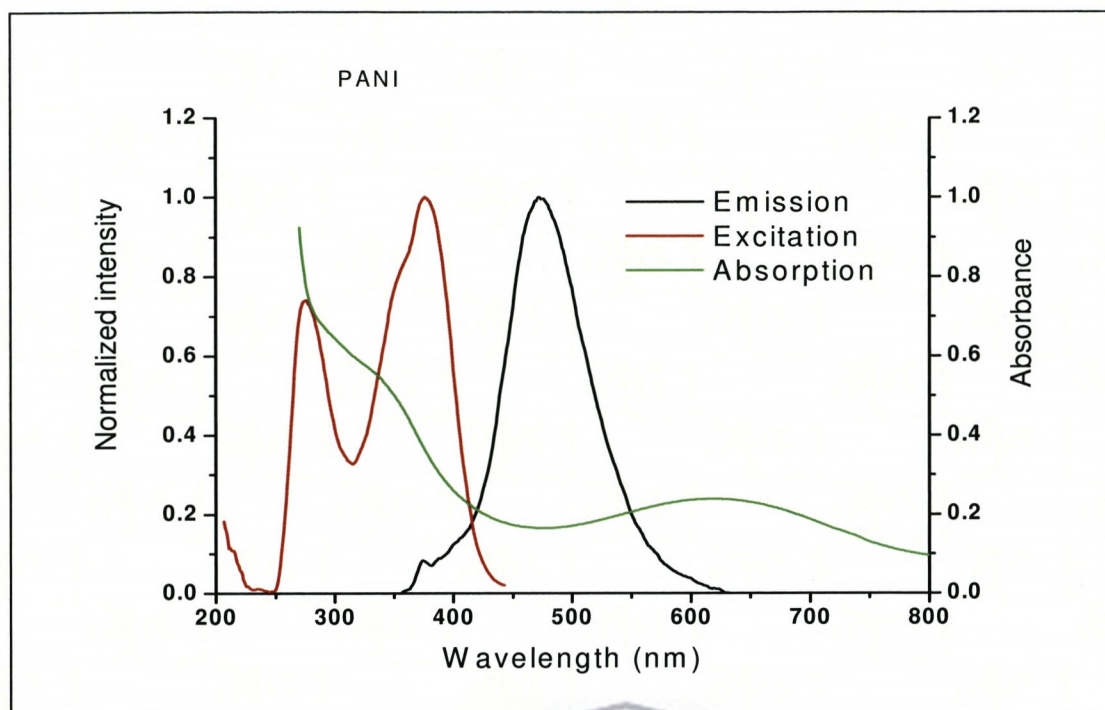


Figure 5.11: Fluorescence excitation, emission and UV-vis absorption spectra of PANI in DMSO, excited at 350 nm.

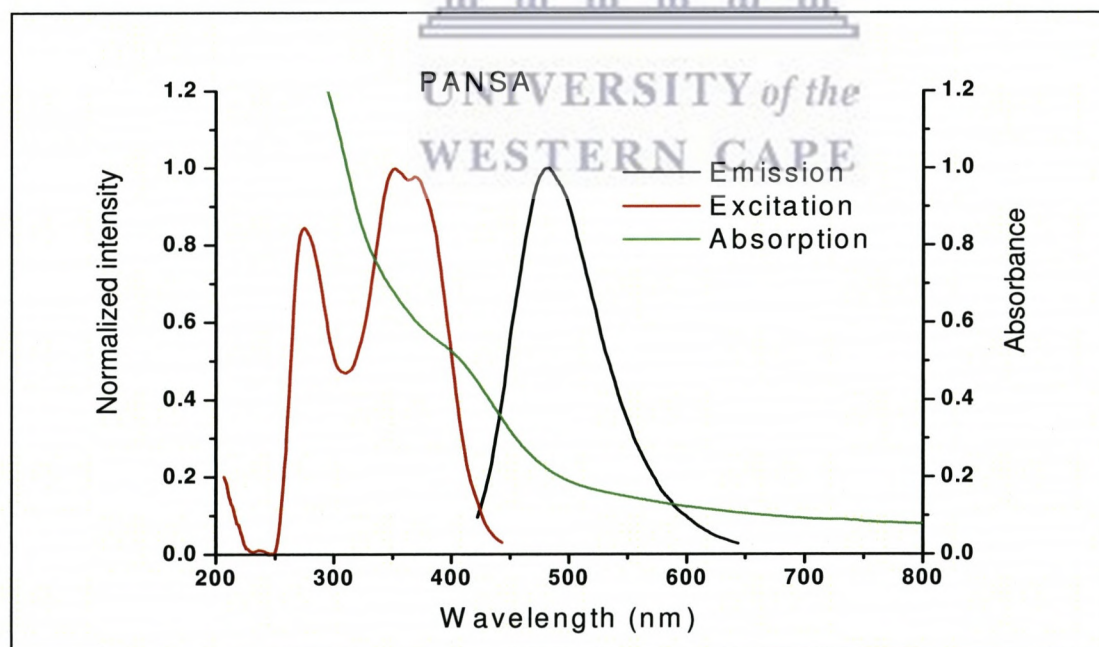


Figure 5.12: Fluorescence excitation, emission and UV-vis absorption spectra of PANSA in DMSO, excited at 350 nm.

5.3.4.2. Effect of dopant on fluorescence spectra of PANI

Figure 5.13 shows photoluminescence spectra of PANI doped with NSA in order to investigate the effect of dopant during the chemical synthesis of PANI. The observed fluorescence and excitation spectra were similar to the chemical synthesized PANI without dopant (Figure 5.11). This indicated that the NSA dopant did not fluoresce, hence, observation of common emission at 470 nm; this showed that the photoluminescence features of PANI were maintained despite the introduction of the NSA dopant.

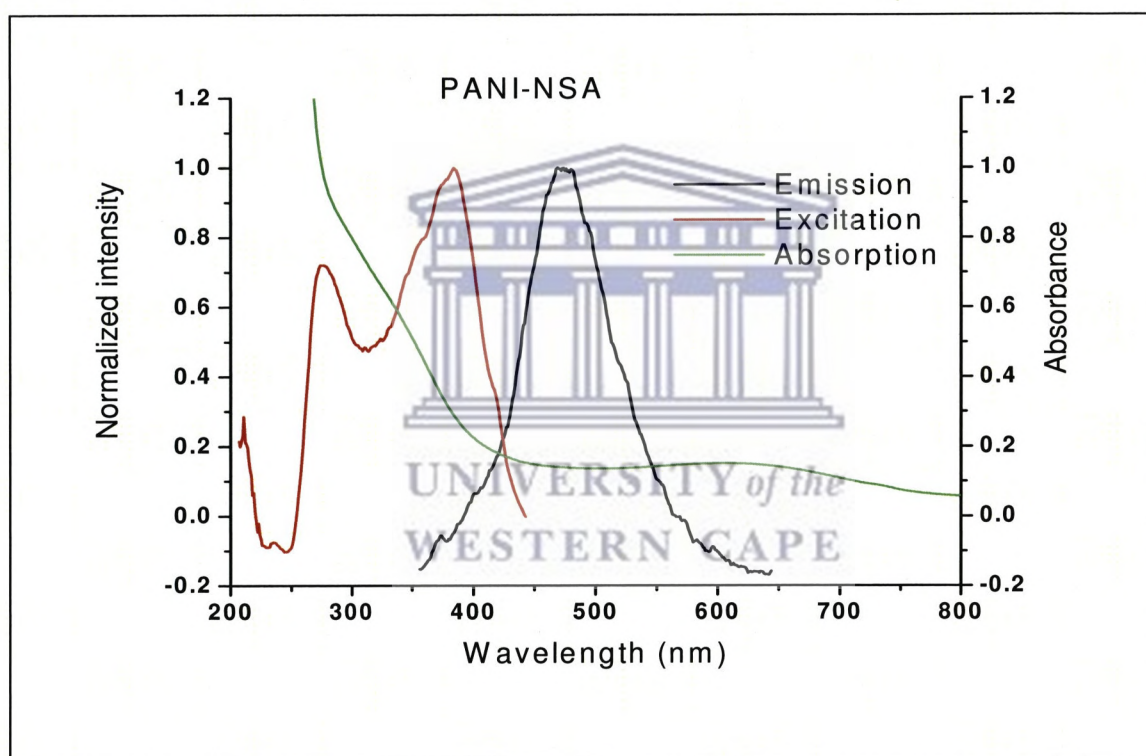


Figure 5.13: Fluorescence excitation, emission and UV-vis absorption spectra of PANI-NSA in DMSO, excited at 350 nm.

5.3.4.3. Fluorescence quantum yield and lifetime of chemical synthesized PANI and PANSA

The fluorescence quantum yields and lifetimes of chemical synthesized PANI, PANSA and PANI-NSA can yield a wealth of information on the relative efficiencies of radiative and non-radiative process, as well as the rates of competing photochemical reactions (Vos, 2003). Most importantly although polyaniline and its derivatives are known to yield low quantum yield values, the study of these properties can give powerful insight into electronic structure of these materials. The quantum yield of PANI, PANSA and PANI-NSA polymers in DMSO were measured using a standard procedure (Williams *et al.*, 1983). The same number of photons was absorbed by the standard and the respective PANI, PANSA and PANI-NSA polymers, because the absorbance is matched at the excitation wavelength. The fluorescence quantum yield (Φ_F) was calculated using Equation 2.41 (as given in chapter two).

$$\Phi_F = \Phi_F^{std} \frac{F_{std} \cdot A_{std} \cdot n^2}{F \cdot A \cdot n^2} \quad [2.41]$$

The quantum yield of all the samples was measured in common de-aerated solution medium of DMSO. Anthracene was used as the standard sample. The fluorescence quantum yield (Φ_F) values for the PANI, PANSA and PANI-NSA conducting polymers (Table 5.3) were found to be 0.0304, 0.005 and 0.0448, respectively. The Φ_F values of PANSA was observed to be lower than PANI, this might be due to the presence of a sulfonic acid unit in the polymer back, which causes steric hindrance of N-substituted naphthalene sulfonic acid group and consequently reducing the number of fluorescing polymer molecules. Relatively higher Φ_F values were observed PANI-NSA as compared to the rest of the polymers due to the addition of NSA as a dopant. Antonel *et al.* (2006), reported very low $\Phi_F \sim 0.001$ for pure EM form PANI, and the results obtained in this study are higher

Table 5.3: Fluorescence quantum yield of PANI, PANSA and PANI-NSA in DMSO

Sample	Absorbance	Area	Quantum yield	Quantum yield %
Anthracene	0.222	5967.21	0.27 (known) ^a	27%
PANI	0.224	583.31	0.0304	3.0%
PANSA	0.226	95.886	0.0050	0.5%
PANI-NSA	0.228	858.78	0.0448	4.4%

a=(Dawson and Windsor, 1968)

The photoluminescence emission lifetime of a polymer usually represents the average amount of time the species remains in the excited state prior to its return to the ground state. In fluorescence, the process is usually a unimolecular and therefore the excited state population established by an impulse of exciting light will generally decay exponentially according to first order kinetics. The impulse response function $I(t)$ will have the form:

$$I(t) = I_0 e^{-kt} \quad [5.1]$$

Where k represents the overall relaxation rate and I_0 is simply a scaling factor. Since the photoluminescence lifetime (t) is by definition the time required for the excited state population to decay to $1/e$ or $\sim 37\%$ of its initial intensity, and it can be determined graphically from the slope of a plot of $\ln(I)$ versus t . The fluorescent lifetimes of the PANI, PANSA and PANI-NSA in DMSO were measured using the FluoTime 100 Time-Correlated Single Photon Counting (TCSPC) instrument.

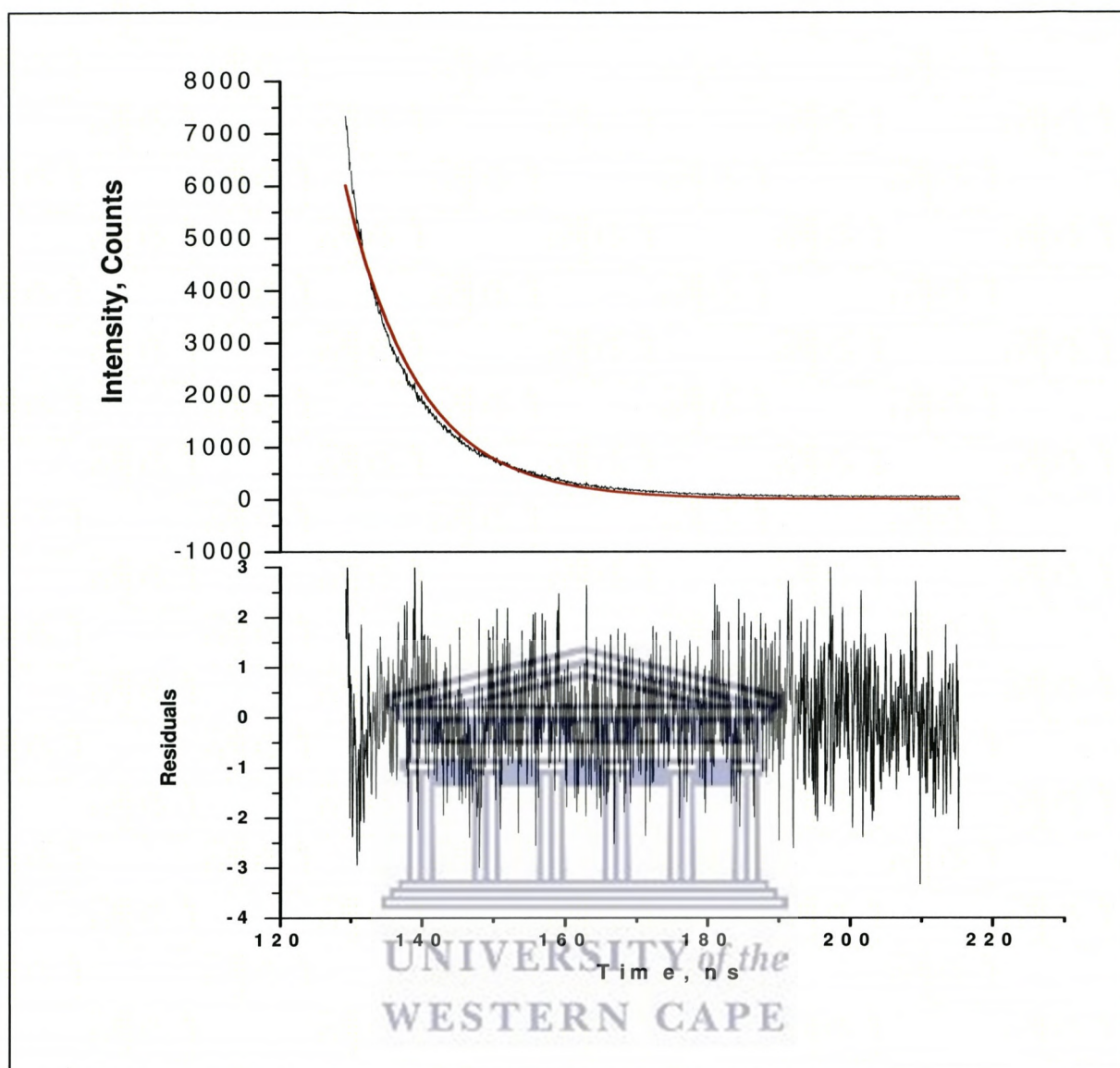


Figure 5.14: Typical fluorescence emission decay of PANSA in DMSO, when pulsed with a 450 nm laser source with a long pass-off filter of 530 nm, and the residual of a mono exponential tail fit.

The lifetime measurements for PANI, PANSA and PANI-NSA were recorded at both aerated and de-aerated conditions since atmospheric oxygen is known as an efficient quencher of luminescence lifetime (Lakowicz, 1999). Figure 5.14 displays the emission decay of PANSA that follows biexponential kinetics and all three polymers gave a similar decay curve. The

first component τ_1 was 11.54 ± 0.066 ns, and while the second component τ_2 was very short lived 3.717 ± 0.123 ns. When the sample was de-aerated for 30 minutes, the life time of τ_1 increased to 11.62 ± 0.06 ns, while τ_2 degreased to 3.44 ± 0.11 ns.

The lifetimes at τ_1 for the PANI, PANI-NSA and PANSA under un-degassed and degassed conditions were almost equal (11.4 ± 0.057 , 11.96 ± 0.087 and 11.54 ± 0.066), which was consistent with the emission behaviour observed previously confirming that, the fluorescing molecule was common in all the polymers, hence, its lifetime was the same. The elimination of collisional oxygen had an effect in the second component τ_2 of all three polymers, as the τ_2 decreased after the samples were degassed. This observation was not expected because it is known that, oxygen is an efficient quencher of luminescence lifetime (Lakowicz, 2006). However, in this study τ_2 of the polymers were found to be longer in the un-degassed samples as compared degassed at τ_2 . The lifetimes at τ_2 were found to be 2.2 ± 0.057 , 3.74 ± 0.087 and 3.717 ± 0.123 ns in un-degassed environment for PANI, PANI-NSA and PANSA, respectively. Whereas in degassed condition the lifetimes that were obtained decreased to 1.23 ± 0.09 , 2.02 ± 0.13 and 3.44 ± 0.11 ns for PANI, PANI-NSA and PANSA, respectively showing that degassing the samples decreased the second τ_2 lifetime. Table 5.4 presents a comparison the different lifetimes of the polymers, in aerated and de-aerated conditions

Table 5.4: Fluorescence lifetime of PANI, PANSa and PANI-NSa in DMSO

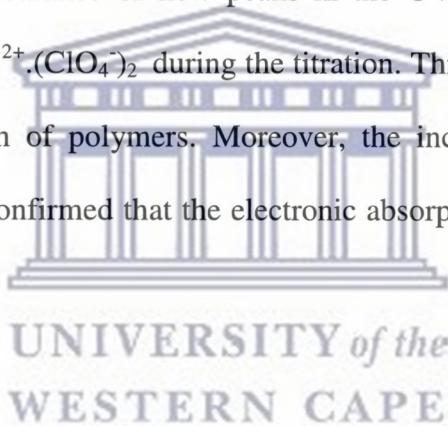
Sample	τ_1 (ns)		τ_2 (ns)	
	Un-degassed	Degassed	Un-degassed	Degassed (30 min)
PANI	11.4 \pm 0.057	12.11 \pm 0.07	2.2 \pm 0.057	1.23 \pm 0.09
PANI-NSA	11.96 \pm 0.087	12.03 \pm 0.06	3.74 \pm 0.087	2.02 \pm 0.13
PANSA	11.54 \pm 0.066	11.62 \pm 0.06	3.717 \pm 0.123	3.44 \pm 0.11

5.3.5. Photoluminescence Studies $[\text{Ru}(\text{bpy})_2(\text{picCOOH})]^{2+} \cdot (\text{ClO}_4^-)_2$ with addition of polymers

5.3.5.1. UV-visible Spectroscopic Characterization of $[\text{Ru}(\text{bpy})_2(\text{picCOOH})]^{2+} \cdot (\text{ClO}_4^-)_2$ with addition of chemically synthesized polymers

Figure 5.15 illustrates the electronic absorption spectra of $[\text{Ru}(\text{bpy})_2(\text{picCOOH})]^{2+} \cdot (\text{ClO}_4^-)_2$ (Ru complex) in acetonitrile with addition of either PANI, PANSa or PANI-NSa in DMSO, in order to investigate the effect of polymer on the $[\text{Ru}(\text{bpy})_2(\text{picCOOH})]^{2+} \cdot (\text{ClO}_4^-)_2$. That is whether the presence of the polymer will influence the energy of the excited state of the Ru complex, which is responsible for the photoluminescence. The spectra in Figure 5.15(a) displays the UV-Vis spectrums of Ru complex (20 mM) alone, and also shows the effect of adding aliquots of 10 μl of polymers (1% solution of polymer dissolved in DMSO). The results show that $[\text{Ru}(\text{bpy})_2(\text{picCOOH})]^{2+} \cdot (\text{ClO}_4^-)_2$ before and after titrating it with aliquots of 10 μl of polymer solutions exhibited intense peak between 300-350 nm and this was ascribed

to the ligand centred (LC) $\pi \rightarrow \pi^*$ transition of the Ru complex (Venkatanarayanan, 2010). In addition to that, a strong absorption maximum at ~ 460 nm was also observed and this was due to $d \rightarrow \pi^*$ MLCT of Ru complex (Hughes *et al.*, 1993). The absorption peaks of $[\text{Ru}(\text{bpy})_2(\text{picCOOH})]^{2+} \cdot (\text{ClO}_4^-)_2$ alone were identical to the ones observed after titrating it with aliquots of 10 μl of polymer solution. However, there might have been some overlapping of $\pi \rightarrow \pi^*$ transitions of the polymer with the $\pi \rightarrow \pi^*$ transition of the Ru complex. The effect of the interaction of Ru complex with polymers was further investigated by titrating $[\text{Ru}(\text{bpy})_2(\text{picCOOH})]^{2+} \cdot (\text{ClO}_4^-)_2$ with 10 μl aliquots of polymer until a total volume of 150 μl polymer solution was added. And the results are presented in Figure 5.15(b)-(d) and showed that there was no appearance of new peaks in the UV absorption spectra of the polymer- $[\text{Ru}(\text{bpy})_2(\text{picCOOH})]^{2+} \cdot (\text{ClO}_4^-)_2$ during the titration. This implied that the Ru cores were stable under the addition of polymers. Moreover, the increase in absorbance upon addition of polymer aliquots, confirmed that the electronic absorption of polymers were also taking place.



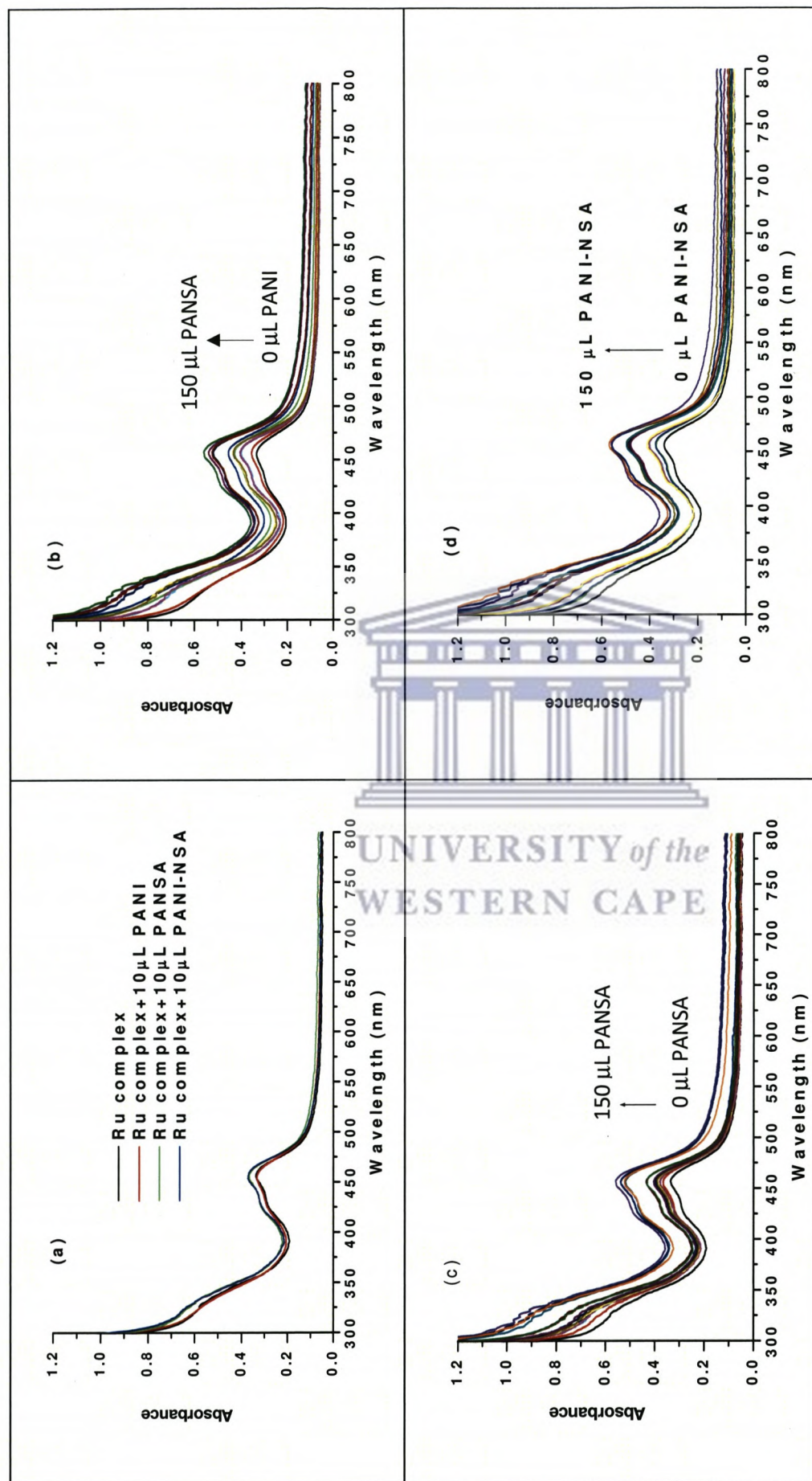


Figure 5.15: UV-vis absorption spectra of [Ru(bpy)₂(picCOOH)]²⁺·(ClO₄)₂ complex in MeCN (a) with addition of 10 μL of polymers and with addition of 10-150 μL of polymers dissolved in DMSO (b) PANI, (c) PANSA and (d) PANI-NSA.

$[\text{Ru}(\text{bpy})_2(\text{picCOOH})]^{2+} \cdot (\text{ClO}_4^-)_2$ with addition of chemically synthesized polymers

To explore the impact of the polymers on the photophysics of $[\text{Ru}(\text{bpy})_2(\text{picCOOH})]^{2+} \cdot (\text{ClO}_4^-)_2$ was also investigated via luminescence studies Figure 5.16(a), The $[\text{Ru}(\text{bpy})_2(\text{picCOOH})]^{2+} \cdot (\text{ClO}_4^-)_2$ alone exhibited an intense luminescence centered between 500 and 650 nm, and another peak observed at ~640nm when excited at 330 nm. The peak observed at ~640nm was due an overtone, which was arises from scanning beyond double the excitation wavelength. Upon titration with 10 μL of PANI or PANI-NSA, the overtone peak, exhibited a bathochromic shift with respect to the one obtained in $[\text{Ru}(\text{bpy})_2(\text{picCOOH})]^{2+} \cdot (\text{ClO}_4^-)_2$ alone and its intensity also increased, while when titrating $[\text{Ru}(\text{bpy})_2(\text{picCOOH})]^{2+} \cdot (\text{ClO}_4^-)_2$ with PANSA, this peak remained the same (Figure 5.16a).

As observed in Figure 5.16(b)-(d) from the interaction of the polymer (PANI, PANSA or PANI-NSA) with $[\text{Ru}(\text{bpy})_2(\text{picCOOH})]^{2+} \cdot (\text{ClO}_4^-)_2$, it was seen that the emission peak of the Ru metal centered between 500 and 650 nm increased with progressive addition of the polyaniline in to the Ru complex, until the maximum ruthenium emission intensity was reached. The nature of interaction probed by the addition of polymers showed that emission properties of $[\text{Ru}(\text{bpy})_2(\text{picCOOH})]^{2+} \cdot (\text{ClO}_4^-)_2$ were not quenched by its interaction with the polymer. In fact, $[\text{Ru}(\text{bpy})_2(\text{picCOOH})]^{2+} \cdot (\text{ClO}_4^-)_2$ was quenching the polymer emissions. This observation was ascribed to the excited state electron transfer from the polymer which resulted in an enhancement of the ruthenium emission. The increase in the luminescence peak centered between 500 and 650 nm was favoured the presence of maximum concentration of the polymer, because the greater the concentration of the polymer, the more the peak increases.

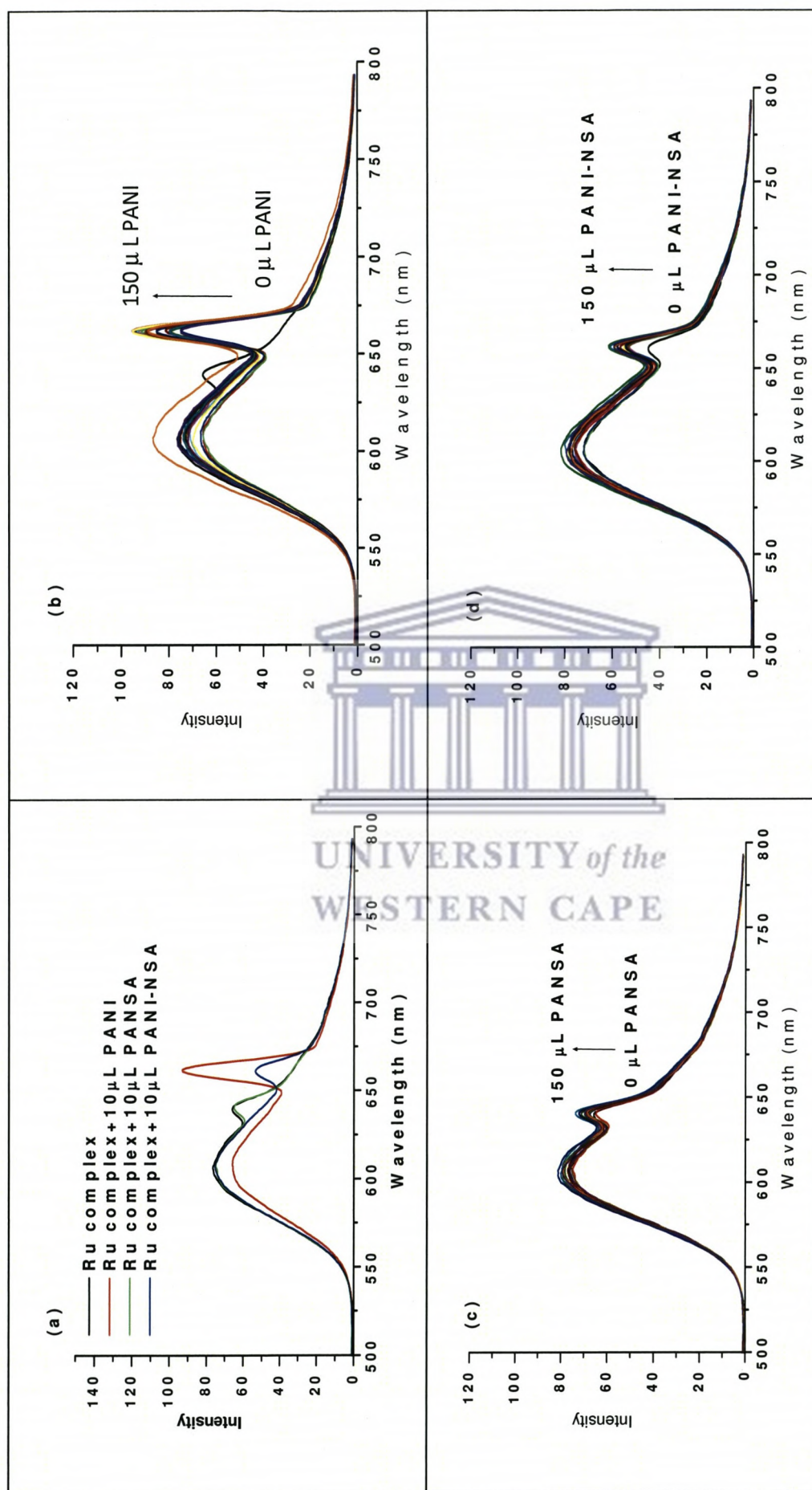


Figure 5.16: Fluorescence emission spectra of Ru complex in MeCN (a) with addition of 10 μL of polymers and with addition of 10-150 μL of polymers dissolved in DMSO (b) PANI, (c) PANSA and (d) PANI-NSA

5.3.5.3. Fluorescence lifetime of Ru complex with addition of chemical synthesized polymers

The fluorescence lifetime can provide useful insights into the excited state interactions between the Ru complex and polymers. Figure 5.17 shows free $[\text{Ru}(\text{bpy})_2(\text{picCOOH})]^{2+} \cdot (\text{ClO}_4^-)_2$ dissolved in acetonitrile exhibited a mono exponential decay with a lifetime of $0.171 \pm 0.0070 \mu\text{s}$ and $0.257 \pm 0.0054 \mu\text{s}$ after titration with 150 μL PANSA.

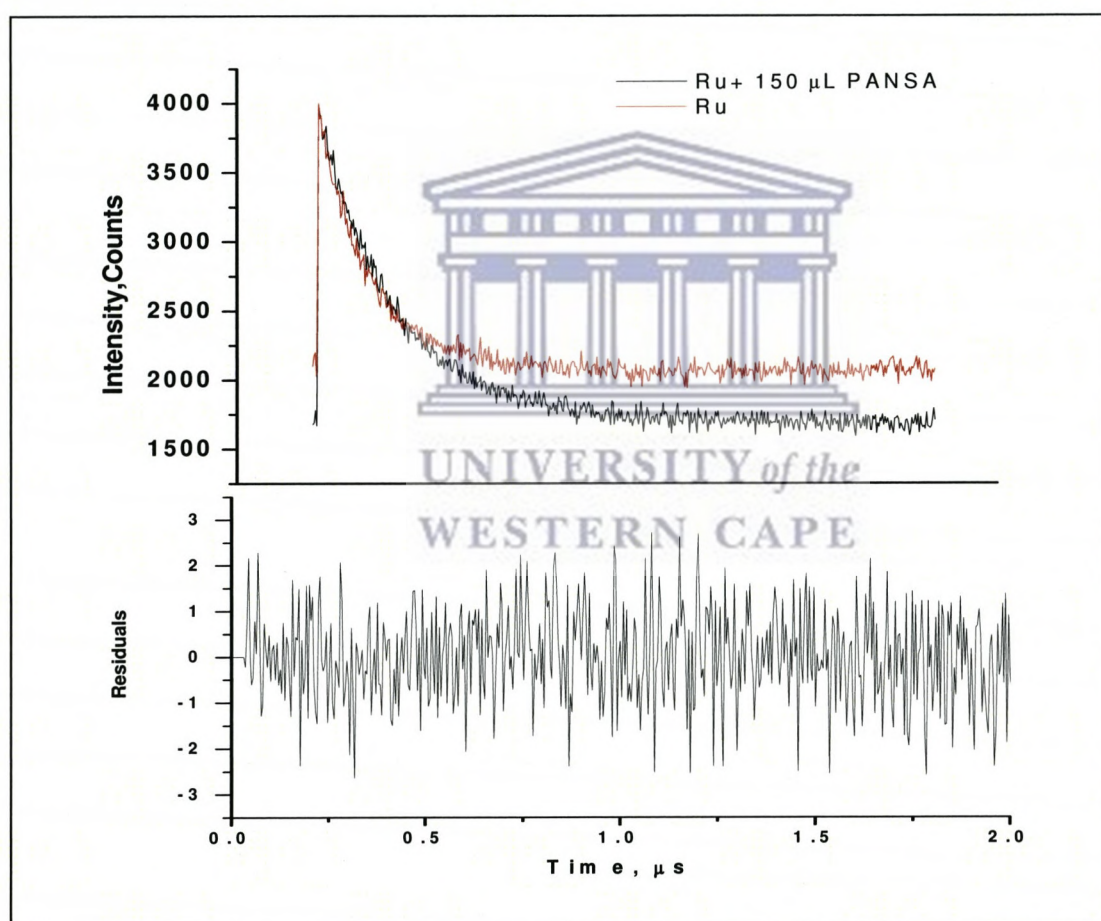


Figure 5.17: A typical fluorescence emission decay of PANSA in DMSO, when pulsed with a 450 nm laser source with a long pass-off filter of 530 nm, and the residual of a mono exponential tail fit.

The results show that $[\text{Ru}(\text{bpy})_2(\text{picCOOH})]^{2+} \cdot (\text{ClO}_4^-)$ conformed to a mono-exponential-model yielding one lifetime, which was longer than that of the polymers (ns). The free $[\text{Ru}(\text{bpy})_2(\text{picCOOH})]^{2+} \cdot (\text{ClO}_4^-)_2$ which was present in excess at this initial stage before titration with PANSA has a lifetime of $0.171 \pm 0.0070 \mu\text{s}$. As the relative concentration of the PANSA increased with progressive additions of $10 \mu\text{L}$ aliquots, the lifetime increased gradually from 0.171 ± 0.0070 to $0.257 \pm 0.0054 \mu\text{s}$ when a final titration volume was $150 \mu\text{L}$ added. These results were consistent with the previous results, that demonstrated that there is a positive electron energy transfer, from the polymer to the $[\text{Ru}(\text{bpy})_2(\text{picCOOH})]^{2+} \cdot (\text{ClO}_4^-)_2$ which resulted in increase lifetime, and was consistent with increasing absorption as concentration of PANSA increases observed in Figure.5.15 and yields increased luminescence (Figure 5.16). Titration with PANI-NSA, exhibited the same behaviour with an increase of lifetime from $0.175 \pm 0.0061 \mu\text{s}$ to $0.180 \pm 0.00521 \mu\text{s}$. PANI also followed the same trend, however, the initial lifetime of free $[\text{Ru}(\text{bpy})_2(\text{picCOOH})]^{2+} \cdot (\text{ClO}_4^-)_2$ was higher $0.259 \pm 0.0043 \mu\text{s}$ and it increased to $0.339 \pm 0.0079 \mu\text{s}$. The free $[\text{Ru}(\text{bpy})_2(\text{picCOOH})]^{2+} \cdot (\text{ClO}_4^-)_2$ should essentially have a similar lifetime, to the ones reported before titration with PANSA or PANI-NSA, since, it was the same complex used. However in the PANI experiments the solution was degassed during the experiments, which involved titration with PANI, which resulted in higher lifetimes. The comparison of the results are shown in Table 5.5.below.

Table 5.5: Fluorescence lifetime of $[\text{Ru}(\text{bpy})_2(\text{picCOOH})]^{2+} \cdot (\text{ClO}_4^-)_2$ in MeCN with addition of chemically synthesized PANI, PANSA and PANI-NSA dissolved in DMSO

Sample	PANI (degassed) Life time (μs)	PANSA Life time (μs)	PANI-NSA Life time (μs)
Ru	0.259 ± 0.0043	0.171 ± 0.0070	0.175 ± 0.0061
Ru +30	0.258 ± 0.0057	0.186 ± 0.0130	0.177 ± 0.0059
Ru +60	0.288 ± 0.0066	0.173 ± 0.0165	0.176 ± 0.0054
Ru+90	0.298 ± 0.0125	0.177 ± 0.0164	0.178 ± 0.0061
Ru +120	0.325 ± 0.0080	0.189 ± 0.0214	0.176 ± 0.0062
Ru +150	0.339 ± 0.0079	0.257 ± 0.0054	0.180 ± 0.00521



5.4. Conclusion

Photoluminescence properties of electro- and chemically synthesized PANSA and PANI with dopants were presented in this chapter. The electronic absorption of these polymers showed to exhibit the absorption bands corresponding to the polyemeraldine salt and base in electro- and chemical synthesized polymers, respectively. The effect of dopants resulted in the increase of the solubility of the materials. It was shown the electronic absorption of chemical synthesized PANI with and without dopants showed to have a band corresponding to the quinoidic ring of the polyemeraldine base. However, in both chemical and electro synthesized PANSA showed disappearance of the quinoidic band due to the presence of naphthalene sulfonic acid group which reduced the conjugation length along the polymer. The fluorescence emission spectra of the electrochemically synthesized PANSA with and without dopants were similar and mirror image of the excitation spectra and corresponding to the

electronic band of the benzoid ring in the polyemeraldine form. The chemically synthesized PANSA and PANI showed that emission spectra were different to excitation spectra suggesting loss of symmetry upon excitation. The effects of polyaniline and its derivatives on the electronic absorption and fluorescence properties of Ru complex were investigated. The analysis revealed that the presence of polyaniline and its derivatives enhanced the Ru complex luminescence by means of electron transfer.



5.5. References

Ameen, S., Lakshmi, G. B. V. S., Husain, M. Synthesis and characterization of polyaniline prepared with the dopant mixture of (ZrO₂/PbI₂), *Journal of Physics D Applied Physics*, (2009) 42, 105104-105109.

Antonel, P. S., Molina, F. V., Andrade, E. M. Fluorescence of polyaniline films on platinum surfaces. Influence of redox state and conductive domains, *Journal of Electroanalytical Chemistry*, (2007) 599, 52-58.

Bansal, V., Bhandari, H., Bansal, M. C., Dhawan, S. K. Electrical and optical properties of poly(aniline-co-8-anilino-1-naphthalene sulphonic acid)- A material for ESD applications, *Indian journal of pure and applied physics* (2009) 47, 667-675.

Bhandari, H., Choudhary, V., Dhawan, S. K. Influence of self-doped poly(aniline-co-4-amino-3-hydroxy-naphthalene-sulfonic acid) on corrosion inhibition behaviour of iron in acidic medium, *Synthetic Metals*, (2011) 161, 753-762.

Bosco, S. J., Zettl, H., Crassous, J., Ballauff, M., Krausch, G. Interactions between methyl cellulose and sodium dodecyl sulfate in aqueous solution studied by single molecule fluorescence correlation spectroscopy, *Macromolecules*, (2006) 39, 8793–8798.

Chen, Y.G., Zhao, D., He, Z. K., Ai, A. P. Fluorescence quenching of water-soluble conjugated polymer by metal cations and its application in sensor, *Spectrochimica Acta Part A*, (2007) 66, 448-452, 2007.

Cochet, M., Buisson, J.P., Wery, J., Jonusauskas, G., Faulques, E., Lefrant, S., A complete optical study of the conductive form of polyaniline: the emeraldine salt, *Synthetic Metals*, (2001) 119, 389-390.

Draman ,S.F.S., Daik, R., and Musa, A., Synthesis and fluorescence spectroscopy of sulphonic acid-doped polyaniline when exposed to oxygen gas, *International Journal of Chemical and Biological Engineering*, (2009) 2, 112-119.

Dawson, W. R., Windsor, M. W. Fluorescence yields of aromatic compounds, *Journal of Physical Chemistry* (1968) 72, 3251-3260.

Dong, B., He, B. L., Xu, C.L., Li, H. L. Preparation and electrochemical characterization of polyaniline/multi-walled carbon nanotubes composites for supercapacitor, *Materials Science and Engineering* (2007) 143,7-13.

Gfroerer, T. H., Mayers, R. A. Encyclopedia of analytical chemistry: photoluminescence in analysis of surfaces and interfaces, *John Wiley & Sons Ltd, Chichester* (2000) 12 , 9209–9231.

Heeger, A.J.Semiconducting and Metallic Polymers: The Fourth Generation of Polymeric Materials, *Journal of Physical Chemistry B* (2001) 105, 8475-8491.

Hopkins, A. R., Rasmussen, P. G., Basheer, R. A., Characterization of solution and solid state properties of undoped and doped polyanilines processed from hexafluoro-2-propanol, *Macromolecules* (1996) 29 , 7838-7846.

Huang, W. S., MacDiarmid, A. G. Optical properties of polyaniline, *Polymer*, (1993) 34, 1833-1845.

Hughes, H. P., Martin D., Bell S., McGarvey, J. J., Vos, J. G., Photophysical and photochemical properties of dinuclear ruthenium(ii) complexes containing 2,2'-bipyridine and 1,10-phenanthroline moieties, *Inorganic Chemistry* (1993) 32, 4402-4408.

Kane-Maguire, L. A. P., Causley, J. A., Wallace G. G. Photoluminescence and photo-redox reactions of poly(2-methoxyaniline-5-sulfonic acid), *Current Applied Physics* (2004) 4, 394–397.

Kohut-Svelko N., Reynaud, S., François J. Synthesis and characterization of polyaniline prepared in the presence of nonionic surfactants in an aqueous dispersion, *Synthetic Metals* (2005) 150,107-114.

Kulkarni, M.V., Viswanath, A.K., Comparative studies of chemically synthesized polyaniline and poly(o-toluidine) doped with p-toluene sulphonic acid, *European Polymer Journal* (2004) 40, 379-384.

Lakowicz, J. R., Principles of Fluorescence Spectroscopy, 3rd ed, Springer, (2006).

Lakowicz, J. R., Long-Lifetime Metal-Ligand Complexes; Principles of Fluorescence Spectroscopy; Plenum Publisher, New York, (1999), 573-594.

Lin, Y.W., Wu, T.M. Synthesis and characterization of externally doped sulfonated polyaniline multi-walled carbon nanotube composites, *Composites science and Technology*. (2009) 69, 559-2565.

Masdarolomoor , F., Innis, P.C., Wallace, G.G., Electrochemical synthesis and characterisation of polyaniline poly(2-methoxyaniline-5-sulfonic acid) composites, *Electrochimica Acta* (2008) 53, 4146–4155.

Mavundla, S. E. One-dimensional nanostructured polymeric materials for solar cells applications, PhD Thesis, Department of Chemistry, University of the Western Cape, (2010).

Mehamod, F. S., Daik, R., Musa, A., Poly(1,3-phenylenediphenylvinylene), as sensing reagent for oxygen gas detection, *Malaysian Journal of Chemistry* (2002) 4, 035-040.

Michira, I., Akinyeye, R., Somerset ,V., Klink, M.J., Sekota, M., Al-Ahmed A., Baker P.G.L., Iwuoha, E.I., Synthesis, characterization of novel polyaniline nanomaterials and application in amperometric biosensors, *Macromolecular Symposia* (2007) 255 ,57-69.

Misra, A., Kumar, P., Srivastava, R., Dhawan, S. K., Kamalasanan, M. N., Chandra S., Electrochemical and optical studies of conjugated polymers for three primary colours, *Indian Journal of Pure and Applied Physics* (2005) 43, 921-925.

Shimano, J.Y., MacDiarmid, A.G. Polyaniline, a dynamic block copolymer: key to attaining its intrinsic conductivity, *Synthetic Metals* (2001) 123, 251-262.

Son, Y., Patterson, H. H., Carlin, C. M., Potential-dependent photoluminescence of conductive polymers: Simple quenching model and experimental results for poly(aniline), *Chemical Physics Letters* (1989) 162, 461-466.

Thorne, J.R.G., Masters, J.G., Williams, S.A., MacDiarmid, A.G., Hochstrasser, R.M. Time-resolved fluorescence of polyaniline, *Synthetic Metals* (1992) 49, 159-165.

Williams, A.T. R., Winfield, S. A., Miller J.N. Relative fluorescence quantum yields using a computer controlled luminescence spectrometer, *Analyst* (1983) 108, 1067-1071.

CHAPTER SIX:

ELECTROCHEMILUMINESCENCE of POLY (8-ANILINO-1-NAPHTHALENE SULFONIC ACID) and POLYANILINE DERIVATIZED with *RUTHENIUM (II) (bis-2,2-BIPYRIDYL)-2(4-CARBOXYLPHENYL) IMIDAZO[4,5-f][1,10]PHENANTHROLINE*

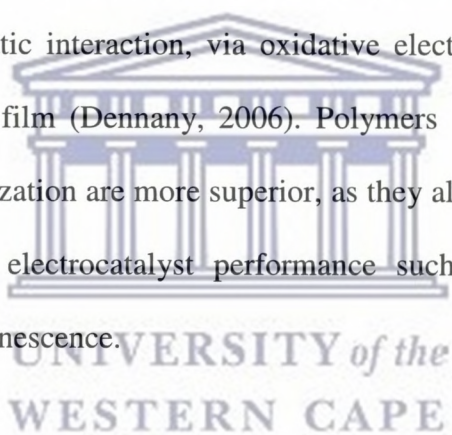
6.1. Introduction

Conjugated organic compounds are known as those with a balanced electronic structure and they possess a spatially delocalised band-like electronic structure. Hence electrochemical processes which take place in these compounds have the ability to bring about huge changes to the compounds electronic properties (Doblhofer, 1998). The changes are induced by processes such as removal or addition of electrons to or from the HOMO or LUMO (Ding *et al.*, 2002; Myung *et al.*, 2003). Owing to this reason conjugated organic compounds offer the possibility of being applied in electrochemically driven applications such as ECL, photovoltaics and electrochromism assembly. Other applications include sensors, rechargeable batteries, and corrosion resistant coatings.

Electrically conducting polymers (ECPs) are examples of conjugated organic polymers. They have been and continue to be a subject of great interest to many researchers. Specific examples of ECPs are; polyimidazole, polyaniline, polypyrrole and phenylene (Wallace *et al.*, 2009). In an electrochemical system, ECL can be generated with great control, *i.e.* the imposition of current and potential value. Dini (2005) explained that for a conjugated organic compound to be applied in ECL production, there are several structural prerequisites which the compound has to meet; such as the material must have a network of conjugated π

electrons. Furthermore, its ionization energy must range in the interval 6.5 to 8.5eV, which will induce electronic transitions within the energy range 1.5-3.5eV in the ground or excited state of the molecule.

ECPs meet the above mentioned prerequisites, and hence incorporating transition metal complexes within these polymers can lead to improvement in their optical and redox properties. Dennany (2006) explained that this is due to their desirable redox, catalytic and optical properties. According to Richter (2004), ECL of complexes and/or clusters containing Ag, Al, Au, Cd, Cr, Cu, Eu, Hg, Ir, Mo, W, Os, Pd, Pt, Re, Ru, Si, and Tb have been reported. The incorporation of these complexes into polymers can be achieved through covalent bonding or electrostatic interaction, via oxidative electropolymerization polymer, giving rise to a thin polymer film (Dennany, 2006). Polymers which possess π network resulting from electropolymerization are more superior, as they allow the rapid movement of electrons necessary for high electrocatalyst performance such as that involved in the generation of electrochemiluminescence.



Owing to the reason that the polymer backbone can supply extra electrons, provided that it is electroactive over the appropriate potential range, or other nearby metal centres. Polymers coupled with metal complexes can offer advantages such as enhanced rates of metal to metal charge transport and increased luminescence due to energy transfer from the polymer to metal, this via interaction between the d orbitals of the metal and π orbitals of the polymer (Pickup, 1999). In addition, there are three proposed mechanisms (Figure 6.1-6.3) through which the process of electron transfer between immobilized metal centres in a polymer film can take place and these are; polymer mediated pathway, super-exchange pathway and the Outer sphere electron transfer (Inzelt, 1999).

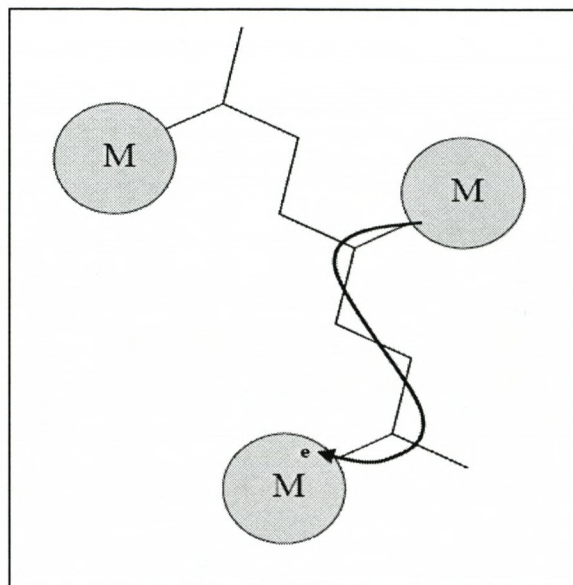


Figure 6.1: Polymer mediated pathway, which takes place via polymer based charge carriers (Pickup, 1999).

There is one prerequisite for polymers to be able to transfer electrons via its charge carriers that is the polymer backbone should be electronically conductive. Furthermore, it should either be p-doped or n-doped at potentials close to the formal potential of the metal centre (Pickup, 1999).

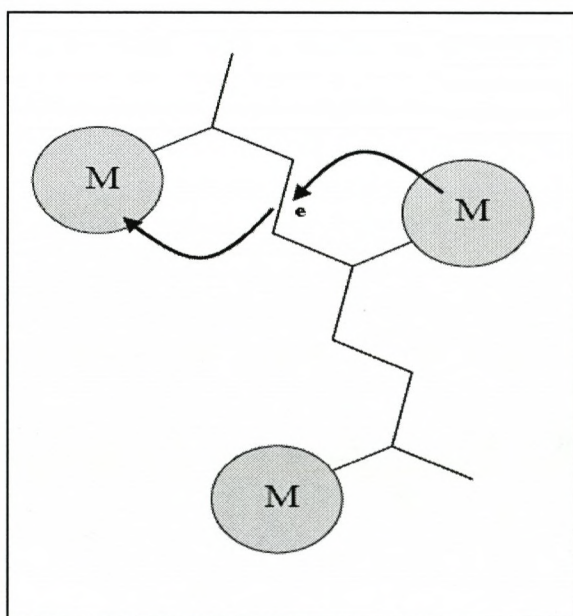


Figure 6.2: Super-exchange pathway (Pickup, 1999).

This is an electron transfer process through the polymer that takes place via metal-metal electronic interaction.

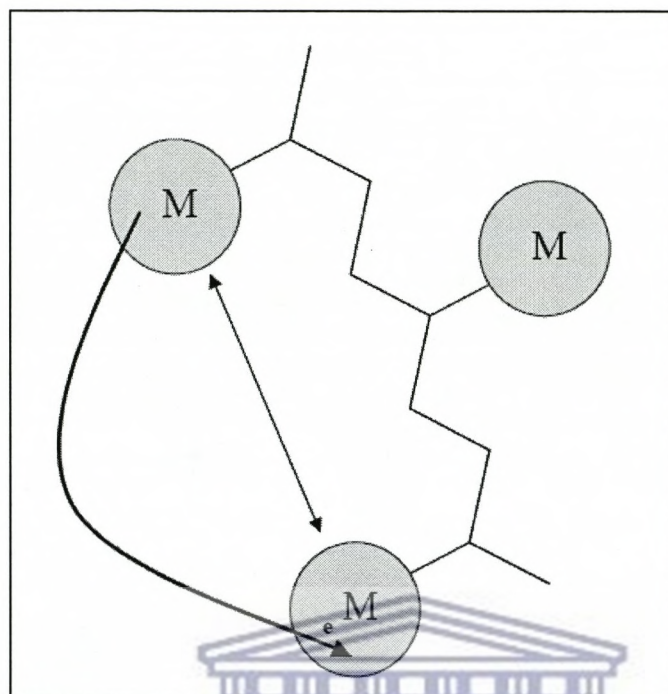


Figure 6.3: Outer sphere electron transfer (Pickup, 1999).

Studies carried out by (Be' langer, 1998) have demonstrated that incorporation of transition metals such as Ru^{2+} into polymer films via electrochemical polymerization, yielded good surface coverage and highly electroactive polymer films. Dennany *et al.* (2008) has also demonstrated that the electrochemical polymerization of methoxy-aniline in the presence of $[\text{Ru}(\text{bpy})_3]^{2+}$ resulting in ruthenium based luminescence and electrochemiluminescence as well as enhanced rates of charge transport. Furthermore, these electron and energy transfer processes can often quench the luminescence that is required to produce ECL.

Hence, the current chapter reports on the electropolymerization of aniline (ANI) and 8-anilino-1-naphthalene sulfonic acid (ANSA) in the presence of $[\text{Ru}(\text{bpy})_2(\text{picCOOH})]^{2+} \cdot (\text{ClO}_4^-)$

)₂ in acidic conditions hydrochloric acid and sulphuric acid, respectively, to give rise to polyaniline (PANI) and poly –anilino –naphthalene sulfonic acid (PANSA) Ru complex films. The $[\text{Ru}(\text{bpy})_2(\text{picCOOH})]^{2+} \cdot (\text{ClO}_4^-)$ electrostatically associates with the anionic polymer backbone. The resulting electrodeposited film was mainly being investigated for electrochemiluminescence (ECL) in the presence of tripropylamine (TPA) as a coreactant. This approach of polymer and Ru complex interaction added advantage for ECL production.

6.2. Experimental method

6.2.1. Reagents and materials

The $[\text{Ru}(\text{bpy})_2(\text{picCOOH})]^{2+} \cdot (\text{ClO}_4^-)_2$ was kindly synthesized and provided by Mr Ciaran Dolan of the Tia Keyes research group according to a synthetic procedure described elsewhere (Yam *et al.*, 2008). Aniline (99%), 8-anilino-1-naphthalene sulfonic acid, ammonium hydrate salt 97%, sulfuric acid (98%), tripropylamine (TPA) were all purchased from Sigma-Aldrich, hydrochloric acid (36% Mw) was purchased from Fluka. All solutions were made using deionized water purified with a Milli-Q plus 18.5 M Millipore installation.

6.2.2. Apparatus and measurement

6.2.2.1. Electrochemistry

Electrochemical measurements were carried out with a CH instrument, (model 900 A) electrochemical workstation. The three electrode cell configuration consisted of a three electrode system where the working electrode was an Indium tin oxide electrode (7 x 50 x 0.9 mm unpolished float glass with $R_s = 8 - 12 \Omega$), and the Ag/AgCl with 3 M KCL as the reference and platinum wire as the auxiliary electrode. All the measurements were carried out at room temperature.

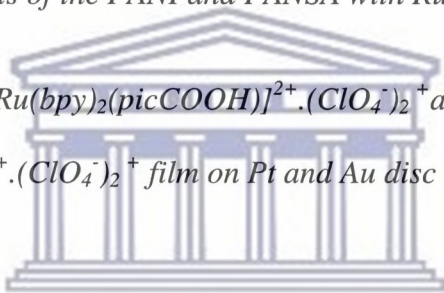
6.2.2.2. Electrochemiluminescence Measurements

ECL measurements, utilized an Oriel 70680 photo multiplier tube (PMT) equipped with a high voltage power supply, (Oriel, model 70705), which was used at a bias of -900 V, and amplifier / recorder (Oriel, model 70701) (in Dublin City University, Ireland). During experiments, the ITO modified the electropolymerized film as placed inside Helma quartz cuvette and this was held in place by specially constructed holder. The optic face of the optic fibre was placed directly towards the cuvette; it should directly phase the ITO glass, the other end of which was coupled to the PMT.

6.2.3. Electro chemical synthesis of the PANI and PANSA with Ru complex

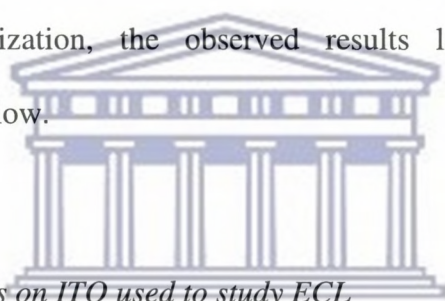
6.2.3.1. Preparation of PANI-[Ru(bpy)₂(picCOOH)]²⁺.(ClO₄⁻)₂⁺ and

PANSA[Ru(bpy)₂(picCOOH)]²⁺.(ClO₄⁻)₂⁺ film on Pt and Au disc electrode respectively.



Experiments were carried out to determine the optimal volumes of the monomers, the ruthenium complex and the acidic medium which should be added to the electropolymerization solution to yield a film with maximum loading of the ruthenium complex. The [Ru(bpy)₂(picCOOH)]²⁺.(ClO₄⁻)₂ and PANSA-[Ru(bpy)₂(picCOOH)]²⁺.(ClO₄⁻)₂ film was prepared by electropolymerization of ANI or ANSA in the presence of the ruthenium complex via in situ deposition onto a Pt or Au electrode for ANI and ANSA respectively. The Pt and Au surface was cleaned by polishing in aqueous slurries of 1, 0.3 and 0.05 µm alumina powder respectively (Buehler, Dorset England) and before proceeding to the next alumina powder; the electrode was rinsed with deionized water and sonicated for 10 minutes. The polished electrodes were then scanned in H₂SO₄ (0.1 M) from - 0.025 to 0.12 V with reference to an Ag/AgCl electrode, to ascertain they were clean bare electrodes. The

cyclic voltametric polymerization of ANI was initially carried out in a 5 mL cell solution containing, 0.2 M ANI, HCL (1 M) and $\text{Ru}(\text{bpy})_2(\text{picCOOH})]^{2+}$ (1 M) and for ANSA the polymerization was carried in 20 mL solution contain, 0.2 M ANSA, H_2SO_4 (0.5 M) and $\text{Ru}(\text{bpy})_2(\text{picCOOH})]^{2+}$ (1 M), by cycling between -0.2 (initial potential E_{initial}) to 1.2 V (final potential, E_{final}), at a potential scan rate of 100 V s^{-1} for ANI and 50 Vs^{-1} for ANSA. The electropolymerization was stopped after 20 voltametric cycles. The Pt-PANI- $[\text{Ru}(\text{bpy})_2(\text{picCOOH})]^{2+} \cdot (\text{ClO}_4^-)_2$ and the Au-PANSA- $[\text{Ru}(\text{bpy})_2(\text{picCOOH})]^{2+} \cdot (\text{ClO}_4^-)_2$ electrodes, were then removed from the electropolymerization solution, and were rinsed off with deionized water to remove excess monomer and they characterized in HCL(1 M) and H_2SO_4 (0.5 M) respectively. From the CV recorded during the electropolymerization processes and the characterization, the observed results lead to carrying out the polymerization as described below.



6.2.3.2. Preparation of the films on ITO used to study ECL

Electropolymerization was carried out by employing amperometric i-t mode, by constantly applying an oxidation potential of 0.7 V for polymerization of ANI and 0.5 V for ANSA on the working electrode and at different run timings. For the electropolymerization of ANI, the electropolymerization solution was prepared by mixing HCL (0.1 mM), aniline (0.2 M) and $[\text{Ru}(\text{bpy})_2(\text{picCOOH})]^{2+} \cdot (\text{ClO}_4^-)_2$ (1 mM) and for polymerization of ANSA a mixture of H_2SO_4 (0.1 mM), 8-anilino-1-napthalene sulfonic acid (0.2 M), and $[\text{Ru}(\text{bpy})_2(\text{picCOOH})]^{2+} \cdot (\text{ClO}_4^-)_2$ (1 mM) was prepared. The resulting film were rinsed off with deionized water, to remove excess monomer which may still be on the electrode, and they were characterized in 0.1 mM HCL and 0.1 mM H_2SO_4 for the PANI and PANSA, respectively.

6.3. Results and Discussion

6.3.1. Preliminary results

6.3.1.1. Film preparation and optimization

The key objective of this work was to electrosynthesize PANI and PANSA which incorporated $[\text{Ru}(\text{bpy})_2(\text{picCOOH})]^{2+} \cdot (\text{ClO}_4^-)_2$, and to study their ECL behaviour. As any ECL is expected to originate from the Ruthenium centres it was important, to optimize the polymerization process, so that the resulting film would have maximum loading of the ruthenium complex. As previously elaborated, polymers which have a metal complex in their backbone do not only possess a π network, often exhibit superior conductivity, permitting the rapid movement of electrons necessary for high electrocatalyst performance such as that involved in the generation of electrochemi-luminescence. Bachas *et al.* (1997) showed that the metal centre served as the means to transport the electrons between the polymer film and the surface of the electrode. The initial step in the optimization process was to characterize $[\text{Ru}(\text{bpy})_2(\text{picCOOH})]^{2+} \cdot (\text{ClO}_4^-)_2$ complex by employing CV on the Pt, Au and ITO electrodes in HCl and H₂SO₄. This was carried out in order to establish the potential region in which the $[\text{Ru}(\text{bpy})_2(\text{picCOOH})]^{2+} \cdot (\text{ClO}_4^-)_2$ peak is normally observed, in the different electrodes and acidic mediums. For example, Figure 6.4 shows a representative cyclic voltammogram of the Ru complex, using indium tin oxide (ITO) as the working electrode in HCl and H₂SO₄. The results showed that $[\text{Ru}(\text{bpy})_2(\text{picCOOH})]^{2+} \cdot (\text{ClO}_4^-)_2$ displays an electrochemically reversible response centered at $\sim +1.2$ V associated with the $\text{Ru}^{2+/3+}$ couple (Pellegrin *et al.*, 2008).

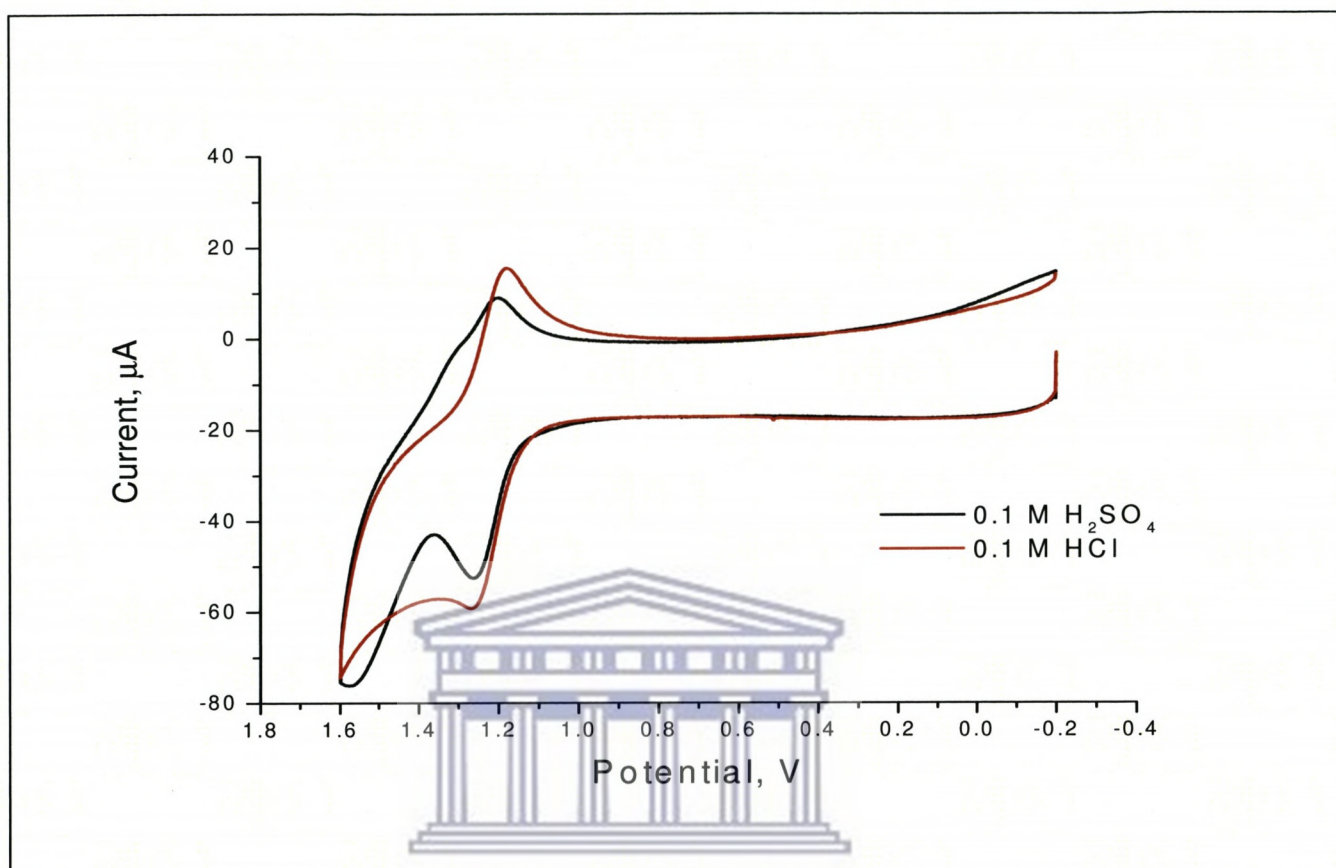


Figure 6.4: CV characterization of $[\text{Ru}(\text{bpy})_2(\text{picCOOH})]^{2+} \cdot (\text{ClO}_4^-)_2$ complex on ITO electrode in 0.1 M H_2SO_4 and HCl .

This observation is consistent with the behaviour reported of the Ru complex, where the Ru metal to monomer unit was not altered, the redox couple ranges from 0.8 to 1.2 V depending on the pH of the contacting electrolyte solution (Pellegrin *et al.*, 2008).

6.3.1.2. Electropolymerization of aniline (ANI) and $[Ru(bpy)_2(picCOOH)]^{2+}.(ClO_4^-)_2$

It is well known that PANI is synthesized electrochemically in acidic medium via anodic oxidation of aniline (Bansal *et al.*, 2009). The polymerization is initiated by formation of a resonance stabilized aniline radical cations from the protonated monomer (Bansal *et al.*, 2009). After electropolymerization of PANI- $[Ru(bpy)_2(picCOOH)]^{2+}.(ClO_4^-)_2$ process was completed; a green film was formed on the Pt electrode. The CV of PANI- $[Ru(bpy)_2(picCOOH)]^{2+}.(ClO_4^-)_2$ electro synthesized at 0.1 Vs^{-1} for 20 voltammetric cycles is illustrated in Figure 6.5, it demonstrates that as the number of voltammetric cycles increased, polymerization peak currents also increased. Mathebe *et al.* (2004) explained that this indicates that polymer was conducting. Figure 6.6 presents typical multi sweep rate voltammograms of the Pt-PANI- $[Ru(bpy)_2(picCOOH)]^{2+}.(ClO_4^-)_2$ which displays well defined oxidation-reduction responses indicating that the PANI- $[Ru(bpy)_2(picCOOH)]^{2+}.(ClO_4^-)_2$ composite was electroactive (Iwuoha *et al.*, 1997). It was seen that there were three redox couples, which were three anodic (A, B, C) and three cathodic peaks (A', B', C'). The oxidation peak (A) could be ascribed to polyleucoemeraldine radical cation, and as the potential sweep proceeded to more higher (positive) values, this caused formation of polyemeraldine radical cation (B), which was also further oxidized to polypernigraniline (C) which is the fully oxidized form of PANI. On the reverse scan the first cathodic peak was attributed to polypernigraniline (C') which was initially reduced, giving rise to polyleucoemeraldine (B'). As the potential sweep proceeded to lower (negative) values, a fully reduced polyleucoemeraldine (A') was formed. Michira *et al.* (2007) also observed the similar redox couples behaviour for electrochemical properties polyaniline nanomaterials for biosensors.

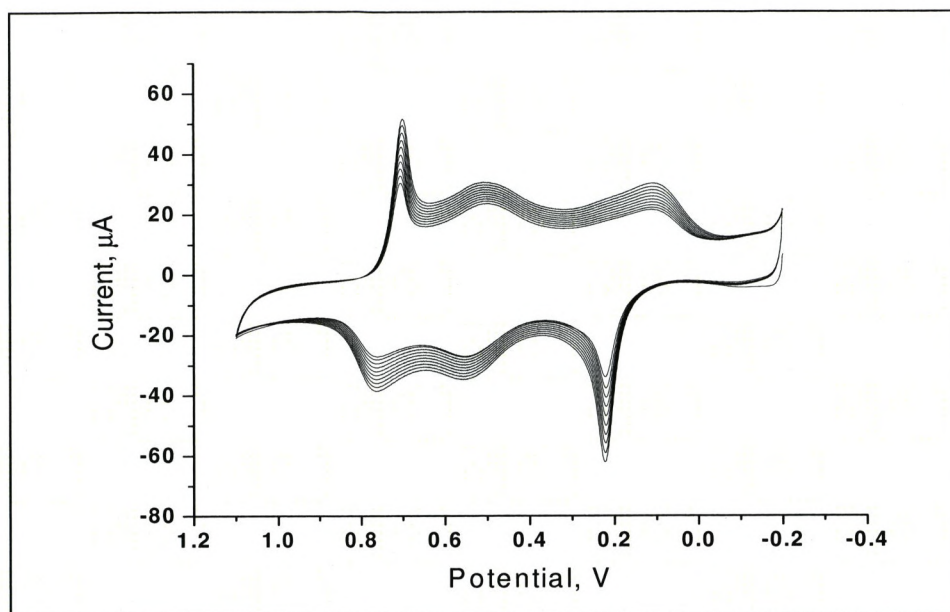


Figure 6.5: Electrosynthesis of PANI and $[\text{Ru}(\text{bpy})_2(\text{picCOOH})]^{2+} \cdot (\text{ClO}_4^-)_2$ on a 0.072 cm^2 Pt electrode at a scan rate 0.1 Vs^{-1} in HCl (1 M), the CV 1st to the 20th of the polymerization cycle.

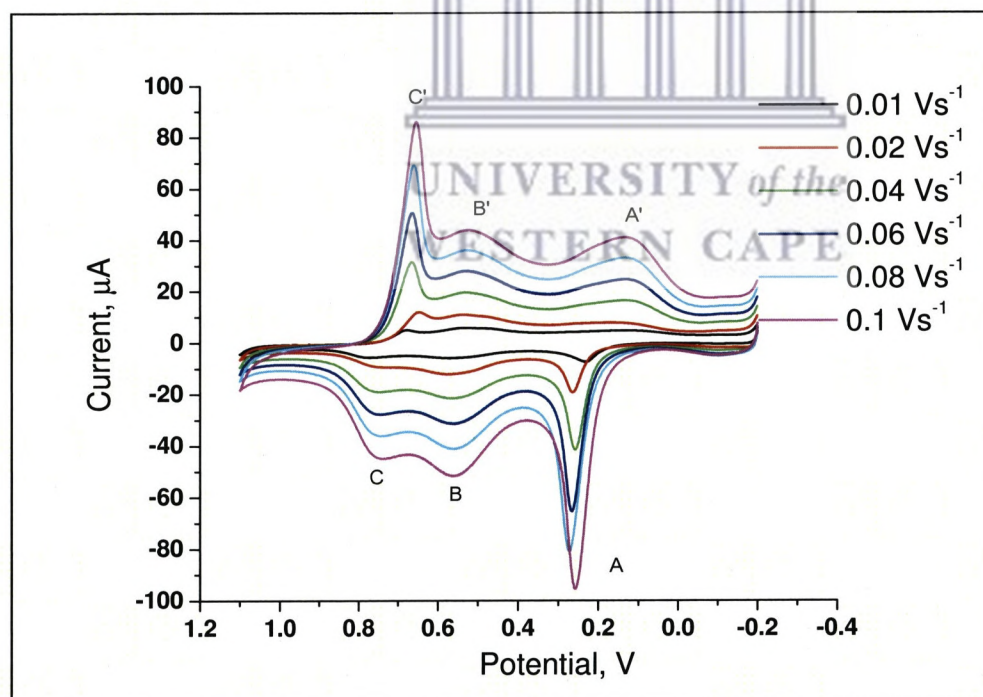


Figure 6.6: Cyclic voltammogram characterization at 0.01, 0.02, 0.04, 0.08 and 0.1 V s^{-1} for Pt-PANI- $[\text{Ru}(\text{bpy})_2(\text{picCOOH})]^{2+} \cdot (\text{ClO}_4^-)_2$ in 1 M HCl film grown at 0.1 Vs^{-1} .

Figure 6.7 below is a CV typical of PANI in an extended potential window of 0.2 -1.6 V s⁻¹. This characterization of extended potential window was done in order to verify if the Ru complex was successfully incorporated into the polymer backbone.

A typical Ru complex peak on a Pt electrode is normally observed ~ between 1.2-1.4 V (Pellegrin *et al.*, 2008). However, in Figure 6.7, such a feature was not observed, suggesting that the incorporation of [Ru(bpy)₂(picCOOH)]²⁺.(ClO₄)₂ into the polymer backbone was not successfully.

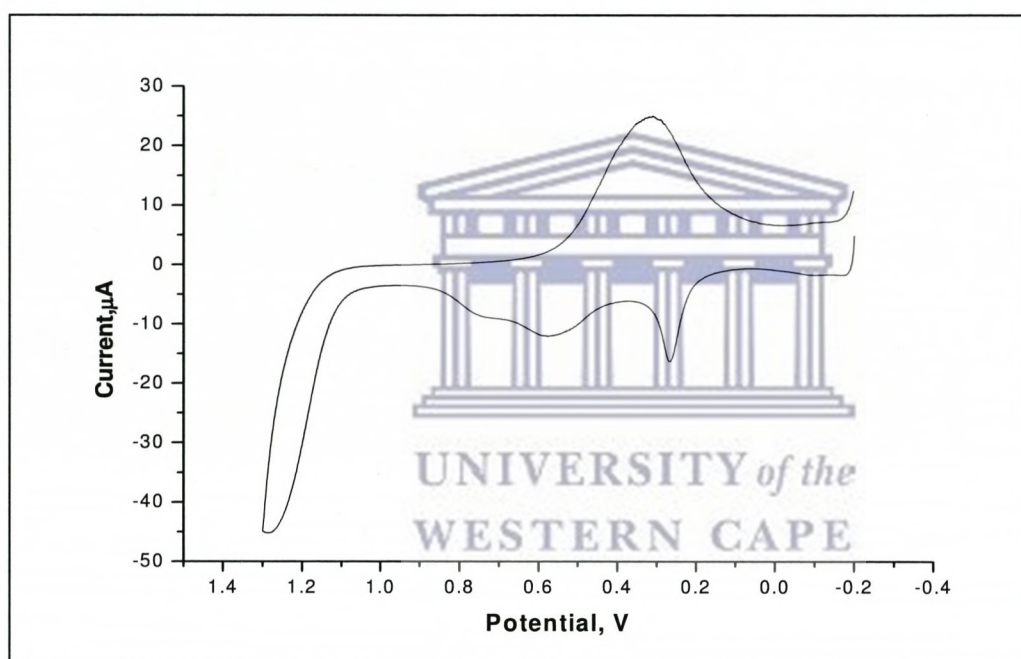


Figure 6.7: Cyclic voltammogram characterization of Pt -PANI-[Ru(bpy)₂(picCOOH)]²⁺.(ClO₄)₂ in an extended potential window of (0.02-0.16 V s⁻¹) at a scan rate of 0.1 V s⁻¹ in HCl (0.1 M),

These results of optimization lead to a conclusion that, in order for the polymerization process of aniline in the presence of [Ru(bpy)₂(picCOOH)]²⁺.(ClO₄)₂ to take place, a potentiostatic technique should be used instead of cycling between potentials. This would force

the Ru complex to get incorporated, because by holding the potential at a certain value for a certain period of time rather than cycling, this would allow the $[\text{Ru}(\text{bpy})_2(\text{picCOOH})]^{2+} \cdot (\text{ClO}_4^-)_2$ to incorporate into the film without moving out of the polymer.

6.3.1.3. Electropolymerization of ANSA and $[\text{Ru}(\text{bpy})_2(\text{picCOOH})]^{2+} \cdot (\text{ClO}_4^-)_2$

A typical CV indicative of ANSA electropolymerization in the presence of $[\text{Ru}(\text{bpy})_2(\text{picCOOH})]^{2+} \cdot (\text{ClO}_4^-)_2$ is illustrated in Figure 6.8 below, and Figure 6.9 for multiscan CV characterization. Showing the polymer growth which was believed to arise from the anilinium ions formed in the acidic medium interacting with free ANSA monomer to form PANSA prior to electropolymerization (Ngece *et al.*, 2011). The PANSA film showed a typical redox response exhibiting one redox couple in the potential under study, confirming that the polymer was electroactive. Ngece (2007) explained that this redox couple is ascribed to the electrochemistry of *p*-benzoquinone formed during polymerisation process. Mazeikiene *et al.* (2006) observed similar behaviour of one redox couple in electropolymerization of ANSA in the presence of 0.1 M sulphuric acid and as well as PANI polymerized in the presence and absence of sodium dodecyl sulphate. Furthermore an increase in number of polymerization cycles is accompanied by peak current increase, confirming that the polymer is conductive (Iwuoha *et al.*, 1997). Moreover between potential 0.8 -1 V there is a peak observed during the polymerization cycle, and it can be ascribed to incorporation of low levels of the $[\text{Ru}(\text{bpy})_2(\text{picCOOH})]^{2+} \cdot (\text{ClO}_4^-)_2$.

These results show that it is possible to incorporate $[\text{Ru}(\text{bpy})_2(\text{picCOOH})]^{2+} \cdot (\text{ClO}_4^-)_2$ into the polymer, but only at low Ru loadings. This could be rationalized by the fact that in the electropolymerization solution there is a high concentration of protons (H^+). As previously

explained these protons are very essential, because they are needed to protonate the ANSA monomer, in order to initiate the polymerization process (Iwuoha *et al.*, 1997). However, in the presence of $[\text{Ru}(\text{bpy})_2(\text{picCOOH})]^{2+} \cdot (\text{ClO}_4^-)_2$ (1 mM), these protons are of very high concentration, as the concentration of H_2SO_4 was 0.5 M and this causes competition between the Ru (1 mM) and the protons for occupation of anionic sites within the polymer. In order to achieve higher loading of the Ru complex in the polymer, the electropolymerization solution should rather contain a low concentration of the acidic medium, in order to have less H^+ and a high concentration of Ru. Hence, the optimized polymerization mixture was finally made up of H_2SO_4 (0.1 mM), $[\text{Ru}(\text{bpy})_2(\text{picCOOH})]^{2+}$ (1 mM) and ANSA (0.2 M), and the results are demonstrated in section 6.3.1.4.

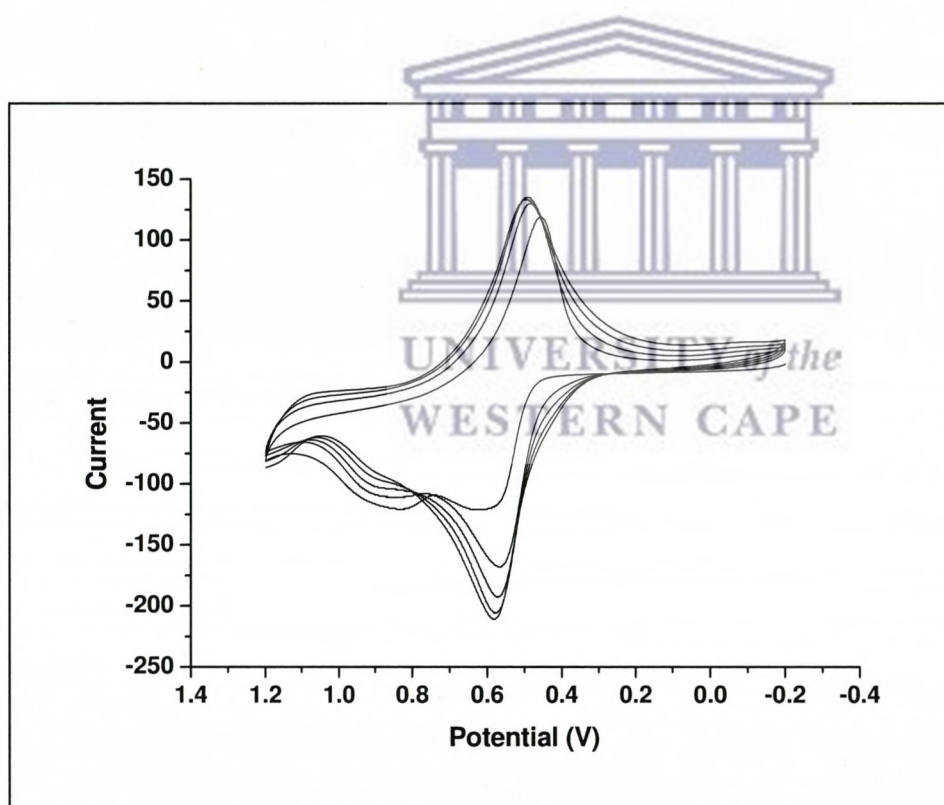


Figure 6 .8: Electrosynthesis of PANSA and $[\text{Ru}(\text{bpy})_2(\text{picCOOH})]^{2+} \cdot (\text{ClO}_4^-)_2$ on a 0.0172 cm^2 Au electrode at a scan rate 0.05 V s^{-1} in H_2SO_4 (0.5 mM), the CV illustrates the 1st to the 10th of the polymerization cycle is shown.

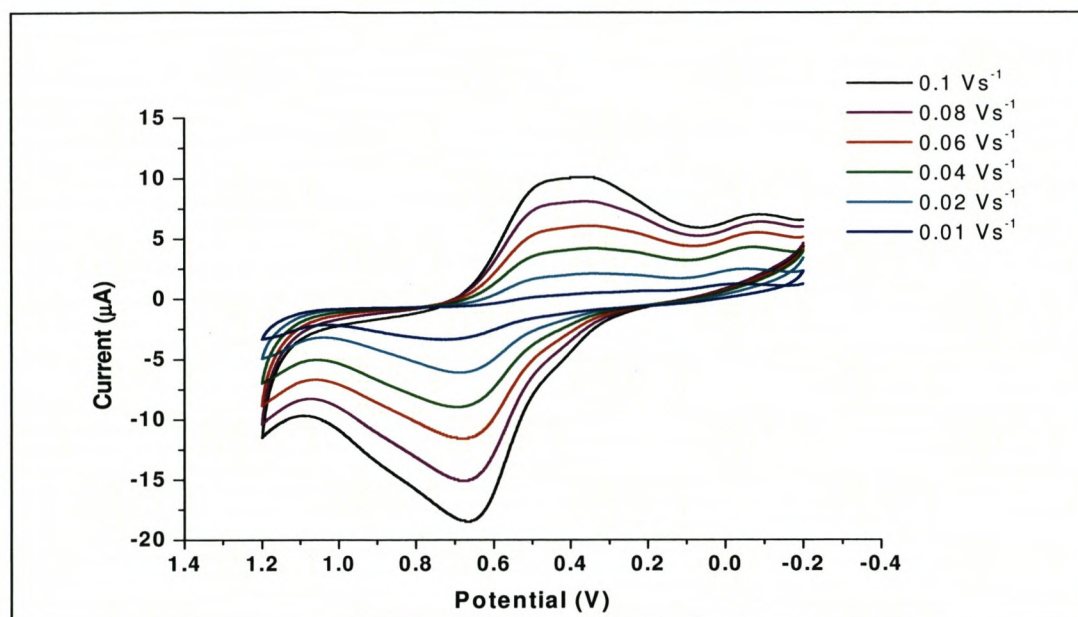


Figure 6.9: Multi scan CV of Au-PANSA-[Ru(bpy)₂(picCOOH)]²⁺.(ClO₄)₂ at 0.01, 0.02, 0.04, 0.08 and 0.1 V s⁻¹ in 0.5 M H₂SO₄, film grown at 0.05 V s⁻¹.

6.3.1.4. Optimized electropolymerization of ANSA and [Ru(bpy)₂(picCOOH)]²⁺.(ClO₄)₂

The results (Figure 6.10) show similar behaviour, as described in section 6.3.1.3 above, whereby during polymerization one redox couple was observed. The polymerization peak current increases as the voltammetric cycles increase, also indicating that polymer was conducting (Iwuoha *et al.*, 1997). Figure 6.11 presents typical multi sweep rate voltammograms of the Au-PANSA-[Ru(bpy)₂(picCOOH)]²⁺.(ClO₄)₂ which displays well defined oxidation-reduction responses indicating that the PANSA-[Ru(bpy)₂(picCOOH)]²⁺.(ClO₄)₂ composite was electroactive (Michira *et al.*, 2007). Furthermore, during polymerization (Figure 6.10), at E_{pa} ~0.95 and 1.1 V, two peaks were present, and the might be due to the presence of [Ru(bpy)₂(picCOOH)]²⁺.(ClO₄)₂, and its successful incorporated into the polymer.

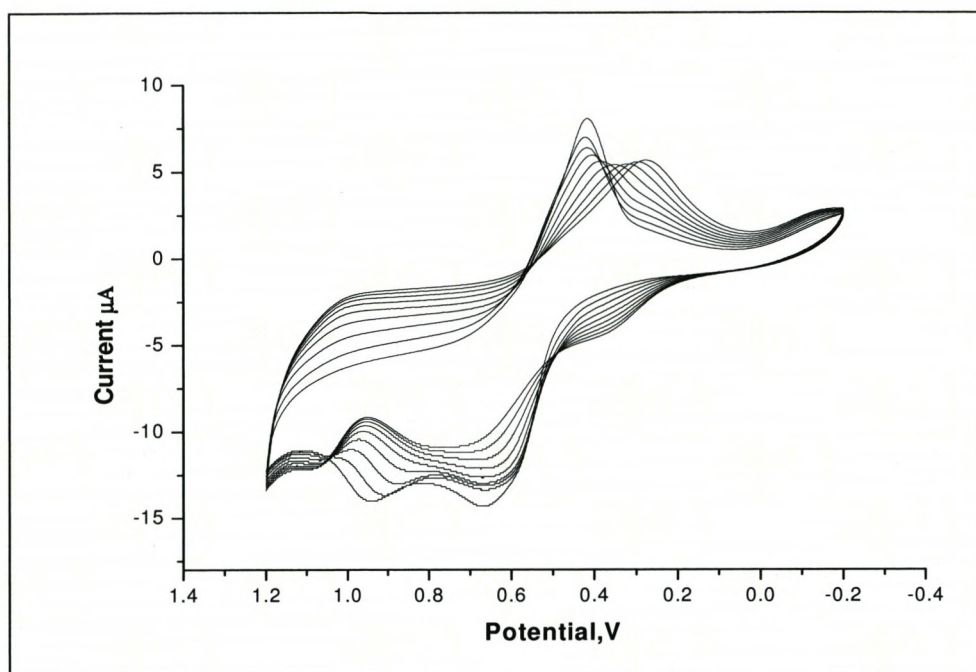


Figure 6.10: Electro-synthesis of PANSA and $[\text{Ru}(\text{bpy})_2(\text{picCOOH})]^{2+} \cdot (\text{ClO}_4^-)_2$ on a 0.0177 cm^2 Au electrode at a scan rate 0.1 V s^{-1} in H_2SO_4 (0.1 mM), the CV illustrates the 1st to the 10th of the polymerization cycle is shown.

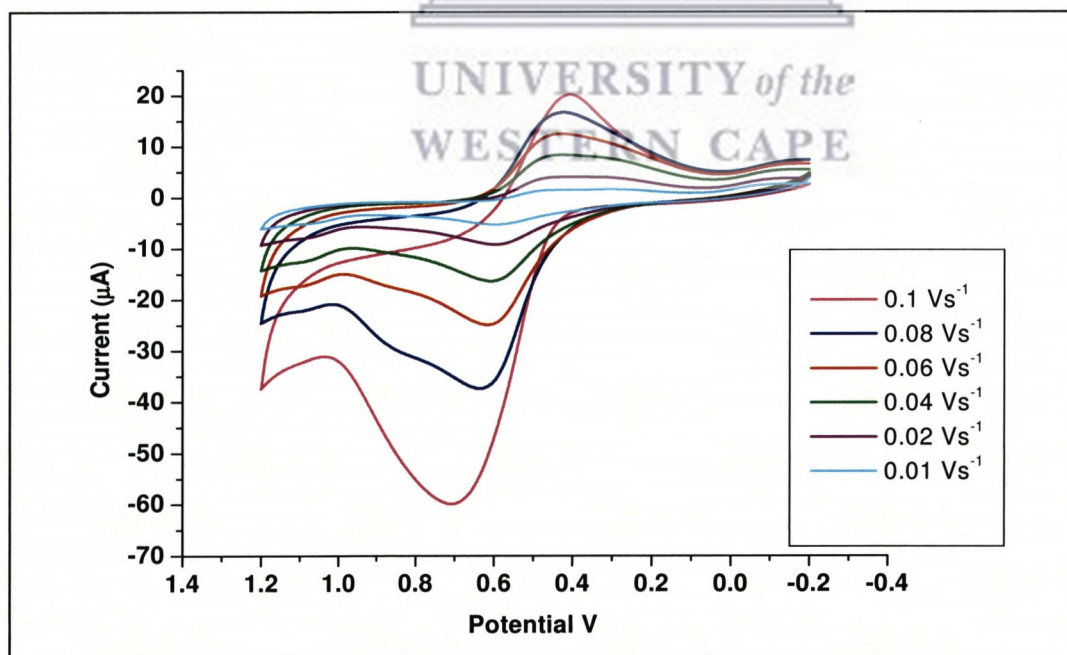


Figure 6.11: Cyclic voltammogram characterization at 0.01, 0.02, 0.04, 0.08 and 0.1 V s^{-1} for Au-PANSA- $[\text{Ru}(\text{bpy})_2(\text{picCOOH})]^{2+} \cdot (\text{ClO}_4^-)_2$ in H_2SO_4 (0.1 mM), film grown at 0.05 V s^{-1} .

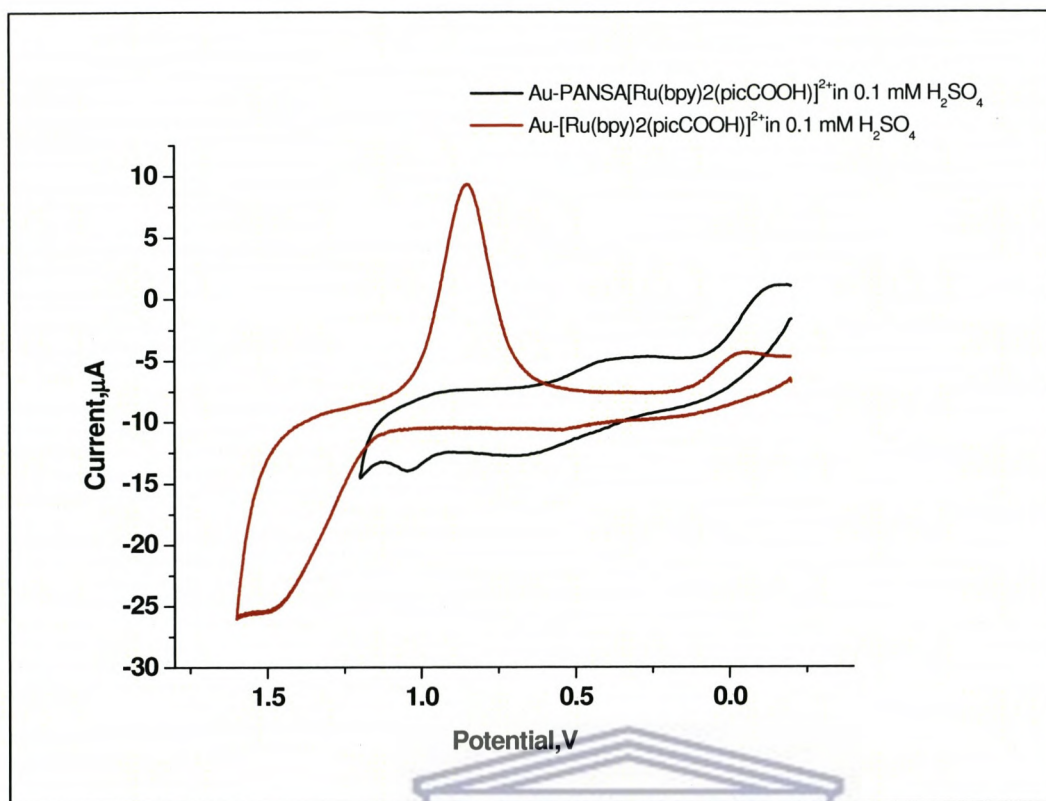


Figure 6.12: Cyclic voltammogram characterization, of Au-PANI-[Ru(bpy)₂(picCOOH)]²⁺.(ClO₄)₂ in an extended potential window of (0.02-0.16 V s⁻¹) at a scan rate of 0.1 Vs⁻¹ in H₂SO₄ (0.1 mM).

This was further investigated by characterizing this film in H₂SO₄ (0.1 mM) in an extended potential window of 0.02-0.16 V s⁻¹ illustrated in Figure 6.12 which presents a comparison of cyclic voltammograms of bare gold electrode in a solution of [Ru(bpy)₂(picCOOH)]²⁺.(ClO₄)₂ and H₂SO₄ and Au electrode modified with PANSA-[Ru(bpy)₂(picCOOH)]²⁺.(ClO₄)₂ film in H₂SO₄. The peak at E_{pa} equal 1.1 V was clearly observed and was due to the presence of the ruthenium complex in polymer film, although there was a shift in the peak potential, as in the bare gold the [Ru(bpy)₂(picCOOH)]²⁺.(ClO₄)₂ peak was observed at E_{pa} ~ 1.4 V.

From the results presented in the preliminary studies above, the conclusion that was reached was that, successful electropolymerization of the PANI and PANSA with incorporation of

$[\text{Ru}(\text{bpy})_2(\text{picCOOH})]^{2+} \cdot (\text{ClO}_4^-)_2$ is possible, provided that the polymerization contains a lower concentration of the acidic medium, which will just be enough to initiate the polymerization process. However, $[\text{Ru}(\text{bpy})_2(\text{picCOOH})]^{2+} \cdot (\text{ClO}_4^-)_2$ concentration should be higher than that of the acidic medium, so as the Ru would be able to get incorporated into the polymer. Although, some incorporation of the Ru complex was demonstrated in PANSA, cycling between potential ranges, may also encourage the shuttling of $[[\text{Ru}(\text{bpy})_2(\text{picCOOH})]^{2+} \cdot (\text{ClO}_4^-)_2]$, instead of its incorporation in the polymer, leading to low loading of the Ru complex into the polymer. Therefore, it was concluded that in order to maximize its incorporation in both PANI and PANSA, and to have a common polymerization technique for both the polymers the most suitable technique for growing the polymers is by employing potentiostatic technique, such as amperometry. From the resulting CV's recorded during the polymerization processes, it was deduced that a suitable potential for potentiostatic growth of PANI was approximately 0.7 V and 0.5 V for PANSA. Applying a potential above these values caused over oxidation of the polymers. Hence, the final method of polymerization which was employed is described in section 6.2.3.2 of the experimental method and it yielded the following results.

6.3.2. Potentiostatic growth of PANI and PANSA in the presence $[\text{Ru}(\text{bpy})_2(\text{picCOOH})]^{2+} \cdot (\text{ClO}_4^-)_2$ on ITO in HCL and H_2SO_4 respectively

As previously explained from preliminary results, it was deduced that the suitable method for potentiostatic growth of PANI, is by constantly applying an oxidation potential of 0.7 V for polymerization of ANI and 0.5 V for ANSA on the working electrode at different run timings. PANI was grown at 0.7 V for 810 and 1600 s, while PANSA was grown at 0.5 V for 90 and 810 s. This was conducted to study the effect of time on the incorporation of $[\text{Ru}(\text{bpy})_2(\text{picCOOH})]^{2+} \cdot (\text{ClO}_4^-)_2$ in the polymer backbone, i.e. to study whether increasing

the time for the potentiostatic growth, would increase or decrease the amount of the Ru loading in the polymer.

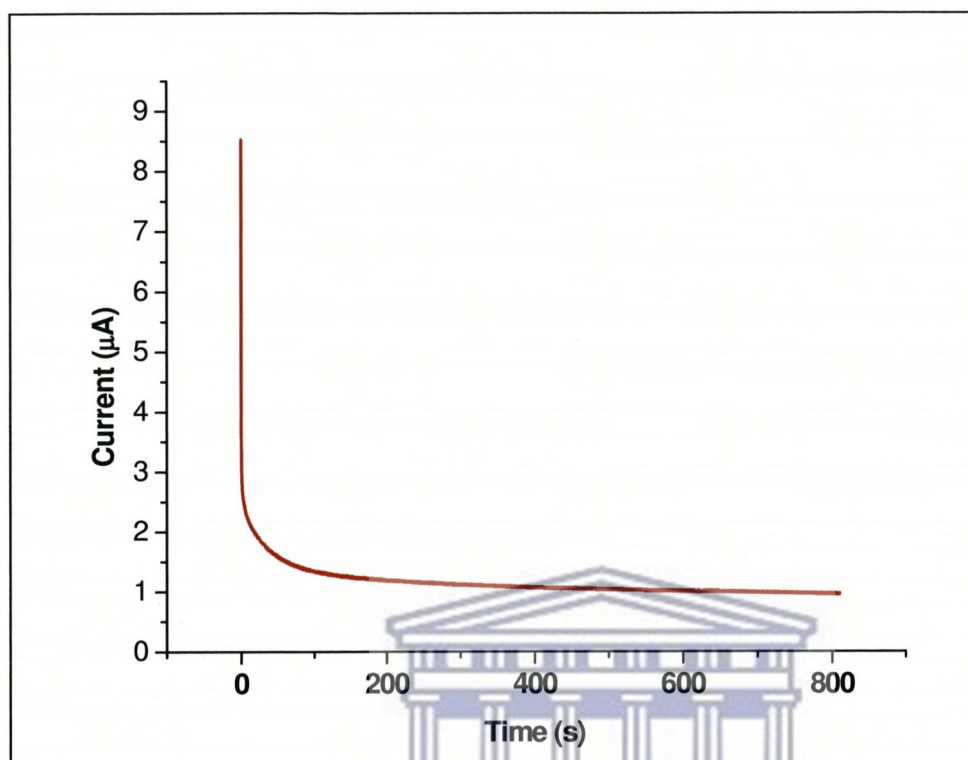


Figure 6.13: Amperometric i-t response of PANI-[Ru(bpy)₂(picCOOH)]²⁺.(ClO₄)₂ film modified ITO electrode upon applying a constant oxidative potential of 0.7 V for 810 s.

During the amperometric experiments, for polymerization of PANI-[Ru(bpy)₂(picCOOH)]²⁺.(ClO₄)₂ the electrode potential was held at an oxidative potential of 0.7 V for 810 and 1600 s. Figure 6.13 shows the amperometric i-t response obtained for the film electropolymerized for 810 s. It was clear that, the composite film exhibited a consistent and well-defined amperometric response. The film prepared for 1600 s, gave the same amperometric i-t response as the one prepared for 810 s.

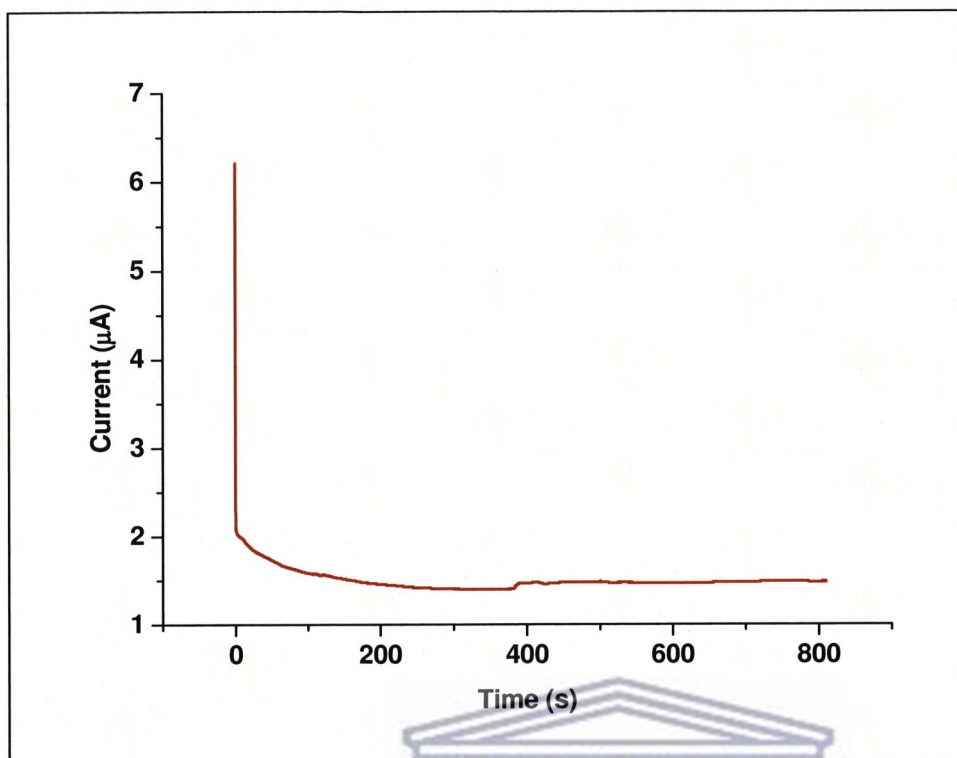


Figure 6.14: Amperometric i-t response of PANSA-[Ru(bpy)₂(picCOOH)]²⁺.(ClO₄)₂ film modified ITO electrode upon applying a constant oxidative potential of 0.5 V for 810 s.

For polymerization of PANSA-[Ru(bpy)₂(picCOOH)]²⁺.(ClO₄)₂ the electrode potential was held at an oxidative potential of 0.5 V for 90 and 810 s. Figure 6.14 displays the amperometric i-t response obtained for this film electropolymerized for 810 s, the composite film also exhibited well-defined amperometric response, with a slight increased in current at ~390 s. The PANSA-[Ru(bpy)₂(picCOOH)]²⁺.(ClO₄)₂ film prepared for 90 s, gave the same amperometric i-t response as the one prepared for 810 s. Table 6.1 below summarizes the response results from amperometric experiments.

Table 6.1: Showing a summary of results obtained PANI and PANSA Films modulated with $[Ru(bpy)_2(picCOOH)]^{2+}.(ClO_4^-)_2$, electropolymerized at different run timings at potential 0.7 and 0.5 V respectively and the final charge during the electropolymerization.

Polymer	Time (s)	Potential (V)	Charge passed (C)
PANI- $[Ru(bpy)_2(picCOOH)]^{2+}.(ClO_4^-)_2$	810	0.7	5.346×10^{-9}
PANI- $[Ru(bpy)_2(picCOOH)]^{2+}.(ClO_4^-)_2$	1600	0.7	6.423×10^{-7}
PANSA- $[Ru(bpy)_2(picCOOH)]^{2+}.(ClO_4^-)_2$	90	0.5	1.13×10^{-6}
PANSA - $[Ru(bpy)_2(picCOOH)]^{2+}.(ClO_4^-)_2$	810	0.5	7.39×10^{-6}

The summary of results indicated by Table 6.1 above shows that during electropolymerization of PANSA, greater charge passed compared to that of PANI. Furthermore, when increasing polymerization time for PANSA from 90 to 810 s, also resulted increased final charge applied. These films were further characterized, using CV to ascertain whether the polymerization was successful and their ECL behaviour was also studied.

6.3.3. CV characterization of PANI- $[Ru(bpy)_2(picCOOH)]^{2+}.(ClO_4^-)_2$ and PANSA- $[Ru(bpy)_2(picCOOH)]^{2+}.(ClO_4^-)_2$ films

The Figure 6.15 illustrates a blank ITO, in the presence of 1 mM of $[Ru(bpy)_2(picCOOH)]^{2+}.(ClO_4^-)_2$ overlaid with ITO-PANI- $[Ru(bpy)_2(picCOOH)]^{2+}.(ClO_4^-)_2$, which was characterized in 0.1 mM HCL at a scan rate of 0.1 V s^{-1} . The blank was ran to

establish the potential range in which the $[\text{Ru}(\text{bpy})_2(\text{picCOOH})]^{2+} \cdot (\text{ClO}_4^-)_2$ peak would be observed, and the characterization of the ITO-PANI- $[\text{Ru}(\text{bpy})_2(\text{picCOOH})]^{2+} \cdot (\text{ClO}_4^-)_2$ was carried out to ascertain whether the Ru complex was incorporated into the polymer and if the polymerization was successful. The results from the blank revealed that $[\text{Ru}(\text{bpy})_2(\text{picCOOH})]^{2+} \cdot (\text{ClO}_4^-)_2$ displays an electrochemically reversible response centered at $\sim +1.25$ V associated with the $\text{Ru}^{2+/3+}$ couple (Pellegrin, 2008), and the peak is also observed at the same potential in the ITO-PANI- $[\text{Ru}(\text{bpy})_2(\text{picCOOH})]^{2+} \cdot (\text{ClO}_4^-)_2$, confirming the successful incorporation of the Ru into the polymer. The redox couple observed ~ 0.5 V, can be attributed to the polymer.

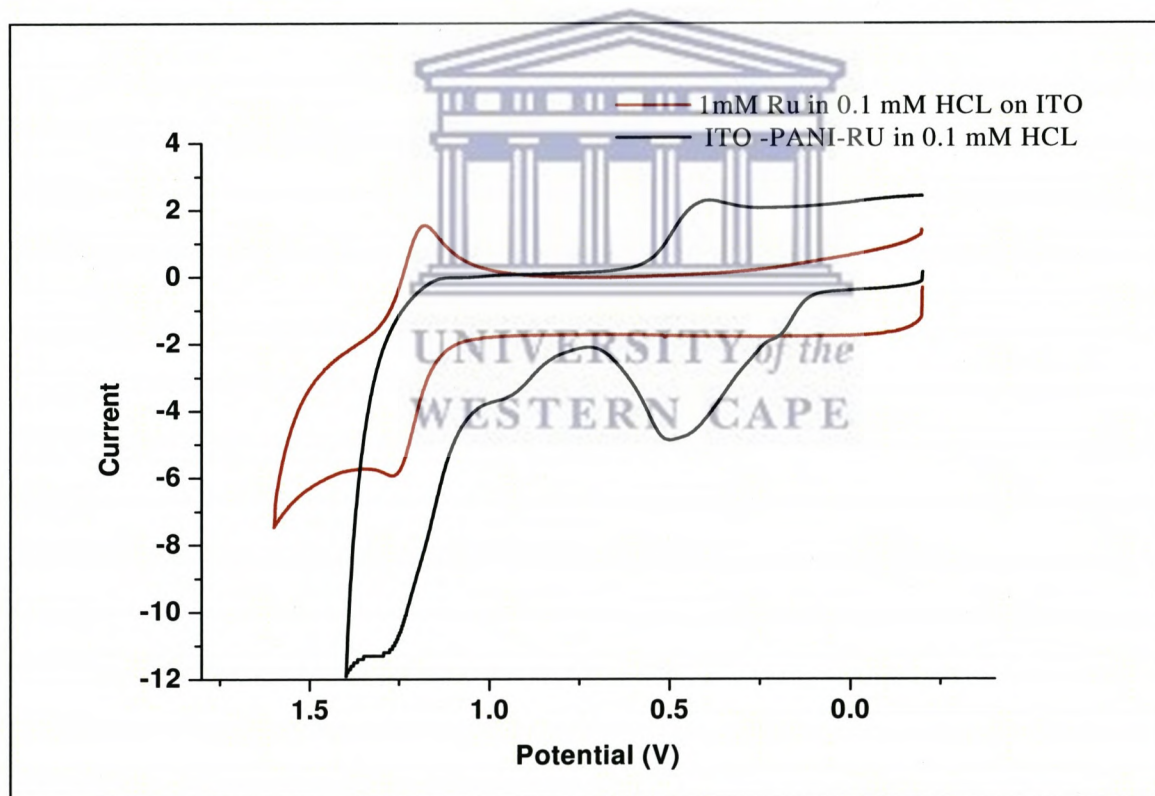


Figure 6.15: Illustrating Blank ITO, in 1 Mm $[\text{Ru}(\text{bpy})_2(\text{picCOOH})]^{2+} \cdot (\text{ClO}_4^-)_2$ and 0.1 mM HCL (—) and (—) illustrates characterization of ITO-PANSA $[\text{Ru}(\text{bpy})_2(\text{picCOOH})]^{2+} \cdot (\text{ClO}_4^-)_2$ at a scan rate of 0.1 V s^{-1} in 0.1 mM HCL electropolymerized by potentiostatic growth for 810 s.

The ITO-PANSA- $[\text{Ru}(\text{bpy})_2(\text{picCOOH})]^{2+} \cdot (\text{ClO}_4^-)_2$, also showed successful incorporation of the ruthenium complex, confirmed by the peak observed $\sim 1.25\text{V}$, and one redox couple which could be ascribed to the PANSA polymer as shown in Figure 6.16 below.

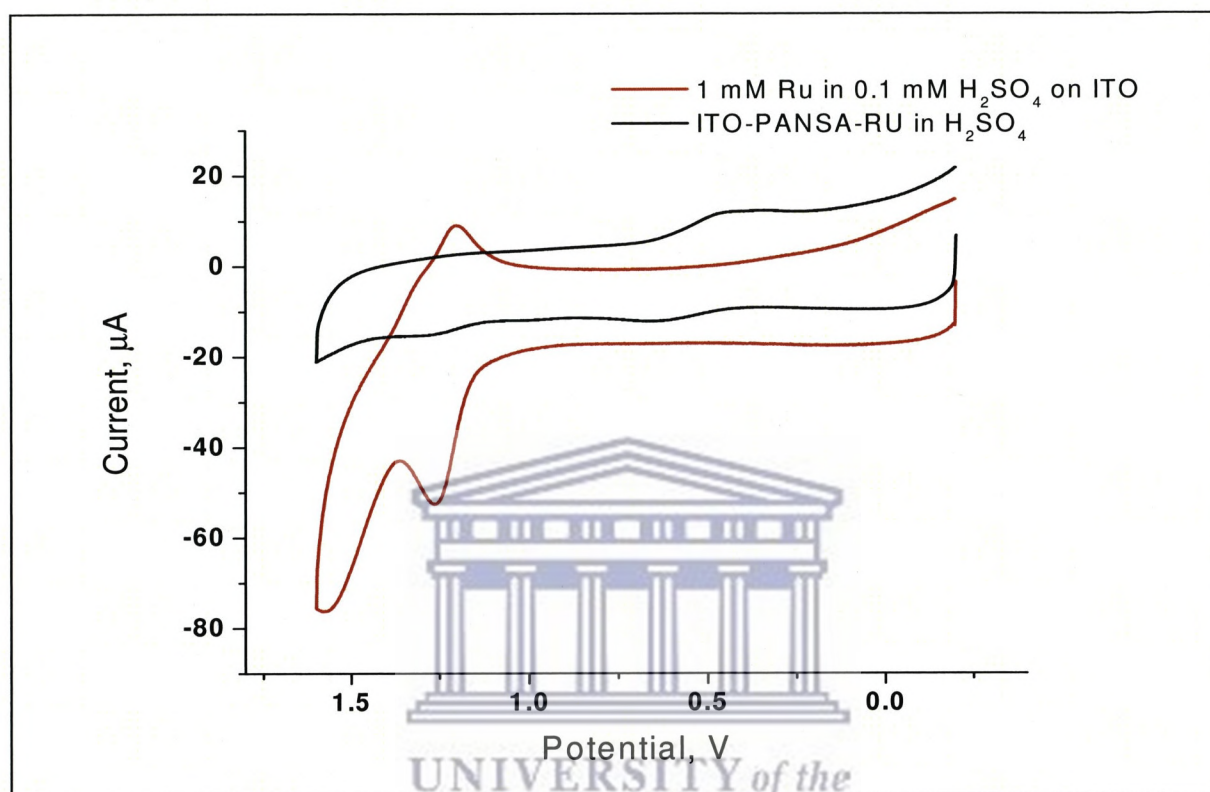


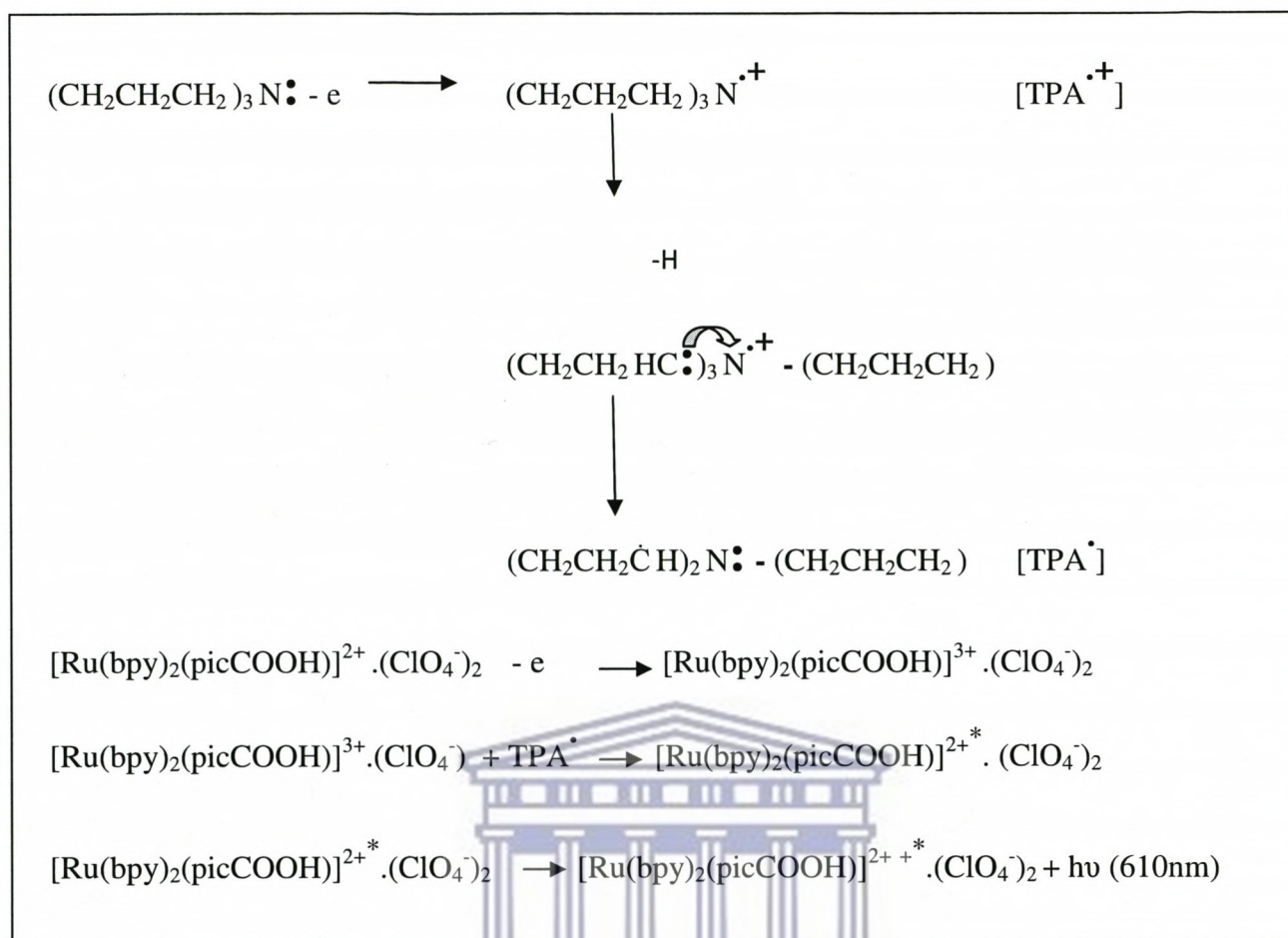
Figure 6.16: Illustrating Blank ITO, in 1 Mm $[\text{Ru}(\text{bpy})_2(\text{picCOOH})]^{2+} \cdot (\text{ClO}_4^-)_2$ and 0.1 mM H_2SO_4 (—), and the characterization ITO-PANSA- $[\text{Ru}(\text{bpy})_2(\text{picCOOH})]^{2+} \cdot (\text{ClO}_4^-)_2$ (—) at a scan rate of 0.1 V s^{-1} in 0.1 mM H_2SO_4 electropolymerized by potentiostatic growth for 810 s.

6.3.4. Electrochemiluminescence study

6.3.4.1. ECL response of PANI-[Ru(bpy)₂(picCOOH)]²⁺.(ClO₄)₂ film

The current section reports, the ECL of the polymers which were prepared in the above section, employing TPA [(CH₂CH₂CH₂)₃ N:] as a representative coreactant. The ECL mechanism of TPA/ [Ru(bpy)₃]²⁺ ECL is a well investigated system (Richter, 2004). Richter (2004) explained about the different possible reaction pathways have been proposed for TPA/ [Ru(bpy)₃]²⁺ ECL system. In general, the reaction pathway takes according to the following direction; oxidation of TPA at the electrodes takes place, to give rise to a radical cation (TPA^{•+}). This radical cation loses a proton from its α carbon, resulting in the formation of an intermediate TPA[•], which is strong reducing agent. TPA[•] reacts with the electrogenerated Ru³⁺ species, forming the excited state reduced product Ru^{2+*} which then relaxes to the electronic ground state by emission of light at 610 nm (Richter, 2004). The results of the ECL behaviour using PANI-[Ru(bpy)₂(picCOOH)]²⁺.(ClO₄)₂ and PANSA-[Ru(bpy)₂(picCOOH)]²⁺.(ClO₄)₂ films, in the presence of 50 Mm TPA as a coreactant are represented below.

The ECL behaviour of [Ru(bpy)₂(picCOOH)]²⁺.(ClO₄)₂ incorporated into PANI-modified ITO electrode has been studied with tripropylamine (TPA). Figure 6.17 illustrates the voltammetric behaviour of a thin layer of PANI-[Ru(bpy)₂(picCOOH)]²⁺.(ClO₄)₂ deposited on ITO at a scan rate of 0.1 V s⁻¹ for 1600 s in 0.1 mM HCL as a supporting electrolyte. The cyclic voltammogram in the presence of TPA shows broad irreversible anodic peak starting at ~0.80 V and peaking at ~1.4 V vs Ag/Ag/Cl. Fan *et al.* (2008) explained that this observation can be ascribed to the direct oxidation of TPA at the electrode surface (refer to Scheme 6.1).



Scheme 6.1: Above shows the proposed tri-*n*-propylamine (TPA) and $[\text{Ru}(\text{bpy})_2(\text{picCOOH})]^{2+} \cdot (\text{ClO}_4^-)_2$ oxidation reaction sequence with abbreviations in parentheses.

The CV measurements also aided in determining effective surface coverage (Γ) of $[\text{Ru}(\text{bpy})_2(\text{picCOOH})]^{2+} \cdot (\text{ClO}_4^-)_2$. The surface coverage was calculated by integration of the anodic peak current when thin-films were characterized in their respective supporting electrolyte medium where Γ was calculated using Equation 2.39 (as shown in chapter two).

$$\Gamma = Q/nFA \quad [2.39]$$

The surface coverage for PANI- $[\text{Ru}(\text{bpy})_2(\text{picCOOH})]^{2+} \cdot (\text{ClO}_4^-)_2$ electropolymerized for 1600 s was $1.29 \times 10^{-9} \text{ mol cm}^{-2}$.

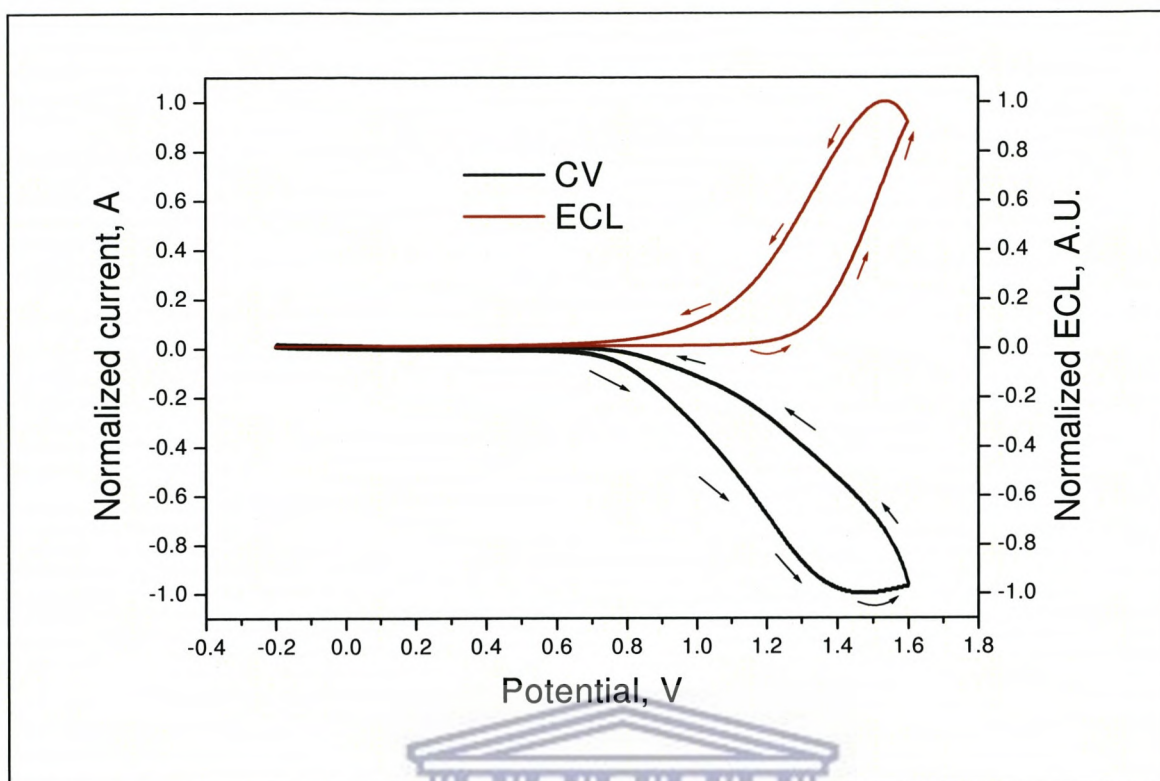


Figure 6.17: Shows simultaneously recorded: Cyclic voltammogram (—) and electrochemiluminescence response (—) of ITO modified with PANI- $[\text{Ru}(\text{bpy})_2(\text{picCOOH})]^{2+} \cdot (\text{ClO}_4)_2$ film electrodeposited for 1600 seconds from hydrochloric acid. TPA (50 mM) dissolved in PBS was the co-reactant used. The electropolymerization and the ECL were performed at a scan rate of 0.1 Vs^{-1} and Γ was $1.29 \times 10^{-9} \text{ mol.cm}^{-2}$.

Figure 6.17 also shows the electrochemiluminescence response after the addition of TPA. The shape of the corresponding ECL with potential was very similar to the one observed in the CV. The results showed that the presence of TPA caused the oxidation peak current observed for the modified electrode surface to increase dramatically. This oxidation of TPA was accompanied by emission from the layer illustrated by the dramatic peak current increase. Forster and Hogan (2000) explained that this observation demonstrated the reduction of Ru^{3+} to Ru^{2+*} (refer to Scheme 6.1). This was observed by an ECL signal, which

was initially at zero intensity, it then starts to increase dramatically at $\sim E_p$ 1.2 V and reached a maximum intensity at $E_p \sim 1.58$ V. The ECL signal then decreased back to zero, indicating relaxation to ground state via emission of light of the molecule.

Figure 6.18 shows cyclic voltammograms and ECL response of PANI $[\text{Ru}(\text{bpy})_2(\text{picCOOH})]^{2+} \cdot (\text{ClO}_4^-)_2$ film electrodeposited for 810 seconds on ITO electrode in the presence of a solution of 50 mM TPA in 0.05 M phosphate buffer. It presents the ECL response recorded simultaneously with CV. The ECL intensity appeared to be initially consistent at 0.3 A.U. As the potential of the ITO electrode modified with PANI - $[\text{Ru}(\text{bpy})_2(\text{picCOOH})]^{2+} \cdot (\text{ClO}_4^-)_2$ for 810 s which is in contact with the TPA solution approaches 1.2 V, an onset increase in the ECL signal is observed initially. This was indication that the reaction of Ruthenium and TPA, giving rise to electrochemical production of the ruthenium excited state species. This ECL peak intensity increased till it reached its maximum intensity at potential 1.6 V, thereby generating luminescence as it decayed to the ground state, and decreasing back to the initial intensity (0.3 A.U).

On the basis of the results above and previous proposal for pathways for ECL generation by Richter (2004) for the reaction ruthenium tris(bipyridyl) with TPA $[(\text{CH}_2\text{CH}_2\text{CH}_2)_3 \text{N}:]$ in solution, the results can be elucidated with a mechanism of the ECL reaction represented by in Scheme 6.1.

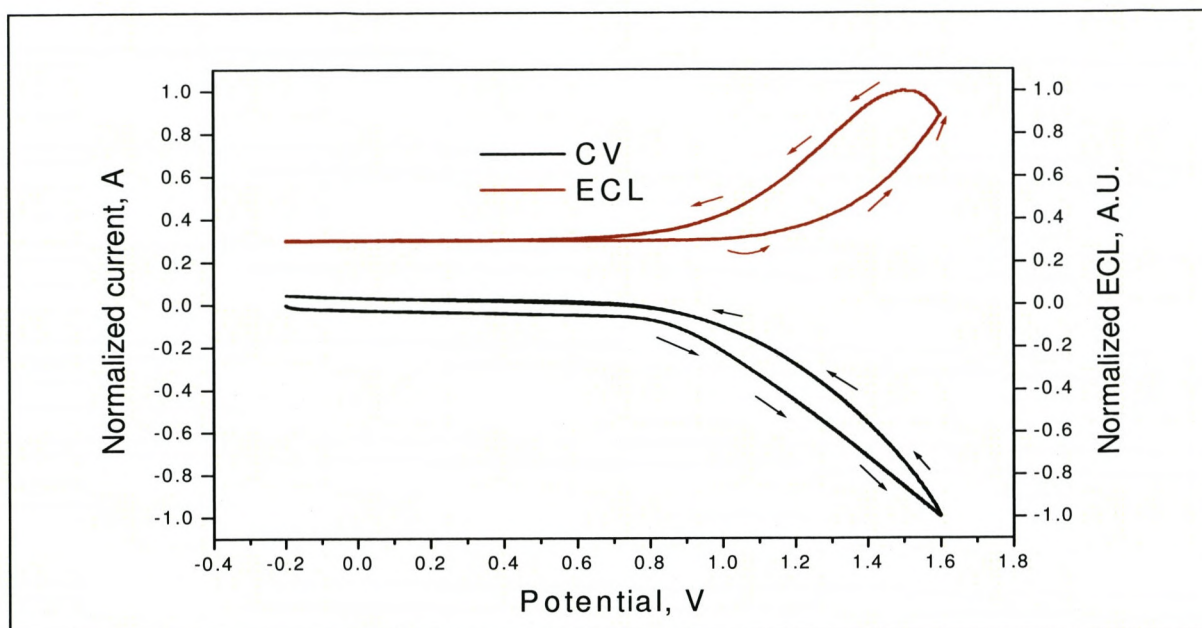


Figure 6.18: Cyclic voltammogram (—) and electrochemiluminescence response (—) of ITO modified with PANI-[Ru(bpy)₂(picCOOH)]²⁺.(ClO₄⁻)₂ film electrodeposited for 810 seconds from hydrochloric acid. TPA (50 mM) dissolved in PBS was the co-reactant used. The electropolymerization and the ECL were performed at a scan rate of 0.1 Vs⁻¹ and Γ was 2.56×10^{-10} mol.cm⁻².

UNIVERSITY of the
WESTERN CAPE

The Figure 6.19 below displays a comparison between ECL response of a PANI-[Ru(bpy)₂(picCOOH)]²⁺.(ClO₄⁻)₂ film electrodeposited for 810 and 1600 seconds. The ECL intensity observed with the PANI-[Ru(bpy)₂(picCOOH)]²⁺.(ClO₄⁻)₂ film electrode, electrodeposited for 1600 s is 25-folds greater than that obtained at the film which was electrodeposited for 810 s.

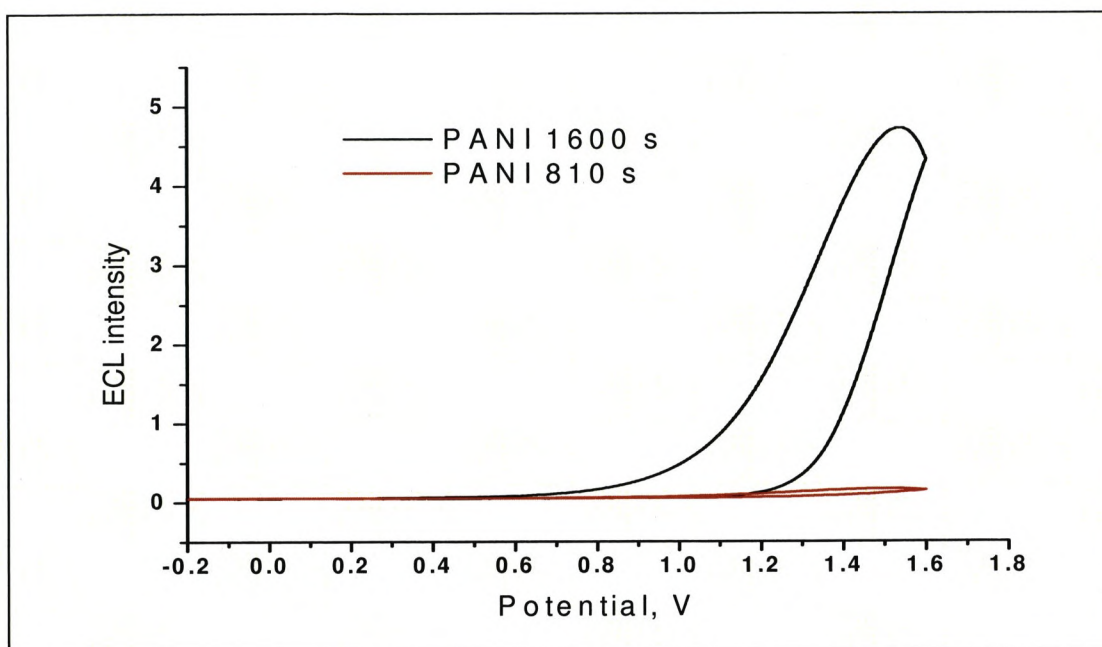


Figure 6.19: The ECL responses of ITO modified with PANI-[Ru(bpy)₂(picCOOH)]²⁺·(ClO₄)₂ film electrodeposited for 810 and 1600 s from hydrochloric acid. TPA (50 mM) dissolved in PBS was the co-reactant used. The electropolymerization and the ECL was performed at a scan rate was 0.1 V s⁻¹

When comparing the surface coverages (Γ) of ruthenium in the two films, that is the amount of ruthenium that was loaded into the polymer, during the electropolymerization of PANI- - [Ru(bpy)₂(picCOOH)]²⁺·(ClO₄)₂ carried out for 1600 seconds yielded, Γ of 1.29×10^{-9} mol cm⁻² was obtained while the film that was electropolymerized for 810 seconds gave rise to a Γ of 2.56×10^{-10} mol cm⁻². The Γ value PANI-Ru complex electropolymerized for 810 seconds was on the same range with the one reported by Venkatanarayanan (2010) of $4.6 \pm 0.5 \times 10^{-10}$ mol cm⁻² in the studies of [Ru(aphen)₃]²⁺ film electrodeposited from acetonitrile and co-reactant used 0.1 M TPA dissolved in acetonitrile. It was clear that extending the electropolymerization time for PANI and -[Ru(bpy)₂(picCOOH)]²⁺·(ClO₄)₂, aided in achieving a higher ruthenium loading. This was consistent with the result observed in Figure

6.19 above, demonstrating that the ECL intensity of PANI (1600 s) was much greater than that of PANI (810 s). Choi *et al.* (2006) explained that direct oxidation of the TPA amine at the electrode surface plays an important role in ECL process. Hence, the film exhibiting greater open structure leads to the faster diffusion of TPA into the film and also the increased charge transport which results in a much greater ECL response and those that do not exhibit open pore structure and have very low rates of charge transfer (Choi *et al.*, 2006). Figure 6.20 and 6.21 display a simultaneous detection of both the amperometric and electrochemiluminescent signals from the PANI-[Ru(bpy)₂(picCOOH)]²⁺.(ClO₄)₂ films, electrodeposited at 810 and 1600 seconds. When the potential was repeatedly stepped at the electrode, in the TPA-PBS electrolyte as demonstrated in Figure 6.20, a current and an emission response was generated. The results demonstrated that repeated stepping of the potential, resulting in emission that was reversibly switched on and off as observed in Figure 6.21. This figure also shows that the emission response from PANI-[Ru(bpy)₂(picCOOH)]²⁺.(ClO₄)₂ electrodeposited for 1600 s was initially very high (~0.65 V) compared to that polymerized for 810 s (0.19 V), but with 10 seconds intervals it gradually decreased. On the contrary, the film prepared for 810 s, showed to have a steady state emission throughout the stepping period of 50 s. Forster and Hogan (2000) explained that this emission of light results from those reactants capable of undergoing a sufficiently exergonic reaction with Ru³⁺ to create the excited-state Ru^{2+*}. In the current study it can be deduced that the emission is caused by the reaction of TPA[•] and [Ru(bpy)₂(picCOOH)]³⁺.(ClO₄)₂, giving rise to an excited state [Ru(bpy)₂(picCOOH)]^{2+*}.(ClO₄)₂, which undergoes further reactions to give [Ru(bpy)₂(picCOOH)]²⁺.(ClO₄)₂ and light at 620 nm (refer to Scheme 6.1).

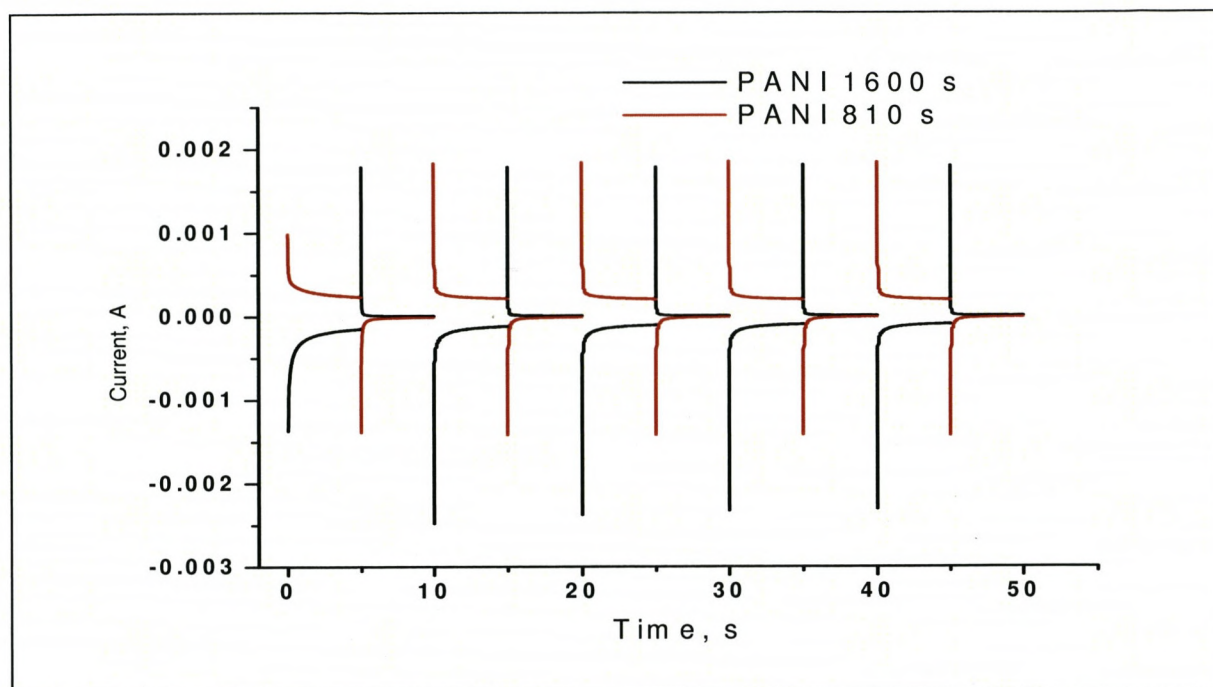


Figure 6.20: Shows the potential waveform of PANI-Ru complex that involves stepping 10 times from 5 to 16 V with a pulse width of 5 s, the supporting electrolyte is PBS that contains 50 mM TPA.

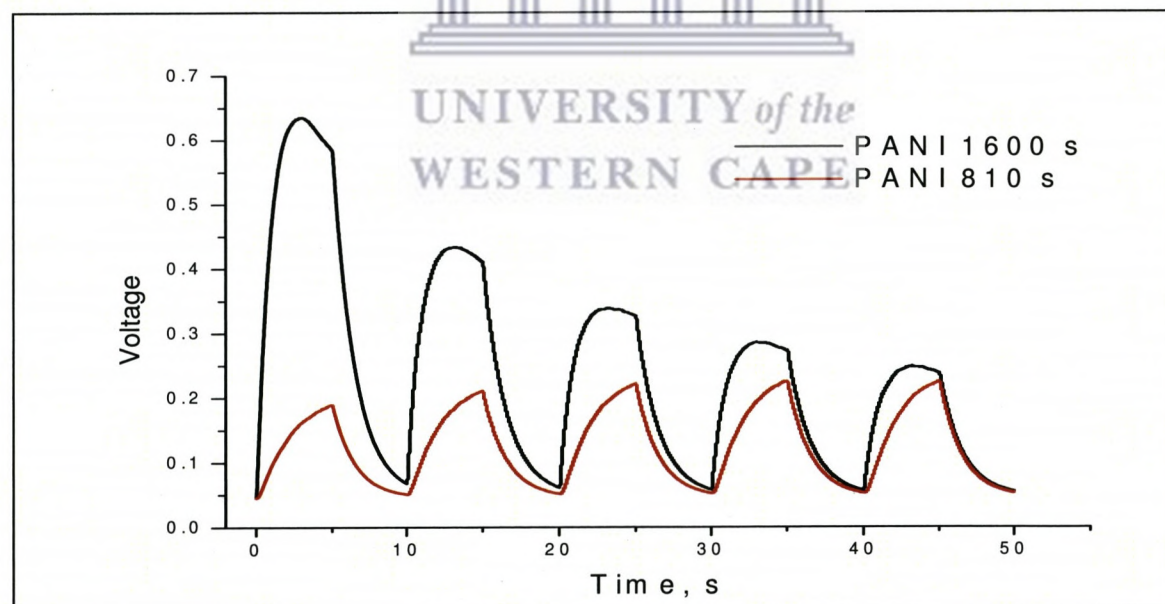


Figure 6.21: Shows the corresponding light signals of PANI-Ru complex, which are triggered by the potential stepping 10 times from 5 to 16 V with a pulse width of 5 seconds, the supporting electrolyte is PBS that contains 50 mM TPA.

6.3.4.1. ECL response of PANSA- $[\text{Ru}(\text{bpy})_2(\text{picCOOH})]^{2+} \cdot (\text{ClO}_4)_2$ film

Typical CVs, recorded at a scan rate of 0.1 V s^{-1} , PANSA - $[\text{Ru}(\text{bpy})_2(\text{picCOOH})]^{2+} \cdot (\text{ClO}_4)_2$ film on ITO in an aqueous TPA (50 mM) dissolved in PBS is shown in Figure 6.22. At the scan rate of 0.1 V s^{-1} . The CVs in the presence of TPA display a broad irreversible anodic peak starting at $\sim 0.5 \text{ V}$ and peaking at $\sim 1.4 \text{ V}$ vs Ag/Ag/Cl. This observation could be ascribed to the direct oxidation of TPA at the electrode surface (Fan *et al.*, 2009).

The surface coverage was calculated by integration of the anodic peak current when thin-layer was characterized, using CV and it was determined to be $5.16 \times 10^{-13} \text{ mol cm}^{-2}$, and this shows that the Ru loading into the polymer was very low. Figure 6.22 also shows the ECL response recorded simultaneously with CV.

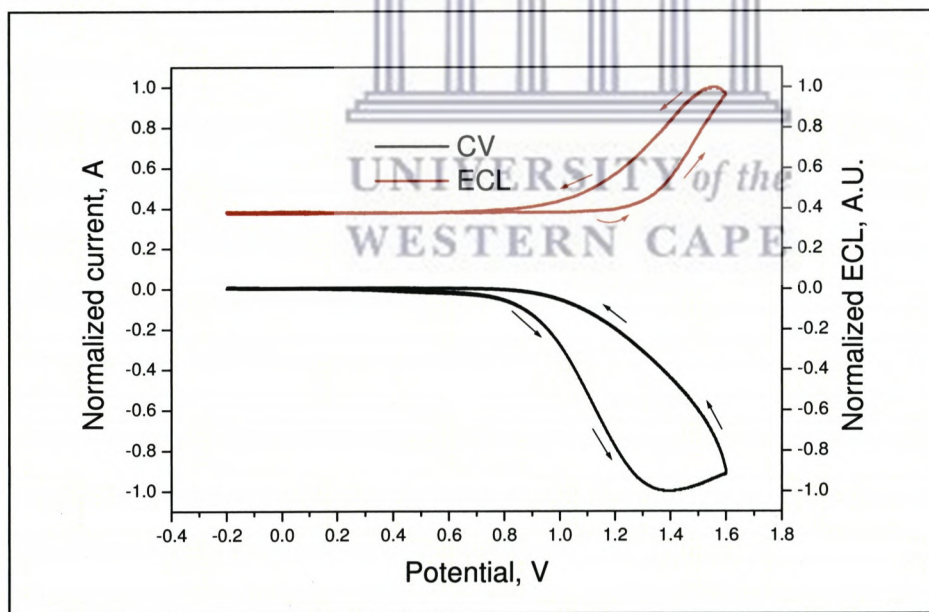


Figure 6.22: Cyclic voltammogram (—) and electrochemiluminescence response (—) ITO modified with PANSA - $[\text{Ru}(\text{bpy})_2(\text{picCOOH})]^{2+} \cdot (\text{ClO}_4)_2$ film electrodeposited for 810 s from sulphuric acid. TPA (50 mM) dissolved in PBS was the co-reactant used during ECL

detection. The electropolymerization and the ECL were performed at scan rates of 0.05 and 0.1 V s⁻¹ respectively. Γ was 5.16×10^{-13} mol cm⁻²

The ECL intensity appeared to be initially consistent at 0.4 A.U. As the potential was scanned linearly towards positive values, an onset increase in the ECL signal was observed at 1.2 V, indicating the reaction of Ruthenium and TPA^{*}, which react together giving rise to an electrochemical production of the ruthenium excited. This ECL peak intensity increased until it reached its maximum intensity at potential 1.6 V thereby generating luminescence as it decays to the ground state, and decreasing back to the initial intensity (0.4. A.U).

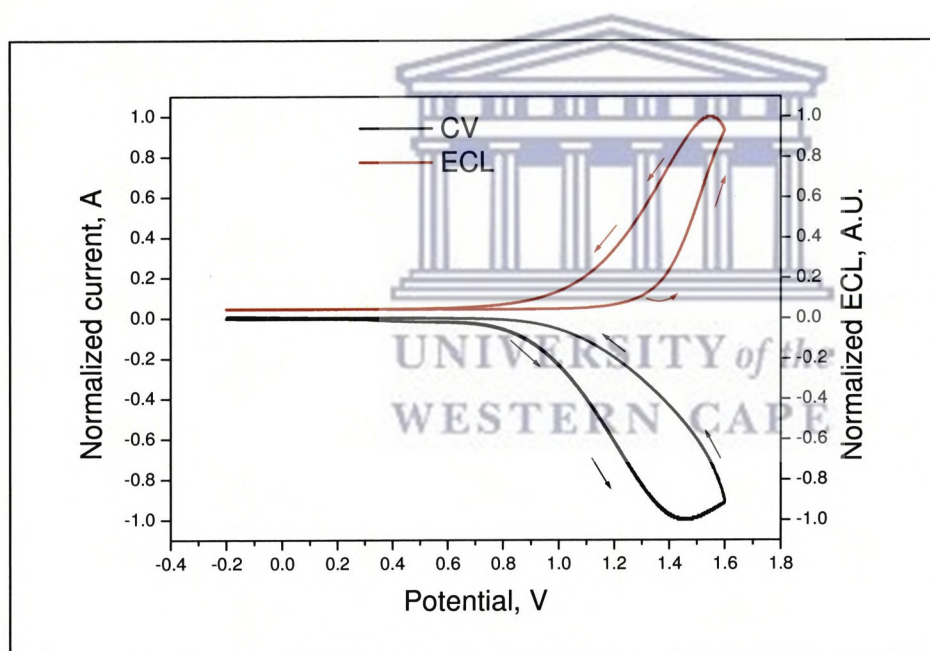


Figure 6.23: Cyclic voltammogram (—) and electrochemiluminescence response (—) of ITO modified with PANSa - $[\text{Ru}(\text{bpy})_2(\text{picCOOH})]^{2+} \cdot (\text{ClO}_4^-)_2$ film electrodeposited for 90 s from sulphuric acid. TPA (50 mM) dissolved in PBS was the co-reactant used. The electropolymerization and the ECL were performed rates of 0.05 and 0.1 V s⁻¹, respectively. Γ was 7.99×10^{-12} mol cm⁻².

The PANSA -[Ru(bpy)₂(picCOOH)]²⁺.(ClO₄⁻)₂ film electrodeposited for 90 seconds (Figure 6.23), displayed the same cyclic voltamogram and ECL as the one electrodeposited for 810 seconds, only that the ECL intensity was initially observed at 0.2 A.U, and as the potential reached 1.2 V an initial increase in ECL signal was observed. This ECL intensity continued to increase till it reached its maximum intensity at potential 1.6 V thereby generating luminescence as it decayed to the ground state, and decreasing back to the initial intensity (0.2 A.U). What was interesting about this film, was that the Γ was calculated to be 7.99×10^{-12} mol.cm⁻². This surface coverage, was higher than that achieved when electropolymerizing the film for 810 s. That is a higher loading of Ru is achieved at shorter periods of polymerization time, in the PANSA film. This observation was further illustrated by comparing the ECL intensity of intensity of PANSA-Ru complex electropolymerized for 90 s and 810 s (Figure 2.24). The figure reveals that the ECL intensity of PANSA-Ru complex electropolymerized for 90 s was greater than the PANSA-Ru complex film electropolymerized at 810 s. This observation was different from the one obtain using PANI-Ru complex film, whereby increasing the polymerization time, yielded higher loading of the Ru in the polymer.

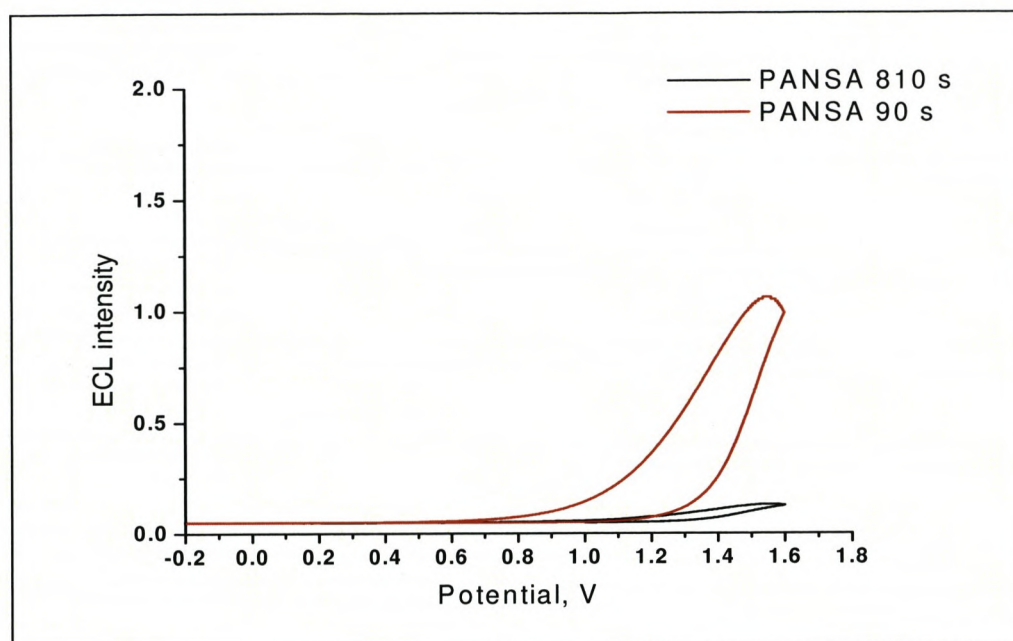


Figure 6.24: The ECL responses of ITO modified with PANSAs - $[\text{Ru}(\text{bpy})_2(\text{picCOOH})]^{2+}$ film electrodeposited for 90 and 810 s from hydrochloric acid. TPA (50 mM) dissolved in PBS was the co-reactant used. The electropolymerization and the ECL were performed at a scan rate of 0.05 and 0.1 V s^{-1} , respectively.

Figure 6.25 and 6.26 illustrate combined light and current detection by simultaneously detecting both the amperometric and electrochemiluminescent signals. The figures display current-time and ECL-time responses for ITO electrodes modified with PANSAs $[\text{Ru}(\text{bpy})_2(\text{picCOOH})]^{2+} \cdot (\text{ClO}_4^-)_2$ (for both 90 and 810 s) following a repeated potential step. The potential was stepped 10 times from 5 to 16 V with a pulse width of 5 seconds over a period of 50 seconds. The solvent used was PBS containing 50 mM TPA as supporting electrolyte. As the potential was stepped, an ECL signal was generated (Figure 6.26) and the results showed that it was possible to switch the light signal on and off. During the process of potential stepping, the Ru^{3+} species was generated which then reacts with TPA producing the excited state Ru^{2+*} , which then relaxed back to the ground state by emission of light at 620 nm (refer to Scheme 6.1). The emission of light in PANSAs-Ru complex

electropolymerized for 90 s was initially high at ~ 0.45 V as compared to the one of PANSA-Ru complex electropolymerized for 810 s, but also gradually decreases as time increases, while the (810 s) gave a steady emission of ~ 0.09 V.

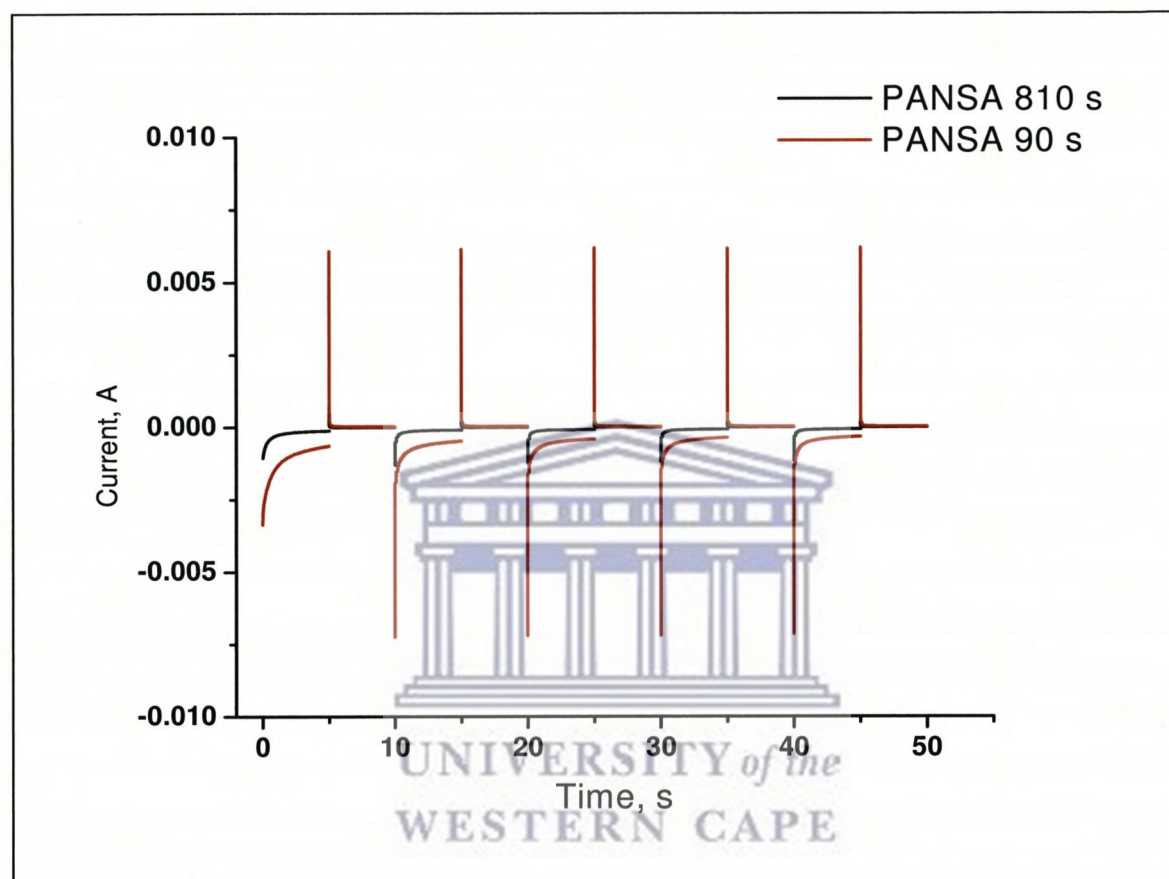


Figure 6.25: Shows the potential waveform that involves stepping 10 times from 5 to 16 V with a pulse width of 5 s, the supporting electrolyte is PBS that contains 50 mM TPA of ITO-PANSA - $[\text{Ru}(\text{bpy})_2(\text{picCOOH})]^{2+} \cdot (\text{ClO}_4^-)_2$ prepared for 90 s.

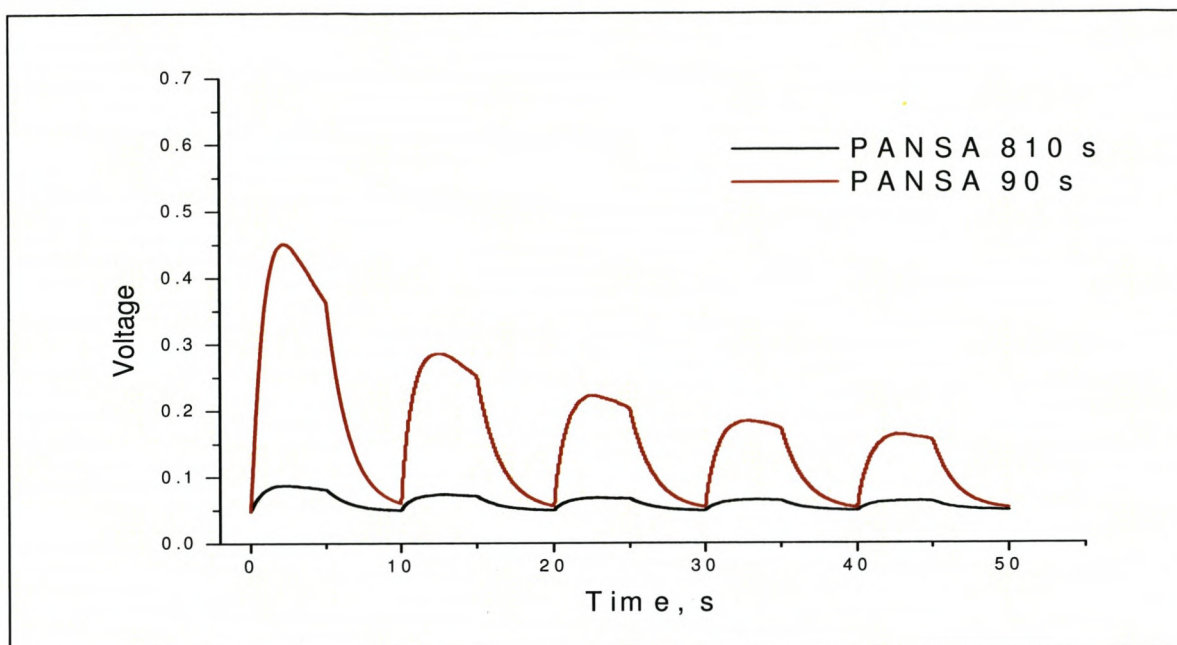
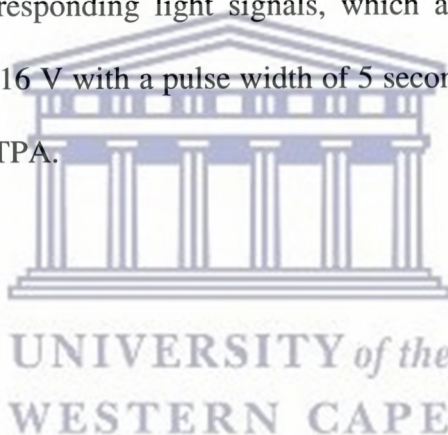


Figure 6.26: Shows the corresponding light signals, which are triggered by the potential stepping, 10 times from 5 to 16 V with a pulse width of 5 seconds, the supporting electrolyte is PBS that contains 50 mM TPA.



6.4. Conclusion

In conclusion, the two electropolymerization approaches were employed for the development of polymer- ruthenium complex for electrochemiluminescence. The electropolymerization of the conducting polymer in the presence of $[\text{Ru}(\text{bpy})_2(\text{picCOOH})]^{2+} \cdot (\text{ClO}_4^-)_2$ complex on ITO electrode was successfully achieved only by using potentiostatic growth method. The resultant film was further characterized in order to verify if the $[\text{Ru}(\text{bpy})_2(\text{picCOOH})]^{2+} \cdot (\text{ClO}_4^-)_2$ complex was incorporated in the conducting polymer. The conducting polymers (PANI and PANS A) used in this work, and resulted in the enhancement of the ECL signal. The increase in ECL signal was due to a positive energy transfer from the conducting polymer (PANI and PANS A) to $[\text{Ru}(\text{bpy})_2(\text{picCOOH})]^{2+} \cdot (\text{ClO}_4^-)_2$ complex, via interaction between the d orbitals of the metal and π orbitals of the polymer.

6.5. References

Bansal, V., Bhandari, H., Bansal, M. C., Dhawan, S. K. Electrical and optical properties of poly(aniline-co-8-anilino-1-naphthalene sulphonic acid) -A material for ESD applications, *Indian Journal of Pure and Applied Physics*, (2009) 47, 667-675.

Bard, A. J., Introduction. In *Electrogenerated Chemiluminescence*, Bard, A.J.; Marcel Dekker. Inc: New York, (2004).

Bachas, L.G., Cullen, L., Hutchins, R. S., Scott, D. L. Synthesis, characterization and electrochemical polymerization of eight transition-metal complexes of 5-amino-1,10-phenanthroline, *Journal of Chemical Society*, (1997) 9;1571-1577.

Choi, H.N., Cho, S.N., Lee, W.Y., Tris(2,2-bipyridyl)ruthenium(II) Immobilized in Titania-Perfluorosulfonated Ionomer Composite Films, *Analytical Chemistry*, (2003) 16; 4250-4256.

Dennany, L., Hogan, C. F., Keyes, T. E., Forster, R. J. Effect of Surface immobilization Electrochemiluminescence. *Analytical Chemistry*, (2006) 78; 1412-1417

Dennany, L., O'Reilly, E. J., Innis, P. C., Wallace, G. G., Forster, R. J. The influence of poly(2-methoxyaniline-5 sulfonic acid) on the electrochemical and photochemical properties of a highly luminescent ruthenium complex, *Electrochimica Acta*, (2008) 53, 4599-4605.

Doblhofer, K., Rajeshwar, K. In *Handbook of Conducting Polymers*, Skotheim, T. A., Elsenbaumer, R. L., Reynolds, J. R., Eds: Marcel Dekker: New York, (1998) 531-588.

Dini, D., Electrochemiluminescence from Organic Emitters , *Chemistry Materials* (2005) 17; 1933-1945.

Ding, Z., Quinn, B.M ., Haram, S.K., Pell, L.E., Korgel, B.A., Bard ,A.J . Electrochemistry and electrogenerated chemiluminescence from silicon nanocrystal quantum dots. *Journal of Science*, (2002) 290, 1293-1297.

Fan, F., Park, S., Zhu .Y., Ruoff, R.S., Bard, A. J. Electrogenerated Chemiluminescence of Partially Oxidized Highly Oriented Pyrolytic Graphite Surfaces and of Graphene Oxide Nanoparticles. *Journal of American Society* (2009) 131; 937–939.

Forster, R.J., Hogan, C.F. Electrochemiluminescent MetallopolymerCoatings: Combined Light and Current Detection Flow Injection Analysis. *Analytical Chemistry*, (2000) 72, 5576-5582.

Inzelt, G., Bard, A.J., (Ed) *Electroanalytical Chemistry*, M. Dekker, New York, (1994) 18.

Iwuoha, E.I., De-Villaverde, D.S., Smyth, M.R. Reactivities of organic phase biosensors. The amperometric behaviour of horseradish peroxidase immobilised on a platinum electrode modified with an electrosynthetic polyaniline film, *Biosensors and Bioelectronic*, (1997) 12,753-754

Mathebe, N. G. R., Morrin, A., Iwuoha, E. I. Electrochemistry and scanning electron microscopy of polyaniline/peroxidase-based biosensor, *Talanta* (2004) 64,115-120.

Mazeikiene ,R., Niaura, G., Malinauskas, A. Raman spectroelectrochemical study of self-doped copolymers of aniline and selected aminonaphthalenesulfonates, *Electrochimica Acta*, (2006) 51, 1919-1920.

Michira, I., Akinyeye, R., Somerset ,V., Klink, M.J., Sekota, M., Al-Ahmed A., Baker P.G.L., Iwuoha, E.I., Synthesis, characterization of novel polyaniline nanomaterials and application in amperometric biosensors, *Macromolecular Symposia*, (2007) 255 , 57–69.

Ngece, R. F. Electrochemical dynamics of cytochrome p450 (2d6) biosensors for selective serotonin re-uptake inhibitors (SSRIs), Msc thesis, University of the Western Cape, South Africa, (2007).

Ngece, R. F., West, N., Ndangili, P.M., Olowu, R., Williams, A., Hendricks, N., Mailu, S., Baker, P. , Iwuoha, E. A silver nanoparticle/poly (8-anilino-1-naphthalene sulphonic acid) bioelectrochemical biosensor system for the analytical determination of ethambutol, *International Journal of Electrochemical Science*, (2011) 6, 1820 –1834.

Myung, N., Lu, X., Johnston, K.P., Bard, A.J. Electrogenerated Chemiluminescence of Ge Nanocrystals , *Nano letters*, (2004) 4, 183-185.

O'Reilly, E. Conjugated metallopolymer systems for electrochemiluminescence enhancement; new approaches and materials, PhD thesis, Dublin City University, Ireland (2008).

Pellegrin, Y., Forster, R.J., Keys, T.E. pH-Modulated photoinduced electron transfer in a {[ruthenium adamantyl].[b-cyclodextrin-methylviologen]} inclusion complex, *Inorganica Chimica Acta*, (2008) 361, 2683-2691.

Pickup, P.G. Conjugated metallopolymer. Redox polymers with interacting metal based redox sites, *Journal of Materials Chemistry*, (1999) 9, 1641-1653.

Richter M. M., Electrochemiluminescence (ECL), *Chemical Reviews*, (2004) 104, 3003-3036

Venkatanarayanan, A. Nanomaterials for Electrochemiluminescent Biosensor, PhD Thesis. Dublin City University, Ireland (2010).

Wallace, G. G., Spinks, G.M., Kane-Maguire, L. A. P., Teasdale, P.R. *Conductive Electroactive Polymers: Intelligent Polymer Systems*, 2nd ed., CRC Press: Boca Raton, (2009).

CHAPTER SEVEN:

CONCLUSIONS AND RECOMMENDATIONS

7.1. Conclusion

The chapter deals with conclusions of the results presented in the study and make further recommendations for photo and eletrochemiluminescence research. This study has been directed towards the development of novel electrochemiluminescent material using conducting, electro-active nanostructured polyanilines and its derivatives. The approach taken involved electrosynthesis of PANSA in the presence of dopants such ASA, CNT and NSA, and from this approach mechanisms of polymerization process have been developed and proposed in the current study. The UV-vis spectroscopic signatures of these polymers yielded powerful insight information of electronic band gaps of the polymers, which could be directly linked to the redox states of the polymer. Since PANSA is a mixed oxidation state polymer, results revealed that the polymers exhibited two UV-vis absorption bands (274 and 368 nm),corresponding to the absorption of benzoid groups and quinoid groups respectively ,which are in the polymer structure. Each absorption band could be related to a band gap and a redox state of the polymer. The band at 274 nm yielded a band gap of 3.95 eV indicating the polyleucoemeraldine state of the polymer while the second band at 368 nm gave a band gap of band gap of 2.85 eV, which is indicative of polyemeraldine state of the polymer. From the study it was seen that all the doped polymers also showed similar results

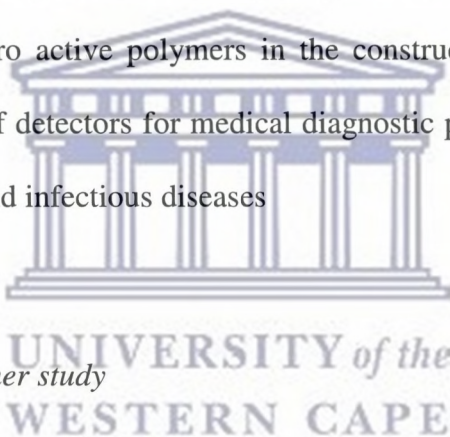
Another approach which was taken in the study was to chemically prepare PANI and PANSA , and PANI modulated with NSA. Conductivity of these materials was investigated and results showed that doping increased the conductivity significantly. The electrical

conductivity measurements showed to increase in this order PANI < PANSA < PANI-NSA (2.3×10^{-4} , 3.5×10^{-3} and $1.72 \times 10^{-2} \text{ Sm}^{-1}$). The increase in conductivity of PANI-NSA and PANSA were due to the electron transfer from the dopant and naphthalene sulfonic acid group to polymer, respectively. From these observations, it can be deduced that PANSA and PANI-NSA have better plastic electronics than pure PANI and are good candidates for being used as Organic light emitting diodes (OLED), since the valence band electrons can be easily excited to the conduction band of the polymeric materials.

Furthermore luminescence studies of these materials and their interaction with $[\text{Ru}(\text{bpy})_2(\text{picCOOH})]^{2+} \cdot (\text{ClO}_4^-)_2$ complex were also investigated. What was of importance is the finding that PANI and its derivatives showed an increase in emission intensity upon addition of polyaniline and its derivatives to the Ru. This was also evident by the increased lifetime which was observed. The enhancement of luminescence emission intensities, were due to the electron transfer from the polymers to the Ru complex. Hence this also shows that PANI and its derivatives are suitable for application as OLED. Moreover these polymers have showed to have added advantages of not having the undesired long wavelength excimer emission, which is normally caused by π - π stacking in conjugated polymers and makes them susceptible poor emission.

This was confirmed by electrochemiluminescence studies, in these studies composites of the polymer (PANSA or PANI) and $[\text{Ru}(\text{bpy})_2(\text{picCOOH})]^{2+} \cdot (\text{ClO}_4^-)_2$ complex were prepared by electropolymerization from monomer aniline and 8-anilino-1-naphthalene sulfonic acid in the presence of $[\text{Ru}(\text{bpy})_2(\text{picCOOH})]^{2+} \cdot (\text{ClO}_4^-)_2$ complex on ITO electrode using potentiostatic growth method at different run timings. The ECL studies involved using TPA as a correagent, on the PANI- $[\text{Ru}(\text{bpy})_2(\text{picCOOH})]^{2+} \cdot (\text{ClO}_4^-)_2$ or PANSA-

$[\text{Ru}(\text{bpy})_2(\text{picCOOH})]^{2+} \cdot (\text{ClO}_4^-)$ ITO modified electrodes. An ECL signal was observed in both composites. An interesting finding from this was that ECL emission was high in intensity, despite having low molar concentrations of Ru in polymer and the intensity was dependent on the time taken to form the film on the ITO electrode. This ECL enhancement signal observed was due to energy transfer from the conductive polymers to Ru complex from the PANI and PANSA. Results revealed that increasing polymerization time for PANI resulted in increased ECL intensity, while for PANSA it decreased the intensity. This shows that the PANI- $[\text{Ru}(\text{bpy})_2(\text{picCOOH})]^{2+} \cdot (\text{ClO}_4^-)$ was in the pernigraniline redox state, while PANSA- $[\text{Ru}(\text{bpy})_2(\text{picCOOH})]^{2+} \cdot (\text{ClO}_4^-)$ was in polyemeraldine radical cation state. This shows that the state that gives higher ECL is the pernigraniline redox state. This can be very useful in application of electroactive polymers in the construction of ECL detectors and assays which are the choice of detectors for medical diagnostic purposes such as monitoring pregnancy, thyroid diseases and infectious diseases.



7.2. Recommendation for further study

The following aspects of the development of an electrochemiluminescence materials using interaction of the Ru complex and conducting, electro-active, nanostructured polyaniline and its derivatives need further investigation:

- ✓ One important factor that should be considered is that in the current study, during the ECL detection, ECL measurements, utilized the photo multiplier tube (PMT) equipped with a high voltage power supply, which was used at a bias of -900 V. Normally the voltage power supply is set at -850 V. This raises concern whether the enhanced ECL signal observed, despite low molar ratio concentrations of the luminophore $[\text{Ru}(\text{bpy})_2(\text{picCOOH})]^{2+} \cdot (\text{ClO}_4^-)_2$ in the polymer occurred due to an increase in voltage supply during ECL measurement or due to energy transfer from

the conductive polymers to metal from the PANI and PANSA. Hence a point of reference measurement will need to be carried out in future, were the voltage supply will be set at a normal -850V and this will allow for the results obtained to be compared with other literature values, which did not use conducting polymers.

- ✓ In photophysics of the material, the energy transfer properties are not only the ground state but also the excited state need serious consideration. While fast rates of charge transfer are required it should be noted that deactivation of the ruthenium excited state by the polymer backbone is also possible.
- ✓ More experimental work needs to be done on optimization of the ITO/polymer/Ru complex for ECL. That includes: using different ratios of polymer and dopants, using different pH's and different temperatures.

